Summer 8-10-2010

Nuclear Pyruvate Kinase M2 Functional Study in Cancer Cells

Xueliang Gao
Georgia State University

NUCLEAR PYRUVATE KINASE M2 FUNCTIONAL STUDY IN CANCER CELLS

by

XUELIANG GAO

Under the Direction of Zhi-Ren Liu

ABSTRACT

Cancer cells take more glucose to provide energy and phosphoryl intermediates for cancer progression. Meanwhile, energy-provider function of mitochondria in cancer cells is disrupted. This phenomenon is so-called Warburg effect, which is discovered over eighty years ago. The detail mechanisms for Warburg effect are not well defined. How glycolytic enzymes contribute to cancer progression is not well known. PKM2 is a glycolytic enzyme dominantly localized in the cytosol, catalyzing the production of ATP from PEP. In this study, we discovered that there were more nuclear PKM2 expressed in highly proliferative cancer cells. The nuclear PKM2 levels are correlated with cell proliferation rates. According to our microarry analyses, MEK5 gene was upregulated in PKM2 overexpression cells. Our studies showed that PKM2 regulated MEK5 gene transcription to promote cell proliferation. Moreover, nuclear PKM2 phosphorylated Stat3 at Y705 site using PEP as a phosphoryl group donor to regulate MEK5 gene transcription. Our study also

showed that double phosphorylated p68 RNA helicase at Y593/595 interacted with PKM2 at its FBP binding site. Under the stimulation of growth factors, p68 interacted with PKM2 to promote the conversion from tetrameraic to dimeric form so as to regulate its protein kinase activity. Overexpression PKM2 in less aggressive cancer cells induced the formation of multinuclei by regulating Cdc14A gene transcription. Overall, this study presents a step forward in understanding the Warburg effect.

INDEX WORDS: PKM2, P68 RNA helicase, MEK5, Stat3, Cdc14A, Tyrosine phosphorylation, Gene transcription, Cell cycle, Glycolysis.

NUCLEAR PYRUVATE KINASE M2 FUNCTIONAL STUDY IN CANCER CELLS

by

XUELIANG GAO

A Dissertation Submitted in Partial Fulfillment of the Requirements for the Degree of

Doctor of Philosophy

in the College of Arts and Sciences

Georgia State University

2010

NUCLEAR PYRUVATE KINASE M2 FUNCTIONAL STUDY IN CANCER CELLS

by

XUELIANG GAO

Committee Chair: Dr. Zhi-Ren Liu

Committee: Dr. E. Shyam P. Reddy
Dr. Shi-Yong Sun
Dr. Susanna Greer

Electronic Version Approved:

Office of Graduate Studies
College of Arts and Sciences
Georgia State University
Aug 2010

ACKNOWLEDGEMENTS

I would like to sincerely acknowledge my mentor, Dr. Zhi-Ren Liu, for all his excellent instructions and scientific support in the past six years. Especially, I thank Dr. Zhi-Ren Liu recruited me in his lab to carry out this fascinating project. Dr. Zhi-Ren Liu gave me very encouraging advises in my research study.

I would like to earnestly acknowledge the support from my doctoral committees. Dr. E. Shyam P. Reddy gave so much brilliant suggestions and technical supports in my research. Dr. Shi-Yong Sun gave me excellent and helpful suggestions in my research project. Dr. Susanna Greer showed me very patient, superb and detailed instruction in my study.

Specially, I would like to thank Dr. Jenny Y Yang for her great help in my Ph.D. study and her guidiance in developing my future career life. I would like to acknowledge Dr. Phang Tai for his grand help in my Ph.D. study in the past years.

Especiallly, I would like to thank Ms. Haizhen Wang for her enormous suggestions and great contributions to my research. I would like to acknowledge all my labmates, past and current, for their wonderful technical assistances.

Last but not least, I would like to thank my parents for giving me strong support to let me complete my Ph.D. study.

TABLE OF CONTENTS

LIST OF TABLES

LIST OF FIGURES

CHAPTER I

GENERAL INTRODUCTION

Cancer is a serious human disease and the detail mechanism is not well understoond. Cancer cells uptake more glucose to provide energy and phosphoryl intermediates for macromolecule systhesis, and their oxidative phosphorylation activity is decreased, so-called Warburg effect. Warburg effect has been known for decades and the detail mechanisms are not well defined. In this project, we studied how a glycolytic protein played a role to regulate gene transcription in cells. Moreover, we investigated how phosphorylated proteins affect the glycolytic process by regulating the quaternary structure of a glycolytic enzyme, which provided part explanations for Warburg effect.

1.1 Cancer Metabolism

1.1.1 Tumors and Cancer

In general, tumors are the outcome of abnormal growth of normal cells. There are three continuous stages normal cells go through to completely develop into tumor cells. The first stage is hyperplasia, and at this stage the cells grow out of control but still behave like normally physiological cells. At this stage, tumors can be removed by surgery; also at this point they are called benign tumors. The second stage is dysplasia, which is also called the early form of cancerous lesions. At this stage, cells change their behavior and the differentiation and mature processes of cells are delayed. However, cells are not invasive to the basement membrane of the soft tissues. Dysplasic cells can be further graded into different levels even though cells at the highest level of this stage are still considered very low level cancers. The third stage is anaplasia, which is a reversion

process of cell differentiation. At this stage, cells lose their functional and structural differentiations at physiological conditions. The nuclei of anaplasic cells become astoundingly hyper-chromatic and large. The nuclear-cytoplasmic ratio increases to 1:1 instead of 1:4~1:6 for normal cells. At this stage, cells gain the ability to invade the blood system as well as neighboring tissues, which are called malignant tumors; these are also defined as cancers.

According to their original tissue location, cancers are further divided into five groups: Carcinoma is originally generated from epithelial cells covering the surface of internal organs. Sarcoma is a cancer initially from muscle, bone or connective tissues. Leukemia is generated from white blood cells. Lymphoma is originally from lymphatic cells. Myeloma is from mature B lymphocyte.

Cancer cells are characteristically different from normal cells. For example, the disruption of cytoskeletons in cancer cells, such as microfilaments and microtubules, changes their interactions with neighboring cells as well as their appearances. The change in cell to cell adhesion helps cancer cells to lose the restrictions of contact inhibition so that cancer cells can grow unlimitedly even surrounded by other cells. The secretion of enzymes from cancer cells facilitates them in degrading the basement membrane to invade into deep tissues. Therefore, these changes create six functional characteristics for cancer cells with the presence of variously genetic alterations, such as avoidance of apoptosis, constant reaction to growth signals or stimuli, unrestricted replicative capability, angiogenesis capacity, invasion ability and metastasis potential.

1.1.2 Cancer Metabolism and Warburg Effect

The metabolism in cancer cells is, to a certain extent, different from normal cells (Merida and Avila-Flores 2006). One important characteristic of cancer cell metabolism is the consistent switch of the energy production pathway from oxidative phosphorylation to glycolysis (Kondoh, Lleonart et al. 2007). In most normal mammalian cells, glycolysis flux is tightly regulated, and the glycolysis process is inhibited by the presence of oxygen, which was first discovered by Louis Pasteur. For decades, it has been known that cancer cells utilize more glucose and display a higher glycolysis rate than normal cells. In the 1920s, Otto Warburg found that even in the presence of sufficient oxygen, cancer cells consume glucose for ATP production instead of using the oxidative phosphorylation pathway (Warburg 1956; Warburg 1956).

In general, through the glycolysis process, one molecule of glucose generates two molecules of pyruvate and produces two molecules of ATP. In mammals, the product of the glycolysis process, pyruvate, has diverse fates. In an environment with limited oxygen, pyruvate is catalyzed into lactate by lactate dehydrogenase, a process which is called anaerobic glycolysis. In the presence of efficient oxygen, pyruvate is catalyzed into acetyl coenzyme A by the pyruvate dehydrogenase complex. Acetyl coenzyme A is consumed in the citric acid cycle to generate electrons in the mitochondria. The electrons create an electron gradient which generates a pH gradient across the mitochondrial membrane. The force motive produced by the pH gradient generates ATP by ATP synthases. This process is called aerobic oxidative phosphorylation. Overall, one acetyl CoA molecule through citric acid cycle produces two molecules of NADH, one molecule

of FADH2, and eight molecules of electrons. Compared to the aerobic oxidative phosphorylation pathway, anaerobic glycolysis only produces a small fraction of the total energy of glucose. One molecule of glucose can be completed degraded into H_2O and CO_2 in the oxidative phosphorylation process to produce 38 molecules of ATP. Overall, the oxidative phosphorylation process is more efficient in producing ATP than glycolysis.

However, cancer cells desire the glycolysis process to produce ATP instead of the oxidative phosphorylation pathway. The reason why cancer cells prefer consuming glucose to produce ATP is not well defined yet. One fact is that the glycolysis process provides a lot of phosphointermediates besides ATP for cells to synthesize macromolecules such as lipids, proteins, and nucleic acids.

1.2 Possible Causes of Metabolic Changes in Cancer Cells

1.2.1 Tumor Microenvironment Affects Tumor Metabolism

The metabolism in cancer cells is regulated by many effectors at diverse levels. Firstly, tumor microenvironment is, to a certain extent, different from normal cells, characterized by being surrounded with disorganized microvasculature (Allinen, Beroukhim et al. 2004; Joyce 2005; Anderson, Weaver et al. 2006; Fukumura and Jain 2007; Mohla 2007). Tissues of human bodies need nutrients and oxygen to keep their normal functions, which is provided through surrounding capillary vessels. Even though the growth and proliferation of cancer cells is not totally controlled by the same mechanisms as normal cells, cancer cells still need nutrients as well as oxygen provided by blood vessels. In most conditions, cancer cells proliferate and grow so fast that the

surrounding blood vessels can not provide enough oxygen or other nutrients to them. Under these conditions, the solid tumor grows in a hypoxic environment (normally below 3%–5% O_2). Without enough oxygen provided to the cancer cells they begin to rely on glycolysis to produce ATP as the major energy providing source. Meanwhile, the hypoxic environment surrounding cancer cells induces continuous expression and activation of hypoxia-inducible transcription factor (HIF-1) to regulate the expression of glycolytic enzymes as well as glucose transporters. Under anoxic conditions, HIF-1 is degraded by proteasomes due to the recognition by the von Hippel-Lindau (VHL) tumor suppressor (Mahon, Hirota et al. 2001). Under hypoxic conditions, HIF-1 is activated and translocates into the nucleus and binds to β-subunit of aryl hydrocarbon receptor nuclear translocator (ARNT) to regulate O_2-induced gene transcriptions (Wiesener and Maxwell 2003). Nearly all the expression of the glycolysis enzymes, such as hexokinase, phosphofructokinase, aldolase, glyceraldehyde 3-phosphate dehydrogenase, phosphoglycerate kinase, enolase, pyruvate kinase, lactate dehydrogenase is regulated by HIF-1 activity (Semenza 2007). The overexpression of these glycolysis enzymes enhances the glycolysis process to provide more energy to cancer cells. On the other hand, under hypoxic conditions, HIF-1 induces VEGF expression from cancer cells which facilitates the growth of blood vessels to provide more oxygen. However, the blood vessels surrounding tumor cells are so disorganized that they can not provide enough oxygen and nutrients as in normal physiological conditions. Under these conditions, the blood vessels surrounding tumor cells still can not alleviate the hypoxic levels of cancer cells. Therefore, aerobic glycolysis is still dominant in these tumor cells.

1.2.2 Oncogenes and Tumor Suppressor Genes Regulate Cancer Cell Metabolism

Some oncogenes and tumor suppressor genes regulate the glycolysis process in cancer cells, such as c-Myc, AKT, AMPK, Ras and p53.

Akt, a Serine/Theronine kinase, was initially discovered as a cellular homolog of a viral oncoprotein; this protein is amplified in diverse cancers, such as ovarian, breast carcinomas, and gastric adenocarcinoma (Vivanco and Sawyers 2002). Akt is the downstream target of phosphatidylinositide-3-kinase (PI-3 kinase) in growth factor induced signal pathways. Under the stimulation of diverse survival signals such as IL-6 and IGF-1, PI-3K is activated by phosphorylation to generate phosphoinositides. Akt is then recruited by phosphoinositides to the cellular membrane to be phosphorylated at Serine 473 and Threonine 308 residues (Kitamura, Kitamura et al. 1999). Akt can be dephophorylated by protein phosphatase 2A (PP2A). The PI3K-Akt pathway is an important signal transduction pathway, playing crucial roles in regulating the cell cycle, apoptosis, cell survival and cell proliferation (Thompson and Thompson 2004). Cellular Akt is also activated by the deletion of phosphatase and tensin homolog on chromosome 10 (PTEN), an antagonist of PI-3, in many cancers, such as brain, breast, and prostate cancers (Li, Yen et al. 1997). In addition, Akt is activated by a number of oncoproteins, such as Bcr-Abl in chronic myelogenous leukemia, Her2 in breast cancer, as well as Ras. Activated Akt has many downstream targets, such as nuclear factor-kappa B (NF-κB), GSK-3, and Bad. Activated Akt is pluripotent in contributing to tumorigenisis, such as avoiding apoptosis and promoting cell proliferation. In leukemia cells, the overexpression

of Akt promotes its survival capability by inceasing glycolysis levels. Akt regulates glycolysis though many aspects. Firstly, the activated Akt pathway in respiration deficient cancer cells increases glucose consumption by regulating the transcription and translation of glucose transporter1 (GLUT1) to support their survival and growth (Plas, Talapatra et al. 2001; Rathmell, Fox et al. 2003). Second, activated Akt stimulates hexokinase activity to convert glucose to glucose-6-phosphate, a modified form of glucose which can not diffuse freely out of the cell, so as to increase the cellular amount of glucose (Gottlob, Majewski et al. 2001) (Rathmell, Fox et al. 2003). Third, Akt regulates phosphofructokinase (PFK-1) activity, a key enzyme in controlling the glycolysis rate, through phosphorylating and activating PFK-2. PFK-2 catalyze the production of fructose 2,6-bisphosphate, which is an allosteric regulator of PFK-1 to overcome the inhibition effect of high ATP levels on PFK-1 (Deprez, Vertommen et al. 1997). In addition, it is reported that the overexpression of Akt is sufficient to promote transformed cells' aerobic glycolysis without affecting their oxidative phosphorylation level (Elstrom, 2004 #5019). Furthermore, the inactivation of mitochondrial respiration in human leukemia and lymphoma cell activates PI-3K-Akt pathway by oxidating the tumor suppressor PTEN. The activated PI-3K-Akt pathway benefits cell survival (Pelicano, Xu et al. 2006). The direct effect of Akt on glycolysis may contribute to the Warburg effect (Coloff and Rathmell 2006).

c-Myc is a nuclear oncoprotein, which is constantly active in many malignant tumor cells independent of growth factor stimulations (Elliott, Ge et al. 2000). It is reported that c-Myc regulates many glycolysis-related gene transcriptions to control energy production, such as glucose transporters, hexokinase, phosphoglucose isomerase,

phosphofructokinase, aldolase, enolase and pyruvate kinase (Gordan, Bertout et al. 2007). Interestingly, c-Myc not only upregulates glycolysis-related genes transcriptions for energy production, but also promotes mitochondrial biosynthesis through targeting the mitochondrial transcription factor A (TFAM) (Li, Wang et al. 2005). The products from mitochondrial biosynthesis provide intermediates for macromolecular synthesis, such as fatty acid, nucleotide, polyamine as well as amino acids (Coller et al., 2000; O'Connell et al., 2003).

AMP-activated protein kinase (AMPK), is a master regulator controlling energy metabolism, which was first identified in 1994 as an inhibitor of acetyl-CoA carboxylase and 3-hydroxy-3-methylglutaryl-CoA reductase (HMGR) (Kemp, Stapleton et al. 2003). AMPK activity is stimulated by its upstream effetor, AMPK kinases (AMPKKs), with the phosphorylation at Threonine172 residue. AMPK is also directly activated by AMP. AMPK is reported to regulate glucose consumption by controlling the transcription of GLUT1 and the translocation of GLUT1 to cellular surface (Russell, Bergeron et al. 1999). AMPK activates 6-phosphofructo-2-kinase (PFK-2), the enzyme that synthesizes fructose 2,6-bisphosphate in cardiac muscle cells under ischaemic conditions (Marsin, Bertrand et al. 2000).

p53, an important tumor suppressor, plays important roles in regulating apoptosis, cell cycle arrest, and DNA replication. p53 is inactive in more than half of cancers (Hainaut and Hollstein 2000). It is reported that the activation of p53 causes the downregulation of several glycolytic enzymes' transcription, such as phosphoglycerate mutase (PGM), and GLUT (Schwartzenberg-Bar-Yoseph, Armoni et al. 2004). In the glycolysis process, PGM converts 3-phosphoglycerate to 2-phosphoglycerate to decrease

the glycolysis flux. Interestingly, the activation of p53 increases the oxidative phosphorylation rate by upregulation of the synthesis of cytochrome oxidase 2 (SCO2). SOC2 is crucial for regulating cytochrome c oxidase (COX) complex activity to use oxygen in oxidative phosphorylation pathway. Therefore, the loss of p53 activity benefits cell proliferation by increasing the glycolysis rate and decreasing mitochondrial oxidative phosphorylation activity, which is another possible explanation for the Warburg effect (Matoba, Kang et al. 2006). p53 is a nuclecytoplasmic shuttling protein which depends on its leucine-rich nuclear export signal (Stommel, Marchenko et al. 1999). It is reported that p53 also translocates to mitochondria under stimuli to induce apoptosis by directly interacting with a Bcl-2 family protein (Erster, Mihara et al. 2004). Moreover, p53 plays important functions in maintaining mtDNA integrity in response to mtDNA damage by interacting with mtDNA and DNA polymerase γ to enhance poly γ transcriptional activity (Achanta, Sasaki et al. 2005).

1.2.3 Mitochondrial Malfunction in Cancer Cells

Mitochondrion is an important cellular organelle which takes part in regulating cell metabolism, producing reactive oxygen species (ROS) as well as inducing apoptosis (Lu, Sharma et al. 2009). Mitochondria have their own DNA as well as DNA transcription, replication and repair system to encode 13 polypeptides as the components of oxidative phosphorylation chain (Anderson, Bankier et al. 1981). In cancer cells the energy producer function of mitochondria is decreased for many reasons. First, in cancer cells, the transcription rate of the mitochondrial genome is reduced to a certain level compared to normal cells (Gogvadze, Orrenius et al. 2008; Bellance, Lestienne et al. 2009). Second,

mtDNA lacks histone protection from damages. Third, mitochondrial DNA is circular, supercoiled, and is easily damaged due to diverse exogenous or endogenous effects, such as radiation and ROS. Fourth, there are few DNA repair mechanisms in mitochondria compared to the nuclear genome (Achanta, Sasaki et al. 2005). All these properties make mitochondrial DNA to be easily affected by mutations, which disrupts the electron transport chain to decrease mitochondrial respiration rate. In addition, the malfunction of the electron transport chain in cancer cells produces superoxide, which forms ROS with other radicals. The accumulation of ROS damage mtDNA and nuclear DNA causes genetic instability as well as cancer progression (Pelicano, Carney et al. 2004). Usually, there are two characteristics of mtichondrial DNA mutations in cancer cells. First, the mutations are base transitions from T to C or G to A. Second, the mutations in the mitochondrial genome frequently occur in the 1.1 kb displacement-loop region (Ding, Ji et al. 2009).

The malfunction of mitochondrial genome decreases oxidative phosphorylation efficiency for ATP production. On the other hand ATP produced in the oxidative phosphorylation process is an inhibitor for phosphofructokinase 1 (PFK1) in glycolysis. PFK1 is the major pace-keeping enzyme in glycolysis, and activated PFK1 increases glycolysis flux, which makes a transition for energy production from oxidative phosphorylation to glycolysis in cancer cells. Moreover, studies show that the disruption of mitochondrial respiration function in cancer cells induces tumorigenesis. For example, the interruption of mitochondrial respiration with genetic, chemical and microenvironmental methods, activates the PI3K-Akt pathway (Robey and Hay 2009). It is well known that the PI3K-Akt pathway in cancer cells plays important functional roles

in cell survival, proliferation and migrations (Robey and Hay 2009). In mitochondria-deficient human leukemia and lymphoma cells, glycogen synthase kinase-3 (GSK-3), the substrate of Akt, is activated by Akt phoshphorylation. Therefore, the malfunctions of mitochondrial respiration in cancer cells may present part of the full explanation for the Warburg effect.

1.2.4 Metabolic Malfunction is a Potential Cancer Therapy Method.

Even though the mechanisms of the Warburg effect are not fully understood, thus far, the theory of the Warburg effect has been applied clinically in cancer diagnosis and therapy. For example, the Warburg effect has been used in cancer imaging for tumor detection by a glucose analogue, fluorodeoxyglucose, Positron Emission Tomography (FdG-PET) (Weber, Schwaiger et al. 2000). The fact that cancer cells require more glucose for energy production leads to FdG-PET, a powerful method in cancer diagnosis and prognosis (Kelloff, Hoffman et al. 2005). In addition, the increase of protein expression in glycolysis in cancer cells, such as HK2, and the decrease of the expression of components in the oxidative phosphorylation pathway, such as β-F1-ATPase, are also applied as biomarkers for cancer diagnosis (Cuezva, Ortega et al. 2009).

On the other hand, Akt/mTOR/HIF-1, a major regulatory signal pathway for the Warburg effect, has been targeted as a cancer therapy method to switch the energy production sources, that is, to decrease glycolysis efficiency and increase oxaditive phosphorylation competence (Jiang and Liu 2008). The activation of HIF-1 induced by Akt under hypoxia environment promotes cancer cell survival. By these methods, the survival advantages of cancer cells in hypoxic environments will be removed so that the

cancer cells cannot survive in the abnormal physiological conditions. For this purpose, some inhibitors for mTOR, such as RAD001, AP-23573 and CCI-779, and HIF-1a inhibitors, such as NSC644221, PX-478 and YC-1 are applied to impact cancer cell metabolism (Yeo, Chun et al. 2004; Smolewski 2006; MacKenzie and von Mehren 2007; Sun, Liu et al. 2007; Wan and Helman 2007; Gridelli, Maione et al. 2008; Jiang and Liu 2008).

Moreover, the fact that cancer cells depend on increased glycolysis as an ATP provider in hypoxic environments, brings a basis for disruption glycolysis as a potent cancer therapy. The disruption of the glycolytic pathway in order to limit the energy production has been studied as a promising cancer therapeutic method (Pelicano, Martin et al. 2006). For example, 3-BrPa, a hexokinase inhibitor, shows effective anti-cancer properties in colon cancer cells and lymphoma cells (Chen, Hewel et al. 2007). 2-deoxyglucose, a glucose analogue, which cannot be metabolized to produce ATP, is in clinical trails as an interruptor of the glycolytic pathway which induces tumor cell death (Mohanti, Rath et al. 1996). A hexokinase inhibitor, lonidamine, releases hexokinase bound to mitochondria, and inhibits oxygen consumption and glycolysis effectively in cancer cells (Brawer 2005). Glufosfamide, an alkylating agent from D-glucose, which damages DNA and activates PARP, is also in phase II clinical trials in patients with advanced non-small cell lung cancer (Giaccone, Smit et al. 2004). Evasion from apoptosis is one of the characteristics of cancer cells. Tumor cells that are defective in cell apoptosis can be diverted into another cell death pathway, necrosis (Zong and Thompson 2006) (Nelson and White 2004). Necrosis is happening in tumor cells when the cell cannot provide itself enough energy for consumption. The dismantling of the

glycolysis pathway may induce tumor cell necrosis. Even though chronic necrosis may trigger chronic inflammation, it still is a potent method for tumor therapy.

1.3 The Introduction of Glycolysis---Functional and Regulational Mechanisms of Glycolysis in Cancer Cells

Glucose is a very important energy source for the human body, and the body can use many sources for producing glucose. Glucose is a monosaccharide which can be generated from the hydrolysis of polysaccharides and disaccharides, such as starch and lactose. In some tissues, such as brain cells, glucose is the only available energy source, under non-starvation conditions. Glucose can also be synthesized from non-carbohydrate precursors, such as lactate, amino acids and glycerol. The formation of glucose from other non-cabohydrate carbon substrates, such as glycerol, lactate and glucogenic amino acides is called gluconeogenesis. The gluconeogenic pathway occuring in mitochondrial and cytosol, converts pyruvate into glucose. Gluconeogenesis is not simply the reverse process of glycolysis, as it takes two steps to convert pyruvate into PEP. The first step is the carboxylation of pyruvate to generate oxaloacetate catalyzed by pyruvate carboxylase at an expense of one molecule of ATP. The second step is under the function of phosphoenolpyruvate carboxykinase to generate PEP from oxaloacetat at the expense of one molecule of GTP.

Glycolysis is the metabolic process for cells to catalyze one molecule of glucose to produce two molecules of pyruvate, with a net energy production of two molecules of ATP. There are 10 reaction steps in this process carried out by 10 distinct enzymes. In mammals, glucose is first taken into cells with a family of glucose transporters (GLUT).

The sequence of glucose transporters is 500 amino acids long and consists of 12 transmembrane α helices. There are five members of GLUT family presented in specific tissues. GLUT1 and GLUT3 are responsible for controlling basal glucose uptake. GLUT2 exists in liver and pancreatic β cells to control glucose uptake from the blood with a very high Km value. GLUT4 is present in muscle and fat cells. GLUT5 exists in the small intestine. Once glucose is transported into the cells through GLUT, hexokinase, the first enzyme in the glycolysis process, phosphorylates glucose to form glucose 6-phosphate. Once phosphorylated, glucose 6-phosphate can not diffuse through the cell membrane and is trapped in the cytosol. Glucose 6-phosphate is further converted into fructose-6-phosphate through the function of phosphoglucose isomerase. In the next stage, the six-carbon fructose is cleaved by aldolase to generate two molecules of three-carbon fructose, glyceraldehyde 3-phosphate (GAP) and dihydroxyacerone phosphate (DHAP). GAP is the only form of the two, three-carbon molecules that can be used in the glycolysis process. Triose phosphate isomerase converts one molecule of DHAP into one molecule of GAP. Next, glyceraldehyde 3-phosphate dehydrogenase (GAPDH) catalyzes the formation of 1,3-bisphosphoglycerate (1,3-BPG) from GAP with the production of NADH. In this step, phosphorylation is coupled to the oxidation of three-carbon molecules. 1,3-BPG is an acyl phosphate, which has a high phosphoryl-transfer potential. The phosphate is transferred to ADP in the next step under the catalytic function of phsophglycerate kinase with the production of ATP. In the next step, the phosphoryl group is shifted with the conversion of 3-phosphoglycerate to 2-phosphoglycerate by phosphoglycerate mutase. Enolase catalyzes the conversion from 2-phosphoglycerate to phosphoenolpyruvate (PEP) with the formation of an enol in PEP and the production of a

molecule of H_2O. The enol phosphate in PEP has a high potential to transfer phosphate. In the final step, pyruvate kinase catalyzes this reaction and a phosphate is transferred to ADP with the production of a molecule of ATP committed with the formation of pyruvate.

The fates of pyruvate are diverse in different living organisms. In yeast and some other microorganisms, pyruvate is converted into ethanol catalyzed by pyruvate decarboxylase. In mammalian cells pyruvate is catalyzed into lactate by lactate dehydrogenase when oxygen is lacking. Most pyruvate produced in the glycolysis process enters into the citric acid cycle and the electron-transport chain in mitochondria to generate energy needed for higher organisms.

The pace of glycolysis is tightly regulated by the catalytic enzymes. Three glycolytic enzymes, which catalyze these irreversible glycolytic reactions, are involved in the regulatory process; they are hexokinase, phosphofructokinase and pyruvate kinase (Weber, Convery et al. 1966). Among these three enzymes, phosphofructokinase is the predominant regulator in the glycolytic pathway whose enzymatic activity is tightly controlled by the ATP/AMP ratio in mammalian cells. Phosphofrucokinase catalyzes the third step in the glycolysis process, which is the conversion from fuctose 6-phosphate to fructose-1,6-bisphosphate (FBP). During this process, fructose 2,6-bisphosphate formed from the phosphorylation of fructose 6-phosphate by phosphofuctokinase 2, regulates the activity of phosphofuctokinase. Fructose 2,6-bisphosphate activates phosphofructoskinase by increasing the affinity for fructose 6-phosphate as well as decreasing the ATP inhibitory effect to phosphofructokinase. Meanwhile, as an important regulator in the glycolytic pathway, the concentration of fructose 2,6-bisphosphate is

tightly controlled by its phosphorylation status. Fructose 2,6-bisphosphate can be dephosphorylated by fructose bisphosphatase 2 (FBPase 2). Phosphofuctokinase 2 and FBPase 2 are in a single peptide chain as a bi-functional enzyme. This bi-functional enzyme has five isoforms presenting as tissue specific. Overexpression of fructose 2,6-bisphosphatase decreases glycolysis flux and delays cell cycle progression (Perez, Roig et al. 2000).

Hexokinase is the second control element for the glycolytic pathway and it phosphorylates glucose to phospholate-6-glucose in the first step of the glycolysis process. Hexokinase activity is inhibited by its catalytic product, phospholate-6-glucose. Under these circumstances in which cells have enough energy production or high sources for macromolecule biosynthesis, phospholate-6-glucose will pass these signals to decrease the glycolysis process. In livers hexokinase has another isozyme, glycokinase, whose affinity to glucose is 50 folds lower than that of hexokinase. The function of glycokinase in liver is to provide phospholate-6-glucose for glycogen synthesis as well as fatty acid synthesis.

1.4 Pyruvate Kinase Type M2

Pyruvate kinase (PK) is the third rate-limiting enzyme in glycolysis process. Pyruvate kinase catalyzes the transfer of phosphoryl group from phosphoenolpyruvate (PEP) to ADP to produce pyruvate and ATP ($\Delta G°'$PEP=58 kJ/mol, $\Delta G°'$ATP=29 kJ/mol). This reaction is chemically irreversible. In mammalian cells, there are four types of pyruvate kinases in different tissues. L type is expressed exclusively in liver and R type is found in erythrocytes. M1 type is dominant in adult muscles tissues. M2 type is

expressed in fetal tissues and some proliferating tissues, such as tumor cells. During tumorigenesis, the tissue specific forms of PK, such as L and M1 types, lose their expression and M2 type is expressed (van Berkel, de Jonge et al. 1974; Miwa, Nakashima et al. 1975; Etiemble and Boivin 1976; Marie, Kahn et al. 1976). The L and R types are generated from one gene with different transcriptional start sites. M1 and M2 types are isoforms derived from the same gene but are different due to alternative splicing (Saheki, Saheki et al. 1982; Noguchi, Inoue et al. 1986). The M gene consists of 12 exons and 11 introns. In M2 type, exon 10 is spliced out, and in M1 type, exon 9 is spliced out. The splicing generates 23 different amino acids in a 56 stretch between M1 and M2 types at the carboxyl terminal from 378-434. During tumorigenesis, M1 type expression is replaced by M2 type. The replacement of M1 type by M2 type changes the glycolysis rate to produce more phosphoryl intermediates for cell proliferation.

The PKM2 protein consists of 531 amino acids and each monomer has four designated domains, such as A, B, C and N domains. Two monomers contact each other through the A domain interface to form a dimeric structure. Two dimers form a tetramer through the A and C domain interface (Dombrauckas, Santarsiero et al. 2005). The N-domain consists of residues 1-43. The A domain, consisting of residues 44-116 and 219-389, and is the core structure of the monomer. The B domain comprises residues 117-218. The C-domain is made of residues 390-531. The active site of PKM2 is located in the cleft constructed by A and B domains. The FBP binding site for PKM2 is positioned at the C-domain. Lysine 433, Serine 434, Serine 437, and Glycine 520 residues are backbone amides that bond to the 6'-phosphate oxygens of FBP. Among these residues, Lysine 433 is important for the binding of FBP to PKM2 as well as for PKM2 binding to

Tyrosine phosphorylated peptides (Christofk, Vander Heiden et al. 2008; Christofk, Vander Heiden et al. 2008; Spoden, Morandell et al. 2009). Lysine 270 is a conserved site for all four types of pyruvate kinases and is crucial for its kinase activity (Dombrauckas, Santarsiero et al. 2005).

In mammalian cells PKM2 has two known quaternary structures, dimeric and tetrameric forms. Tetrameric PKM2 has a higher affinity to its glycolysis substrate, PEP, compared to its dimeric form. In tumorigenesis, there is more dimeric PKM2 expressed with low affinity to PEP, which is called human tumor PKM2. The presence of dimeric PKM2 in patients feces, blood is utilized as a biomarker for the diagnosis of many cancers, such as colorectal cancer, prostate cancer and pancreatic cancer (Hardt, Ngoumou et al. 2000; Ahmed, Dew et al. 2007; Chung-Faye, Hayee et al. 2007; Dube, Grigull et al. 2007; Ewald, Schaller et al. 2007; Goonetilleke, Mason et al. 2007; Haug, Rothenbacher et al. 2007).

The low affinity of tumor PKM2 (dimeric PKM2) to PEP decreases the glycolysis rate so as to produce more phosphor intermediates, which are used to synthesize lipids, amino acids and some other macromolecules for cell growth and proliferation. The quaternary structure of PKM2 is regulated by many factors, such as fructose 1, 6-bisphosphorylate (FBP), Serine and some oncoproteins (Mazurek, Grimm et al. 2002). Fructose 1, 6-bisphosphate (FBP), a proceeding molecule in the glycolysis process, binds to PKM2 to induce its conformational change to the exposed active sites binding to PEP. The allosteric activity of PK is also regulated both by ATP and alanine, an important amino acid used in the building blocks for macromolecular synthesis. The activities of

PK are also controlled by reversible phosphorylation. Phosphorylated PK is less active than non-phosphorylated form.

Tetrameric PKM2, not dimeric PKM2, is associated with many other glycolytic enzymes to perform its glycolytic function, such as hexokinase (HK), glyceraldehyde 3-P dehydrogenase (GAPDH), phosphoglycerate kinase, phoglyceromutatse (PGM), enolase and lactate dehydrogenase (LDH) (Mazurek, Hugo et al. 1996). However, the interaction of PKM2 with some other proteins in the cytosol may change its glycolytic activity. Some oncoproteins, such as pp60V-src kinase and HPV-16E7 proteins directly interact with PKM2, individually to help the conversion of dimeric forms from tetrameric form, which results in a decreased ATP/ADP ratio and upregulated FBP level in the cytosol (Zwerschke, Mazurek et al. 1999). On the other hand, some tumor suppressor proteins, such as promyelocytic leukemia (PML), also interact with tetrameric PKM2 to suppress its glycolytic activity (Shimada, Shinagawa et al. 2008). Interestingly, PKM2 is a phosphoTyrosine binding protein, and the binding of Tyrosine phosphorylated peptides to PKM2 decreases its enzymatic activity (Christofk, Vander Heiden et al. 2008). Moreover, it is reported that the cytosolic monomer of PKM2 binds to cytoplasmic thyroid hormone 3,3',5-triiodo-L-thyronine (T3) to regulate transcription activity of thyroid hormone receptors (Ashizawa and Cheng 1992).

Besides its well-known glycolytic function in the cytosol, it is not known whether PKM2 have any other biological functions. Under the stimulation of interleukin 3 (IL-3), more PKM2 localizes to the nucleus to regulate cell proliferation in an IL-3-dependent hematopoietic cell line, Ba/F3 (Hoshino, Hirst et al. 2007). There are many reported nuclear partners of PKM2, such as Oct-4 and PIAS3. PKM2 interacts with Oct-4, an

important transcription factor for regulating the pluripotent state of embryonic stem cells, to positively modulate gene transcription (Lee, Kim et al. 2008). Interestingly, the N-terminal (a.a.1–348) of PKM2, interacts with the SUMO-E3 ligase protein PIAS3 (inhibitor of activated STAT3) in the nucleus of many cell lines, such as NIH3T3 and U-2 OS (Spoden, Morandell et al. 2009). SUMO, the small ubiquiting modification, is a post-translational modification occurring at lysine residues in many proteins (Miller, Levy et al. 2005). Sumoylation modification changes protein properties including transcriptional activity, nuclear-cytosolic translocation as well as protein stability. For example, sumoylation of interferon regulatory factor-1 (IRF-1) induced by PIAS3, represses its transcriptional activity (Nakagawa and Yokosawa 2002). The transcriptional activity of microphthalmia transcription factor (MITF) is suppressed due to sumoylation, it is dependent on the targeting sequence in the promoter of TRPM1 (Miller, Levy et al. 2005). PIAS, the protein inhibitor of activated STAT family, was originally identified as a cytokine-induced inhibitor of Stat3 and appears to have SUMO-E3 ligase activity (Chung, Liao et al. 1997; Nishida and Yasuda 2002). PIAS has several family members (PIAS1, PIAS2, PIAS3 PIAS3b, PIASxa, PIASxb, PIASy, and PIASyE6) sharing similar protein structures, such as the RING finger-like structure (Shuai and Liu 2005). PKM2 is sumoylated in U-2 OS cells affected by PIAS3, a human bone osteosarcoma. The overexpression of PIAS3 increases the sumoylation level of PKM2, which leads to the accumulation of nuclear PKM2 (Spoden, Morandell et al. 2009). According a SUMO prediction program and PKM2 X-ray structure analyses, there are eight lysine sites in PKM2 exposed on the protein surface possibly modified by PIAS3 (Spoden, Morandell et al. 2009).

On the other hand, somatosatin, a neuropeptide hormone and its anti-cancer analogues, TT-232, interact with pyruvate kinase in COS-7 cells. The interaction induces nuclear accumulation of PKM2 from cytosol to trigger caspase-independent apoptosis (Stetak, Veress et al. 2007). Moreover, UV and H_2O_2 also cause PKM2 nuclear accumulation independent of its kinase activity to induce apoptosis (Stetak, Veress et al. 2007). PKM2 also has its function in regulating viral replication abilities. For example, PKM2 interacts with NS5B, the Hepatitis C virus (HCV) RNA-dependent RNA polymerase, in HCV replicon 9B cells (Wu, Zhou et al. 2008). The downregulation of PKM2 by shRNA in n HCV replicon 9B cells reduces the replication of HCV (Wu, Zhou et al. 2008).

Besides its transcriptional regulatory activity, nuclear PKM2 also shows a kinase activity. It is reported that nuclear PKM2 isolated from Morris hepatoma 7777 tumor cell nuclei has kinase activity to phosphorylate histone H1 and it is speculated that PKM2 transfers phosphate from PEP to the ε-amino group of L-lysine (Ignacak and Stachurska 2003).

1.5 p68 RNA Helicase

p68 RNA helicase is a member of the DEAD box family proteins which share a conserved an Aspartic acid–Glutamic acid–Alanine–Aspartic acid (D-E-A-D) sequence motif (Hirling, Scheffner et al. 1989). There are many members in the DEAD family, such as p68, p72 and eIF-4a. All the members of the DEAD box family have a conserved amino acid motif, which includes the conserved DEAD box (Petry, Johnson et al. 1995; Shin, Rossow et al. 2007; Wilson and Giguere 2007). The conserved regions can be

found in many species, such as mouse, human, *Escherichia coli, Drosophila* and *Saccharomyces cerevisiae* (Jost, Schwarz et al. 1999). The DEAD box family proteins show RNA binding and unwinding activities through the conserved DEAD box amino acids sequence (Iggo and Lane 1989). DEAD box proteins have been shown to be involved in a wide range of biological processes involving interaction with specific RNA substrates; examples include pre-mRNA splicing, ribosome biogenesis, translation and embryogenesis (Stevenson, Hamilton et al. 1998).

Many homologs of p68 RNA helicase have been discovered in chickens, yeast, frogs, human and mice. In humans, p68 RNA helicase is encoded by a single gene locus. The transcribed part of human p68 gene is ~6.7 kb long and is split into 13 exons. Human p68 RNA helicase was first identified as an antigen cross reacting with a monoclonal antibody to SV40 large-T antigen, which is a DNA dependent ATPase (Huang and Liu 2002).

P68 RNA helicase plays important roles in pre-mRNA splicing process (Huang and Liu 2002; Liu 2002). Pre-mRNA splicing is an accurate process, which requires four small nuclear ribonucleoprotein particles (snRNPs): U1, U2, U4/U6 and U5 as well as some other non-snRNPs proteins. U1 snRNP binds to the 5' splicing site of pre-mRNA and U2 snRNP binds to the branch point. The spliceosome is formed when the U4/U6/U5 triRNPs joins the intermediate spliceosome complex. The 5' splice site is cleaved and the exposed 5' end of the intron links to the branching site. Next, the 3'-OH end of the first exon adds to the 5' end beginning site of the second exon. The whole intron between the two exons is cut off and released as a lariat and the two exons are jointed together to form a mature mRNA. p68 RNA helicase unwinds the transient U1-5' splice site duplex during

the spliceosome assembly process. The ATPase and helicase activities of p68 are required for the dissociation of U1 snRNA from the 5' slice site, which indicates that p68 RNA helicase might play roles in unwinding U1 snRNA and 5' splicing site complex. p68 RNA helicase might have functions in the formation of the spliceosome with the adding of U4/U6 and U5 snRNPs, which does not require the ATPase and helicase activities of p68 (Lin, Yang et al. 2005). As an RNA helicase, p68 is required for microRNA duplex unwinding, which is required for the unwinding of the transient RNA duplex to single stranded RNA, to take into the Argonaute protein to perform its silencing activity (Salzman, Shubert-Coleman et al. 2007). p68 RNA helicase plays important roles in early organ development and maturation. In mouse embryonic fibroblasts, the lack of p68 is related to the depression of many microRNAs (Salzman, Shubert-Coleman et al. 2007).

In the nucleus, p68 RNA helicase interacts with many other proteins to regulate its gene transcription as a co-activator (Warner, Bhattacherjee et al. 2004; Fuller-Pace, Jacobs et al. 2007). p68 interacts with p53 through the C-terminal region of p53 to regulate p53 downstream targeting genes, such as p21, Fas, PIG3 and mdm2 (Bates, Nicol et al. 2005). p68 RNA helicase is reported to be recruited to pS2 gene promoter, a downstream target of estrogen receptor alpha (ERα), to regulate its transcription (Watanabe, Yanagisawa et al. 2001). In these studies, neither the ATPase activity nor the RNA helicase activity of p68 is required for its co-activator function. p68 also interacts with CBP through the C-terminal of CBP to enhance CBP-mediated transcription (Rossow and Janknecht 2003). p68 RNA helicase interacts with Smad3, specifically the MH2 domains of Smad3, to form an active transcription regulator complex (Warner,

Bhattacherjee et al. 2004). Recently it is reported that p68 RNA helicase interacts with the androgen receptor (AR) in the nucleus and regulate gene transcription as a co-activator for androgen-dependent and androgen-independent prostatic malignancy (Clark, Coulson et al. 2008).

There are many post-translational modifications of p68 RNA helicase in mammalian cells, such as sumoylation, polyubiquitylation and phosphorylation. p68 was first reported to be polyubiquitylated in colorectal cells (Causevic, Hislop et al. 2001). Sumoylation is found at a single site of p68, Lysine 53, which is enhanced by PIAS1 (protein inhibitor of activated STAT1) (Jacobs, Nicol et al. 2007). The sumoylated p68 co-represses gene transcription through interacting with HDAC1 for p300 and Elk1 (Ets-like kinase 1) (Jacobs, Nicol et al. 2007). Recombinant p68 RNA helicase purified from *E.Coli*, is phosphorylated at Serine, threonine and Tyrosine residues (Yang and Liu 2004). In many cancer cells, p68 is phosphorylated at Tyrosine residues but not in their corresponding normal cell lines (Yang, Lin et al. 2005). p68 is phosphorylated at the Tyrosine 593 residue under the stimulation of PDGF-β in colorectal cells. The Tyrosine phosphorylated p68 blocks the phosphorylation of β-catenin by GSK-3β and displaces Axin from β-catenin distruction complex. The released β-catenine is shuttled into the nucleus by p68 RNA helicase which interacts with the LEF/TCF site to regulate gene expressions, which are required for EMT process (Yang, Lin et al. 2006). p68 is also double phosphorylated at Tyrosine 593 and Tyrosine 595 residues in T98G glioblastoma cells as well as HeLa cells. The double phosphorylation of p68 facilitates its apoptosis resistance to some TRAIL-induced apoptosis. The double phosphorylation of p68 RNA

helicase protects T98G cells from caspase-8 activation to trigger apoptosis (Yang, Lin et al. 2007).

Immunohistochemical examination shows p68 RNA helicase is dominantly localized in the nucleus in mammalian cells. p68 is detected in the cytosol depending on the cell cycle (Yang, Lin et al. 2007). Under the stimulation of growth factors, such as EGF, PDGF, some p68 comes out of the nucleus into the cytosol. According to the sequence analysis, there are many putative NES and NLS signals in p68. Two NES and two NLS functional signals are discovered in p68 RNA helicase sequence. Interestingly, the shuttling capability of p68 RNA helicase is not dependent on its ATPase activity. The nucleocytoplasmic shuttling function of p68 is CRM-1 dependent.

1.6 MEK5 and MAP Kinase Pathway

1.6.1 MAPK Family Members and Their Biological Functions

The mitogen-activated protein kinase (MAPK) family is an important kinase family in mammalian cells, consisting of four subfamilies: extracellular-regulated protein kinase1 and 2 (ERK1/2), ERK5, c-jun NH2-terminal protein kinases (JNK), and p38 MAPKs (Graves, Campbell et al. 1995; Seger and Krebs 1995; Attar, Atten et al. 1996; Hu and Plaxton 1996). The biological functions of MAPK pathways are diverse, playing roles in many cellular processes. In general, ERK subfamilies are related to cell growth, proliferation and survival, induced by growth factor stimulations. JNK and p38 MAPKs are associated with inflammation, apoptosis, cell growth and differentiation induced by cytokine stimulation, as well as extracellular stresses (Obata, Brown et al. 2000;

Hardwick, van den Brink et al. 2001; Papatsoris and Papavassiliou 2001; Saldeen, Lee et al. 2001).

All the MAPK family members are activated by phosphorylation at Threonine and Tyrosine residues within the activation loop TxY of kinase subdomain VIII by diverse activators: mitogen-activated protein kinase kinase (MEK1) and MEK2 for ERK1/2, MEK5 for ERK5, MKK4 and MKK7 for JNKs, MKK3 and MKK6 for p38 MAPKs (Graves, Campbell et al. 1995). The x in the TxY motif of the kinase subdomain VIII is diverse in MAPKs. For example, x is proline in JNK, glutamate in ERK, glycine in p38 MAP kinases. MEKs are activated by an upstream activator, MEK kinase. There are many MEK kinases that activate MEKs: Raf-1, A-Raf, B-Raf, c-Raf, Mos, Tpl2 are for MEK1 and MEK2; MEKK1, MEKK2, MEKK3, Tpl2 are for MEK5; PAK is for MKK3 and MKK6; MEKK4 and DLK are for MKK4 and MKK7. Cross-talk is always occurring among these MAPK signaling pathways. In addition, some activators are involved in more than one MAPK pathway. For example: the activators for MEK5 can also activate MEK1 and MEK2. In general, MAPK cascade members use docking interactions to regulate the efficiency and specificity between upstream activators and downstream substrates (Hu, Shen et al. 2007). In MAP2ks, such as MKK6, the docking domains are located at the N-terminal or C-terminal to bind its activator, MAP3Ks. The docking domain of MEK5, consisting of amino acids sequence, EYEDEDGD, is located in its N-terminus which interacts with its upstream regulator, MEKK2 or its downstream substrate, ERK5 (Seyfried, Wang et al. 2005). For MAPKs, such as ERK2, the docking domain is located in both the N- and C-terminals. ERK2 has a CD domain (common domain) consisting of a group of negatively charged amino acids, which is located in the

C-terminal region just after its kinase domain. ERK2 also has a docking domain named the ED site, which is located at its N-terminal region in front of its kinase domain. MAPK substrates have docking domains for their regulation by MAPK. C-Jun has a D domain to interact with its activator, JNK. c-Fos has DEF (docking site for ERK or FX) domain in its C-terminal region to interact with ERK. Some ERK substrates have both D domain and DEF domain to interact with their activators, such as JNK and ERK. In addition, some MAPK cascades use scaffold proteins to assemble functional MAPK modules to increase the interaction specificity. For example, JIP-1, a scaffold protein in the JNK pathway, contains a D domain to bind JNK (Dickens, Rogers et al. 1997)

On the other hand, the activation of MAPK is negatively controlled by MAPK phosphatase activity. Any dephosphorylation at either Threonine or Tyrosine residues in TxY motif inactivates MAPK. The dephosphorylation and inactivation process in the activation loop in MAPK last from minutes to hours depending on cell type and stimuli. Serine/Threonine protein phosphotases, such as PP2A, a member from the PPP family, inactivates ERKs. Members of Tyrosine protein phosphotase, such as PTP-SL, STEP, and HePTP, also dephosphorylate and inactivate ERKs. MAPK phosphatase plays important roles in diverse biological functions. For example, the JNK phosphatase family, the puckered mutation leads to cytoskeletal defects resulting in dorsal closure during Drosophola embryogensis. Interestingly, a subclass of the tyrosine phosphotase family called dual specificity phosphatase (DSP) dephosphorylate both tyrosine and threonine residues to inactivate MAPKs (Camps, Nichols et al. 2000). There are nine members identified in DSP family, such as CL100/MKP-1, PAC1, hVH-2/MKP-2, hVH3/B23, hVH-5, MKP-3/PYST1, B59, and MKP-5. PAC1, hVH-2/MKP-2,

hVH3/B23, hVH-5 are expressed exclusively in the nucleus and MKP-3/PYST1 is expressed in the cytosol. MKP-4 is expressed in both the cytosol and the nucleus.

1.6.2 ERK5-MEK5 Signal Pathway

Extracellular signal-regulated kinase 5 (ERK5), which is also named big-MAPK or BMK1, is one of the important MAPK family members, and it is activated through a cascade of signal transduction by MAP3Ks (MEKK2/3 and Cot), MEK5 and ERK5. ERK5 activation is exclusively activated by MEK5. The MEK5 signal pathway was first discovered in 1995 by Dixon and co-workers with a yeast two-hybrid screen experiment. ERK5 was used as the bait to interact with MEK5. ERK5-MEK5 signal pathway plays important roles in cell growth, cell differentiation, neuronal survival and embryonic angiogenesis (Sohn, Sarvis et al. 2002; Wang, Merritt et al. 2005). There are many transcription factors that can be phosphorylated by ERK5, such as c-Myc, MEF2 family members and c-Fos (Kamakura, Moriguchi et al. 1999) (Yang, Ornatsky et al. 1998). ERK5 has two splicing variants, ERK5 and ERK5b. ERK5b is shorter in the N-terminal compared with ERK5. ERK5b is a naturally dominant negative mutant which regulates ERK5 kinase activity. Overexpression of ERK5b inhibits ERK5b kinase function on nuclear substrate, such as MEF2C.

The MEK5 gene codes a 444 amino acids protein, which has two splicing variants, MEK5a and MEK5b (English, Vanderbilt et al. 1995; Chao, Hayashi et al. 1999). MEK5a is a protein with 89 amino acids longer than MEK5b at the N-terminal.

Both of MEK5a and MEK5b can individually interact with ERK5. Double phosphorylated MEK5a at Serine 311 and Threonine 315 activates ERK5 as well as its

nuclear translocation, but not MEK5b (Kato et al., 1997). MEK5a directly interacts and stimulates ERK5 kinase activity by phosphorylating threonine and Tyrosine residues in the TxY motif. On the other hand the overexpression of MEK5b disrupts the interaction of MEK5a with ERK5, which indicates MEK5b is a putative dominant negative mutant which regulates MEK5a kinase function to activate ERK5.

The expression and cellular localization of MEK5a and MEK5b are tissue specific (English, Vanderbilt et al. 1995). MEK5a is localized dominantly in the cytosol and MEK5b is distributed evenly in the whole cell. MEK5a expression is abundant in actively mitotic tissues, such as liver and brain (English, Vanderbilt et al. 1995). MEK5b has more expression than MEK5a in differentiated tissues, such as muscle, lung, kidney et al.

Many studies showed the expression of MEK5 is closely related with tumorigenesis. MEK5 is overexpressed in human prostate cancer cells as detected by antibodies that recognize the specific N-terminal of MEK5a (Mehta, Jenkins et al. 2003). Immunohistostaining results also show that MEK5 is overexpressed in human prostate cancer but not in benign prostate tissues (Mehta, Jenkins et al. 2003). Moreover, the expression level of MEK5 in malignant prostate cancer is correlated with its bone metastases (Mehta, Jenkins et al. 2003). Patients with higher expression of MEK5 had a shorter disease-specific survival time (52 months) compared to those with weaker MEK5 expression which survived in 58 months. The activation of MEK5 induces prostate cancer cell proliferation. The overexpression of a constitutively active MEK5 mutant (MEK5D) in LNCaP cells, a metastatic prostatic adenocarcinoma cell line derived from the lymph node, induces a 3.7 fold higher cell proliferation compared to control vectors. In our experiments the expression of MEK5 is upregulated by PKM2 overexpression,

which results in cell proliferation, especially in more metastatic cancer cell lines compared to the less aggressive cell lines. Moreover, MEK5D overexpression in LNCaP cells increases cell migration by 1.8 fold and invasion ability by 2.1 fold compared to control vectors, which indicates that MEK5 plays a role in tumor metastasis as well as invasion. MEK5 is a putative modulator in regulating gene expression involved in tumor metastasis and migration processes. Matrix metalloproteinases 9 (MMP9), a zinc-dependent enzyme involved in the metastasis process, is transcriptionally upregulated by MEK5 overexpression (Mehta, Jenkins et al. 2003).

1.7 Stat Family and the Biological Function of Stat3

Signal transducer and activator of transcriptions (Stat) is an important transcription factor family playing crucial roles in cell differentiation, proliferation, cell survival as well as other cellular activities (Johnston, Bacon et al. 1995; Ripperger, Fritz et al. 1995; DaSilva, Rui et al. 1996). Stat family proteins were first identified as a molecule required for interferon (IFN)-triggered gene expression around 15 years ago (Yang, Shi et al. 1996). Stat is highly expressed in a large number of human malignant tumor cells, such as breast cancer, lung cancer, colorectal cancer and hematological malignancies. The Stat family consists of seven members, such as Stat1, Stat2, Stat3, Stat4, Stat5 (Stat5a, Stat5b) and Stat6. Stat1 and Stat2 were first identified as transcriptional factors binding to a consensus sequence TT(C/A)YNR(G/T)AA (Schindler, Shuai et al. 1992). Stat family members share a number of well conserved domains. The N-terminal domain is a binding region for some other transcription co-activators, such as CBP/p300, c-Jun, and Nmi (Giraud, Bienvenu et al. 2002; Cvijic, Bauer et al. 2009). In the middle of the sequence is

a DNA binding domain, which binds to cognate targeting DNA sequences. A flexible linker connects DNA binding domain with SH2 domain, which is required for the dimerization of Stat proteins as well as for Tyrosine phosphorylation binding. The C-terminal region of Stat protein is a transactivation domain and the phosphorylation of Tyrosine/Serine residues at this domain is required for Stat protein activation.

In general, Stat is a transcription factor family activated by phosphorylation through a cascade of signal transductions induced by interleukins or growth factors (Wen, Zhong et al. 1995). The Stat family of proteins is latent and inactive within the cytosol under normal conditions. Once ligands bind to the receptors on cellular membrane, autophosphorylation of the receptors is triggered, which induces the dimerization of these receptors. The dimerization of growth factor receptors activates their intrinsic Tyrosine phosphorylation activity. The phosphroylated receptors at Tyrosine residues subsequently create docking sites at their cytoplasmic tails for Stat proteins via their Src-homology (SH2) domain. Stat proteins binding to the phosphorylated receptors are phosphorylated by the receptors and form an activated form. In some cases the engagement of cytokines to their receptors results in the activation of these receptor-associated Tyrosine kinases, such as Janus kinase (JAK). Subsequently, JAK kinase phosphorylates Stat proteins at their C-terminals. The phosphorylated Stat proteins are released from the binding sites on the membrane and form homodimers or heterodimers. The dimerized Stat proteins then translocate into the nucleus and bind to promoter regions bearing conserved DNA sequences. Once bound, Stat proteins recruit other transcription elements at the promoter site to trigger gene transcription.

Stat family members can be activated by many cell-surface binding ligands involved in diverse signal pathways. Stat1 activation is induced by interferon signaling exclusively (Qing and Stark 2004; Ho and Ivashkiv 2006). Stat3 activation can be inducible by many cytokinses, such as interleukin-6 (IL-6) and growth factors, such as EGF, PDGF, VEGFR, FGFR and IGFR. In transformed cells, some oncoproteins, such as Src and Abl, can also activate Stat3 (Yu, Meyer et al. 1995). The activation of the Stat family requires Tyrosine phosphorylation at the C-terminal region, which is adjacent to its transcriptional activation domain. For example, Y705 in Stat3, Y694 in Stat5a and Y699 in Stat5b are the activation sites for these Stat family members. A phenylalanine substitution of the Tyrosine residue position at 705 of Stat3 results in a reduction in Tyrosine phosphorylation of wild type Stat3 and inhibits its endogeous activity (Kaptein, Paillard et al. 1996). Serine phosphorylation at the C-terminal of the Stat family is also important for regulating their transcriptional activity. For example, phosphorylation at Serine 727 in Stat3 and Stat1 upregulates their transcriptional activity mediated by several kinases, such as p38，JNK and protein kinase C (Nagy, Wang et al. 2002) (Wierenga, Vogelzang et al. 2003) (Pircher, Petersen et al. 1999). On the contrary, Serine phosphorylation at residue 725 in Stat5 down-regulates the transcriptional activity of Stat5 (Yamashita, Nevalainen et al. 2001)　(Yamashita, Xu et al. 1998) .

An important Stat family member is Stat3, whose activity is tightly controlled under diverse physiological conditions. Stat3 is activated/phosphorylated in a low level in normal cells, which is negatively regulated by many inhibitory proteins including Suppressor of Cytokine Signalling (SOCS) and Protein Inhibitor of Activated Stat (PIAS) (Flowers, Subramaniam et al. 2005; Tokumaru, Sayama et al. 2005; Diao, Wang et al.

2009). It is reported that PIAS3 specificly interacts with Stat3, not other members of Stat family. The interaction blocks Stat3 DNA binding activity to inhibit its gene transcriptional regulatory activity in many cell lines, such as HepG2 cells, IL-6-treated M1 and MCF7 cells (Chung, Liao et al. 1997). Some protein Tyrosine phosphatases, such as PTP1B, SHP1, SHP2, CD45 are reported to inhibit the Stat3 pathway as well (Ohtani, Ishihara et al. 2000; Zhang, Chan et al. 2009). In cancer cells, such as breast cancer, head and neck cancer, prostate cancer, Stat3 is detected with high levels of expression and activation (Bromberg, Wrzeszczynska et al. 1999) (Yu and Jove 2004). Activated Stat3 is sufficient to mediate tumor formation in nude mice (Bromberg, Wrzeszczynska et al. 1999). A constitutively active Stat3 mutant transfected in melanoma cells, enhances its brain metastasis (Xie, Huang et al. 2006). Phosphorylated Stat3 activates many genes related to cell proliferation and differentiation as well as anti-apoptosis, such as c-Myc, Cyclin D1, BCL2 family gene Bcl-XL (Nielsen, Kaestel et al. 1999) (Bienvenu, Gascan et al. 2001), (Song, Ethier et al. 2004). Stat3 also induces the gene expression of HIF-1, MMP-2 and VEGF to promote tumor metastasis and angiogenesis (Niu, Wright et al. 2002).

Moreover, Stat3 plays important roles as a cross-talker in regulating the activities between tumor cells and tumor immune microenvironments by suppressing immune responses from both tumor cells and immune cells (Cheng, Wang et al. 2003; Kortylewski and Yu 2008). In tumor cells, the overexpression of Stat3 inhibits the release of immuno-stimulating molecules so that the tumor cells can prevent the infiltration of immune cells. For example, the overexpression of a Stat3 dominant negative mutant in B16 melanoma, greatly enhances the release of pro-inflammatory mediators to promote

the infiltration of immune cells to B16 melanoma (Wang, Niu et al. 2004). Moreover, the releasing of pro-inflammatory mediators blocked by phosphorylated Stat3 stimulates the activation of innate immune response cells, such as neutrophils and macrophages (Wang, Niu et al. 2004). Activated Stat3 not only inhibits the release of pro-inflammatory mediators from tumor cells, but also prohibits the expression of pro-inflammatory mediators in normal immune cells. For example, the inhibition of Stat3 expression in macrophages results in a high level release of pro-inflammatory mediators found in Stat3-inactiated tumor cells (Takeda, Clausen et al. 1999).

Stat3 is a important mediator playing roles in multiple oncogenic signaling pathways to regulate tumorigenesis as well as immunosuppressive pathways (Yu, Kortylewski et al. 2007). Stat3 has been identified as a potential target for cancer immuno-therapy (Zhang, Zhang et al. 2007; Zhou, Wulfkuhle et al. 2007; Al Zaid Siddiquee and Turkson 2008). The suppression of Stat3 activities in tumor cells induces cell apoptosis, decreases tumor cell proliferation, and inhibits tumor cell migration (Grandis, Drenning et al. 2000; Epling-Burnette, Liu et al. 2001; Wang, Ouyang et al. 2008; Baral, Bose et al. 2009; Xin, Zhang et al. 2009; Yagil, Kay et al. 2009). Disruption of Stat3 activity blocks VEGF expression, a key mediator for solid tumor angiogenesis (Wei, Kuo et al. 2003). The interruption of the Stat3 signaling pathway activates the expression of IP-10 and IFN-β, both of which are inhibitors of solid tumor angiogenesis during malignant process (Niu, Heller et al. 1999; Niu, Bowman et al. 2002). Some Stat3 inhibitors, such as phosphopeptide and platinum (IV) complexes, have been proven to inhibit Stat3 signaling so as to deregulate Stat3-dependent malignant transformation and cell proliferation, and induce apoptosis of cancer cells (Turkson, Ryan et al. 2001;

Turkson, Zhang et al. 2005). The suppression of Stat3 activities in many immune cells decreases the release of negative immune regulators such as immature dendritic cells. The suppression of Stat3 activities also increases the activity of CD8+ T cells, natural killer cells as well as neutrophils.

Stat3 is located in diverse cellular compartments dependent on its phosphorylation status, such as the cytosol and the nucleus. Non-phosphorylated Stat3 shuttles between the nucleus and the cytosol depending on its own NLS and NES. Stat3 binds to α/β importin to translocate into the nucleus, and binds to CRM1 to export from the nucleus (Sato, Tsuruma et al. 2005). Once phosphorylated by its upstream activators, Stat3 is retained in the nucleus, binding to its target DNA sequence to start regulating gene transcription by recruiting other transcriptional factors. Recently, it is reported that Stat3 exists in mitochondria where it interacts with GRIM-19 in complex 1 and 2 to regulate cell respiration (Wegrzyn, Potla et al. 2009). The functional role of Stat3 in regulating energy production in the oxidative phosphorylation pathway is independent of its transcriptional function. Moreover, unlike its transcription role in the nucleus, DNA binding domain, the dimerization motif or Tyrosine phosphorylation at 705, are not required for its mitochondrial function. Interestingly, phosphorylation at Serine 727 is crucial for Stat3 oxidative phosphorylation regulatory function, which indicates the possible involvement of either growth factor triggered phosphorylation signal pathways or non-receptor protein kinase induced phosphorylation pathways (Wegrzyn, Potla et al. 2009).

1.8 Cdc14 Regulates Mitosis Exit in Eukaryotic Cells

Cyclin Dependent Kinases (CDKs) play important roles in regulating the entry from interphase to mitosis. For cells to exit from mitosis, CDKs must be degraded or be dephosphorylated to inhibit their functions. How cells exit from mitosis has been well characterized in the budding yeast, *Saccharomyces cerevisiae* (Jensen and Johnston 2002). In *Saccharomyces cerevisiae*, cells exit from mitosis is regulated by a cascade of reactions named Cdc Fourteen Early Anaphase Release (FEAR) and Mitosis exit network (MEN). MEN are a group of proteins that can inactivate mitotic cyclin-dependent kinases including Tem1p, Lte1p, Cdc5p, Cdc15p, Dbf2p, and Dbf20p, and Mob1p (McCollum and Gould 2001). In anaphase, MEN activated by a small G protein, Tem1, induces the export of Cdc14, which is located in the nucleolus held by inhibitors Cfi1/Net1 during interphase, from the nucleolus into cytoplasm. Cdc14 is a Serine/Threonin phoshpatase. In *Saccharomyces cerevisiae*, Cdc14 antagonize the effect of Cdc28/Clb, a key regulatory kinase for cell cycle in yeast, to regulate cell cycle. Cdc14 dephosphorylates several downstream targets of Cdc28/Clb, such as Hct1, Sic1 and Swi5, to regulate cell cycle. (Toyn, Johnson et al. 1997). The dephosphorylation of Hct1 results in cyclin B degradation. The dephosphorylation of Swi5, a transcription factor, by Cdc14 results in the nuclear accumulation of Swi5. Cdc14 also mediates dephosphorylation of Sic1, an inhibitor of Cdc28/clb, results in the accumulation of Cdc28/clb (Verma, Feldman et al. 1997)

In fission yeast, *Saccharomyces pombe*, Cdc14 has a homologous, Flp1/Clp1, which has a distinct functions in cell cycle regulation from Cdc14 in *Saccharomyces cerevisiae*. Flp1/Clp1 is not an essential gene in fission yeast and regulates G2 phase of the cell cycle.

In higher eukaryotes, two types of anaphase promoting complexes (APC), a large ubiquitin ligase, must be activated for cells to exit from anaphase. APC and their co-effectors, such as Cdc20 and Cdh1, form a complex, such as APC^{Cdc20} and APC^{Cdh1}. During G2/M phase, APC^{cdc20} is activated to ubiquitnate securin so that separase was released into the cytosol to promote sister-chromatid separation. APC^{cdh1} is activated during M/G1 phase and APC^{Cdh1} ubiqutinates mitotic cyclins to allow cells to exit from mitosis. The activity of APC relies on the phosphorylation status of their co-effectors, Cdc20 and Cdh1. Cdh1 is phosphorylated by cyclin B-cdc2 and dephosphorylated by Cdc14A. In addition, Cdc14A is the major phosphatase for Cdh1 (Bembenek and Yu 2001).

In mammalian cells, Cdc14 has two orthologs Cdc14A and Cdc14B, encoding by two distinct genes. Cdc14A and Cdc14B share a conserved amino acid sequences over 80% in their N-terminal and phosphatase domain. Cdc14A and Cdc14B have distinct dynamic cellular localizations spatiotemporally. Cdc14A resides in centrosome in interphase and Cdc14B locates in nucleolus. During mitosis Cdc14A is released into the cytoplasm. Cdc14A was interacted with MTOC in the cytosol.

In human, Cdc14A gene is located on chromosome 1 on the band 1p21 and consists of 16 exons. The expression of Cdc14A is tightly controlled during cell cycle. The expression of Cdc14B is even during whole cell cycle. Cdc14A is highly expressed in brain, heart, small intestine and skeletal muscle. And has a low expression level in kidney, liver, lung, testis and pancreas (Paulsen, Starks et al. 2006). The expression of Cdc14A is quite differentially in cancer cells, even within the same specific tumor type.

In mammalian cells, Cdc14A has several putative downstream targets. Cdc14A interacts with tumor suppressor p53 both *in vitro* and *in vivo*. The interaction is dependent on the N-terminal of Cdc14A and the C-terminal of p53. The phosphorylation site of p53, Ser315, is specifically dephosphorylated by Cdc14A. The other phosphorylation site in p53, such as Ser392, is not dephosphorylated by Cdc14A. The phosphorylaion of p53 protein at Ser315 is related to its DNA binding activity (Li, Ljungman et al. 2000).

As two isoforms, Cdc14A and Cdc14B have distinct functions in regulation centrosome duplication. Studies show that Cdc14A overexpression induce multinucleus in mammalian cells. The depletion of Cdc14A results in centrosome separation and cytokinesis failure (Mailand, Lukas et al. 2002). On the other hand, the depletion of Cdc14B results in amplification of centriole (Wu, Cho et al. 2008).

As an important physiological regulator, the expression of either Cdc14A or Cdc14B affects genomic stability (Mailand, Lukas et al. 2002). So far, the mechanism of Cdc14A gene transcription regulation is not well defined.

1.9 Aims of Dissertation

Aerobic glycolysis is been established as a hallmark for cancer progression, which is well known as Warburg effect. In 1924 Otto Warburg hypothesized that cancer is caused by the metabolism switch from oxidative phosphorylation to glycolysis (Warburg 1956; Warburg 1956). With the development of modern oncology and the discovery of many oncogenes and tumor suppressor genes, cancer is gradually recognized as a genetic disease and the metabolism change in cancer cells is a company phenomenon of

tumorigenesis. Many oncogenes as well as tumor suppressor genes results in the metabolism switch from oxdative phosphorylation to glycolysis by regulating metabolic enzymes activities, such as Ras, Akt and Myc (Gordan, Thompson et al. 2007). However, how glycolysis enzymes directly regulate tumorigenesis is not well studied. In this project, we found that a glycolytic enzyme, pyruvate kinase M2 (PKM2), plays an important role as a transcriptional co-activitor in regulating cell proliferation in the nucleus of cancer cells. PKM2 phosphorylates its downstream target, Stat3, using PEP as a substrate. Morover, phosphorylated p68 RNA helicase Y593/595 interacts with PKM2 to shuttle cytosolic PKM2 into the nucleus. In addition, the interaction between phosphorylated p68 RNA heliase and PKM2 transforms a tetrameric PKM2 into a dimeric form under the stimulation of EGF. Nuclear PKM2 and p68 RNA helicase co-regulates Cdc14A gene transcription to induce multinucleus in less aggressive cancer cells. Overall, this study provides evidences about how glycolytic enzymes affect tumorigenesis, which brings centain levels of explanations about why cancer cells prefer to glycolysis for Warburg effect.

1.10 References

Achanta, G., R. Sasaki, et al. (2005). "Novel role of p53 in maintaining mitochondrial genetic stability through interaction with DNA Pol gamma." EMBO J 24(19): 3482-3492.

Ahmed, A. S., T. Dew, et al. (2007). "M2-PK as a novel marker in ovarian cancer. A prospective cohort study." Eur J Gynaecol Oncol 28(2): 83-88.

Al Zaid Siddiquee, K. and J. Turkson (2008). "STAT3 as a target for inducing apoptosis in solid and hematological tumors." Cell Res 18(2): 254-267.

Allinen, M., R. Beroukhim, et al. (2004). "Molecular characterization of the tumor microenvironment in breast cancer." Cancer Cell 6(1): 17-32.

Anderson, A. R., A. M. Weaver, et al. (2006). "Tumor morphology and phenotypic evolution driven by selective pressure from the microenvironment." Cell 127(5): 905-915.

Anderson, S., A. T. Bankier, et al. (1981). "Sequence and organization of the human mitochondrial genome." Nature 290(5806): 457-465.

Ashizawa, K. and S. Y. Cheng (1992). "Regulation of thyroid hormone receptor-mediated transcription by a cytosol protein." Proc Natl Acad Sci U S A 89(19): 9277-9281.

Attar, B. M., M. J. Atten, et al. (1996). "MAPK activity is down-regulated in human colon adenocarcinoma: correlation with PKC activity." Anticancer Res 16(1): 395-399.

Baral, R., A. Bose, et al. (2009). "Association of early phase of colorectal carcinogenesis with STAT3 activation and its relevance in apoptosis regulation." Exp Mol Pathol 87(1): 36-41.

Bates, G. J., S. M. Nicol, et al. (2005). "The DEAD box protein p68: a novel transcriptional coactivator of the p53 tumour suppressor." EMBO J 24(3): 543-553.

Bellance, N., P. Lestienne, et al. (2009). "Mitochondria: from bioenergetics to the metabolic regulation of carcinogenesis." Front Biosci 14: 4015-4034.

Bembenek, J. and H. Yu (2001). "Regulation of the anaphase-promoting complex by the dual specificity phosphatase human Cdc14a." J Biol Chem 276(51): 48237-48242.

Bienvenu, F., H. Gascan, et al. (2001). "Cyclin D1 represses STAT3 activation through a Cdk4-independent mechanism." J Biol Chem 276(20): 16840-16847.

Brawer, M. K. (2005). "Lonidamine: basic science and rationale for treatment of prostatic proliferative disorders." Rev Urol 7 Suppl 7: S21-26.

Bromberg, J. F., M. H. Wrzeszczynska, et al. (1999). "Stat3 as an oncogene." Cell 98(3): 295-303.

Camps, M., A. Nichols, et al. (2000). "Dual specificity phosphatases: a gene family for control of MAP kinase function." FASEB J 14(1): 6-16.

Causevic, M., R. G. Hislop, et al. (2001). "Overexpression and poly-ubiquitylation of the DEAD-box RNA helicase p68 in colorectal tumours." Oncogene 20(53): 7734-7743.

Chao, T. H., M. Hayashi, et al. (1999). "MEKK3 directly regulates MEK5 activity as part of the big mitogen-activated protein kinase 1 (BMK1) signaling pathway." J Biol Chem 274(51): 36035-36038.

Chen, E. I., J. Hewel, et al. (2007). "Adaptation of energy metabolism in breast cancer brain metastases." Cancer Res 67(4): 1472-1486.

Cheng, F., H. W. Wang, et al. (2003). "A critical role for Stat3 signaling in immune tolerance." Immunity 19(3): 425-436.

Christofk, H. R., M. G. Vander Heiden, et al. (2008). "The M2 splice isoform of pyruvate kinase is important for cancer metabolism and tumour growth." Nature 452(7184): 230-233.

Christofk, H. R., M. G. Vander Heiden, et al. (2008). "Pyruvate kinase M2 is a phosphotyrosine-binding protein." Nature 452(7184): 181-186.

Chung-Faye, G., B. Hayee, et al. (2007). "Fecal M2-pyruvate kinase (M2-PK): a novel marker of intestinal inflammation." Inflamm Bowel Dis 13(11): 1374-1378.

Chung, C. D., J. Liao, et al. (1997). "Specific inhibition of Stat3 signal transduction by PIAS3." Science 278(5344): 1803-1805.

Clark, E. L., A. Coulson, et al. (2008). "The RNA helicase p68 is a novel androgen receptor coactivator involved in splicing and is overexpressed in prostate cancer." Cancer Res 68(19): 7938-7946.
Coloff, J. L. and J. C. Rathmell (2006). "Metabolic regulation of Akt: roles reversed." J Cell Biol 175(6): 845-847.
Cuezva, J. M., A. D. Ortega, et al. (2009). "The tumor suppressor function of mitochondria: Translation into the clinics." Biochim Biophys Acta.
Cvijic, H., K. Bauer, et al. (2009). "Co-activator SRC-1 is dispensable for transcriptional control by STAT3." Biochem J 420(1): 123-132.
DaSilva, L., H. Rui, et al. (1996). "Prolactin recruits STAT1, STAT3 and STAT5 independent of conserved receptor tyrosines TYR402, TYR479, TYR515 and TYR580." Mol Cell Endocrinol 117(2): 131-140.
Deprez, J., D. Vertommen, et al. (1997). "Phosphorylation and activation of heart 6-phosphofructo-2-kinase by protein kinase B and other protein kinases of the insulin signaling cascades." J Biol Chem 272(28): 17269-17275.
Diao, Y., X. Wang, et al. (2009). "SOCS1, SOCS3, and PIAS1 promote myogenic differentiation by inhibiting the leukemia inhibitory factor-induced JAK1/STAT1/STAT3 pathway." Mol Cell Biol.
Dickens, M., J. S. Rogers, et al. (1997). "A cytoplasmic inhibitor of the JNK signal transduction pathway." Science 277(5326): 693-696.
Ding, Z., J. Ji, et al. (2009). "Analysis of mitochondrial DNA mutations in D-loop region in thyroid lesions." Biochim Biophys Acta.
Dombrauckas, J. D., B. D. Santarsiero, et al. (2005). "Structural basis for tumor pyruvate kinase M2 allosteric regulation and catalysis." Biochemistry 44(27): 9417-9429.
Dube, V., J. Grigull, et al. (2007). "Verification of endometrial tissue biomarkers previously discovered using mass spectrometry-based proteomics by means of immunohistochemistry in a tissue microarray format." J Proteome Res 6(7): 2648-2655.
Elliott, K., K. Ge, et al. (2000). "The c-Myc-interacting adaptor protein Bin1 activates a caspase-independent cell death program." Oncogene 19(41): 4669-4684.
English, J. M., C. A. Vanderbilt, et al. (1995). "Isolation of MEK5 and differential expression of alternatively spliced forms." J Biol Chem 270(48): 28897-28902.
Epling-Burnette, P. K., J. H. Liu, et al. (2001). "Inhibition of STAT3 signaling leads to apoptosis of leukemic large granular lymphocytes and decreased Mcl-1 expression." J Clin Invest 107(3): 351-362.
Erster, S., M. Mihara, et al. (2004). "In vivo mitochondrial p53 translocation triggers a rapid first wave of cell death in response to DNA damage that can precede p53 target gene activation." Mol Cell Biol 24(15): 6728-6741.
Etiemble, J. and P. Boivin (1976). "Pyruvate kinase isozymes among human organs and blood cells." Enzyme 21(4): 296-303.
Ewald, N., M. Schaller, et al. (2007). "Fecal pyruvate kinase-M2 (tumor M2-PK) measurement: a new screening concept for colorectal cancer." Anticancer Res 27(4A): 1949-1952.
Flowers, L. O., P. S. Subramaniam, et al. (2005). "A SOCS-1 peptide mimetic inhibits both constitutive and IL-6 induced activation of STAT3 in prostate cancer cells." Oncogene 24(12): 2114-2120.

Fukumura, D. and R. K. Jain (2007). "Tumor microenvironment abnormalities: causes, consequences, and strategies to normalize." J Cell Biochem 101(4): 937-949.
Fuller-Pace, F. V., A. M. Jacobs, et al. (2007). "Modulation of transcriptional activity of the DEAD-box family of RNA helicases, p68 (Ddx5) and DP103 (Ddx20), by SUMO modification." Biochem Soc Trans 35(Pt 6): 1427-1429.
Giaccone, G., E. F. Smit, et al. (2004). "Glufosfamide administered by 1-hour infusion as a second-line treatment for advanced non-small cell lung cancer; a phase II trial of the EORTC-New Drug Development Group." Eur J Cancer 40(5): 667-672.
Giraud, S., F. Bienvenu, et al. (2002). "Functional interaction of STAT3 transcription factor with the coactivator NcoA/SRC1a." J Biol Chem 277(10): 8004-8011.
Gogvadze, V., S. Orrenius, et al. (2008). "Mitochondria in cancer cells: what is so special about them?" Trends Cell Biol 18(4): 165-173.
Goonetilleke, K. S., J. M. Mason, et al. (2007). "Diagnostic and prognostic value of plasma tumor M2 pyruvate kinase in periampullary cancer: evidence for a novel biological marker of adverse prognosis." Pancreas 34(3): 318-324.
Gordan, J. D., J. A. Bertout, et al. (2007). "HIF-2alpha promotes hypoxic cell proliferation by enhancing c-myc transcriptional activity." Cancer Cell 11(4): 335-347.
Gordan, J. D., C. B. Thompson, et al. (2007). "HIF and c-Myc: sibling rivals for control of cancer cell metabolism and proliferation." Cancer Cell 12(2): 108-113.
Gottlob, K., N. Majewski, et al. (2001). "Inhibition of early apoptotic events by Akt/PKB is dependent on the first committed step of glycolysis and mitochondrial hexokinase." Genes Dev 15(11): 1406-1418.
Grandis, J. R., S. D. Drenning, et al. (2000). "Constitutive activation of Stat3 signaling abrogates apoptosis in squamous cell carcinogenesis in vivo." Proc Natl Acad Sci U S A 97(8): 4227-4232.
Graves, J. D., J. S. Campbell, et al. (1995). "Protein serine/threonine kinases of the MAPK cascade." Ann N Y Acad Sci 766: 320-343.
Gridelli, C., P. Maione, et al. (2008). "The potential role of mTOR inhibitors in non-small cell lung cancer." Oncologist 13(2): 139-147.
Hainaut, P. and M. Hollstein (2000). "p53 and human cancer: the first ten thousand mutations." Adv Cancer Res 77: 81-137.
Hardt, P. D., B. K. Ngoumou, et al. (2000). "Tumor M2-pyruvate kinase: a promising tumor marker in the diagnosis of gastro-intestinal cancer." Anticancer Res 20(6D): 4965-4968.
Hardwick, J. C., G. R. van den Brink, et al. (2001). "NF-kappaB, p38 MAPK and JNK are highly expressed and active in the stroma of human colonic adenomatous polyps." Oncogene 20(7): 819-827.
Haug, U., D. Rothenbacher, et al. (2007). "Tumour M2-PK as a stool marker for colorectal cancer: comparative analysis in a large sample of unselected older adults vs colorectal cancer patients." Br J Cancer 96(9): 1329-1334.
Hirling, H., M. Scheffner, et al. (1989). "RNA helicase activity associated with the human p68 protein." Nature 339(6225): 562-564.
Ho, H. H. and L. B. Ivashkiv (2006). "Role of STAT3 in type I interferon responses. Negative regulation of STAT1-dependent inflammatory gene activation." J Biol Chem 281(20): 14111-14118.

Hoshino, A., J. A. Hirst, et al. (2007). "Regulation of cell proliferation by interleukin-3-induced nuclear translocation of pyruvate kinase." J Biol Chem 282(24): 17706-17711.

Hu, Q., W. Shen, et al. (2007). "Insight into the binding properties of MEKK3 PB1 to MEK5 PB1 from its solution structure." Biochemistry 46(47): 13478-13489.

Hu, Z. and W. C. Plaxton (1996). "Purification and characterization of cytosolic pyruvate kinase from leaves of the castor oil plant." Arch Biochem Biophys 333(1): 298-307.

Huang, Y. and Z. R. Liu (2002). "The ATPase, RNA unwinding, and RNA binding activities of recombinant p68 RNA helicase." J Biol Chem 277(15): 12810-12815.

Iggo, R. D. and D. P. Lane (1989). "Nuclear protein p68 is an RNA-dependent ATPase." EMBO J 8(6): 1827-1831.

Ignacak, J. and M. B. Stachurska (2003). "The dual activity of pyruvate kinase type M2 from chromatin extracts of neoplastic cells." Comp Biochem Physiol B Biochem Mol Biol 134(3): 425-433.

Jacobs, A. M., S. M. Nicol, et al. (2007). "SUMO modification of the DEAD box protein p68 modulates its transcriptional activity and promotes its interaction with HDAC1." Oncogene 26(40): 5866-5876.

Jensen, S. and L. H. Johnston (2002). "Complexity of mitotic exit." Cell Cycle 1(5): 300-303.

Jiang, B. H. and L. Z. Liu (2008). "Role of mTOR in anticancer drug resistance: perspectives for improved drug treatment." Drug Resist Updat 11(3): 63-76.

Johnston, J. A., C. M. Bacon, et al. (1995). "Tyrosine phosphorylation and activation of STAT5, STAT3, and Janus kinases by interleukins 2 and 15." Proc Natl Acad Sci U S A 92(19): 8705-8709.

Jost, J. P., S. Schwarz, et al. (1999). "A chicken embryo protein related to the mammalian DEAD box protein p68 is tightly associated with the highly purified protein-RNA complex of 5-MeC-DNA glycosylase." Nucleic Acids Res 27(16): 3245-3252.

Joyce, J. A. (2005). "Therapeutic targeting of the tumor microenvironment." Cancer Cell 7(6): 513-520.

Kamakura, S., T. Moriguchi, et al. (1999). "Activation of the protein kinase ERK5/BMK1 by receptor tyrosine kinases. Identification and characterization of a signaling pathway to the nucleus." J Biol Chem 274(37): 26563-26571.

Kaptein, A., V. Paillard, et al. (1996). "Dominant negative stat3 mutant inhibits interleukin-6-induced Jak-STAT signal transduction." J Biol Chem 271(11): 5961-5964.

Kelloff, G. J., J. M. Hoffman, et al. (2005). "Progress and promise of FDG-PET imaging for cancer patient management and oncologic drug development." Clin Cancer Res 11(8): 2785-2808.

Kemp, B. E., D. Stapleton, et al. (2003). "AMP-activated protein kinase, super metabolic regulator." Biochem Soc Trans 31(Pt 1): 162-168.

Kitamura, T., Y. Kitamura, et al. (1999). "Insulin-induced phosphorylation and activation of cyclic nucleotide phosphodiesterase 3B by the serine-threonine kinase Akt." Mol Cell Biol 19(9): 6286-6296.

Kondoh, H., M. E. Lleonart, et al. (2007). "Protection from oxidative stress by enhanced glycolysis; a possible mechanism of cellular immortalization." Histol Histopathol 22(1): 85-90.
Kortylewski, M. and H. Yu (2008). "Role of Stat3 in suppressing anti-tumor immunity." Curr Opin Immunol 20(2): 228-233.
Lee, J., H. K. Kim, et al. (2008). "Pyruvate kinase isozyme type M2 (PKM2) interacts and cooperates with Oct-4 in regulating transcription." Int J Biochem Cell Biol 40(5): 1043-1054.
Li, F., Y. Wang, et al. (2005). "Myc stimulates nuclearly encoded mitochondrial genes and mitochondrial biogenesis." Mol Cell Biol 25(14): 6225-6234.
Li, J., C. Yen, et al. (1997). "PTEN, a putative protein tyrosine phosphatase gene mutated in human brain, breast, and prostate cancer." Science 275(5308): 1943-1947.
Li, L., M. Ljungman, et al. (2000). "The human Cdc14 phosphatases interact with and dephosphorylate the tumor suppressor protein p53." J Biol Chem 275(4): 2410-2414.
Lin, C., L. Yang, et al. (2005). "ATPase/helicase activities of p68 RNA helicase are required for pre-mRNA splicing but not for assembly of the spliceosome." Mol Cell Biol 25(17): 7484-7493.
Liu, Z. R. (2002). "p68 RNA helicase is an essential human splicing factor that acts at the U1 snRNA-5' splice site duplex." Mol Cell Biol 22(15): 5443-5450.
Lu, J., L. K. Sharma, et al. (2009). "Implications of mitochondrial DNA mutations and mitochondrial dysfunction in tumorigenesis." Cell Res 19(7): 802-815.
MacKenzie, A. R. and M. von Mehren (2007). "Mechanisms of mammalian target of rapamycin inhibition in sarcoma: present and future." Expert Rev Anticancer Ther 7(8): 1145-1154.
Mahon, P. C., K. Hirota, et al. (2001). "FIH-1: a novel protein that interacts with HIF-1alpha and VHL to mediate repression of HIF-1 transcriptional activity." Genes Dev 15(20): 2675-2686.
Mailand, N., C. Lukas, et al. (2002). "Deregulated human Cdc14A phosphatase disrupts centrosome separation and chromosome segregation." Nat Cell Biol 4(4): 317-322.
Marie, J., A. Kahn, et al. (1976). "Pyruvate kinase isozymes in man. I. M type isozymes in adult and foetal tissues, electrofocusing and immunological studies." Hum Genet 31(1): 35-45.
Marsin, A. S., L. Bertrand, et al. (2000). "Phosphorylation and activation of heart PFK-2 by AMPK has a role in the stimulation of glycolysis during ischaemia." Curr Biol 10(20): 1247-1255.
Matoba, S., J. G. Kang, et al. (2006). "p53 regulates mitochondrial respiration." Science 312(5780): 1650-1653.
Mazurek, S., H. Grimm, et al. (2002). "Pyruvate kinase type M2: a crossroad in the tumor metabolome." Br J Nutr 87 Suppl 1: S23-29.
Mazurek, S., F. Hugo, et al. (1996). "Studies on associations of glycolytic and glutaminolytic enzymes in MCF-7 cells: role of P36." J Cell Physiol 167(2): 238-250.
McCollum, D. and K. L. Gould (2001). "Timing is everything: regulation of mitotic exit and cytokinesis by the MEN and SIN." Trends Cell Biol 11(2): 89-95.

Mehta, P. B., B. L. Jenkins, et al. (2003). "MEK5 overexpression is associated with metastatic prostate cancer, and stimulates proliferation, MMP-9 expression and invasion." Oncogene 22(9): 1381-1389.
Merida, I. and A. Avila-Flores (2006). "Tumor metabolism: new opportunities for cancer therapy." Clin Transl Oncol 8(10): 711-716.
Miller, A. J., C. Levy, et al. (2005). "Sumoylation of MITF and its related family members TFE3 and TFEB." J Biol Chem 280(1): 146-155.
Miwa, S., K. Nakashima, et al. (1975). "Four new pyruvate kinase (PK) variants and a classical PK deficiency." Br J Haematol 29(1): 157-169.
Mohanti, B. K., G. K. Rath, et al. (1996). "Improving cancer radiotherapy with 2-deoxy-D-glucose: phase I/II clinical trials on human cerebral gliomas." Int J Radiat Oncol Biol Phys 35(1): 103-111.
Mohla, S. (2007). "Tumor microenvironment." J Cell Biochem 101(4): 801-804.
Nagy, Z. S., Y. Wang, et al. (2002). "Interleukin-2 family cytokines stimulate phosphorylation of the Pro-Ser-Pro motif of Stat5 transcription factors in human T cells: resistance to suppression of multiple serine kinase pathways." J Leukoc Biol 72(4): 819-828.
Nakagawa, K. and H. Yokosawa (2002). "PIAS3 induces SUMO-1 modification and transcriptional repression of IRF-1." FEBS Lett 530(1-3): 204-208.
Nelson, D. A. and E. White (2004). "Exploiting different ways to die." Genes Dev 18(11): 1223-1226.
Nielsen, M., C. G. Kaestel, et al. (1999). "Inhibition of constitutively activated Stat3 correlates with altered Bcl-2/Bax expression and induction of apoptosis in mycosis fungoides tumor cells." Leukemia 13(5): 735-738.
Nishida, T. and H. Yasuda (2002). "PIAS1 and PIASxalpha function as SUMO-E3 ligases toward androgen receptor and repress androgen receptor-dependent transcription." J Biol Chem 277(44): 41311-41317.
Niu, G., T. Bowman, et al. (2002). "Roles of activated Src and Stat3 signaling in melanoma tumor cell growth." Oncogene 21(46): 7001-7010.
Niu, G., R. Heller, et al. (1999). "Gene therapy with dominant-negative Stat3 suppresses growth of the murine melanoma B16 tumor in vivo." Cancer Res 59(20): 5059-5063.
Niu, G., K. L. Wright, et al. (2002). "Constitutive Stat3 activity up-regulates VEGF expression and tumor angiogenesis." Oncogene 21(13): 2000-2008.
Noguchi, T., H. Inoue, et al. (1986). "The M1- and M2-type isozymes of rat pyruvate kinase are produced from the same gene by alternative RNA splicing." J Biol Chem 261(29): 13807-13812.
Obata, T., G. E. Brown, et al. (2000). "MAP kinase pathways activated by stress: the p38 MAPK pathway." Crit Care Med 28(4 Suppl): N67-77.
Ohtani, T., K. Ishihara, et al. (2000). "Dissection of signaling cascades through gp130 in vivo: reciprocal roles for STAT3- and SHP2-mediated signals in immune responses." Immunity 12(1): 95-105.
Papatsoris, A. G. and A. G. Papavassiliou (2001). "Molecular 'palpation' of BPH: a tale of MAPK signalling?" Trends Mol Med 7(7): 288-292.

Paulsen, M. T., A. M. Starks, et al. (2006). "The p53-targeting human phosphatase hCdc14A interacts with the Cdk1/cyclin B complex and is differentially expressed in human cancers." Mol Cancer 5: 25.
Pelicano, H., D. Carney, et al. (2004). "ROS stress in cancer cells and therapeutic implications." Drug Resist Updat 7(2): 97-110.
Pelicano, H., D. S. Martin, et al. (2006). "Glycolysis inhibition for anticancer treatment." Oncogene 25(34): 4633-4646.
Pelicano, H., R. H. Xu, et al. (2006). "Mitochondrial respiration defects in cancer cells cause activation of Akt survival pathway through a redox-mediated mechanism." J Cell Biol 175(6): 913-923.
Perez, J. X., T. Roig, et al. (2000). "Overexpression of fructose 2,6-bisphosphatase decreases glycolysis and delays cell cycle progression." Am J Physiol Cell Physiol 279(5): C1359-1365.
Petry, P., K. R. Johnson, et al. (1995). "Assignment to chromosome 11 of mouse p68 RNA helicase gene (Hlr1) and pseudogene (Hlr1-ps1)." FEBS Lett 363(1-2): 25-28.
Pircher, T. J., H. Petersen, et al. (1999). "Extracellular signal-regulated kinase (ERK) interacts with signal transducer and activator of transcription (STAT) 5a." Mol Endocrinol 13(4): 555-565.
Plas, D. R., S. Talapatra, et al. (2001). "Akt and Bcl-xL promote growth factor-independent survival through distinct effects on mitochondrial physiology." J Biol Chem 276(15): 12041-12048.
Qing, Y. and G. R. Stark (2004). "Alternative activation of STAT1 and STAT3 in response to interferon-gamma." J Biol Chem 279(40): 41679-41685.
Rathmell, J. C., C. J. Fox, et al. (2003). "Akt-directed glucose metabolism can prevent Bax conformation change and promote growth factor-independent survival." Mol Cell Biol 23(20): 7315-7328.
Ripperger, J. A., S. Fritz, et al. (1995). "Transcription factors Stat3 and Stat5b are present in rat liver nuclei late in an acute phase response and bind interleukin-6 response elements." J Biol Chem 270(50): 29998-30006.
Robey, R. B. and N. Hay (2009). "Is Akt the "Warburg kinase"?-Akt-energy metabolism interactions and oncogenesis." Semin Cancer Biol 19(1): 25-31.
Rossow, K. L. and R. Janknecht (2003). "Synergism between p68 RNA helicase and the transcriptional coactivators CBP and p300." Oncogene 22(1): 151-156.
Russell, R. R., 3rd, R. Bergeron, et al. (1999). "Translocation of myocardial GLUT-4 and increased glucose uptake through activation of AMPK by AICAR." Am J Physiol 277(2 Pt 2): H643-649.
Saheki, S., K. Saheki, et al. (1982). "Peptide structures of pyruvate kinase isozymes: 2. Origins of types M1 and M2 isozymes suggested from species-variations in their peptide maps." Biochim Biophys Acta 704(3): 494-502.
Saldeen, J., J. C. Lee, et al. (2001). "Role of p38 mitogen-activated protein kinase (p38 MAPK) in cytokine-induced rat islet cell apoptosis." Biochem Pharmacol 61(12): 1561-1569.
Salzman, D. W., J. Shubert-Coleman, et al. (2007). "P68 RNA helicase unwinds the human let-7 microRNA precursor duplex and is required for let-7-directed silencing of gene expression." J Biol Chem 282(45): 32773-32779.

Sato, N., R. Tsuruma, et al. (2005). "Nuclear retention of STAT3 through the coiled-coil domain regulates its activity." Biochem Biophys Res Commun 336(2): 617-624.
Schindler, C., K. Shuai, et al. (1992). "Interferon-dependent tyrosine phosphorylation of a latent cytoplasmic transcription factor." Science 257(5071): 809-813.
Schwartzenberg-Bar-Yoseph, F., M. Armoni, et al. (2004). "The tumor suppressor p53 down-regulates glucose transporters GLUT1 and GLUT4 gene expression." Cancer Res 64(7): 2627-2633.
Seger, R. and E. G. Krebs (1995). "The MAPK signaling cascade." FASEB J 9(9): 726-735.
Semenza, G. L. (2007). "HIF-1 mediates the Warburg effect in clear cell renal carcinoma." J Bioenerg Biomembr 39(3): 231-234.
Seyfried, J., X. Wang, et al. (2005). "A novel mitogen-activated protein kinase docking site in the N terminus of MEK5alpha organizes the components of the extracellular signal-regulated kinase 5 signaling pathway." Mol Cell Biol 25(22): 9820-9828.
Shimada, N., T. Shinagawa, et al. (2008). "Modulation of M2-type pyruvate kinase activity by the cytoplasmic PML tumor suppressor protein." Genes Cells 13(3): 245-254.
Shin, S., K. L. Rossow, et al. (2007). "Involvement of RNA helicases p68 and p72 in colon cancer." Cancer Res 67(16): 7572-7578.
Shuai, K. and B. Liu (2005). "Regulation of gene-activation pathways by PIAS proteins in the immune system." Nat Rev Immunol 5(8): 593-605.
Smolewski, P. (2006). "Recent developments in targeting the mammalian target of rapamycin (mTOR) kinase pathway." Anticancer Drugs 17(5): 487-494.
Sohn, S. J., B. K. Sarvis, et al. (2002). "ERK5 MAPK regulates embryonic angiogenesis and acts as a hypoxia-sensitive repressor of vascular endothelial growth factor expression." J Biol Chem 277(45): 43344-43351.
Song, H., S. P. Ethier, et al. (2004). "Stat3 modulates heat shock 27kDa protein expression in breast epithelial cells." Biochem Biophys Res Commun 314(1): 143-150.
Song, H., X. Jin, et al. (2004). "Stat3 upregulates MEK5 expression in human breast cancer cells." Oncogene 23(50): 8301-8309.
Spoden, G. A., D. Morandell, et al. (2009). "The SUMO-E3 ligase PIAS3 targets pyruvate kinase M2." J Cell Biochem 107(2): 293-302.
Stetak, A., R. Veress, et al. (2007). "Nuclear translocation of the tumor marker pyruvate kinase M2 induces programmed cell death." Cancer Res 67(4): 1602-1608.
Stevenson, R. J., S. J. Hamilton, et al. (1998). "Expression of the 'dead box' RNA helicase p68 is developmentally and growth regulated and correlates with organ differentiation/maturation in the fetus." J Pathol 184(4): 351-359.
Stommel, J. M., N. D. Marchenko, et al. (1999). "A leucine-rich nuclear export signal in the p53 tetramerization domain: regulation of subcellular localization and p53 activity by NES masking." EMBO J 18(6): 1660-1672.
Sun, H. L., Y. N. Liu, et al. (2007). "YC-1 inhibits HIF-1 expression in prostate cancer cells: contribution of Akt/NF-kappaB signaling to HIF-1alpha accumulation during hypoxia." Oncogene 26(27): 3941-3951.

Takeda, K., B. E. Clausen, et al. (1999). "Enhanced Th1 activity and development of chronic enterocolitis in mice devoid of Stat3 in macrophages and neutrophils." Immunity 10(1): 39-49.
Thompson, J. E. and C. B. Thompson (2004). "Putting the rap on Akt." J Clin Oncol 22(20): 4217-4226.
Tokumaru, S., K. Sayama, et al. (2005). "SOCS3/CIS3 negative regulation of STAT3 in HGF-induced keratinocyte migration." Biochem Biophys Res Commun 327(1): 100-105.
Toyn, J. H., A. L. Johnson, et al. (1997). "The Swi5 transcription factor of Saccharomyces cerevisiae has a role in exit from mitosis through induction of the cdk-inhibitor Sic1 in telophase." Genetics 145(1): 85-96.
Turkson, J., D. Ryan, et al. (2001). "Phosphotyrosyl peptides block Stat3-mediated DNA binding activity, gene regulation, and cell transformation." J Biol Chem 276(48): 45443-45455.
Turkson, J., S. Zhang, et al. (2005). "A novel platinum compound inhibits constitutive Stat3 signaling and induces cell cycle arrest and apoptosis of malignant cells." J Biol Chem 280(38): 32979-32988.
van Berkel, T. J., H. R. de Jonge, et al. (1974). "Kinetic evidence for the presence of two forms of M2-type pyruvate kinase in rat small intestine." Biochem Biophys Res Commun 60(1): 398-405.
Verma, R., R. M. Feldman, et al. (1997). "SIC1 is ubiquitinated in vitro by a pathway that requires CDC4, CDC34, and cyclin/CDK activities." Mol Biol Cell 8(8): 1427-1437.
Vivanco, I. and C. L. Sawyers (2002). "The phosphatidylinositol 3-Kinase AKT pathway in human cancer." Nat Rev Cancer 2(7): 489-501.
Wan, X. and L. J. Helman (2007). "The biology behind mTOR inhibition in sarcoma." Oncologist 12(8): 1007-1018.
Wang, J., C. Ouyang, et al. (2008). "STAT3 inhibits apoptosis of human renal tubular epithelial cells induced by ATP depletion/recovery." Nephron Exp Nephrol 108(1): e11-18.
Wang, T., G. Niu, et al. (2004). "Regulation of the innate and adaptive immune responses by Stat-3 signaling in tumor cells." Nat Med 10(1): 48-54.
Wang, X., A. J. Merritt, et al. (2005). "Targeted deletion of mek5 causes early embryonic death and defects in the extracellular signal-regulated kinase 5/myocyte enhancer factor 2 cell survival pathway." Mol Cell Biol 25(1): 336-345.
Warburg, O. (1956). "On respiratory impairment in cancer cells." Science 124(3215): 269-270.
Warburg, O. (1956). "On the origin of cancer cells." Science 123(3191): 309-314.
Warner, D. R., V. Bhattacherjee, et al. (2004). "Functional interaction between Smad, CREB binding protein, and p68 RNA helicase." Biochem Biophys Res Commun 324(1): 70-76.
Watanabe, M., J. Yanagisawa, et al. (2001). "A subfamily of RNA-binding DEAD-box proteins acts as an estrogen receptor alpha coactivator through the N-terminal activation domain (AF-1) with an RNA coactivator, SRA." EMBO J 20(6): 1341-1352.

Weber, G., H. J. Convery, et al. (1966). "Feedback inhibition of key glycolytic enzymes in liver: action of free fatty acids." Science 154(754): 1357-1360.
Weber, W. A., M. Schwaiger, et al. (2000). "Quantitative assessment of tumor metabolism using FDG-PET imaging." Nucl Med Biol 27(7): 683-687.
Wegrzyn, J., R. Potla, et al. (2009). "Function of mitochondrial Stat3 in cellular respiration." Science 323(5915): 793-797.
Wei, L. H., M. L. Kuo, et al. (2003). "Interleukin-6 promotes cervical tumor growth by VEGF-dependent angiogenesis via a STAT3 pathway." Oncogene 22(10): 1517-1527.
Wen, Z., Z. Zhong, et al. (1995). "Maximal activation of transcription by Stat1 and Stat3 requires both tyrosine and serine phosphorylation." Cell 82(2): 241-250.
Wierenga, A. T., I. Vogelzang, et al. (2003). "Erythropoietin-induced serine 727 phosphorylation of STAT3 in erythroid cells is mediated by a MEK-, ERK-, and MSK1-dependent pathway." Exp Hematol 31(5): 398-405.
Wiesener, M. S. and P. H. Maxwell (2003). "HIF and oxygen sensing; as important to life as the air we breathe?" Ann Med 35(3): 183-190.
Wilson, B. J. and V. Giguere (2007). "Identification of novel pathway partners of p68 and p72 RNA helicases through Oncomine meta-analysis." BMC Genomics 8: 419.
Wu, J., H. P. Cho, et al. (2008). "Cdc14B depletion leads to centriole amplification, and its overexpression prevents unscheduled centriole duplication." J Cell Biol 181(3): 475-483.
Wu, X., Y. Zhou, et al. (2008). "Isoform-specific interaction of pyruvate kinase with hepatitis C virus NS5B." FEBS Lett 582(15): 2155-2160.
Xie, T. X., F. J. Huang, et al. (2006). "Activation of stat3 in human melanoma promotes brain metastasis." Cancer Res 66(6): 3188-3196.
Xin, H., C. Zhang, et al. (2009). "Sunitinib inhibition of Stat3 induces renal cell carcinoma tumor cell apoptosis and reduces immunosuppressive cells." Cancer Res 69(6): 2506-2513.
Yagil, Z., G. Kay, et al. (2009). "A specific epitope of protein inhibitor of activated STAT3 is responsible for the induction of apoptosis in rat transformed mast cells." J Immunol 182(4): 2168-2175.
Yamashita, H., M. T. Nevalainen, et al. (2001). "Role of serine phosphorylation of Stat5a in prolactin-stimulated beta-casein gene expression." Mol Cell Endocrinol 183(1-2): 151-163.
Yamashita, H., J. Xu, et al. (1998). "Differential control of the phosphorylation state of proline-juxtaposed serine residues Ser725 of Stat5a and Ser730 of Stat5b in prolactin-sensitive cells." J Biol Chem 273(46): 30218-30224.
Yang, C. C., O. I. Ornatsky, et al. (1998). "Interaction of myocyte enhancer factor 2 (MEF2) with a mitogen-activated protein kinase, ERK5/BMK1." Nucleic Acids Res 26(20): 4771-4777.
Yang, C. H., W. Shi, et al. (1996). "Direct association of STAT3 with the IFNAR-1 chain of the human type I interferon receptor." J Biol Chem 271(14): 8057-8061.
Yang, L., C. Lin, et al. (2005). "Phosphorylations of DEAD box p68 RNA helicase are associated with cancer development and cell proliferation." Mol Cancer Res 3(6): 355-363.

Yang, L., C. Lin, et al. (2006). "P68 RNA helicase mediates PDGF-induced epithelial mesenchymal transition by displacing Axin from beta-catenin." Cell 127(1): 139-155.
Yang, L., C. Lin, et al. (2007). "A double tyrosine phosphorylation of P68 RNA helicase confers resistance to TRAIL-induced apoptosis." Oncogene 26(41): 6082-6092.
Yang, L., C. Lin, et al. (2007). "Phosphorylation of p68 RNA helicase plays a role in platelet-derived growth factor-induced cell proliferation by up-regulating cyclin D1 and c-Myc expression." J Biol Chem 282(23): 16811-16819.
Yang, L. and Z. R. Liu (2004). "Bacterially expressed recombinant p68 RNA helicase is phosphorylated on serine, threonine, and tyrosine residues." Protein Expr Purif 35(2): 327-333.
Yeo, E. J., Y. S. Chun, et al. (2004). "New anticancer strategies targeting HIF-1." Biochem Pharmacol 68(6): 1061-1069.
Yu, C. L., D. J. Meyer, et al. (1995). "Enhanced DNA-binding activity of a Stat3-related protein in cells transformed by the Src oncoprotein." Science 269(5220): 81-83.
Yu, H. and R. Jove (2004). "The STATs of cancer--new molecular targets come of age." Nat Rev Cancer 4(2): 97-105.
Yu, H., M. Kortylewski, et al. (2007). "Crosstalk between cancer and immune cells: role of STAT3 in the tumour microenvironment." Nat Rev Immunol 7(1): 41-51.
Zhang, W., R. J. Chan, et al. (2009). "Negative regulation of Stat3 by activating PTPN11 mutants contributes to the pathogenesis of Noonan syndrome and JMML." J Biol Chem.
Zhang, X., J. Zhang, et al. (2007). "STAT3-decoy oligodeoxynucleotide inhibits the growth of human lung cancer via down-regulating its target genes." Oncol Rep 17(6): 1377-1382.
Zhou, J., J. Wulfkuhle, et al. (2007). "Activation of the PTEN/mTOR/STAT3 pathway in breast cancer stem-like cells is required for viability and maintenance." Proc Natl Acad Sci U S A 104(41): 16158-16163.
Zong, W. X. and C. B. Thompson (2006). "Necrotic death as a cell fate." Genes Dev 20(1): 1-15.
Zwerschke, W., S. Mazurek, et al. (1999). "Modulation of type M2 pyruvate kinase activity by the human papillomavirus type 16 E7 oncoprotein." Proc Natl Acad Sci U S A 96(4): 1291-1296.

CHAPTER 2

PYRUVATE KINASE M2 PROMOTES CELL PROLIFERATION BY REGULATING GENE TRANSCRIPTION

2.1 Abstract

Alterations in metabolism may play a critical role in the transformation to malignancy during tumor progression. However, the ways by which the metabolism alterations affect tumor progression are not well understood. Here, we show that PKM2, a glycolysis enzyme, localizes to the cell nucleus. The nuclear PKM2 levels correlate with cell proliferation rates. Expression of PKM2 promotes cell proliferation. Nuclear PKM2 promotes cell proliferation by upregulating transcription of MEK5, a MAP kinase associated with cell proliferation. PKM2 regulates the MEK5 transcription by promoting stat3 phosphorylation at Y705 and facilitating stat3 binding to MEK5 promoter. Our studies reveal an important molecular link that connects metabolic alterations with gene expressions during tumor progression.

2.2 Introduction

Most cancer cells utilize aerobic pathways for glucose metabolism. Upon tumor progression, the oxidative phosphorylation in mitochondria is usually dramatically reduced even in the presence of oxygen (Warburg effects) (Warburg, 1956). Although it is still debatable whether the metabolic alteration is just a symptom of cell transformation or a causative factor in tumorigenesis, the evidence suggests that metabolic adjustments by tumor cells are necessary processes for tumorigenesis and tumor progression

(Deberardinis et al., 2008; Garber, 2006). It is generally believed that oncogenic products regulate the metabolic pathways (Matoba et al., 2006). Expression of oncogenes can result in substantial changes in composition of metabolism isoenzymes that regulate the flows of metabolites (Dang & Lewis, 1997; Elstrom et al., 2004; Semenza, 2007). However, it is not well understood whether, and how, metabolic changes during tumor progression will produce a feedback effect on cell proliferation. An important molecular signature of tumor development and progression is a shift in expression of pyruvate kinase isoenzymes. The tissue specific isoform (L, R, or M1) disappears and is replaced by pyruvate kinase isoenzyme type M2 (PKM2) in cancer cells (Elbers et al., 1991; Hacker et al., 1998). The glycolysis catalytically active PKM2 exists as a tetramer and associates with a glycolytic enzyme complex in normal cells (Altenberg & Greulich, 2004; Dombrauckas et al., 2005; Zwerschke et al., 1999). In tumor cells, it is believed that PKM2 dominantly forms a dimer, and appears to be catalytically inactive for conversion of PEP to pyruvate (Ashizawa et al., 1991; Mazurek et al., 2005). The inactive PKM2 actually provides an advantage for metabolism as it helps to channel the carbon source from glycolytic intermediates to biosynthesis, especially syntheses of nucleic acids, lipids, and proteins, to meet the demands for tumor cell proliferation. Recent studies have suggested that PKM2 changes its catalytic activity, consequently facilitating cell proliferation by binding to tyrosine phosphor-proteins (Christofk et al., 2008a; Christofk et al., 2008b). The observations suggest that growth signals regulate the flow of carbon sources from glucose.

2.3 Results

2.3.1 Nuclear PKM2 Levels Correlate with Tumor Progression and Expression of PKM2 Promotes Cell Proliferation

PKM2 is an enzyme that catalyzes the last step of glycolysis converting PEP to pyruvate. Several independent studies have revealed that the protein may localize to the cell nucleus (Hoshino et al., 2007; Schneider et al., 2002; Stetak et al., 2007). We further verified the nuclear localization of PKM2 in different cancer cells by immunostaining using antibody raised against a peptide spanning aa 399 – 412 of PKM2 (PabPKM2) (Fig. S1A). To understand the functional significance of nuclear localization of PKM2, we examined nuclear PKM2 levels in ten different cancer cell lines by immunoblot of nuclear extracts and whole cell lysates using the antibody PabPKM2. These ten different cell lines represented different cancer progression stages and are derived from cancers of different organs/tissue types. SW480 and SW620 are colon cancer cell lines derived from the same cancer patient. LN686 is a head-neck squamous cell carcinoma cell line while the M4C1 is derived from LN686 by selecting high metastatic and high proliferation sub-lines in nude mice (Zhang et al., 2002). WM115 and WM266 are melanoma cell lines from the same patient. T98G and U87MG are cell lines of glioblastoma. H146 and H460 are cell lines derived from lung cancer patients. Cell proliferation analyses demonstrated that M4C1, SW620, WM266, and H460 are more proliferated than their corresponding lines in the matched pairs (Fig. 2.1A). Immunoblot analyses indicated much higher nuclear levels of PKM2 in the more proliferated cancer cells than those in the corresponding less proliferated cells (Fig. 2.1B), The higher nuclear PKM2 levels were

not attributed to differences in PKM2 expression levels in different cells, as shown in figure 1B whereas no significant differences were observed in total PKM2 in cell lysates in all test cells. The detection of PKM2 in the nuclear extracts was not due to contamination of cytoplasmic proteins as demonstrated by lack of GAPDH in the immunoblot analyses of the nuclear extracts.

We next investigated the effects of expression of PKM2 on cell proliferation with these ten different cell lines. HA-PKM2 was exogenously expressed in the cells using a commercially available Adeno-viral expression system. Quantization of PKM2 before and after exogenous expression revealed an approximately ~30% increase in cellular levels of PKM2 (Fig. 2.7 B). No significant differences in expression of HA-PKM2 were observed among the different cells (Fig. 2.1C). The expressed HA-PKM2 was distributed similarly to the endogenous PKM2 between the nucleus and the cytoplasm, as shown by immunoblot analyses using anti-HA antibody (Fig. 2.7C). It was evident that all cells that exogenously expressed HA-PKM2 experienced some degree of cell proliferation, with more proliferated cancer cells experiencing a higher proliferation rate increase than those of corresponding less proliferated cancer cells (Fig. 2.1D). The results suggested that expression of PKM2 promoted cell proliferation. To further test the role of PKM2 in promoting cell proliferation, we used a smartpool RNAi to knock down PKM2 in SW620 and SW480 cells (Fig. 2.1E). The cell growth rate of the more proliferated SW620 was dramatically reduced by PKM2 knockdown, while the growth rate of the less proliferated SW480 cells was moderately reduced by PKM2 knockdown (Fig. 2.1E). Similar results were also observed with the pair of melanoma cell lines (WM115/WM266, Fig 2.1E). Thus, both PKM2 expression and knockdown experiments indicated that PKM2 plays a

role in promoting cell proliferation with stronger effects on the more proliferated cancer cells. The effects of expression of PKM2 in different cancer cells on cell proliferation correlated very well with nuclear levels of PKM2 in different cancer cells.

2.3.2 PKM2 Activates Transcription of MEK5

The observations that the nuclear PKM2 levels completely correlated with the cell proliferation and that the expression of HA-PKM2 promoted cell proliferation led us to believe that nuclear PKM2 plays an important role in promoting cell proliferation by action other than that in the glycolysis. One possibility is that nuclear PKM2 is involved in regulation of gene expressions. To explore this possibility, we carried out gene expression array analyses with SW620 cells that exogenously expressed HA-PKM2. Expressions of 350 genes were upregulated, and expressions of 359 genes were downregulated, by at least two fold under the expression of HA-PKM2 (Table S1). Among those affected genes, expression of MEK5 (also named MAP2K5), a MAP kinase closely associated with cell proliferation, was affected by over seven fold. The expression array analyses indicated that nuclear PKM2 may function as a regulator for gene transcription. Expression and activation of MEK5 plays a very important role in cell proliferation (Diaz-Meco & Moscat, 2001). Expression and activation of MEK5 have also been shown to closely associate with cancer progression, including prostate cancer and breast cancer (McCracken et al., 2008; Mehta et al., 2003; Song et al., 2004). Thus, we reasoned that upregulation of MEK5 may mediate, at least partially, the effects of nuclear PKM2 on promoting cell proliferation. To test this conjecture, we first verified the effects of expression of PKM2 on the expression of MEK5 by RT-PCR. Consistent

with the gene expression array analyses, RTPCR demonstrated a marginal increase in MEK5 expression in SW480 cells following the expression of PKM2. However, the changes in the MEK5 expression in SW620 cells were much more dramatic (Fig. 2.2A). Similar patterns were also observed with another pair of cell lines, WM115 and WM266. The effects on the expressions of MEK5 by the expression of PKM2 were further confirmed by immunoblot analyses of cellular MEK5. It was clear that the cellular MEK5 levels increased subsequent to expression of PKM2. The more aggressive cancer cells experienced more dramatic increases in MEK5 levels upon expression of PKM2 (Fig. 2.2B). Interestingly, immunoblot of MEK5 using antibody against the phosphorylated MEK5 revealed a strong increase in the cellular levels of phosphorylated MEK5 (activated MEK5) in aggressive cancer cells compared to the less aggressive cancer cells upon exogenous expression of PKM2 (Fig. 2.2B). To further verify the role of PKM2 in transcriptional regulation of MEK5 gene, PKM2 was knocked down in SW620 and SW480 cells. Immunoblot analyses showed an approximately 80% PKM2 knockdown efficiency (Fig. 2.2C). It was evident that MEK5 expression was slightly reduced in SW480. However, the reduction in cellular levels of MEK5 in SW620 cells was dramatic upon knockdown of PKM2 (Fig. 2.2C). Again, the phosphorylated MEK5 experienced a sharp reduction in SW620 upon PKM2 knockdown, which was not observed in SW480 cells (Fig. 2.2C). We also analyzed the MEK5 mRNA levels in SW620 and WM266 cells upon PKM2 knockdown. Quantitative RT-PCR analyses demonstrated a strong reduction in cellular MEK5 mRNA in both PKM2 knockdown SW620 and WM266 cells (Fig. 2.2D). Thus, it is clear that PKM2 regulates the expression of MEK5. Expression of PKM2 appeared to also regulate MEK5 activation in

the more aggressive cancer cells. We further probed whether PKM2 regulates the transcription of the MEK5 gene directly, or if the regulatory effects were mediated through other cellular factor(s). To this end, we examined whether PKM2 interacted with the MEK5 promoter by chromatin immunoprecipitation (ChIP). We carried out the ChIP experiments with SW620 cells using the PCR primer pair that spanned the region of nt – 1,621 – -1,366 of MEK5 promoter. Our ChIP assays clearly demonstrated that PKM2 indeed interacted with the MEK5 promoter (Fig. 2.2E), indicating that PKM2 most likely regulates the transcription of the MEK5 gene directly. The preceding experiments suggested that PKM2 plays an active role in regulating the transcription of the MEK5 gene. We next sought to test whether up-regulation of MEK5 by PKM2 contributed to cell proliferation. We first knocked down MEK5 by RNAi in SW620 and WM266 cells. As a result, the cell proliferation rate was dramatically reduced (Fig. 2.3A). The proliferation rate increases stimulated by expression of HA-PKM2 in MEK5 knockdown SW620 and WM266 cells were also largely reduced (Fig. 2.3A), suggesting that up-regulation of MEK5, at least partially, mediated the effects of HA-PKM2 overexpression on cell proliferation. Moreover, we analyzed the MEK5 expression levels and phosphorylation status in these ten different cancer cell lines. MEK5 was expressed in all ten cell lines, but there were substantially higher levels of MEK5 in the more proliferated cancer cells than in the less proliferated cancer cells. Strikingly, the levels of phosphorylated MEK5 were also consistently higher in more proliferated cancer cells than in less proliferated cancer cells (Fig. 2.3B). Clearly, there is a close correlation between cellular MEK5 expression levels, the MEK5 phosphorylation levels and nuclear PKM2 levels, and all were correlated closely with the cell proliferation status of the cells

(comparing Fig. 2.3B with Fig. 2.1B). We concluded from these studies that up-regulation and activation of MEK5 by nuclear PKM2 contributed to cell proliferation.

2.3.3 PKM2 Upregulates MEK5 Transcription by Activation of Stat3

In searching for the proteins (possibly transcription factor) that may interact with nuclear PKM2, we noted that stat3 regulates transcription of MEK5 gene and the protein interacts with MEK5 promoter at -1776 nt – -1520 nt region by the ChIP assay (Song et al., 2004). Interestingly, PKM2 also interacts with MEK5 promoter at the same region by ChIP assay (Fig. 2.2E). Thus, we wondered whether PKM2 would interact with stat3 in the cell nucleus. To probe the interaction between PKM2 and stat3, we carried out co-immunoprecipitation with nuclear extracts made from SW620 and SW480 cells. Clearly, stat3 co-precipitated with PKM2. As a control, stat3 was not precipitated using rabbit IgG as IP antibody (Fig. 2.3C). Consistent with our previous observations, there were substantially less PKM2 and stat3 co-immunoprecipitation in the nuclear extracts prepared from SW480 than in the extracts made from SW620 cells. The coimmunoprecipitation was also carried out using reversed IP and IB antibodies, and with exogenously expressed HA-PKM2 (Fig. 2.8 A&B). These co-immunoprecipitation experiments indicated that PKM2 indeed interacted with stat3 in the nuclear extracts. We next tested whether the activation of stat3 was required for the effects of PKM2 on upregulation of MEK5 transcription. To this end, we first knocked down stat3 using RNAi in SW620/SW480 and WM266/WM115 cells and subsequently HA-PKM2 was expressed in the stat3 knockdown cells. It was clear that expression of HA-PKM2 could no longer upregulate MEK5 gene transcription as measured by cellular levels of both

mRNA and protein of MEK5 (Fig. 2.4 A&B, C&D). To further test the role of stat3 in mediating the effects of PKM2 on upregulation of MEK5 transcription, we used a dominate-negative mutant stat3 (Y705F) (Xie et al., 2006). The wild-type or dominate negative mutant was co-expressed with HA-PKM2 in SW620/SW480 and WM266/WM115 cells. Expression of MEK5 in both mRNA and protein levels was examined. It was evident that expression of dominate-negative stat3 mutant largely diminished the effects of PKM2 on upregulating MEK5 transcription (Fig. 2.8 C&D, E&F). It is well documented that the activity of the active stat3 can be inhibited by specific inhibitor (Xu et al., 2008). We therefore tested the effects of a stat3 inhibitor on the upregulation of MEK5 by expression of HA-PKM2 in SW620 and WM266 cells. Treatment of the HA-PKM2 expressing cells with the inhibitor resulted in a decrease in MEK5 transcription (Fig. 2.8 G&H). Thus, we concluded that activation of stat3 mediated the regulatory effects of PKM2 on MEK5 transcription.

We further investigated whether expression of PKM2 affected the stat3 binding to its target DNA at the MEK5 promoter. We first carried out ChIP analyses with SW620 cells using the PCR primer pair span the region -1621 nt - -1366 nt. Our ChIP assays showed that interaction of stat3 with the MEK5 promoter can be detected by this PCR primer pair (Fig. 2.9A). To probe whether knockdown or expression of PKM2 affected the interaction of stat3 with the MEK5 promoter, we performed ChIP experiments in SW620 cells in which the endogenous PKM2 was knocked down or HA-PKM2 was expressed. Clearly, the stat3 and MEK5 promoter interaction was strengthened by HA-PKM2 expression and was weakened by PKM2 knockdown (Fig. 2.5A). To further analyze the effects of PKM2 on the interaction between stat3 and its target DNA, we

carried out gel mobility shift assays using a 32P-labled oligonucleotide duplex containing a stat3 binding sequence (Xie et al., 2006). The gel-shift experiments were carried out with nuclear extracts made from SW620 cells with/without PKM2 knockdown or with/without HA-PKM2 expression. Autoradiography indicated that a slow migration complex was assembled with the labeled oligonucleotide and addition of the antibody against stat3 or PKM2 resulted in a supershift complex (Fig. 2.5B). The supershift complexes clearly indicated the coexistence of both PKM2 and stat3 in the assembled oligo-protein complex. Interestingly, knockdown of PKM2 substantially decreased the assembly of the oligo-protein complex and assembly of stat3 in the complex (the weak supershift) (Fig. 2.5D), while expression of HA-PKM2 dramatically increased assembled complex and assembly of both stat3 and PKM2 in the complex (Fig. 2.5C). The gelshift and supershift experiments suggested that PKM2 and stat3 might participate in transcription complex at the same stat3 DNA binding site, and PKM2 facilitated stat3 binding to its target DNA sequence. To further test this notion, we carried out ChIP/Re-ChIP experiments with the MEK5 promoter using antibody against stat3 and the antibody PabPKM2. The ChIP/Re-ChIP experiment clearly indicated that both PKM2 and stat3 interacted simultaneously with MEK5 promoter at the region of -1621 – -1366 nt (Fig. 2.5E). Stat3 is a transcription activator that is activated by phosphorylation at Y705 mainly by JAK or Src kinase. The phosphorylation increased the stat3 and DNA binding affinity (Sehgal, 2008). We observed the interaction between stat3 and PKM2 in the cell nucleus and PKM2 increased the stat3 binding to its target sequence both *in vitro* and *in vivo*. We suspected that PKM2 may play a role in stat3 phosphorylation at Y705. To test this conjecture, we analyzed the stat3 phosphorylation in SW620 cells in which the HA-

PKM2 was exogenously expressed. The phosphorylation of stat3 at Y705 in the nuclear extracts was examined by immunoblot using antibody against the Y705 phosphorylated stat3. Clearly, a significant increase in Y705 phosphorylation of stat3 in the nuclear extracts was evident by the immunoblot, upon expression of HA-PKM2 in the cells. Examination of the cellular levels of stat3 by immunoblot indicated that the expression levels of stat3 were not affected by the PKM2 expression (Fig. 2.6A). We further examined the effects of knockdown of PKM2 on the phosphorylation of stat3. Immunoblot analyses demonstrated that the phosphorylation levels of stat3 were significantly reduced upon PKM2 knockdown. The cellular levels of stat3 were not affected by PKM2 knockdown (Fig. 2.6B). It is known that JAK2 and c-Src are the most common protein tyrosine kinases that phosphorylate stat3. We therefore probed whether JAK2 and c-Src were activated by the HA-PKM2 expression. We examined JAK2/activated JAK2 and c-Src/activated c-Src by immunoblot using antibodies against JAK2, the phosphorylated (Y1007/1008) JAK2 (activated), c-Src, and the phosphorylated c-Src (Y530) with the cell lysate made from SW620 cells with/without HA-PKM2 expression. Clearly, JAK2 and c-Src were not activated upon the HAPKM2 expression (Fig. 2.6 C&D). The experiments suggested that expression of PKM2 promoted stat3 phosphorylation (activation), and the phosphorylation was not due to activation of JAK2 and c-Src.

2.3.4 Expression of PKM2 did not Alter Production of Pyruvate and Lactate

PKM2 is an enzyme that acts in the glycolysis pathway. We therefore analyzed production of lactate and pyruvate in two pairs of cells, SW620/SW480 and

WM266/WM115, in which the HA-PKM2 was exogenously expressed. Upon exogenous expression of HA-PKM2, there were no significant changes in cellular lactate and pyruvate for either WM266 or SW620 cells (the more proliferated cell lines). Cellular pyruvate and lactate increased slightly in SW480 and WM115 cells (the less proliferated cell lines), indicating a slight increase in glycolytic pyruvate kinase activity upon exogenous expression of HA-PKM2 in the less aggressive cancer cells, while expression of PKM2 did not lead to any changes in glycolytic pyruvate kinase activity in the more proliferated cancer cells. Overall, no substantial changes in cellular pyruvate and lactate were observed (Fig. 2.9 B-E), suggesting that the differences in stimulating cell proliferation by expression of HA-PKM2 in more proliferated and less proliferated cancer cells were not simply due to the effects on the carbohydrate metabolism.

2.4 Discussion

During tumor progression, growth signals stimulate the conversion of glycolytically active PKM2 to an inactive form of the enzyme, consequently regulating the glycolysis pathway to channel the carbon source from glucose for biosynthesis (Christofk et al., 2008a; Deberardinis et al., 2008; Garber, 2006; Mazurek & Eigenbrodt, 2003). It is conceivable that tumor cells need to coordinate the metabolism alterations with expression of genes that are related to cell proliferation during tumor progression. PKM2 has long been recognized as a so-called ‘moonlight’ enzyme that plays a very important role in tumor progression (Sriram et al., 2005). Clearly, the activity of PKM2 in transcription regulation is an important ‘moonlight’ activity of the protein. The functions of PKM2 in regulating expression of genes fulfill the role of feedback

signaling from metabolic alterations to gene regulation during tumor malignancy transformation (see model in Fig. 2.6E). It is intriguing that a glycolytic enzyme can translocate to the nucleus and act in gene transcription. Our co-immunoprecipitation experiments demonstrated that nuclear PKM2 coimmunoprecipitated with stat3, a transcription activator whose activations response to various growth factor and cytokines stimulations. PKM2 activates stat3 and increases the capability of the transcription activator binding to its target DNA, thus consequently activates transcription. This is a new pathway that leads to activation of stat3. Stat3 is a transcription activator that is activated in response to inflammatory cytokines, such as IL-6 (Gao et al., 2007; Watson & Neoh, 2008). Strikingly, activation of stat3 represents probably one of the most important molecular signatures involved in promoting cancer progression. It has been observed that activation of stat3 is detected in almost all cancer types (Frank, 2007; Groner et al., 2008; Huang, 2007; Kim et al., 2007). However, it is generally believed that activations of stat3 in response to growth factor and cytokines are usually transient. A long standing question is "How do the malignant cancer cells maintain constitutive activation of stat3?" Currently, mutation(s) that lead to constitutive activation of stat3 have not been identified. Thus, activation of stat3 by PKM2 in malignant cancer cells potentially provides a very attractive explanation for this long-standing question. The increase in nuclear stat3 phosphorylation at Y705 by expression of PKM2 implies a possibility that PKM2 may function as a protein kinase in the cell nucleus. Consistent with this conjecture, it was observed that PKM2 purified from extracts of hepatoma cells could phosphorylate histone H1 *in vitro* (Ignacak & Stachurska, 2003). We attempted to test possible kinase activity of the recombinant PKM2 expressed in *E. coli* with a

commercial recombinant GST-stat3 in the presence of ATP. No phosphorylation of stat3 was observed (data not shown). However, it is possible that PKM2 expressed in bacteria did not adapter the same structural or conformational properties. Alternatively, PKM2 may interact with tyrosine phosphorylated stat3 and the interaction helps redistribution of the phosphorylated stat3 to the cell nucleus. PKM2 is demonstrated to interact with tyrosine-phosphor-peptide. It is believed that interaction of PKM2 with tyrosine phosphor-protein confers the functional role of PKM2 in promoting cell proliferation (Christofk et al., 2008a; Christofk et al., 2008b). However, the interaction of PKM2 with a particular tyrosine phosphorylated protein has not been identified. Here, we demonstrated an example that PKM2 targeted a cellular tyrosine phosphor-protein stat3. PKM2 interacts with the phosphorylated stat3 and aids the activity of the phosphorylated protein in gene transcription, which consequently confers the functional role of PKM2 in promoting cell proliferation.

2.5 Materials and Methods

2.5.1 Reagents, Cell lines, and Antibodies

The KLH conjugated peptide spans aa 399 – 412 of PKM2 was synthesized by Global Peptide Services. PKM2 polycolonal antibody and anti-HA antibody was raised in the animal facility of Georgia State University. Antibodies against Lamin A/C, Histone 2A, MEK5, MEK5(pSer311/Thr315), stat3, stat3(pY705), JAK2, JAK2(p-1007/1008), c-Src, p-c-Src(pY530), and _-actin were purchased from Cell Signaling, Abnova, Invitrogen, SantaCruz, Abcam, and AnaSpec respectively. Recombinant GST-stat3 was purchased from Abcam. Cell lines LN686 and M4C1 were gifts from Dr. Georgia Chen,

Emory University. Cell lines SW480, SW620, WM115, WM266, T98G, U87MG, H146 and H460 were purchased from ATCC and cultured by following the vendor's instructions. The vector for expression of dominate negative stat3 (Y705F) was a kind gift from Dr. Suyan Huang, The University of Texas, M.D. Anderson Cancer Center (Xie et al., 2006). Stat3 inhibitor, Ethyl-1-(4-cyno-2,3,5,6-tetrafluorophenyl)-6,7,8-trifluoro-4-oxo-1,4-dihydroquinoline-3-carboxylate (Xu et al., 2008) was purchased from Calbiochem and used without further purification.

2.5.2 RNA Interference, Subcellular Extracts Preparation, Co-immunoprecipitation, immunoblot, Cell Proliferation Assays, and Chromatin immunoprecipitation (ChIP)

The siRNA duplexes for PKM2, stat3, and MEK5, siGENOME ON-TARGETplus SMARTpool duplex, were purchased from Dharmacon RNA technologies. The experimental procedures for preparation of subcellular extracts, co-immunoprecipitation, RNA interference knockdown, immunoblot, cell proliferation assays, and chromatin immunoprecipitation (ChIP) were similar to that of our previous reports (Yang et al., 2006; Yang et al., 2007b). Cell proliferations were measured using the commercial cell proliferation kit (Calbiochem) that monitors incorporation of BrdU (Yang et al., 2006; Yang et al., 2007a).

2.5.3 Expression of PKM2 by Adenovirus Using Commercial AdEasy System

The cDNA encoding PKM2 was purchased from OriGene Technologies. PKM2 cDNA was cloned into a shuttle vector pAdEasy-1 with EcoRI and NotI restriction endonuclease sites. The resultant plasmid was digested with Pme1 and transformed into

competent AdEasier cells containing the adenovirail backbone plasmid pAdEasy-1 by electroporation (BJ5183-AD-1, Stratagene). Recombinants were selected for kanamycin resistance and further confirmed by restriction endonuclease analyses and DNA autosequencing. The confirmed plasmid with PKM2 cDNA was digested with PacI restriction endonuclease and transformed into HEK-293 cells expressing adenovirus E1 (Stratagene). The production of recombinant adenoviruses in HEK-293 cells was examined under fluorescent microscope and collected in three weeks. The recombinant viruses were amplified three rounds in HEK-293 cells to increase virus titer (1x1013 Pfu/ml). The viruses were collected by centrifugation and stored at -80oC. The cells were seeded in a 48 well plate to 70% – 80% confluence. Viruses stock (50 _l at 1x1013 Pfu/ml) were added to each well and incubated for 3 – 5 hours following by changing fresh culture medium. The expression of HA-PKM2 was examined 48 hours after incubation.

2.5.4 Cellular Pyruvate and Lactate

Cellular pyruvate and lactate were analyzed by commercially available kits (BioVision). Cells (WM115, WM266, SW480, and SW620) were infected with adeno-viruses for overexpression of

HA-PKM2 or control vectors, and were lysed in lysis buffers that were included in the kits. The lysates were centrifuged at 13,000g to remove the precipitates. The prepared extracts (10 _l) were applied to the assay test. The standard curves were made using probes included with the kits. Pyruvate and lactate amounts were measured by following the vendor's instructions.

2.5.5 Microarray Analyses of Gene Expressions

Total RNA from cells expressing HA-tagged PKM2 or control was extracted with an RNeasy kit by following the vendor's instructions (Qiagen). The total RNA concentration was determined by spectrometer reading at OD 280 nm. The isolated total RNA (10 _g) of each sample was used for synthesizing cDNA using the ImProm-II reverse transcription system (Promega). Synthesized cDNA was purified by phenol-chloroform extraction and ethanol precipitation. The cDNA was labeled using the GeneChip® IVT Labeling Kit (Affymetrix). The labeled cDNA was fragmented in fragmentation buffer and hybridized to a GeneChip® Human Genome U133 Plus 2.0 Array (Affymetrix). The arrays were scanned with the Affymetrix GeneChip 3000 scanner. The data were analyzed by Affymetrix GeneChip Operating Software (GCOS) Version 1.0. The array data in table S1 obtained with SW620 cells in which PKM2 was exogenously expressed were subtracted from a reference array where the cells were infected with viruses carrying an empty vector. The same expression array experiments were repeated two times.

2.5.6 Real Time PCR and RT-PCR

Total RNA was extracted from the cells using RNeasy kit by following the manufacturer's instruction (Qiagen). Reverse transcription process was performed with ImProm-II reverse transcription system (Promega). Subsequent Polymerase Chain Reactions were carried out with 1 μg of template cDNA mixed with the Fast SYBR green master mix in an Applied Biosystems Real-Time PCR 7500 system (Applied biosystems).

The PCR reactions using standard RT-PCR negative control primer set were performed as reference. The primer pairs, forward 5'-CATGTCCTTGGAAGAATTGC-3', reverse 5'-ATAGAATTCACCAGCTGAGTG-3', that

targeted exon 12 – exon 14/15 regions of the MEK5 gene was used in our RT-PCR experiments.The primer pair for PCR reaction in the ChIP with MEK5 promoter was, forward 5'-GTATGCAAATTTGGCAAATTGAG-3' reverse 5'-CTTCAGATATTCTAGGAATTTCCC-3', targeting nt -1,621 – -1,366 region. The primer pair for ChIP target exon 1 of MEK5 (nt 342– nt 542) was forward 5'-CAGAGACCTTCACCATAGCG-3' and reverse 5'-AACAAGGGAATGGAGGATGAG-3'. The primer pair for PCR reaction in the ChIP withGAPDH gene was forward 5'-CAATTCCCCATCTCAGTCGT-3', reverse 5'-AGTAGCCGGGCCCTACTTT-3' span region of -360 nt - -163 nt.

2.5.7 Gel-Mobility Shift and Super-Shift Assays

The mobility shift assays were carried out with oligonucleotide that harbors a stat3 binding sequence 5'-GATCCTTCTGGGAATTCCTAGATC-3' (Xie et al., 2006). The oligonucleotide was 5'-end 32P-labeled. The labeled oligonucleotide (100 pmole) was incubated with 15% nuclear extracts (20 _l) prepared from appropriate cells as indicated in the figure legends for 30 minutes at room temperature in the binding buffer (5% glycerol, 1mM MgCl2, 0.5mM EDTA, 0.5mM DTT, 50mM NaCl, 10mM Tris-HCl, 0.05mg/ml poly(dI-dC)). The proteinoligonucleotide complexes were separated in 4% native polyacrylamide gel (acrylamide: polyacrylamide 59:1). For supershift analyses, a monoclonal antibody against stat3 (invitrogen) or the antibody PabPKM2 was added to

the oligonucleotide-nuclear extracts mixture and incubated for additional 45 minutes. The complexes in gel were transferred to a membrane and subjected to autoradiography.

2.5.8 ChIP, Re-ChIP

ChIP and Re-ChIP experiments were performed with a commercial ChIP/Re-ChIP kit (Activemotif) by following vendor's instruction. Briefly, the first round of ChIP was carried out s described above. The DNA was recovered from the immunoprecipitates by elution with 1% SDS, and 90% of the eluted chromatin from the first round of immunoprecipation was diluted 10-fold with ChIP buffer. The second round of immunoprecipitation was then carried out with the recovered immunoprecipitates. DNA fragmentations, reverse crosslinking, and PCR reaction was subsequently performed with the second round of immunoprecipitation.

2.6 References

Altenberg B and Greulich KO. (2004). *Genomics*, 84, 1014-20.

Ashizawa K, Willingham MC, Liang CM and Cheng SY. (1991). *J Biol Chem*, 266, 16842-6

Christofk HR, Vander Heiden MG, Harris MH, Ramanathan A, Gerszten RE, Wei R, Fleming MD, Schreiber SL and Cantley LC. (2008a). *Nature*, 452, 230-3.

Christofk HR, Vander Heiden MG, Wu N, Asara JM and Cantley LC. (2008b). *Nature*, 452, 181-6.

Dang CV and Lewis BC. (1997). *J Biomed Sci*, 4, 269-278.

Deberardinis RJ, Sayed N, Ditsworth D and Thompson CB. (2008). *Curr Opin Genet Dev*, 18, 54-61.

Diaz-Meco MT and Moscat J. (2001). *Mol Cell Biol*, 21, 1218-27.

Dombrauckas JD, Santarsiero BD and Mesecar AD. (2005). *Biochemistry*, 44, 9417-29.

Elbers JR, van Unnik JA, Rijksen G, van Oirschot BA, Roholl PJ, Oosting J and Staal GE. (1991). *Cancer*, 67, 2552-9.

Elstrom RL, Bauer DE, Buzzai M, Karnauskas R, Harris MH, Plas DR, Zhuang H, Cinalli RM, Alavi A, Rudin CM and Thompson CB. (2004). *Cancer Res*, 64, 3892-9.

Frank DA. (2007). *Cancer Lett*, 251, 199-210.

Gao SP, Mark KG, Leslie K, Pao W, Motoi N, Gerald WL, Travis WD, Bornmann W, Veach D, Clarkson B and Bromberg JF. (2007). *J Clin Invest*, 117, 3846-56.

Garber K. (2006). *Science*, 312, 1158-9.
Groner B, Lucks P and Borghouts C. (2008). *Semin Cell Dev Biol*, 19, 341-50.
Hacker HJ, Steinberg P and Bannasch P. (1998). *Carcinogenesis*, 19, 99-107.
Hoshino A, Hirst JA and Fujii H. (2007). *J Biol Chem*, 282, 17706-11.
Huang S. (2007). *Clin Cancer Res*, 13, 1362-6.
Ignacak J and Stachurska MB. (2003). *Comp Biochem Physiol B Biochem Mol Biol*, 134, 425-33.
Kim DJ, Chan KS, Sano S and Digiovanni J. (2007). *Mol Carcinog*, 46, 725-31.
Matoba S, Kang JG, Patino WD, Wragg A, Boehm M, Gavrilova O, Hurley PJ, Bunz F and
Hwang PM. (2006). *Science*, 312, 1650-3.
Mazurek S, Boschek CB, Hugo F and Eigenbrodt E. (2005). *Semin Cancer Biol*, 15, 300-8.
Mazurek S and Eigenbrodt E. (2003). *Anticancer Res*, 23, 1149-54.
McCracken SR, Ramsay A, Heer R, Mathers ME, Jenkins BL, Edwards J, Robson CN, Marquez R, Cohen P and Leung HY. (2008). *Oncogene*, 27, 2978-88.
Mehta PB, Jenkins BL, McCarthy L, Thilak L, Robson CN, Neal DE and Leung HY. (2003). *Oncogene*, 22, 1381-9.
Schneider J, Neu K, Grimm H, Velcovsky HG, Weisse G and Eigenbrodt E. (2002). *Anticancer Res*, 22, 311-8.
Sehgal PB. (2008). *Semin Cell Dev Biol*, 19, 329-40.
Semenza GL. (2007). *J Bioenerg Biomembr*, 39, 231-4.
Song H, Jin X and Lin J. (2004). *Oncogene*, 23, 8301-9.
Sriram G, Martinez JA, McCabe ER, Liao JC and Dipple KM. (2005). *Am J Hum Genet*, 76, 911-24.
Stetak A, Veress R, Ovadi J, Csermely P, Keri G and Ullrich A. (2007). *Cancer Res*, 67, 1602-8.
Warburg O. (1956). *Science*, 123, 309-14.
Watson CJ and Neoh K. (2008). *Semin Cell Dev Biol*, 19, 401-6.
Xie TX, Huang FJ, Aldape KD, Kang SH, Liu M, Gershenwald JE, Xie K, Sawaya R and Huang S. (2006). *Cancer Res*, 66, 3188-96.
Xu J, Cole DC, Chang CP, Ayyad R, Asselin M, Hao W, Gibbons J, Jelinsky SA, Saraf KA and Park K. (2008). *J Med Chem*, 51, 4115-21.
Yang L, Lin C and Liu ZR. (2006). *Cell*, 127, 139-55.
Yang L, Lin C, Sun SY, Zhao S and Liu ZR. (2007a). *Oncogene*, 26, 6082-92.
Yang L, Lin C, Zhao S, Wang H and Liu ZR. (2007b). *J Biol Chem*, 282, 16811-9.
Zhang X, Liu Y, Gilcrease MZ, Yuan XH, Clayman GL, Adler-Storthz K and Chen Z. (2002). *Cancer*, 95, 1663-72.
Zwerschke W, Mazurek S, Massimi P, Banks L, Eigenbrodt E and Jansen-Durr P. (1999). *Proc Natl Acad Sci U S A*, 96, 1291-6.

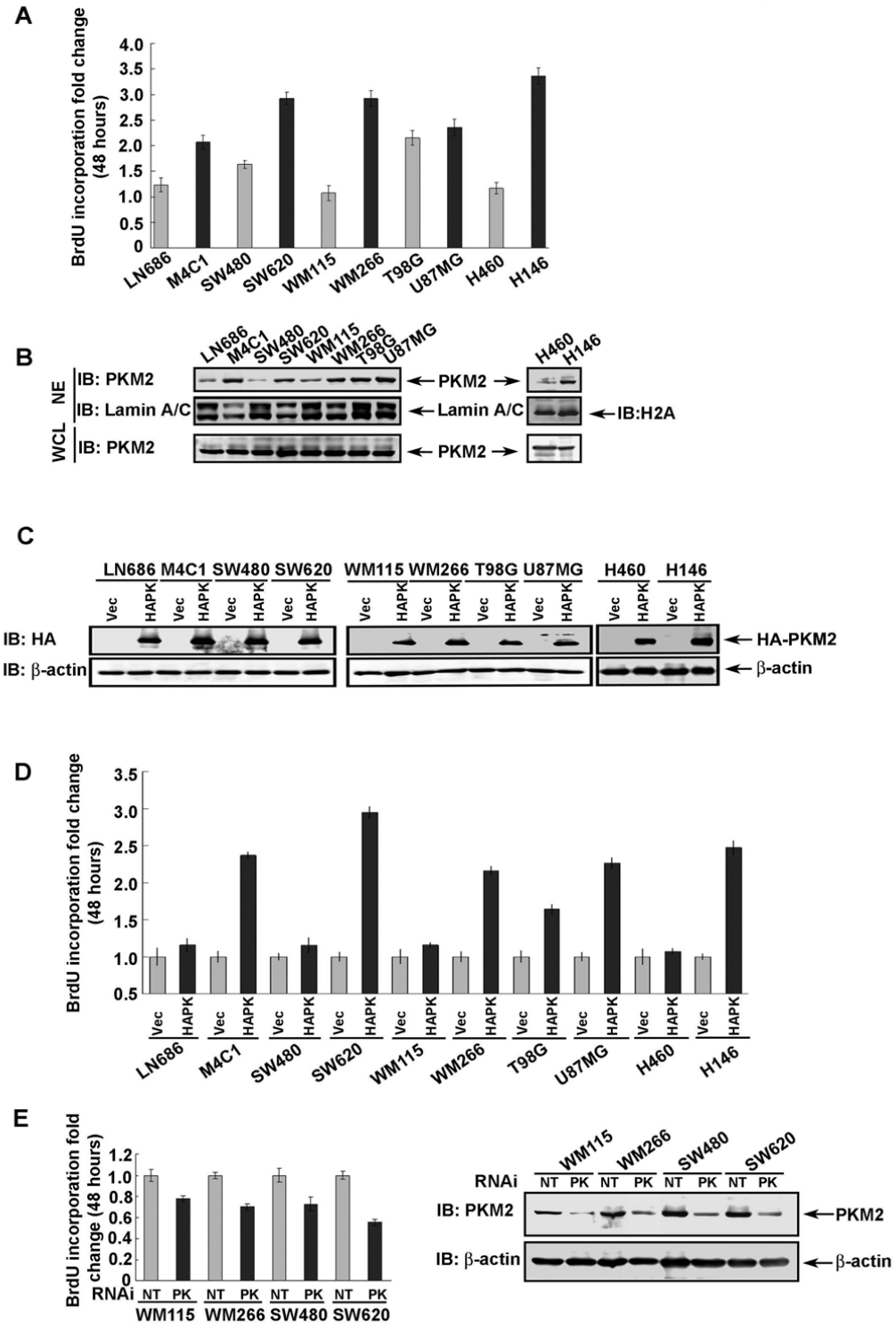
A
BrdU incorporation fold change (48 hours)
4.0
3.5
3.0
2.5
2.0
1.5
1.0
0.5
0
LN686
M4C1
SW480
SW620
WM115
WM266
T98G
U87MG
H460
H146
B
NE
WCL
IB: PKM2
IB: Lamin A/C
IB: PKM2
PKM2
Lamin A/C
PKM2
IB:H2A
C
LN686 M4C1 SW480 SW620 WM115 WM266 T98G U87MG H460 H146
Vec
HAPK
IB: HA
IB: β-actin
HA-PKM2
β-actin
D
BrdU incorporation fold change (48 hours)
3.5
3.0
2.5
2.0
1.5
1.0
0.5
Vec
HAPK
LN686
M4C1
SW480
SW620
WM115
WM266
T98G
U87MG
H460
H146
E
BrdU incorporation fold change (48 hours)
1.2
1.0
0.8
0.6
0.4
0.2
0
RNAi
NT
PK
WM115
WM266
SW480
SW620
IB: PKM2
IB: β-actin
PKM2
β-actin

Figure 2.1 PKM2 Promotes Cell Proliferation
(A) Cell proliferations of ten cancer cell lines (indicated) were measured using a commercial cell proliferation kit. The proliferation rates are presented as fold changes of BrdU incorporation of the same cultured cells before and after 48 hours culturing by defining the initial BrdU incorporation as 1. **(B)** Nuclear localization of PKM2 in different cancer cells. Immunoblot analyses of PKM2 using the antibody PabPKM2 (IB:PKM2) in nuclear extracts (NE) and whole cell lysates (WCL) of ten different cell lines (indicated). Blots of lamin A/C and H2A are loading controls. **(C)** Exogenous HA-PKM2 (HAPK) expression using the adeno-viral expression kit in ten different cell lines (indicated) were analyzed by immunoblot using anti-HA antibody (IB:HA). Immunoblot of _-actin (IB:_-actin) were loading controls. **Vec** were the cells infected with virus that carry an empty vector. **(D)** Cell proliferation rates of ten different cell lines (indicated) in which PKM2 was exogenously expressed using the adeno-viral expression kit were measured using the cell proliferation kit. Cell proliferations are presented as fold changes in BrdU incorporation of the same cultured cells before expression of PKM2 and 48 hours after PKM2 expression. The BrdU incorporation of each cell line without PKM2 expression is defined as 1. **(E) (Top)** Cell proliferations of SW480 and SW620 cells were measured using the cell proliferation kit. Cell proliferations were presented as fold changes in BrdU incorporation before and 48 hours after knockdown of PKM2 using a smart-pool RNAi (PK). NT represents the cells treated with non-target RNAi. The BrdU incorporation of each cell line before PKM2 knockdown was defined as 1. **(Bottom)** Immunoblot analyses of cellular PKM2 using the antibody PabPKM2 (IB:PKM2) 48 hours after RNAi knockdown of PKM2 in different cells (indicated). Immunoblot of β-actin (IB:β-actin) were loading controls. NT represents the cells treated with non-target RNAi. Error bars in **(A), (D),** and **(E)** are standard deviations for three independent experiments.

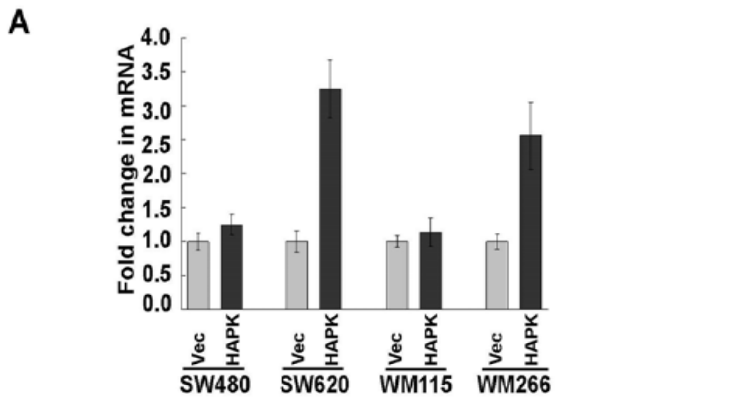
A
Fold change in mRNA
4.0
3.5
3.0
2.5
2.0
1.5
1.0
0.5
0.0
Vec
HAPK
SW480
SW620
WM115
WM266

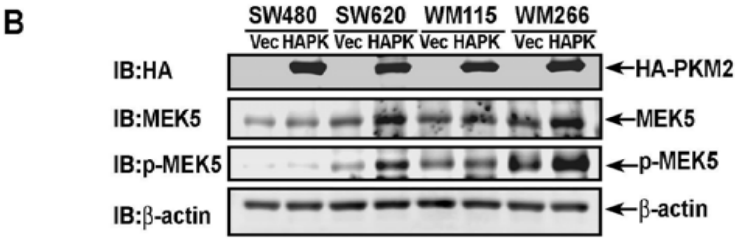
B
SW480
SW620
WM115
WM266
Vec HAPK Vec HAPK Vec HAPK Vec HAPK
IB:HA
HA-PKM2
IB:MEK5
MEK5
IB:p-MEK5
p-MEK5
IB:β-actin
β-actin

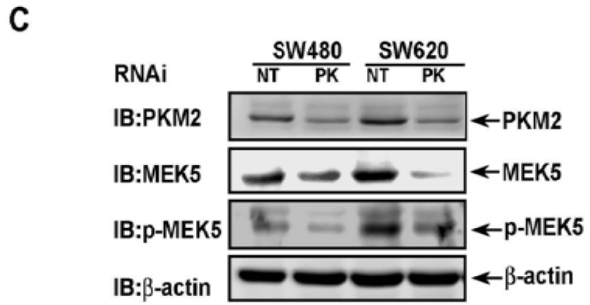
C
SW480
SW620
RNAi
NT PK NT PK
IB:PKM2
PKM2
IB:MEK5
MEK5
IB:p-MEK5
p-MEK5
IB:β-actin
β-actin

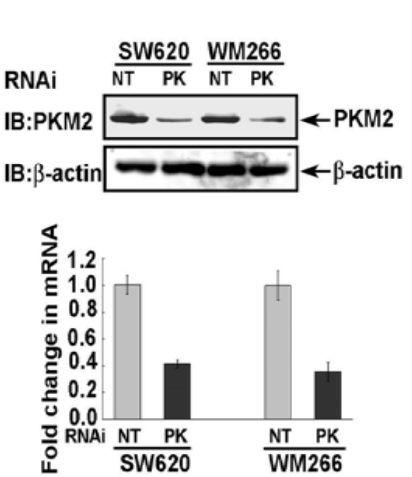
D
SW620
WM266
RNAi
NT PK NT PK
IB:PKM2
PKM2
IB:β-actin
β-actin
Fold change in mRNA
1.2
1.0
0.8
0.6
0.4
0.2
0.0
RNAi
NT PK NT PK
SW620
WM266

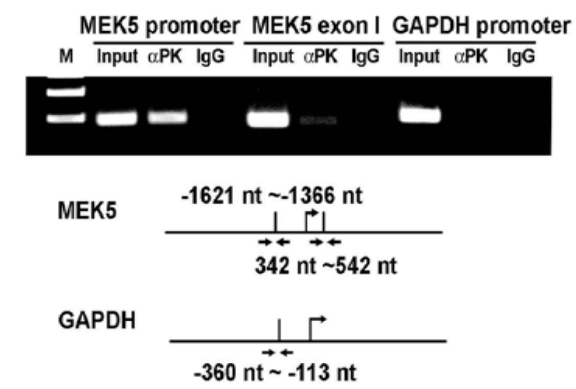
E
MEK5 promoter
MEK5 exon I
GAPDH promoter
M
Input αPK IgG Input αPK IgG Input αPK IgG
MEK5
-1621 nt ~-1366 nt
342 nt ~542 nt
GAPDH
-360 nt ~ -113 nt

Figure 2.2 PKM2 Upregulates MEK5 Transcription
(A) RT-PCR analyses of cellular MEK5 mRNA levels in two pairs of cancer cells (indicated) in which PKM2 was exogenously expressed using the adeno-viral expression kit. The results are presented as fold increase in PCR products before and 48 hours after PKM2 exogenous expression in the same cells. The level of PCR product from each cell line before PKM2 exogenous expression was defined as 1. **(B)** Expressions (IB:MEK5) and phosphorylation (IB:p-MEK5) of MEK5 in different cancer cells (indicated on top) were analyzed by immunoblot using antibodies against MEK5 and phosphorylated MEK5. HA-PKM2 was expressed (HAPK) in the cells using the adeno-viral expression kit (IB:HA). **Vec** were the cells infected with virus that carry the empty vector. **(C)** Expressions (IB:MEK5) and phosphorylation (IB:p-MEK5) of MEK5 in SW480 and SW620 cells (indicated) in which PKM2 was knocked down (PK) using the smart pool RNAi were analyzed by immunoblot using antibodies against MEK5 and phosphorylated MEK5. The cellular levels of PKM2 were analyzed by immunoblot of PKM2 (IB:PKM2). **(D) (Bottom panel)** RT-PCR analyses of cellular MEK5 mRNA levels in SW620 and WM266 cells (indicated) in which PKM2 was knocked down using a smart-pool RNAi (PK). NT represents the cells treated with non-target RNAi. The results are presented as fold changes in PCR products before and 48 hours after PKM2 knockdown in the same cells. The level of PCR products from each cell line that was treated with non-target RNAi was defined as 1. **(Upper panel)** Immunoblot analyses of cellular PKM2 in SW620 and WM266 cells (indicated) in which PKM2 was knocked down using a smart-pool RNAi (PK). **(E)** ChIP of the MEK5 promoter (MEK5 promoter) using antibody against PKM2 in SW620 cells (_PK). ChIP using rabbit IgG was a negative control. ChIP using PCR primer pair targeting a region of exon 1 (MEK5 exon 1) of MEK5 gene (nt 342 – nt 542) is a negative control. ChIP targeting GAPDH promoter (GAPDH promoter) using antibody against PKM2 was another negative control. The primer pair positions are indicated. Inputs were PCR products from DNA extracts without ChIP. In **(B), (C),** and **(D)**, Immunoblot of β-actin (IB:β-actin) is a loading control. Error bars in **(A)** and **(D)** are standard deviations of three measurements

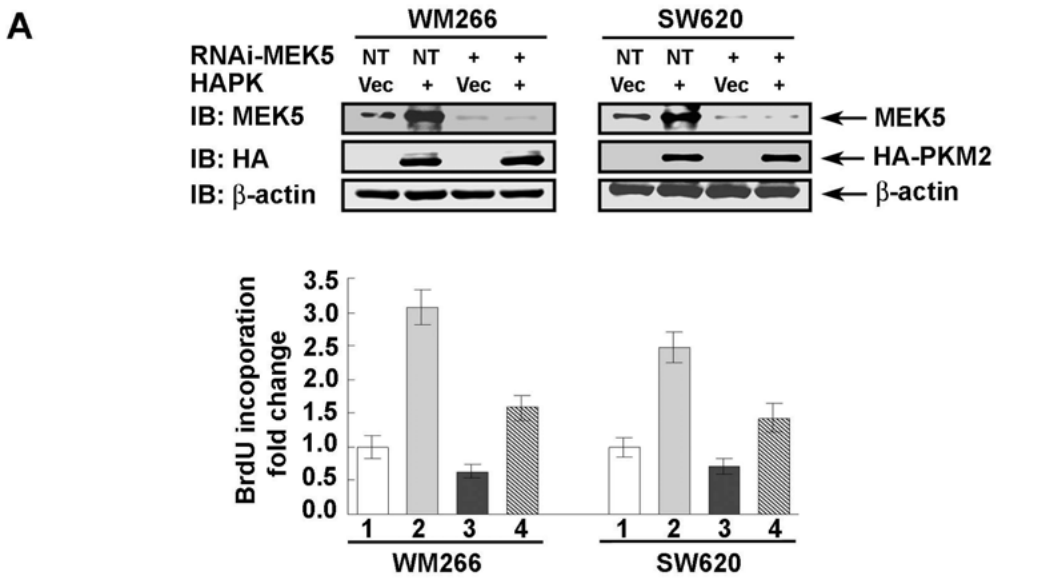
A
WM266
SW620
RNAi-MEK5
HAPK
NT NT + +
Vec + Vec +
IB: MEK5
IB: HA
IB: β-actin
MEK5
HA-PKM2
β-actin
BrdU incoporation fold change
3.5
3.0
2.5
2.0
1.5
1.0
0.5
0.0
1 2 3 4
WM266
SW620

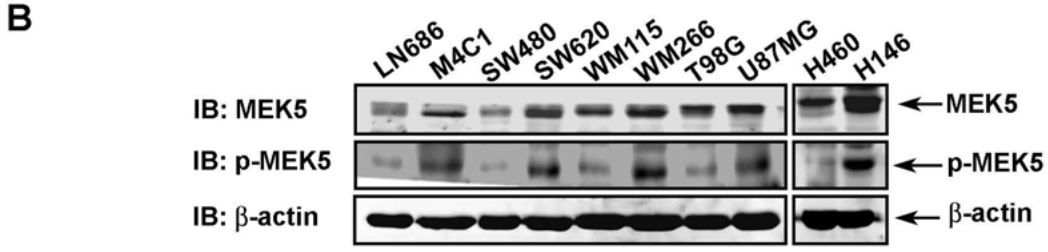
B
LN686
M4C1
SW480
SW620
WM115
WM266
T98G
U87MG
H460
H146
IB: MEK5
IB: p-MEK5
IB: β-actin
MEK5
p-MEK5
β-actin

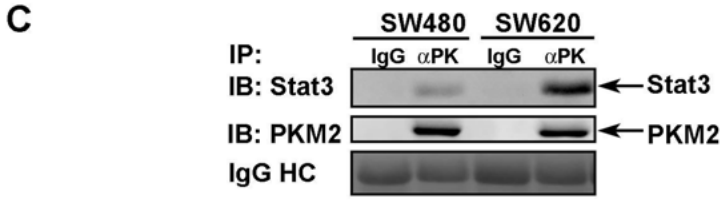
C
SW480
SW620
IP:
IgG αPK IgG αPK
IB: Stat3
IB: PKM2
IgG HC
Stat3
PKM2

Figure 2.3 Expression of MEK5 Mediates the Effects of PKM2 in Cell Proliferation
(A) (Upper panel) Cellular levels of MEK5 and exogenously expressed HA-PKM2 in WM266 and SW620 cells were analyzed by immunoblot using antibodies against MEK5 (IB: MEK5) and HA (IB:HA). MEK5 in the cells was knocked down by RNAi (PK). PKM2 was exogenously expressed in the cells using the adeno-viral expression kit. **(Bottom Panel)** Cell proliferations of WM266 and SW620 cells were measured using the cell proliferation kit. Proliferations of WM266 (1 – 4) or SW620 (5 – 8) cells were measured under following conditions: 1) and 5) Open bars, HA-PKM2 expression and no MEK5 knockdown;. 2) and 6) Gray bars, HA-PKM2 was expressed and no MEK5 knockdown; 3) and 7) Black bars, no PKM2 expression and MEK5 knockdown; and 4) and 8) Striped bars, PKM2 expression and MEK5 knockdown. The proliferations are presented as fold changes of BrdU incorporation before and after indicated treatments. NT represents the cells treated with non-target RNAi. **Vec** were the cells infected with virus that carry the empty vector. Error bars are standard deviations of three measurements. **(B)** Cellular MEK5 levels and phosphorylation of the protein in ten different cell lines (indicated at top) were examined by immunoblot of whole cell lysate using antibodies against MEK5 and phosphorylated MEK5. In **(A)** and **(B)** Immunoblot of β-actin (IB:β-actin) is a loading control. **(C)** Co-immunoprecipitation of PKM2 with stat3. PKM2 was immunoprecipitated from nuclear extracts prepared from SW620 and SW480 cells using the antibody PabPKM2 (IP: αPK). The immunoprecipitates were analyzed by immunoblot using antibodies against stat3 (IB: Stat3) or PKM2 (IB: PKM2). Ponceau S staining of IgG heavy chain (IgG HC) in the immunoprecipitates is the loading control. Immunoprecipitation using rabbit IgG (IP:IgG) was the control immunoprecipitation.

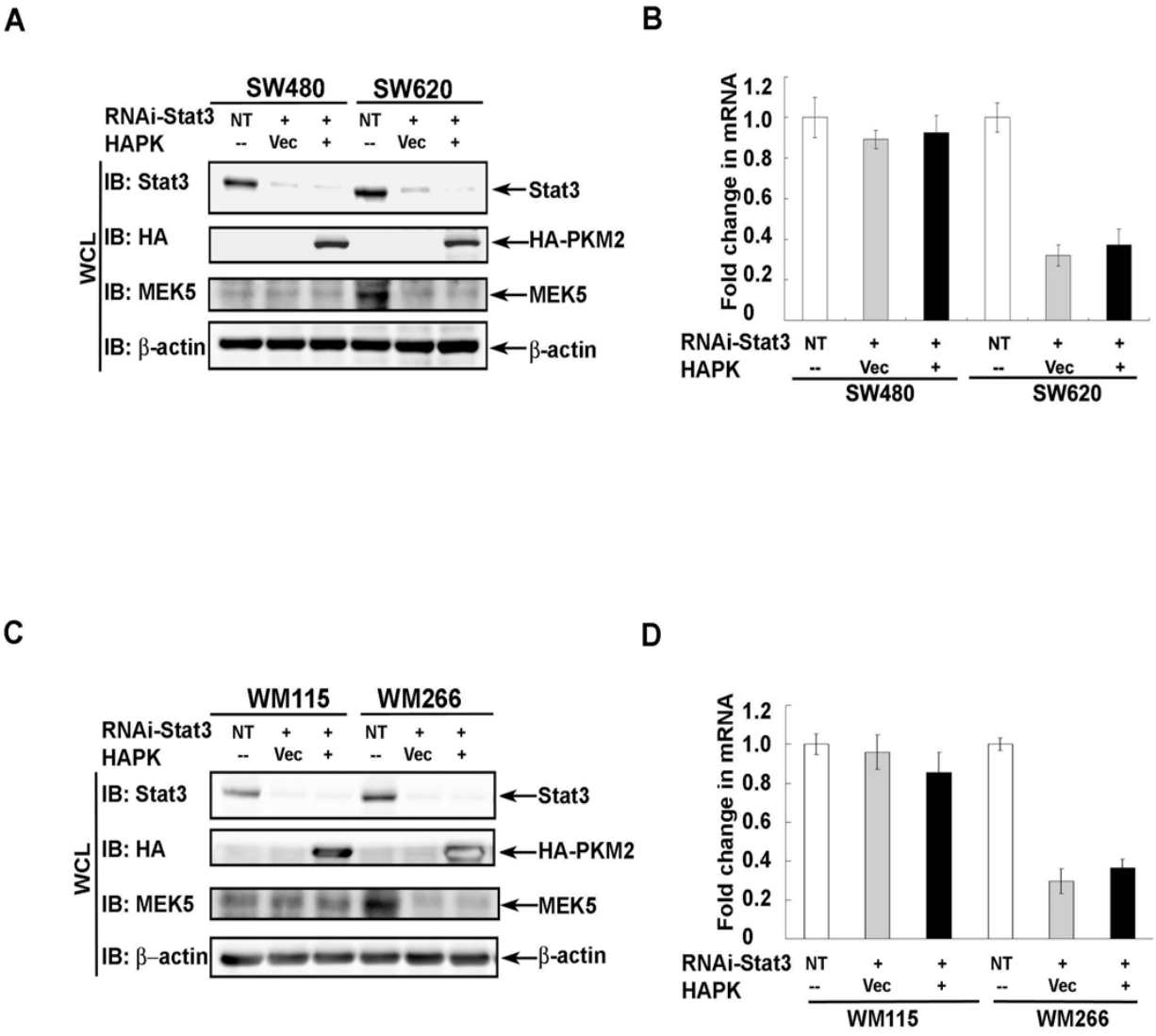
A
SW480
SW620
RNAi-Stat3
NT + + NT + +
HAPK
-- Vec + -- Vec +
WCL
IB: Stat3
IB: HA
IB: MEK5
IB: β-actin
Stat3
HA-PKM2
MEK5
β-actin
B
Fold change in mRNA
1.2
1.0
0.8
0.6
0.4
0.2
0
RNAi-Stat3 NT + + NT + +
HAPK -- Vec + -- Vec +
SW480
SW620
C
WM115
WM266
RNAi-Stat3
NT + + NT + +
HAPK
-- Vec + -- Vec +
WCL
IB: Stat3
IB: HA
IB: MEK5
IB: β–actin
Stat3
HA-PKM2
MEK5
β-actin
D
Fold change in mRNA
1.2
1.0
0.8
0.6
0.4
0.2
0
RNAi-Stat3 NT + + NT + +
HAPK -- Vec + -- Vec +
WM115
WM266

Figure 2.4 PKM2 Upregulates MEK5 Transcription via Activation of Stat3
(A) & (C) Expressions of MEK5 (IB: MEK5) in SW620/SW480 **(A)** and WM115/WM266 cells **(C)** (indicated) were analyzed by immunoblot the cell lysate (WCL) prepared from the cells in which stat3 was knocked down by RNAi (stat3, IB:Stat3). HA-PKM2 was exogenously expressed in the stat3 knockdown cells (IB:HA). The blot of β-actin (IB: β-actin) are the loading controls. **(B) & (D)** RT-PCR analyses of cellular MEK5 mRNA levels in SW620/SW480 **(B)** and WM266/WM115 cells **(D)** (indicated) in which stat3 was knocked down by RNAi (stat3, IB:Stat3). HA-PKM2 was exogenously expressed in the stat3 knockdown cells (IB: HA). The results are presented as fold changes in PCR products before and 48 hours after stat3 knockdown and HA-PKM2 expression in the same cells. The level of PCR products from each cell line that was treated with non-target RNAi was defined as 1. In **(A), (B), (C),** a**nd (D)**, NT represents the cells treated with non-target RNAi. **Vec** were the cells infected with virus that carry the empty vector. Error bars in **(B)** and **(D)** are standard deviations of three measurements.

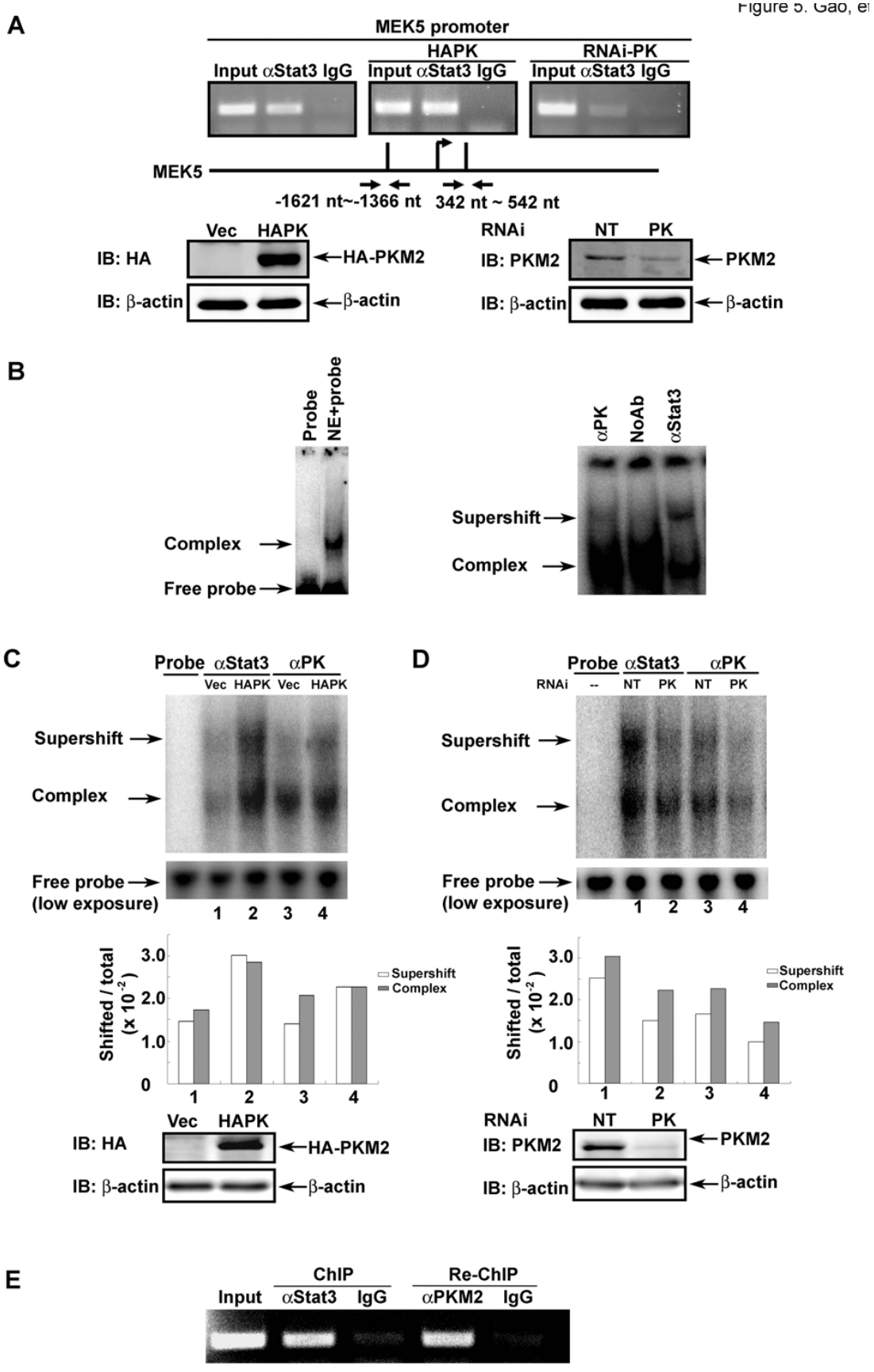
A
MEK5 promoter
HAPK
RNAi-PK
Input αStat3 IgG
Input αStat3 IgG
Input αStat3 IgG
MEK5
-1621 nt~-1366 nt
342 nt ~ 542 nt
Vec HAPK
IB: HA
HA-PKM2
IB: β-actin
β-actin
RNAi NT PK
IB: PKM2
PKM2
IB: β-actin
β-actin
B
Probe
NE+probe
Complex
Free probe
αPK
NoAb
αStat3
Supershift
Complex
C
Probe αStat3 αPK
Vec HAPK Vec HAPK
Supershift
Complex
Free probe
(low exposure)
1 2 3 4
Shifted / total
(x 10-2)
3.0
2.0
1.0
0
Supershift
Complex
Vec HAPK
IB: HA
HA-PKM2
IB: β-actin
β-actin
D
Probe αStat3 αPK
RNAi -- NT PK NT PK
Supershift
Complex
Free probe
(low exposure)
1 2 3 4
Shifted / total
(x 10-2)
3.0
2.0
1.0
0
Supershift
Complex
RNAi NT PK
IB: PKM2
PKM2
IB: β-actin
β-actin
E
ChIP
Re-ChIP
Input
αStat3
IgG
αPKM2
IgG

Figure 2.5 PKM2 Upregulates MEK5 Transcription by Promoting Stat3 DNA Interaction **(A) (Upper panels)** ChIP of the MEK5 promoter (MEK5 promoter) using antibody against stat3 in SW620 cells (αStat3). The cells were treated non-target RNAi (left, NT) or with RNAi target PKM2 (right, RNAi-PK), or HA-PKM2 was exogenously expressed in the cells (middle, HAPK). ChIP using rabbit IgG (IgG) was a negative control. Inputs were PCR products from DNA extracts without ChIP. The primer pair positions are indicated. **(Lower panels)** the cellular PKM2 (right) and HA-PKM2 (left) levels in SW620 cells that were treated with RNAi target PKM2 (PK) or with non-target RNAi (NT), or infected with virus that carry HA-PKM2 expression vector (HAPK) or vector alone (Vec). The blot of β-actin (IB:β-actin) is the loading control. **(B)** DNA-protein complex (Complex) assembled on a 32P-labeled oligonucleotide containing the stat3 targeting sequence in nuclear extracts prepared from SW620 cells (left panel) was detected by gel-shift and autoradiography. Probe indicates the free ^{32}P-labeled oligonucleotide probe without addition of nuclear extracts. The antibodies against PKM2 (αPK), stat3 (αStat3), or no antibody (NoAb) was added to the complex to create supershift (Supershift) (right panel). **(C) & (D)** Supershift complex assembled with the 32P-labeled oligonucleotide and antibodies (indicated) in the nuclear extracts prepared from SW620 cells in which **(D)** PKM2 was knocked down by RNAi (PK) or **(C)** HA-PKM2 was exogenously expressed (HAPK) was detected by gel-shift and autoradiography. NT means the cells were treated with non-target RNAi. Vec means the cells were infected with virus that carried the empty vector. Probe only is the free probe without addition of nuclear extracts. The free probe (low exposure) is the loading control with 1/10 of exposure time in autoradiography. The quantification of the assembled complex and super shift complex were presented as percentage (Shifted/total x102) of probe in the shift complex calculated by Intensities of complex [complex (grey bars) or supershift (open bars)] divided by Intensities of total [free probe + complex + supershift). Immunoblots at bottom of each panel indicate cellular levels of HA-PKM2 (IB:HA) and endogenous PKM2 (IB:PKM2). Immunoblot of β-actin is the loading control. **(E)** ChIP and Re-ChIP of the MEK5 promoter (MEK5 promoter) in SW620 cells. The antibody is against stat3 (αStat3) was used as the first ChIP antibody (ChIP). The antibody PabPKM2 (αPK) was used as Re-ChIP antibody (Re-ChIP). ChIP and Re-ChIP using rabbit IgG (IgG) were the negative control experiments. The primer pair targeting the same region (-1621 nt – -1366 nt) was used in ChIP and Re-ChIP assays.

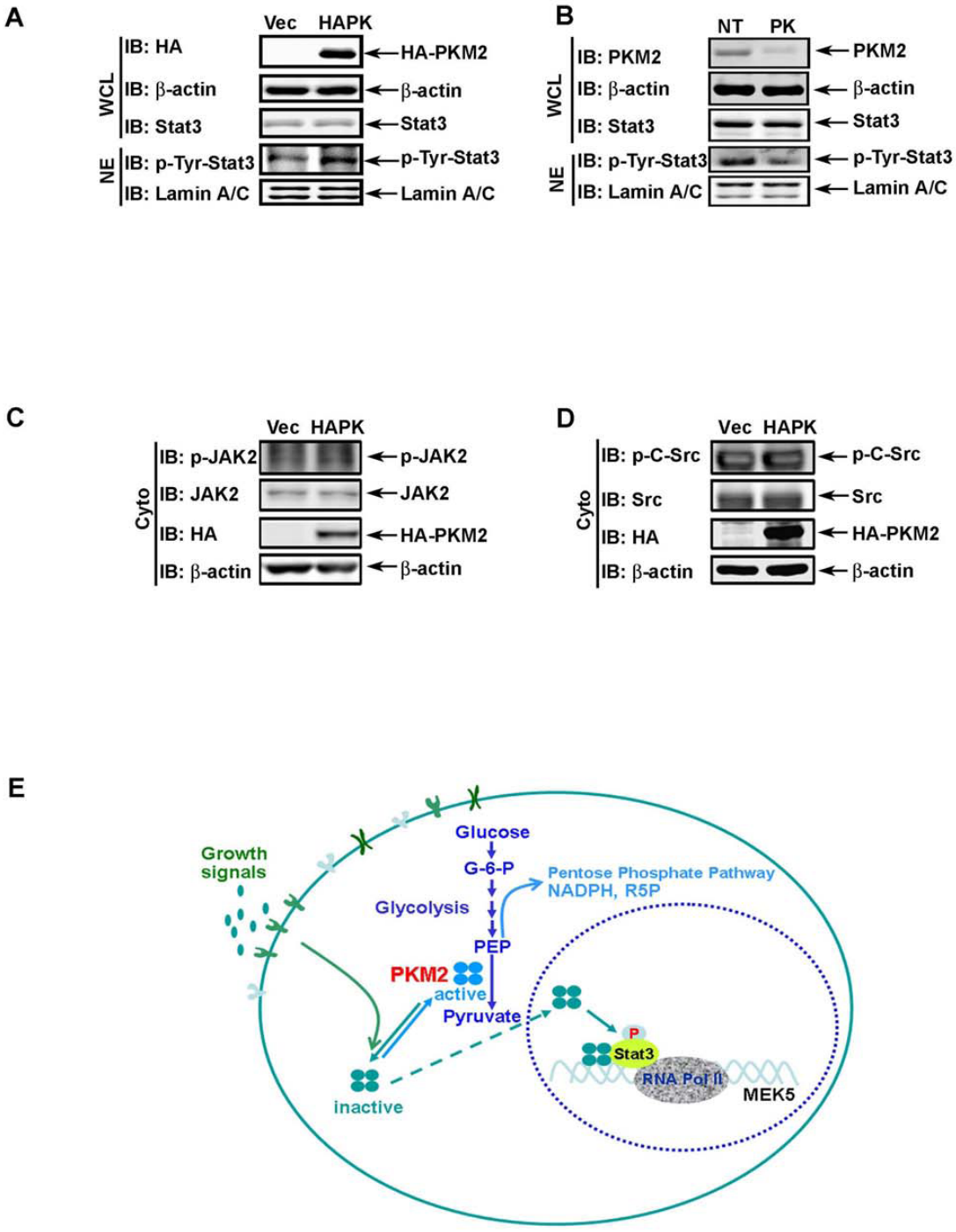
A
Vec
HAPK
WCL
IB: HA
HA-PKM2
IB: β-actin
β-actin
IB: Stat3
Stat3
NE
IB: p-Tyr-Stat3
p-Tyr-Stat3
IB: Lamin A/C
Lamin A/C
B
NT
PK
WCL
IB: PKM2
PKM2
IB: β-actin
β-actin
IB: Stat3
Stat3
NE
IB: p-Tyr-Stat3
p-Tyr-Stat3
IB: Lamin A/C
Lamin A/C
C
Vec
HAPK
Cyto
IB: p-JAK2
p-JAK2
IB: JAK2
JAK2
IB: HA
HA-PKM2
IB: β-actin
β-actin
D
Vec
HAPK
Cyto
IB: p-C-Src
p-C-Src
IB: Src
Src
IB: HA
HA-PKM2
IB: β-actin
β-actin
E
Growth signals
Glucose
G-6-P
Pentose Phosphate Pathway
NADPH, R5P
Glycolysis
PEP
PKM2
active
Pyruvate
inactive
P
Stat3
RNA Pol II
MEK5

Figure 2.6 PKM2 Phosphorylates Stat3
(A) & (B) The levels of Y705 phosphorylated stat3 (IB:p-Tyr-Stat3) in the cell nucleus were analyzed by immunoblot of nuclear extracts (NE) prepared from SW620 cells in which HAPKM2 was expressed **(A. HAPK)** or endogenous PKM2 was knocked down using the smartpool RNAi **(B, PK)**. The total cellular stat3 levels were analyzed by immunoblot analyses of stat3 (IB:Stat3) in whole cell lysate (WCL). In **(A)**, immunoblot of HA-tag (IB:HA) indicates the HA-PKM2 expression levels in the cells. In **(B)**, immunoblot of PKM2 (IB:PKM2) represents cellular PKM2 levels in the cells. Immunoblot of lamin A/C and β-actin are the loading controls. **(C) & (D)** Activation JAK2 **(B)** or c-Src **(C)** in SW620 cells in which HA-PKM2 was expressed **(HAPK)** was analyzed by immunoblot of cytoplasmic extracts (Cyto) using antibody against phosphorylated JAK2 (**B**, IB:p-JAK2) or antibody against phosphorylated c-Src (**C**, IB:p-c-Src). Vec means the cells were infected by virus carry the empty vector. Immunoblots of JAK2 (IB: JAK2) in **(B)** and c-Src (IB:Src) in **(C)** are loading control. Immunoblot of β-actin is another loading control. The expression levels of HA-PKM2 were examined by immunoblot of HA-tag. **(E)** A hypothetic model for the role of PKM2 in promoting cell proliferation.

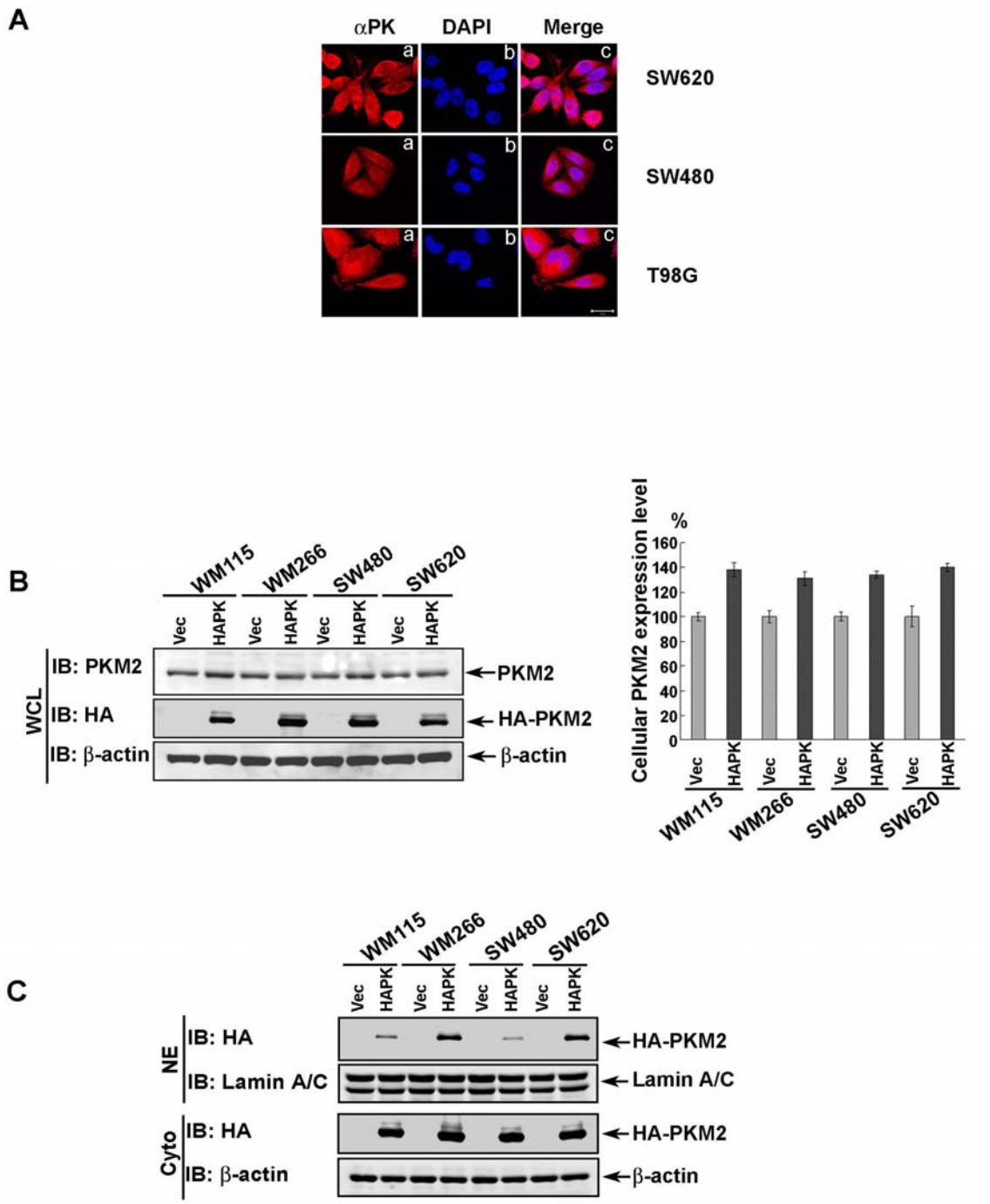
A
αPK
DAPI
Merge
a
b
c
SW620
SW480
T98G
B
WM115
WM266
SW480
SW620
Vec
HAPK
WCL
IB: PKM2
IB: HA
IB: β-actin
PKM2
HA-PKM2
β-actin
Cellular PKM2 expression level
%
160
140
120
100
80
60
40
20
0
C
NE
Cyto
IB: HA
IB: Lamin A/C
IB: β-actin
HA-PKM2
Lamin A/C
β-actin

Figure 2.7 Expression PKM2 in Cancer Cells
(**A)** Immunostaining of PKM2 using the antibody PabPKM2 in SW480, SW620, and T98G cells (indicated). The red signal represents staining of PKM2 in the cells **(a)**. The blue signal represents DAPI staining of DNA **(b)**. **(c)** is the overlay of PKM2 antibody staining and DAPI staining. **(B)** Cellular levels of PKM2 in WM115, WM266, SW480, and SW620 cells (indicated) before and 48 hours after infection of the cells with viruses that carry PKM2 expression vector (HAPK) or empty vector (Vec) were analyzed by immunoblot of PKM2 (IB:PKM2) in cell lysate using the antibody PabPKM2. The exogenously expressed HA-PKM2 was examined by immunoblot using anti-HA antibody. The right panel is quantization of immunoblot signals of IB:PKM2 by defining the IB signal before HA-PKM2 expression as 1 in each cell line. Error bars are standard deviations of three measurements. **(C)** Levels of exogenously expressed HA-PKM2 (HAPK) in the cell nucleus (NE) and the cytoplasm (Cyto) in WM115, WM266, SW480, and SW620 cells (indicated) were analyzed by immunoblot using anti-HA antibody (IB:HA). **Vec** were the cells infected with virus carrying an empty vector. In **(B)** and **(C)**, immunoblot of β-actin (IB: β-actin) and lamin A/C (IB:Lamin A/C) were loading controls.

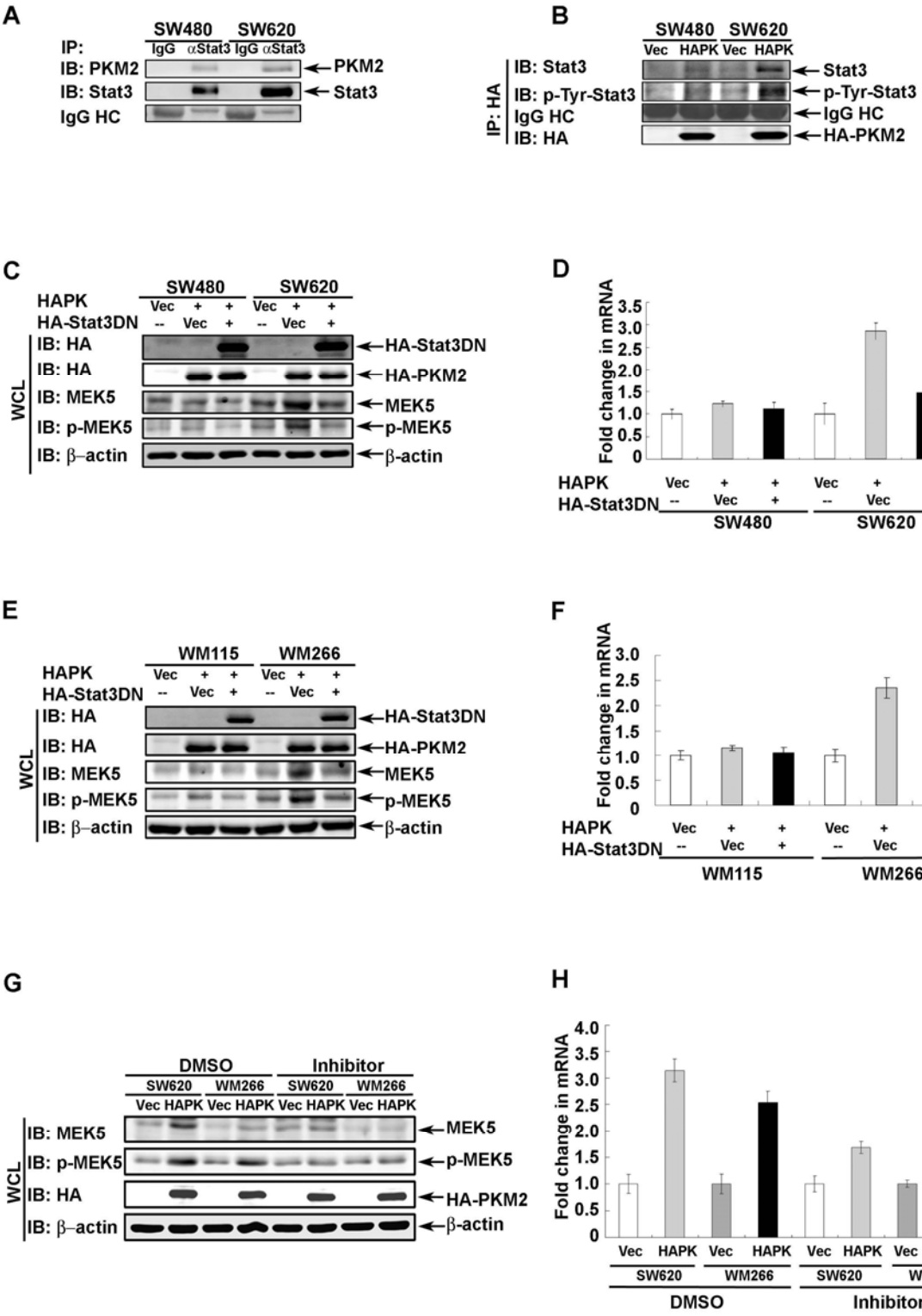
A
SW480
SW620
IP:
IgG
αStat3
IgG
αStat3
IB: PKM2
IB: Stat3
IgG HC
PKM2
Stat3
B
SW480
SW620
Vec
HAPK
Vec
HAPK
IP: HA
IB: Stat3
IB: p-Tyr-Stat3
IgG HC
IB: HA
Stat3
p-Tyr-Stat3
IgG HC
HA-PKM2
C
SW480
SW620
HAPK
HA-Stat3DN
WCL
IB: HA
IB: HA
IB: MEK5
IB: p-MEK5
IB: β–actin
HA-Stat3DN
HA-PKM2
MEK5
p-MEK5
β-actin
D
Fold change in mRNA
HAPK
HA-Stat3DN
SW480
SW620
E
WM115
WM266
HAPK
HA-Stat3DN
WCL
IB: HA
IB: HA
IB: MEK5
IB: p-MEK5
IB: β–actin
HA-Stat3DN
HA-PKM2
MEK5
p-MEK5
β-actin
F
Fold change in mRNA
HAPK
HA-Stat3DN
WM115
WM266
G
DMSO
Inhibitor
SW620
WM266
SW620
WM266
Vec HAPK Vec HAPK Vec HAPK Vec HAPK
WCL
IB: MEK5
IB: p-MEK5
IB: HA
IB: β–actin
MEK5
p-MEK5
HA-PKM2
β-actin
H
Fold change in mRNA
Vec HAPK Vec HAPK Vec HAPK Vec HAPK
SW620
WM266
SW620
WM266
DMSO
Inhibitor

Figure 2.8 PKM2 Interacts with Stat3 to Regulate MEK5 Gene Transcription
(A) & (B) Co-immunoprecipitations of endogenous PKM2 **(A)** and exogenous HAPKM2 **(B)** with stat3 were analyzed by immunoprecipitation using antibody against stat3 (IP: αstat3 in **A**) and anti-HA antibody (IP:HA in **B**) from nuclear extracts prepared from SW620 and SW480 cells. The immunoprecipitates were analyzed by immunoblot using antibodies against stat3 (IB:Stat3) or PKM2 (IB:PKM2). Ponceau S staining of IgG heave chain (IgG HC) in the immunoprecipitates is the loading control. Immunoprecipitation using rabbit IgG (IP:IgG) was the control immunoprecipitation. In **(B)**, the immunoblot using anti-HA antibody was an additional loading control. **(C) & (E)**, Expressions of MEK5 (IB:MEK5) in SW620/SW480 **(C)** and WM115/WM266 **(E)** cells were analyzed by immunoblot the whole cell lysate (WCL) prepared from the cells in which a stat3 dominant negative mutant (DNST) and HA-PKM2 (HAPK) were expressed. Immunoblot of HA-Stat3DN (IB:HA (stat3DN) and HA-PKM2 (IB:HAPK) indicated the exogenous expression levels. The cellular levels of phosphorylated MEK5 were also examined by immunoblot using the antibody against phosphorylated MEK5 (IB:p-MEK5). **(D) & (F)** RT-PCR analyses of cellular MEK5 mRNA levels in SW620/SW480 **(D)** and WM266/WM115 **(F)** cells in which a stat3 dominant negative mutant (DNST) and HAPKM2 (HAPK) were expressed. The results are presented as fold changes in PCR products before and 48 hours after the dominant negative stat3 mutant and HA-PKM2 expression in the same cells. The level of PCR products from each cell line that was infected with virus that carry the empty vector (Vec) and no stat3 mutant expression was defined as 1. **(G)** Expressions of MEK5 (IB: MEK5) in SW620/WM266 cells (indicated) were analyzed by immunoblot the whole cell lysate (WCL) prepared from the cells in which HA-PKM2 was exogenously expressed (HAPK) and that were treated with the stat3 inhibitor (Inhibitor). Cells treated with DMSO (the same amounts as used in inhibitor treatments as solvent for dissolve the inhibitor) are the control treatments. **(H)** RT-PCR analyses of cellular MEK5 mRNA levels in SW620/WM266 cells. The results are presented as fold changes in PCR products before and 48 hours after the dominant negative stat3 mutant and HA-PKM2 expression in the same cells. The level of PCR products from each cell line that was infected with virus that carry the empty vector (Vec) and no stat3 mutant expression was defined as 1. In **(C)**, **(E)**, and **(G)**, immunoblot of β-actin (IB: β-actin) is the loading control. Error bars in **(D)**, **(F),** and **(H)** are standard deviations of three measurements.

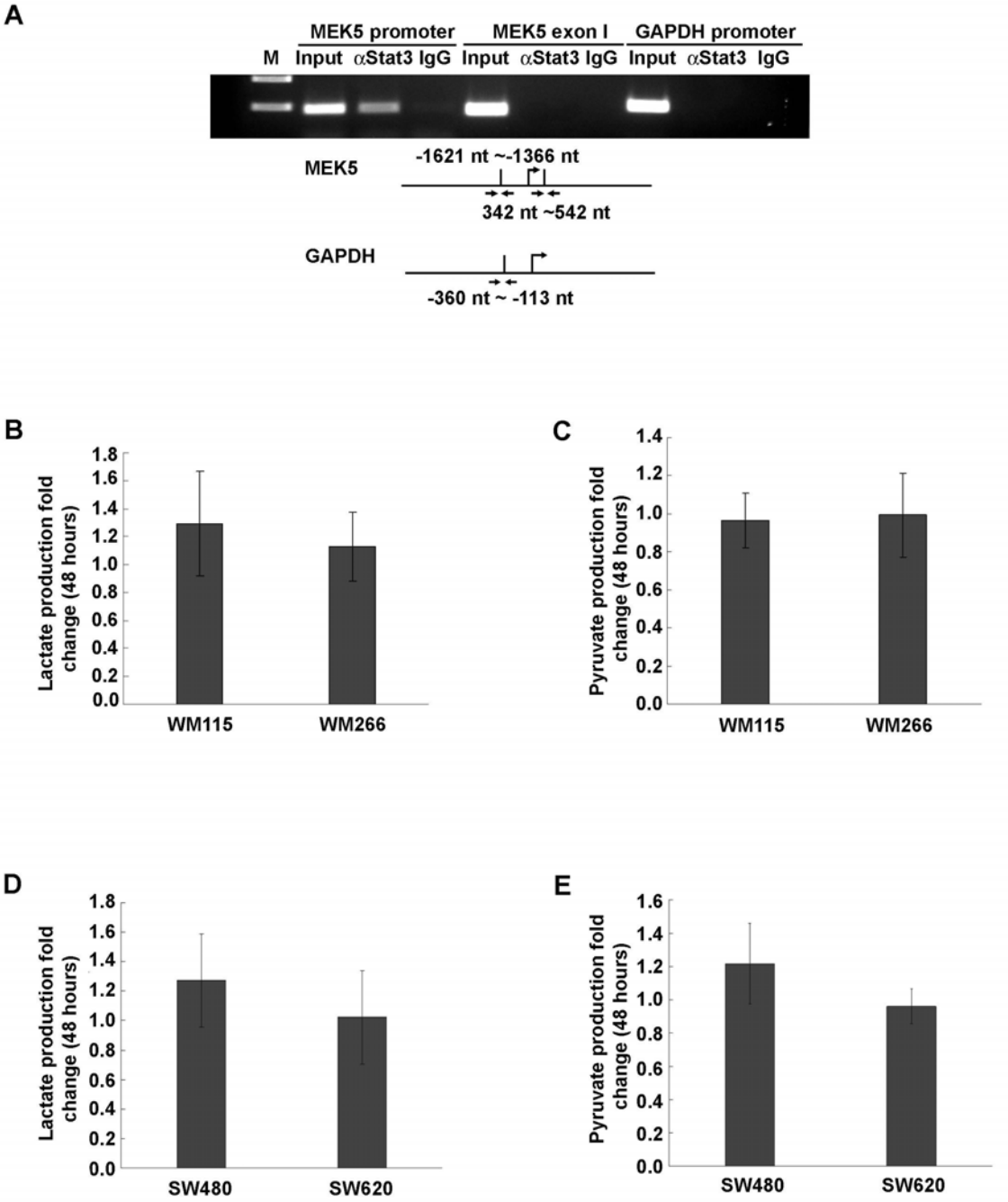
A
MEK5 promoter
MEK5 exon I
GAPDH promoter
M
Input αStat3 IgG
Input αStat3 IgG
Input αStat3 IgG
MEK5
-1621 nt ~-1366 nt
342 nt ~542 nt
GAPDH
-360 nt ~ -113 nt
B
Lactate production fold change (48 hours)
WM115
WM266
C
Pyruvate production fold change (48 hours)
WM115
WM266
D
Lactate production fold change (48 hours)
SW480
SW620
E
Pyruvate production fold change (48 hours)
SW480
SW620

Figure 2.9 PKM2 is Associated with Stat3 Promoter Region
(A) ChIP of the MEK5 promoter (MEK5 promoter) using antibody against stat3 in SW620 cells (α□Stat3). ChIP using rabbit IgG (IgG) was a negative control. ChIP using PCR primer pair targeting a region of exon 1 (MEK5 exon 1) of MEK5 gene (nt 342 – nt 542) is a negative control. ChIP targeting GAPDH promoter (GAPDH promoter) using antibody against stat3 was another negative control. The primer pair positions are indicated. Inputs were PCR products from DNA extracts without ChIP. **(B-E)** The cellular levels of lactate **(B, C)** and pyruvate **(D, E)** in WM115/WM266 **(B, D)**, and SW480/SW620 **(C, E)** cells (indicated) were analyzed using commercial pyruvate and lactate analyses kits. The results were presented as fold changes before and 48 hours after exogenous expression of HA-PKM2 using the adeno-viral system. The cellular levels of pyruvate and lactate measured by the kits in the cells before exogenous expression of HA-PKM2 were defined as 1.

Table 1 List for gene expressions regulated by PKM2 overexpression in SW480 cells

Gene ID	Gene Name	Expression Fold Change (up-regulated)	Description
10862691	ACVR1B	2.02	Homo sapiens activin A receptor, type IB (ACVR1B), transcript variant 2, mRNA
5901887	ADAMTS5	2.04	Homo sapiens a disintegrin-like and metalloprotease (reprolysin type) with thrombospondin type 1 motif
349268	ADCY1	3.51	Human fetal brain adenylyl cyclase mRNA, 3 end.
3139026	AF10	2.09	Homo sapiens type V AF10 protein (AF10) Mrna
4502050	ALOX12	2.31	Homo sapiens arachidonate 12-lipoxygenase (ALOX12)
10190675	ANKRD3	2.85	Homo sapiens ankyrin repeat domain 3 (ANKRD3)
2210410	AP1S2	2.24	adaptor-related protein complex 1, sigma 2 subunit
28771	APOA1	3.65	Human mRNA for apolipoprotein AI (apo AI)
13937840	ATM	2.19	Homo sapiens, Similar to ataxia telangiectasia mutated (includes complementation groups A, C and D), clone MGC:12371
3849111	ATP6H	2.38	ATPase, H+ transporting, lysosomal (vacuolar proton pump) 9kD
13603411	B29	2.67	Homo sapiens B29 mRNA, complete cds.
13111840	BART1	2.18	binder of Arl Two
3307010	BCAA	2.98	RBP1-like protein
219494	BGP	3.14	Human mRNA for biliary glycoprotein, complete cds
19756424	BIRC5	2.46	baculoviral IAP repeat-containing 5 (survivin)
9945321	BNPI	2.11	Homo sapiens brain-specific Na-dependent inorganic phosphate cotransporter (BNPI)
10437300	C14orf85	2.88	Homo sapiens cDNA: FLJ21234 fis, clone COL00841
5361475	C21ORF23	2.20	chromosome 21 open reading frame 23

4188559	CALR	3.05	calreticulin
3049661	CALR	3.07	calreticulin
9966860	CATX-8	2.07	Homo sapiens CATX-8 protein (CATX-8), mRNA.
5450397	CCND1	2.50	cyclin D1 (PRAD1: parathyroid adenomatosis 1)
11141862	CLDN6	2.63	Homo sapiens claudin 6 (CLDN6), mRNA
18141077	CNK2	2.03	Homo sapiens connector enhancer of KSR2A mRNA
5393570	CNN3	2.15	calponin 3, acidic
4503086	CSN2	2.39	Homo sapiens casein, beta (CSN2), mRNA
6807697	DKFZp434A1014	2.36	Homo sapiens mRNA; cDNA DKFZp434A1014 (from clone DKFZp434A1014)
5912137	DKFZp434H168	2.22	hypothetical protein
12053074	DKFZp434N1817	2.98	Homo sapiens mRNA; cDNA DKFZp434N1817 (from clone DKFZp434N1817)
4884089	DKFZp564C196	3.88	Homo sapiens mRNA; cDNA DKFZp564C196 (from clone DKFZp564C196)
13183072	DKFZP586K0717	2.48	Homo sapiens multi-PDZ-domain-containing protein mRNA
10823629	DLG5	2.00	discs, large (Drosophila) homolog 5
2046909	EIF5A	3.36	eukaryotic translation initiation factor 5A
10729178	EPS15R	2.20	epidermal growth factor receptor substrate EPS15R
6505954	ETV5	2.28	ets variant gene 5 (ets-related molecule)
7455945	ETV5	2.16	ets variant gene 5 (ets-related molecule)
11006648	FBXL7	2.67	f-box and leucine-rich repeat protein 7
11056051	FCGR2A	2.24	Homo sapiens Fc fragment of IgG, low affinity IIa, receptor for (CD32) (FCGR2A)
4758357	FGD1	2.03	Homo sapiens faciogenital dysplasia (Aarskog-Scott syndrome) (FGD1),
9622332	FGF5	2.12	Homo sapiens fibroblast growth factor 5 short variant (FGF5), alternatively spliced
13186264	FGFR2	3.72	Homo sapiens fibroblast growth factor receptor 2 (bacteria-expressed kinase, keratinocyte growth factor receptor
814986	FLJ10154	2.32	hypothetical protein FLJ10154
10941605	FLJ10287	2.33	hypothetical protein

5855915	FLJ10342	2.43	hypothetical protein FLJ10342
3483211	FLJ11193	2.27	Homo sapiens full length insert cDNA clone YP41C12
1483671	FLJ13195	2.22	hypothetical protein FLJ13195 similar to stromal antigen 3
22749176	FLJ36779	2.31	Homo sapiens hypothetical protein FLJ36779 (FLJ36779)
27734816	FLJ39058	2.00	Homo sapiens hypothetical protein FLJ39058 (FLJ39058)
1228635	FLRT3	2.40	fibronectin leucine rich transmembrane protein 3
4503734	FOXC1	2.02	forkhead box C1
3416539	FOXD1	2.30	forkhead box D1
6912371	FOXD3	4.64	Homo sapiens forkhead box D3 (FOXD3), mRNA
8393383	G8	2.52	Homo sapiens G8 protein (G8), mRNA.
1754748	GABAA receptor gamma 3 subunit	2.11	GABAA receptor gamma 3 subunit (human, fetal brain, mRNA Partial, 1536 nt)
20202213	GAD2	3.17	glutamate decarboxylase 2 (pancreatic islets and brain)
4406347	GCAP3	3.59	Homo sapiens guanylate cyclase activating protein 3 splice variant (GCAP3) mRNA
4758433	GHSR	3.33	Homo sapiens growth hormone secretagogue receptor (GHSR)
3400047	GLP	2.71	golgin-like protein
28269674	GPR126	3.40	G protein-coupled receptor 126
6006002	GRIN2A	4.39	Homo sapiens glutamate receptor, ionotropic, N-methyl D-aspartate 2A (GRIN2A)
6005773	GUCA2B	5.02	Homo sapiens guanylate cyclase activator 2B (uroguanylin) (GUCA2B), mRNA
9867563	H41	2.02	hypothetical protein
13549111	HBB	2.33	Homo sapiens beta globin chain variant (HBB) mRNA, complete cds.
5928292	HDAC3	2.28	histone deacetylase 3
1597725	HLA-DRB4	2.48	Homo sapiens HLA class II DRB4 null antigen (HLA-DRB4) pseudogene mRNA, null allele HLA-DRB4*0201N
13489076	HOXA6	2.24	Homo sapiens homeo box A6 (HOXA6), mRNA.
3461865	HSPA1L	2.09	Heat shock protein 70 testis variant

7019420	HUMBINDC	2.54	Homo sapiens DNA binding protein for surfactant protein B (HUMBINDC), mRNA.
4504590	IFNA14	2.98	Homo sapiens interferon, alpha 14 (IFNA14), mRNA
10835102	IFNA4	2.71	Homo sapiens interferon, alpha 4 (IFNA4), mRNA.
4504706	INPP4B	2.32	Homo sapiens inositol polyphosphate-4-phosphatase, type II, 105kD (INPP4B), mRNA
13050848	INSIG1	2.03	insulin induced gene 1
4072135	ITGB5	2.13	integrin, beta 5
6912441	KCNE1L	2.08	Homo sapiens potassium voltage-gated channel, Isk-related family, member 1-like (KCNE1L)
7657246	KCNIP1	2.23	Homo sapiens Kv channel-interacting protein 1 (KCNIP1), mRNA
1193698	KIAA0256	2.09	KIAA0256 gene product
3327077	KIAA0632	2.33	Homo sapiens mRNA for KIAA0632 protein, partial cds.
10828334	KIAA0644	2.14	KIAA0644 gene product
11445251	KIAA0847	2.25	KIAA0847 protein
9792490	KIAA0964	2.24	KIAA0964 protein
10940593	KIAA1096	2.02	KIAA1096 protein
1552995	KLF1	2.76	Human erythroid-specific transcription factor EKLF mRNA, complete cds.
6007796	Kv4.3	3.38	Homo sapiens voltage gated potassium channel Kv4.3 short splice variant (Kv4.3)
8923829	LEP503	2.24	Homo sapiens lens epithelial protein (LEP503), mRNA.
4150402	LOC145622	3.45	hypothetical protein LOC145622
21687187	LOC146325	2.63	Homo sapiens similar to hypothetical protein FLJ13841 (LOC146325)
16553309	LOC149086	3.30	Homo sapiens cDNA FLJ33000 fis, clone THYMU1000191.
24270838	LOC283403	2.29	Homo sapiens, clone IMAGE:5268545, mRNA.
3923425	LOC284889	4.76	hypothetical protein LOC284889
13277527	LOC51065	2.07	Homo sapiens, Similar to 40S ribosomal protein S27 isoform, clone MGC:12175

10911294	LOC286411	2.97	hypothetical protein LOC286411
12770474	LOC55884	2.10	CS box-containing WD protein
1720456	LOC56851	2.65	chromosome 11 hypothetical protein ORF3
5394758	LOC56993	2.46	mitochondrial import receptor Tom22
19913482	LOC57821	2.38	Homo sapiens, Similar to hypothetical protein LOC57821, clone MGC:26487
4523295	LOC57863	2.77	hypothetical protein FLJ10698
4505016	LRP6	2.67	Homo sapiens low density lipoprotein receptor-related protein 6 (LRP6), mRNA
11081627	LSP1	2.50	lymphocyte-specific protein 1
3387766	m6b1	2.02	glycoprotein M6B /DEF=Homo sapiens m6b1 mRNA, complete cds.
1616780	MAP2K5	5.04	Human MAP kinase kinase MEK5c mRNA, complete cds.
4885476	MB	2.05	Homo sapiens myoglobin (MB), mRNA
4337095	MEGT1	2.25	Homo sapiens MSH55 gene, partial cds; and CLIC1, DDAH, G6b, G6c,
219881	MS4A1	2.23	Homo sapiens mRNA for IgE receptor beta subunit, complete cds.
12803920	MS4A2	2.11	Homo sapiens, membrane-spanning 4-domains, subfamily A, member 2, clone MGC:3969
5031926	MUSK	2.05	Homo sapiens muscle, skeletal, receptor tyrosine kinase (MUSK), mRNA
4505376	NEUROD1	3.53	Homo sapiens neurogenic differentiation 1 (NEUROD1), mRNA.
6133390	NOLA2	2.24	nucleolar protein family A, member 2 (HACA small nucleolar RNPs)
11452542	NOV	2.01	nephroblastoma overexpressed gene
7669529	NRG2	2.07	Homo sapiens neuregulin 2 (NRG2), transcript variant 3, mRNA
18087816	NY-REN-41	2.03	Homo sapiens NY-REN-41 antigen (NY-REN-41)
5110327	OGT	2.16	O-linked N-acetylglucosamine (GlcNAc) transferase (UDP-N-acetylglucosamine:polypep)
21104485	OKSW-cl.92	2.55	Homo sapiens OKSW-cl.92 mRNA, complete cds.
11545886	OT7T022	2.45	Homo sapiens neuropeptide FF 1; RFamide-related peptide receptor (OT7T022), mRNA.
7524355	PAX3	2.81	Homo sapiens paired box gene 3 (Waardenburg syndrome 1) (PAX3), transcript variant PAX3B

6679187	P-B	3.92	Homo sapiens salivary proline-rich protein (P-B), mRNA.
4406228	PPIE	2.09	Homo sapiens peptidyl-prolyl cis-trans isomerase E (PPIE) mRNA, alternatively spliced
4989070	PPM1A	2.30	protein phosphatase 1A (formerly 2C), magnesium-dependent, alpha isoform
4328589	PRO1073	2.25	PRO1073 protein
7662589	PRO1073	2.22	Homo sapiens PRO1073 protein (PRO1073), mRNA.
7770170	PRO2214	2.25	Homo sapiens PRO2214 mRNA
7770218	PRO2706	2.12	Homo sapiens PRO2706 mRNA
2552941	PSMB4	2.61	proteasome (prosome, macropain) subunit, beta type, 4
726735	RAD23B	2.43	RAD23 (S. cerevisiae) homolog B
6691625	RAGE	3.15	Homo sapiens RAGE mRNA for advanced glycation endproducts receptor
4506420	RARB	3.81	Homo sapiens retinoic acid receptor, beta (RARB), mRNA
1072311	RGN	2.14	Human mRNA for SMP-30 (senescence marker protein-30)
13097176	RPL10	2.06	ribosomal protein L10
4489788	RPL23A	2.52	ribosomal protein L23a
9130191	RPL27	2.52	ribosomal protein L27
10151019	RPL27A	4.56	ribosomal protein L27a
10372131	RPL37A	2.92	ribosomal protein L37a
6712816	RPL38	2.14	ribosomal protein L38
13529169	RPLP2	2.50	ribosomal protein, large P2
11954150	RPS11	6.10	ribosomal protein S11
12652562	RPS19	4.07	Homo sapiens, ribosomal protein S19, clone MGC:1630
6642739	RPS20	2.12	Homo sapiens clone FLB0708 mRNA sequence.
11683880	RREB1	2.09	ras responsive element binding protein 1
4678742	RS1	3.47	retinoschisis (X-linked, juvenile) 1
1052870	SCCA2	2.12	Human squamous cell carcinoma antigen 2 (SCCA2)
11493551	SCD	2.73	Homo sapiens PRO1933 mRNA, complete cds.
820298	SEC14L2	2.96	SEC14 (S. cerevisiae)-like 2

10031679	SEL1L	2.58	sel-1 (suppressor of lin-12, C.elegans)-like
306441	SLC3A1	2.47	Homo sapiens amino acid transport protein
10940859	SMURF2	2.38	E3 ubiquitin ligase SMURF2
6569554	SNRPG	3.46	small nuclear ribonucleoprotein polypeptide G
10863910	SPINK2	4.24	Homo sapiens serine protease inhibitor, Kazal type, 2 (acrosin-trypsin inhibitor) (SPINK2)
4557870	TF	2.67	Homo sapiens transferrin (TF), mRNA
10820568	TGFB2	2.54	transforming growth factor, beta 2
12407428	TRIM14	2.32	Homo sapiens tripartite motif protein TRIM14 alpha (TRIM14) mRNA, alternatively spliced.
3153858	TXN delta 3	2.25	Homo sapiens thioredoxin delta 3 (TXN delta 3) mRNA, partial cds.
3056223	UBE2H	2.16	ubiquitin-conjugating enzyme E2H (homologous to yeast UBC8)
6457377	VIL2	3.64	Homo sapiens cytovillin 2 (VIL2) mRNA, partial cds
4991221	WNT5A	2.83	wingless-type MMTV integration site family, member 5A
22477810		2.40	Homo sapiens, Similar to RIKEN cDNA 4930442L21 gene, clone MGC:34773
18478590		2.58	Homo sapiens prostate-specific KLK2 mRNA, complete cds, alternatively spliced
21750477		2.12	Homo sapiens cDNA FLJ34667 fis, clone LIVER2000769
3017252		2.20	Homo sapiens mRNA; cDNA DKFZp564M243 (from clone DKFZp564M243)
16553266		3.37	Homo sapiens cDNA FLJ32963 fis, clone TESTI2008405.
652989		3.96	Homo sapiens cDNA FLJ34653 fis, clone KIDNE2018287.
21750410		2.51	Homo sapiens cDNA FLJ34611 fis, clone KIDNE2014112.
21706985		3.61	Homo sapiens cDNA FLJ33147 fis, clone UTERU2000218
3483352		2.19	Homo sapiens full length insert cDNA clone YU66F10.
5111893		2.16	Homo sapiens cDNA FLJ37762 fis, clone BRHIP2024347, weakly similar to GALECTIN-3.
18089211		2.29	Homo sapiens, clone IMAGE:4732650, mRNA
13283225		2.05	Human mRNA upregulated during camptothecin-induced apoptosis of U937

			cells.
9325152		2.08	Homo sapiens full length insert cDNA clone ZD79H04
15943770		2.94	Homo sapiens, clone IMAGE:5404026, mRNA
2265537		2.03	Homo sapiens cDNA FLJ36460 fis, clone THYMU2014801.
27694447		2.48	Homo sapiens, clone IMAGE:6155889, mRNA.
21391489		2.13	Homo sapiens D21S2088E mRNA sequence.
4895021		2.55	Homo sapiens clone IMAGE:120631 mRNA sequence.
21752222		2.00	Homo sapiens cDNA FLJ36051 fis, clone TESTI2018083.
23138779		4.45	Homo sapiens, clone IMAGE:4799886, mRNA.
23271185		2.54	Homo sapiens, clone IMAGE:4723617, mRNA.
22749602		2.52	Homo sapiens, clone IMAGE:5167209, mRNA.
24659364		2.17	Homo sapiens, clone IMAGE:5762932, mRNA.
10717930		2.84	chromosome 14 open reading frame 70
10719117		2.02	Homo sapiens, clone IMAGE:4732650, mRNA
16553158		2.11	Homo sapiens cDNA FLJ32886 fis, clone TESTI2004255.
15080371		2.42	Homo sapiens, clone IMAGE:4541510, mRNA.
562424		2.34	Homo sapiens cDNA FLJ33351 fis, clone BRACE2005063.
15929454		6.42	Homo sapiens, clone IMAGE:3885734, mRNA.
27370602		2.60	Homo sapiens, clone IMAGE:5272850, mRNA.
21755882		2.16	Homo sapiens cDNA FLJ39080 fis, clone NT2RP7018197.
23273407		2.09	Homo sapiens, clone IMAGE:4821940, mRNA.
21707002		2.29	Homo sapiens, clone IMAGE:4838775, mRNA, partial cds.
15492406		2.15	Homo sapiens, clone IMAGE:5288527, mRNA
4761757		2.18	Homo sapiens full length insert cDNA clone YP51C12.
16551907		2.99	Homo sapiens cDNA FLJ31929 fis, clone NT2RP7006160.
26251840		3.10	Homo sapiens, clone IMAGE:5270242, mRNA.
23138689		2.01	Homo sapiens, clone IMAGE:5284251, mRNA.
27695778		2.00	Homo sapiens, clone IMAGE:5287262, mRNA.

9368862		5.02	Homo sapiens mRNA; cDNA DKFZp547B124 (from clone DKFZp547B124).
22789247		2.21	Homo sapiens, clone IMAGE:5284619, mRNA.
23243297		2.44	Homo sapiens, Similar to hypothetical protein FLJ1066
26251897		2.45	Homo sapiens, clone IMAGE:5744232, mRNA
15929532		2.93	Homo sapiens, clone IMAGE:4272661, mRNA
21733910		3.02	Homo sapiens mRNA; cDNA DKFZp451E068 (from clone DKFZp451E068).
27693443		5.55	Homo sapiens, clone IMAGE:5297745, mRNA.
21748888		2.02	Homo sapiens cDNA FLJ33360 fis, clone BRACE2005253.
18645132		2.38	Homo sapiens, clone IMAGE:4106638, mRNA, partial cds
18490345		2.24	Homo sapiens, clone IMAGE:4280848, mRNA.
13543960		2.03	Homo sapiens, clone IMAGE:3505629, mRNA, partial cds
7998994		2.28	Human mucin mRNA, partial CDS
19048193		2.56	Homo sapiens, clone IMAGE:4838884, mRNA
27469480		2.46	Homo sapiens, clone IMAGE:5303725, mRNA
21707013		3.17	Homo sapiens, clone IMAGE:5278245, mRNA.
21733665		2.06	Homo sapiens mRNA; cDNA DKFZp451E0119 (from clone DKFZp451E0119).
9880662		3.25	Homo sapiens trapped 3 terminal exon, clone B2D7
23138784		2.14	Homo sapiens, clone IMAGE:4815137, mRNA.
1314791		3.24	Human oral cancer candidate gene mRNA, clone T9, 3 end.
3245917		3.30	Homo sapiens, clone IMAGE:4828827, mRNA
22773448		2.16	Homo sapiens, clone IMAGE:4798439, mRNA.
12872929		2.28	Homo sapiens, clone IMAGE:4295896, mRNA
18266902		2.06	Homo sapiens, clone IMAGE:3920449, mRNA.
19387911		2.13	Homo sapiens, clone IMAGE:4876018, mRNA.
17315156		2.22	Homo sapiens, clone IMAGE:4622909, mRNA.
23138810		2.05	Homo sapiens, clone IMAGE:5285294, mRNA.
23025744		2.09	Homo sapiens, Similar to hypothetical protein MGC5149,
15214740		2.54	Homo sapiens, clone IMAGE:4708704, mRNA.

23272857		2.61	Homo sapiens, clone IMAGE:5583231, mRNA.
21955461		3.82	Homo sapiens, clone IMAGE:4824334, mRNA.
22382161		3.48	Homo sapiens, clone IMAGE:4770655, mRNA.
19387889		2.74	Homo sapiens, clone IMAGE:4544545, mRNA.
18204260		2.21	Homo sapiens, Similar to zinc finger protein
22902336		2.34	Homo sapiens, clone IMAGE:4475530, mRNA.
22658409		2.32	Homo sapiens, clone IMAGE:5106435, mRNA.
14713658		2.43	Homo sapiens, clone IMAGE:4290767, mRNA.
18988609		2.07	Homo sapiens, clone IMAGE:3936226, mRNA
21961399		2.05	Homo sapiens, clone IMAGE:4401081, mRNA.
13543476		2.18	Homo sapiens, hyaluronoglucosaminidase 3, clone MGC:14472
897614		2.17	Homo sapiens transmembrane tyrosine kinase mRNA, complete cds.
5053998		2.05	Human BRCA2 region, mRNA sequence CG011
6698300		2.10	Homo sapiens cDNA: FLJ21771 fis, clone COLF7779
9368876		2.22	Homo sapiens mRNA; cDNA DKFZp547N074 (from clone DKFZp547N074)
10435808		2.10	Homo sapiens cDNA FLJ13712 fis, clone PLACE2000394.
7947076		2.28	Human soluble CD44 (CD44) mRNA, with exon v9 extension, partial cds
10432666		2.35	Homo sapiens cDNA FLJ11412 fis, clone HEMBA1000876
527579		3.28	H.sapiens mRNA for ribosomal protein L18a homologue
7328007		2.30	Homo sapiens mRNA; cDNA DKFZp434H0229
10440237		2.11	Homo sapiens cDNA: FLJ23519 fis, clone LNG04908
6197723		2.32	ESTs, Weakly similar to ALUF_HUMAN
10810430		2.35	ESTs, Weakly similar to AF208855 1 BM-013
4874618		2.64	ESTs, Highly similar to T-box-containing transcriptional activator
12005981		2.06	Homo sapiens DC37 mRNA, complete cds.
11493436		2.41	Homo sapiens clone FLB8034 PRO2158 mRNA, complete cds
6983841		2.73	Homo sapiens mRNA for tomoregulin, complete cds
12006208		3.44	Homo sapiens DC48 mRNA, complete cds.

13623316		3.46	Homo sapiens, clone MGC:10724, mRNA, complete cds
13603378		2.59	Homo sapiens 5-nucleotidase I mRNA, complete cds
1126361		2.40	ESTs
4610307		2.89	Homo sapiens cDNA: FLJ21410 fis, clone COL03938
7246662		2.95	ESTs, Weakly similar to KIAA1204 protein (H.sapiens)
9867611		2.91	ESTs, Weakly similar to ALU7
5448126		2.71	Homo sapiens cDNA: FLJ21042 fis, clone CAE11204
4997672		2.68	ESTs
11263724		2.00	ESTs
10030244		2.33	ESTs
5854418		2.30	ESTs
11130642		2.18	Homo sapiens mRNA; cDNA DKFZp586J0720
5054233		2.89	ESTs
2874383		2.56	Homo sapiens cDNA FLJ10500 fis, clone NT2RP2000369
10825381		2.23	ESTs
5513942		2.67	ESTs, Highly similar to I38945 melanoma ubiquitous mutated protein
9704374		2.14	Homo sapiens cDNA FLJ12936 fis, clone NT2RP2005018
10585982		2.42	ESTs
2898542		2.17	ESTs
2878893		2.40	Homo sapiens cDNA: FLJ21715 fis, clone COL10287, highly similar to AF071569 multifunctional
10301536		2.40	ESTs
11593563		2.40	ESTs
7799136		3.00	Homo sapiens EST from clone 208499, full insert
11007502		2.50	Homo sapiens cDNA FLJ12030 fis, clone HEMBB1001868
11016719		2.01	Homo sapiens cDNA FLJ10941 fis, clone OVARC1001243
2261986		2.25	Homo sapiens HSPC106 mRNA, partial cds
10433162		2.02	Homo sapiens cDNA FLJ11814 fis, clone HEMBA1006381.

10438582		4.22	Homo sapiens cDNA: FLJ22266 fis, clone HRC03089.
10432694		2.51	Homo sapiens cDNA FLJ11437 fis, clone HEMBA1001226
6808434		2.99	Homo sapiens mRNA; cDNA DKFZp434E145
5912099		2.83	Homo sapiens mRNA; cDNA DKFZp566O1624
11008881		2.42	Homo sapiens cDNA FLJ12212 fis, clone MAMMA1000979
10433290		2.04	Homo sapiens cDNA FLJ11919 fis, clone HEMBB1000274.
4406668		5.86	Homo sapiens clone 24894 mRNA sequence.
4884225		3.26	Homo sapiens mRNA; cDNA DKFZp564B032
3766130		3.41	Homo sapiens PAC clone RP4-669B10 from 7q33-q35
10439146		2.25	Homo sapiens cDNA: FLJ22668 fis, clone HSI08585.
10439819		4.20	Homo sapiens cDNA: FLJ23208 fis, clone ADSE01253.
4500031		3.26	Homo sapiens mRNA; cDNA DKFZp564I103
876413		2.59	ESTs
4070155		2.10	ESTs
7247381		2.22	ESTs
10822124		2.05	ESTs
4311165		2.55	ESTs
5741187		2.73	ESTs
4738586		2.23	ESTs
3898470		2.39	ESTs
696583		2.01	ESTs, Weakly similar to alternatively spliced product using exon 13A
4896021		3.37	ESTs
6702839		4.08	ESTs
10939000		2.66	ESTs
3052775		2.23	ESTs
2782919		3.11	ESTs
8909427		2.65	ESTs
9703764		2.68	ESTs

1227643		2.37	ESTs
10301882		2.08	ESTs
9869489		2.25	ESTs
1225259		2.38	ESTs
11592084		2.11	ESTs
697122		4.68	ESTs
4985432		2.32	ESTs
7148710		2.35	ESTs
1505796		2.32	ESTs
8156739		2.64	ESTs
3109118		2.90	ESTs
11547763		2.04	ESTs
8888160		5.14	ESTs
8157795		2.75	ESTs, Weakly similar to AF108460 1 ubinuclein
5340596		2.20	ESTs
2006798		2.38	ESTs
6496811		2.39	ESTs
6496811		2.43	ESTs
9179366		2.26	ESTs
11600065		2.20	ESTs
3427699		3.24	ESTs
5111876		2.56	ESTs
8905208		2.09	ESTs
13340980		2.36	ESTs
2052997		2.25	ESTs
5054311		3.72	ESTs
4083674		3.16	ESTs
7457491		2.76	ESTs

817755		2.66	ESTs
648511		2.04	ESTs
5054307		2.96	ESTs
6661498		2.04	ESTs
11598629		2.54	ESTs
6444844		2.12	ESTs
8007397		2.56	ESTs
8472949		2.23	ESTs, Moderately similar to pyruvate dehydrogenase E1-alpha subunit precursor
10032681		3.27	ESTs, Weakly similar to ALUA_HUMAN
9867191		2.11	ESTs
5887371		2.04	ESTs, Weakly similar to CYA6_HUMAN ADENYLATE CYCLASE, TYPE VI
12057724		4.64	ESTs
821774		2.19	ESTs
6087291		2.06	ESTs
867415		2.03	ESTs
5768395		2.56	ESTs
3143651		2.05	ESTs
11599277		2.20	ESTs
12512341		2.22	ESTs
3959771		2.00	ESTs
3041371		2.05	ESTs
12356555		2.26	ESTs
5393539		2.64	ESTs
3412614		5.54	ESTs
1484744		2.37	ESTs
4147560		2.09	ESTs
2910255		2.40	ESTs

9792941		3.15	ESTs
Gene ID	**Gene Name**	**Expression Fold Change (down regulated)**	**Description**
10321660	ACP1	-4.00	Acid phosphatase 1, soluble
5901889	ADAMTS8	-2.06	Homo sapiens a disintegrin-like and metalloprotease (reprolysin type) with thrombospondin type 1 motif, 8 (ADAMTS8), mRNA
4501922	ADCYAP1R1	-2.05	Homo sapiens adenylate cyclase activating polypeptide 1 (pituitary) receptor type I (ADCYAP1R1)
5453538	ADE2H1	-2.24	Homo sapiens multifunctional polypeptide similar to SAICAR synthetase and AIR carboxylase (ADE2H1)
11061448	ADIR	-2.78	Homo sapiens mRNA for ATP-dependant interferon response protein 2 (ADIR gene)
1306665	AGA	-2.77	aspartylglucosaminidase
2155239	AGPAT2	-2.15	Human lysophosphatidic acid acyltransferase-beta mRNA
5529662	ANXA2	-2.14	annexin A2
11038642	AP2S1	-2.90	Homo sapiens adaptor-related protein complex 2, sigma 1 subunit (AP2S1), transcript variant AP17delta,
5848763	APLP2	-2.02	Amyloid beta (A4) precursor-like protein 2
7662085	ARHGEF11	-2.72	Homo sapiens Rho guanine exchange factor (GEF) 11 (ARHGEF11), mRNA
5031602	ARL4	-2.31	Homo sapiens ADP-ribosylation factor-like 4 (ARL4), mRNA
2094740	ARNTL	-2.26	Homo sapiens mRNA for BMAL1e, complete cds
4757779	ARRB2	-2.47	Homo sapiens arrestin, beta 2 (ARRB2), mRNA
12275865	ATDC	-2.74	Homo sapiens tripartite motif protein TRIM29 beta mRNA, complete cds
5437188	AXIN2	-2.34	Axin 2 (conductin, axil)
13569945	BA108L7.2	-2.46	Homo sapiens similar to rat tricarboxylate carrier-like protein (BA108L7.2), mRNA

12751138	BAL	-2.48	Homo sapiens B aggressive lymphoma long isoform (BAL) mRNA, complete cds
4757837	BAX	-2.19	Homo sapiens BCL2-associated X protein (BAX), mRNA
4502380	BCL2L1	-3.30	Homo sapiens BCL2-like 1 (BCL2L1), mRNA
13112010	BENE	-3.90	Homo sapiens, clone MGC:4419, mRNA, complete cds
9878618	BIG2	-3.68	brefeldin A-inhibited guanine nucleotide-exchange protein 2
17511794	bioref	-2.28	Homo sapiens, clone MGC:31940 IMAGE:4553653, mRNA, complete cds
16359168	BITE	-2.24	Homo sapiens, Similar to p10-binding protein, clone MGC:22949 IMAGE:4858367, mRNA
2778778	BLVRA	-4.31	biliverdin reductase A
686012	BRPF3	-2.27	bromodomain and PHD finger containing, 3
3739598	C11ORF15	-2.87	chromosome 11 open reading frame 15
10287071	CALM3	-2.41	calmodulin 3 (phosphorylase kinase, delta)
4086141	CALR	-3.46	Calreticulin
12056961	CAST	-3.12	Homo sapiens calpastatin mRNA, complete cds
4826664	CCS	-2.15	Homo sapiens copper chaperone for superoxide dismutase (CCS), mRNA
1137068	CD74	-2.63	CD74 antigen (invariant polypeptide of major histocompatibility complex, class II antig
12923866	CDS2	-2.02	CDP-diacylglycerol synthase (phosphatidate cytidylyltransferase) 2
15126732	CGI-18	-2.26	Homo sapiens, Similar to CGI-18 protein, clone MGC:8735 IMAGE:3858865
1230376	CGI-56	-2.41	beta-parvin
4885104	CHAF1B	-4.70	Homo sapiens chromatin assembly factor 1, subunit B (p60) (CHAF1B), mRNA
1905899	CKAP1	-2.03	Homo sapiens DNA from chromosome 19-cosmid f24590 containing CAPNS and POL2RI
4502876	CLDN4	-2.63	Homo sapiens claudin 4 (CLDN4), mRNA
6005734	COPE	-3.15	Homo sapiens coatomer protein complex, subunit epsilon (COPE), mRNA
3641620	CPD	-2.04	Homo sapiens mRNA for gp180-carboxypeptidase D-like enzyme, complete cds

12751066	CRI1	-2.15	Homo sapiens PNAS-26 mRNA, complete cds
15341933	CRYZL1	-2.10	Homo sapiens, clone MGC:8826 IMAGE:3870188, mRNA, complete cds
6397524	CTL1	-2.24	Transporter-like protein
11591983	CTRL	-2.56	chymotrypsin-like
18482479	CXADR	-2.46	Homo sapiens coxsackie-adenovirus-receptor isoform CAR37 (CXADR)
3551833	DAGK1	-2.09	Homo sapiens clone 24 diacylglycerol kinase alpha (DAGK1) mRNA, complete cds
4503318	DGUOK	-3.66	Homo sapiens deoxyguanosine kinase (DGUOK), mRNA
7108341	DHPS	-2.35	Homo sapiens deoxyhypusine synthase (DHPS), transcript variant 1, mRNA
12053302	DKFZp434E229	-3.00	Homo sapiens mRNA; cDNA DKFZp434E229 (from clone DKFZp434E229)
12053188	DKFZp434M182	-2.07	Homo sapiens mRNA; cDNA DKFZp434M182 (from clone DKFZp434M182)
6807975	DKFZp434P072	-3.36	Homo sapiens mRNA; cDNA DKFZp434P072 (from clone DKFZp434P072)
12804040	DKFZP564J0123	-2.69	Homo sapiens, Similar to nuclear protein E3-3 orf1, clone MGC:10527, mRNA
4929614	DKFZP566C134	-3.09	Homo sapiens CGI-73 protein mRNA, complete cds
12053344	DKFZp586H1320	-2.82	Homo sapiens mRNA; cDNA DKFZp586H1320
12053358	DKFZp586H1322	-2.90	Homo sapiens mRNA; cDNA DKFZp586H1322
13276648	DKFZp761J1523	-2.86	Homo sapiens mRNA; cDNA DKFZp761J1523
8393263	DLL3	-2.87	Homo sapiens delta (Drosophila)-like 3 (DLL3), mRNA
11493772	EHF	-2.77	Homo sapiens ETS-family transcription factor EHF (EHF) mRNA
10832596	ENSA	-3.67	endosulfine alpha
11594983	EPB41L2	-2.07	Erythrocyte membrane protein band 4.1-like 2
10439354	FANCA	-2.68	Homo sapiens cDNA: FLJ22829 fis, clone KAIA4075, highly similar to HSCH
5031692	FBRNP	-2.89	Homo sapiens heterogeneous nuclear protein similar to rat helix destabilizing protein (FBRNP), mRNA
10438969	FBXO5	-2.55	Homo sapiens cDNA: FLJ22544 fis, clone HSI00219
13186237	FGFR1	-2.54	Homo sapiens fibroblast growth factor receptor 1 (fms-related tyrosine kinase 2, Pfeiffer syndrome) (FGFR1), transcript variant 5, Mrna
2078479	FHL-1	-2.28	Human heart protein with four and a half LIM domains (FHL-1) mRNA

10436956	FJH1	-2.96	Homo sapiens cDNA: FLJ20982 fis, clone ADSU02018
11056001	FKSG2	-2.55	Homo sapiens apoptosis inhibitor (FKSG2), mRNA
12408251	FKSG30	-2.64	Homo sapiens FKSG30 (FKSG30) mRNA, complete cds
13327692	FLII	-2.13	Flightless I (Drosophila) homolog
8922343	FLJ10308	-2.28	Homo sapiens homolog of rat nadrin (FLJ10308), mRNA
8922412	FLJ10415	-3.95	Homo sapiens hypothetical protein FLJ10415
8922425	FLJ10450	-3.29	Homo sapiens hypothetical protein FLJ10450
8922643	FLJ10751	-2.25	Homo sapiens hypothetical protein FLJ10751
8922715	FLJ10851	-2.78	Homo sapiens hypothetical protein FLJ10851
13280012	FLJ10903	-2.05	Hypothetical protein FLJ10903
12892919	FLJ11126	-2.01	hypothetical protein FLJ11126
11967980	FLJ12538	-3.89	Homo sapiens hypothetical protein FLJ12538 similar to ras-related protein RAB17
12597646	FLJ12572	-2.35	Homo sapiens hypothetical protein FLJ12572 (FLJ12572), mRNA
13376722	FLJ12584	-3.18	Homo sapiens hypothetical protein FLJ12584 (FLJ12584), mRNA
13376330	FLJ12618	-3.18	Homo sapiens hypothetical protein FLJ12618 (FLJ12618), mRNA
13529205	FLJ12644	-3.21	Homo sapiens, hypothetical protein FLJ12644, clone MGC:12483
13376670	FLJ13087	-2.91	Homo sapiens hypothetical protein FLJ13087 (FLJ13087), mRNA
11968026	FLJ13258	-2.38	Homo sapiens hypothetical protein FLJ13258 similar to fused toes (FLJ13258), mRNA
13376616	FLJ14038	-3.14	Homo sapiens hypothetical protein FLJ14038 (FLJ14038), mRNA
12654818	FLJ20071	-3.16	Homo sapiens, Similar to hypothetical protein FLJ20071, clone MGC:4975
8923113	FLJ20113	-3.10	Homo sapiens hypothetical protein FLJ20113 (FLJ20113), mRNA
13581300	FLJ20335	-2.47	hypothetical protein FLJ20335
9134345	FLJ20452	-2.24	Hypothetical protein FLJ20452
10435257	FLJ20542	-3.09	Homo sapiens cDNA FLJ13294 fis, clone OVARC1001232
6228478	FLJ20580	-2.85	Hypothetical protein FLJ20580
13376618	FLJ21168	-2.21	Homo sapiens hypothetical protein FLJ21168 (FLJ21168), mRNA

12232416	FLJ22059	-2.01	Homo sapiens hypothetical protein FLJ22059 (FLJ22059), mRNA
12759062	FLJ22313	-2.00	hypothetical protein FLJ22313
22749272	FLJ35954	-2.14	Homo sapiens hypothetical protein FLJ35954 (FLJ35954), mRNA
5803018	FSHPRH1	-2.74	Homo sapiens FSH primary response (LRPR1, rat) homolog 1 (FSHPRH1), mRNA
4503800	FUBP1	-2.02	Homo sapiens far upstream element (FUSE) binding protein 1 (FUBP1), mRNA
4503870	GABRR2	-2.14	Homo sapiens gamma-aminobutyric acid (GABA) receptor, rho 2 (GABRR2), mRNA
2459950	GART	-2.08	Homo sapiens GARS-AIRS-GART mRNA, partial cds
4503942	GCDH	-2.26	Homo sapiens glutaryl-Coenzyme A dehydrogenase (GCDH), nuclear gene encoding mitochondrial protein, transcript variant 1
5729839	GCP2	-2.36	Homo sapiens gamma-tubulin complex protein 2 (GCP2), mRNA
9970082	GFPT1	-2.21	glutamine-fructose-6-phosphate transaminase 1
4557626	GLE1L	-2.94	Homo sapiens GLE1 (yeast homolog)-like, RNA export mediator (GLE1L), mRNA
4504036	GNA11	-2.69	Homo sapiens guanine nucleotide binding protein (G protein), alpha 11 (Gq class) (GNA11), mRNA
4504184	GSTT1	-2.07	Homo sapiens glutathione S-transferase theta 1 (GSTT1), mRNA
2687868	GTBP	-2.38	Homo sapiens GTBP mRNA for GTBP-ALT, complete cds
4504200	GTF2H4	-2.32	Homo sapiens general transcription factor IIH, polypeptide 4 (52kD subunit) (GTF2H4), mRNA
595266	HADHA	-2.09	Human 78 kDa gastrin-binding protein mRNA, complete cds
8118720	HDAC8	-2.66	Homo sapiens class I histone deacetylase (HDAC8) mRNA, complete cds
5001538	HIBADH	-2.39	Homo sapiens BAC clone GS1-98E2 from 7p11.2-p21
5855963	HKE2	-2.07	HLA class II region expressed gene KE2
1575443	HLA-Cw*1701	-2.30	Homo sapiens HLA class I heavy chain (HLA-Cw*1701) mRNA, complete cds
17736799	hMCLC-3	-2.30	Homo sapiens hMCLC-3 mRNA for Mid-1-related chloride channel 3, complete

			cds
16416450	hMtCCA	-3.47	Homo sapiens hMtCCA mRNA for tRNA-nucleotidyltransferase, complete cds
10434948	HN1L	-3.17	Hypothetical protein similar to mouse HN1 (Hematological and Neurological expressed sequence 1)
10365758	HNRPC	-2.36	Heterogeneous nuclear ribonucleoprotein C (C1C2)
5031752	HNRPH1	-2.07	Homo sapiens heterogeneous nuclear ribonucleoprotein H1 (H) (HNRPH1), mRNA
11875212	HPC2	-2.98	Homo sapiens putative prostate cancer susceptibility protein (HPC2), mRNA
11291478	HPIP	-3.35	Hematopoietic PBX-interacting protein
2853276	HPRP4	-2.66	Homo sapiens WD splicing factor Hprp4p (HPRP4) mRNA, complete cds
5110914	HRB	-2.38	HIV-1 Rev binding protein
12006357	HRIHFB2122	-2.02	Homo sapiens Tara mRNA, complete cds
10703387	HRMT1L1	-2.44	HMT1 (hnRNP methyltransferase, S. cerevisiae)-like 1
5579469	HSPA1A	-2.29	Homo sapiens heat shock 70kD protein 1A (HSPA1A), mRNA
7661727	HSPC003	-2.19	Homo sapiens HSPC003 protein (HSPC003), mRNA
7661735	HSPC018	-3.53	Homo sapiens HSPC018 protein (HSPC018), mRNA
7661741	HSPC023	-3.60	Homo sapiens HSPC023 protein (HSPC023), mRNA
7661793	HSPC134	-2.02	Homo sapiens HSPC134 protein (HSPC134), mRNA
12654148	HSPC154	-2.77	Homo sapiens, HSPC154 protein, clone MGC:4897, mRNA, complete cds
7106781	HSPC196	-2.56	Homo sapiens HSPC196 mRNA, complete cds
5031770	HSPF2	-3.11	Homo sapiens heat shock 40kD protein 2 (HSPF2), mRNA
4617892	ICAM1	-2.40	Intercellular adhesion molecule 1 (CD54), human rhinovirus receptor
7542379	IDS	-2.14	Homo sapiens normal control W-IDS fusion transcript, mRNA sequence
9970542	IGHG3	-3.69	immunoglobulin heavy constant gamma 3 (G3m marker)
4826773	ISG15	-2.31	Homo sapiens interferon-stimulated protein, 15 kDa (ISG15), mRNA
11252643	ITGB4	-3.82	integrin, beta 4
4504808	JUNB	-2.79	Homo sapiens jun B proto-oncogene (JUNB), mRNA
577300	KIAA0090	-2.45	Human mRNA for KIAA0090 gene, partial cds

7661901	KIAA0095	-4.69	Homo sapiens KIAA0095 gene product (KIAA0095), mRNA
10439023	KIAA0197	-2.39	Homo sapiens cDNA: FLJ22583 fis, clone HSI02596
11286290	KIAA0273	-2.41	KIAA0273 gene product
832234	KIAA0285	-2.29	KIAA0285 gene product
5113513	KIAA0414	-2.37	KIAA0414 protein
2887434	KIAA0432	-2.36	Homo sapiens KIAA0432 mRNA, complete cds
1686271	KIAA0470	-2.05	KIAA0470 gene product
7023392	KIAA0713	-2.05	Homo sapiens cDNA FLJ10999 fis, clone PLACE1002529
18256839	KIAA0826	-3.92	Homo sapiens, clone MGC:25069 IMAGE:4498553, mRNA, complete cds
7662331	KIAA0844	-2.11	Homo sapiens KIAA0844 protein (KIAA0844), mRNA
4665833	KIAA0872	-3.88	KIAA0872 protein
12784477	KIAA1150	-2.05	KIAA1150 protein
11546048	KIAA1247	-4.09	Human DNA sequence from clone RP5-1049G16 on chromosome 20q12-13.2
10434518	KIAA1250	-2.06	Likely homolog of rat kinase D-interacting substance of 220 kDa; KIAA1250 protein
7959294	KIAA1514	-2.95	Homo sapiens mRNA for KIAA1514 protein, partial cds
10047238	KIAA1582	-2.63	Homo sapiens mRNA for KIAA1582 protein, partial cds
12697944	KIAA1700	-2.08	Homo sapiens mRNA for KIAA1700 protein, partial cds
1928356	KNS2	-2.14	Kinesin 2 (60-70kD)
2588629	LOC51666	-2.81	Human BAC clone GS1-303P24 from 7q21-22
10435318	LOC51729	-4.73	Homo sapiens cDNA FLJ13336 fis, clone OVARC1001879
9910351	LOC56904	-3.13	Homo sapiens SH3-containing protein SH3GLB2 (LOC56904), mRNA
12768600	M11S1	-2.10	Membrane component, chromosome 11, surface marker 1
5454183	MAP3K12	-2.58	Homo sapiens mitogen-activated protein kinase kinase kinase 12 (MAP3K12), mRNA
4505098	MAP4	-3.16	Homo sapiens microtubule-associated protein 4 (MAP4), mRNA
795931	MFAP3	-2.70	microfibrillar-associated protein 3
13128987	MGC3103	-3.01	Homo sapiens hypothetical protein MGC3103

22749020	MGC39558	-2.52	Homo sapiens hypothetical protein MGC39558
5803089	MLN64	-2.25	Homo sapiens steroidogenic acute regulatory protein related
7019460	MLX	-2.15	Homo sapiens MAX-like bHLHZIP protein (MLX), mRNA
6006024	MPP1	-2.02	Homo sapiens membrane protein, palmitoylated 1 (55kD)
13549066	MST4	-3.78	Homo sapiens serinethreonine protein kinase MST4 (MST4) mRNA
5174602	MYRL2	-2.57	Homo sapiens myosin regulatory light chain 2, smooth muscle isoform (MYRL2), mRNA
9502399	MYRL2	-2.70	Homo sapiens chromosome 19, BAC CIT-HSPC_204F22 (BC228680)
6912523	NARF	-2.28	Homo sapiens nuclear prelamin A recognition factor (NARF), mRNA
1480645	NCOA1	-2.51	Human steroid receptor coactivator-1 F-SRC-1 mRNA, complete cds
4826853	NDUFB8	-3.68	Homo sapiens NADH dehydrogenase (ubiquinone) 1 beta subcomplex, 8 (19kD, ASHI)
4505370	NDUFS8	-2.17	Homo sapiens NADH dehydrogenase (ubiquinone) Fe-S protein 8 (23kD) (NADH-coenzyme Q reductase)
506817	NFE2	-2.75	Human leucine zipper mRNA, complete cds
17391108	NFS1	-2.14	Homo sapiens, Similar to nitrogen fixation gene 1 (S. cerevisiae, homolog)
1669493	NFYC	-2.36	Human transcription factor NF-YC subunit mRNA
10864008	NLI-IF	-2.07	Homo sapiens nuclear LIM interactor-interacting factor (NLI-IF)
4534208	NMT1	-2.24	N-myristoyltransferase 1
12803666	NR2F6	-2.81	Homo sapiens, nuclear receptor subfamily 2, group F, member 6, clone MGC:4277, mRNA, complete cds
4505274	NUDT1	-2.25	Homo sapiens nudix (nucleoside diphosphate linked moiety X)-type motif 1 (NUDT1), mRNA
7019476	OMI	-3.11	Homo sapiens HtrA-like serine protease (OMI), mRNA
5663957	OSBP	-2.59	Oxysterol binding protein
13699862	OTRPC4	-2.47	Homo sapiens vanilloid receptor-related osmotically activated channel; OTRPC4 protein (OTRPC4)
4505548	P2RX4	-2.67	Homo sapiens purinergic receptor P2X, ligand-gated ion channel, 4 (P2RX4),

			mRNA
12906073	PHB	-2.07	Prohibitin
10824430	PICALM	-2.23	Phosphatidylinositol binding clathrin assembly protein
10818329	PICALM	-2.35	Phosphatidylinositol binding clathrin assembly protein
1743874	PIP5K1A	-2.08	Human 68 kDa type I phosphatidylinositol-4-phosphate 5-kinase alpha mRNA, clone PIP5KIa3
9966876	PIST	-3.33	Homo sapiens PIST (PIST), mRNA
10742618	PL6	-2.08	PL6 protein
12654620	PMP24	-2.30	Homo sapiens, 24 kDa intrinsic membrane protein, clone MGC:1213
4505944	POLR2E	-2.12	Homo sapiens polymerase (RNA) II (DNA directed) polypeptide E (25kD)
10435912	PPFIA3	-2.42	protein tyrosine phosphatase, receptor type, f polypeptide (PTPRF), interacting protein (liprin), alpha 3
4505990	PPIC	-2.09	Homo sapiens peptidylprolyl isomerase C (cyclophilin C) (PPIC), mRNA
5031988	PPP3CC	-2.71	Homo sapiens protein phosphatase 3 (formerly 2B), catalytic subunit, gamma isoform (calcineurin A gamma)
13699864	PRO1853	-2.21	Homo sapiens hypothetical protein PRO1853 (PRO1853), mRNA
12771232	PRO2706	-2.08	Hypothetical protein PRO2706
6807722	PRO2730	-3.71	Homo sapiens mRNA; cDNA DKFZp434C0814
8924201	PRO2801	-2.47	Homo sapiens hypothetical protein PRO2801 (PRO2801), mRNA
4506192	PSMB1	-2.08	Homo sapiens proteasome (prosome, macropain) subunit, beta type, 1 (PSMB1), mRNA
11445036	PSMD11	-2.48	Proteasome (prosome, macropain) 26S subunit, non-ATPase, 11
16580750	PTBLP	-3.47	Homo sapiens PTBLP mRNA for PTB-like protein S, complete cds
4506278	PTMS	-2.18	Homo sapiens parathymosin (PTMS), mRNA
4506310	PTPRF	-3.22	Homo sapiens protein tyrosine phosphatase, receptor type
2281288	PTPRN2	-4.50	Human tyrosine phosphatase IA-2beta mRNA, complete cds
13376819	PUS1	-5.14	Homo sapiens pseudouridine synthase 1 (PUS1), mRNA
4896040	RASA3	-3.20	RAS p21 protein activator (GTPase activating protein) 3 (Ins(1,3,4,5)P4-

			binding
9256633	RASSF1	-3.54	Homo sapiens Ras association (RalGDSAF-6) domain family 1, mRNA
8400719	RBMS1	-3.09	Homo sapiens RNA binding motif, single stranded interacting protein 1, transcript variant MSSP-3
6677700	RE2	-2.50	Homo sapiens G-protein coupled receptor
6677722	RFC5	-2.79	Homo sapiens replication factor C (activator 1) 5 (36.5kD), mRNA
5231227	RNASE6PL	-2.39	Homo sapiens ribonuclease 6 precursor
12656362	RNF6	-2.47	Homo sapiens RNF6 protein, alternatively spliced
10811717	RP42	-3.57	RP42 homolog
13528944	RPA3	-2.08	Homo sapiens, replication protein A3 (14kD), clone MGC:12305
4506680	RPS11	-2.48	Homo sapiens ribosomal protein S11
4506690	RPS16	-2.09	Homo sapiens ribosomal protein S16
4506762	S100A3	-3.22	Homo sapiens S100 calcium-binding protein A3
13540474	SAA2	-2.51	Homo sapiens serum amyloid A2
758680	SAA2	-2.10	Homo sapiens serum amyloid A2-alpha mRNA, complete cds
5730024	SAD1	-3.08	Homo sapiens SnRNP assembly defective 1 homolog, mRNA
10584719	SAT	-2.06	Spermidinespermine N1-acetyltransferase
7023794	SEC15L	-3.77	Homo sapiens cDNA FLJ11251 fis, clone PLACE1008813
7661681	SENP3	-2.05	Homo sapiens sentrinSUMO-specific protease 3 (SENP3), mRNA
7021892	SENP3	-2.49	Homo sapiens cDNA FLJ10061 fis, clone HEMBA1001413.
15430748	SEPTIN6	-2.92	Homo sapiens SEPTIN6 type IV (SEPTIN6) mRNA, complete cds
11141876	SIGIRR	-2.69	Homo sapiens single Ig IL-1R-related molecule
5803168	SIPA1	-2.69	Homo sapiens signal-induced proliferation-associated gene 1
5436769	SLC12A4	-2.49	solute carrier family 12 (potassiumchloride transporters), member 4
4759111	SLC16A3	-2.12	Homo sapiens solute carrier family 16 (monocarboxylic acid transporters), member 3
4507006	SLC25A12	-2.01	Homo sapiens solute carrier family 25 (mitochondrial carrier, Aralar), member 12

4826715	SLC29A1	-2.52	Homo sapiens solute carrier family 29 (nucleoside transporters), member 1
4507022	SLC4A2	-2.80	Homo sapiens solute carrier family 4, anion exchanger, member 2 (erythrocyte membrane protein band 3-like 1)
10946127	SMARCA4	-2.03	SWISNF related, matrix associated, actin dependent regulator of chromatin, subfamily a, member 4
10432598	SMARCB1	-2.63	SWISNF related, matrix associated, actin dependent regulator of chromatin, subfamily b, member 1
21739263	Spir-1	-2.91	Homo sapiens mRNA; cDNA DKFZp434O034
11127696	SSXTSSX4v fusion	-2.28	Homo sapiens SYTSSX4v fusion protein (SSXTSSX4v fusion) mRNA
7305524	ST7	-2.85	Homo sapiens potential tumor suppressor (ST7), mRNA
2443360	STATI2	-3.19	Homo sapiens mRNA for STAT induced STAT inhibitor-2, complete cds
12893045	STIP1	-2.11	Stress-induced-phosphoprotein 1 (Hsp70Hsp90-organizing protein)
6991686	SYK	-2.50	spleen tyrosine kinase
5454101	TACC3	-3.67	Homo sapiens transforming, acidic coiled-coil containing protein 3 (TACC3), mRNA
10439398	TAF1B	-2.67	Homo sapiens cDNA: FLJ22868 fis
2961148	TASR1	-2.13	Homo sapiens TLS-associated protein TASR mRNA, complete cds
4507372	TBCC	-2.99	Homo sapiens tubulin-specific chaperone c (TBCC), mRNA
4507384	TCEA2	-3.12	Homo sapiens transcription elongation factor A (SII), 2 (TCEA2), mRNA
5886115	TCF7	-2.24	transcription factor 7 (T-cell specific, HMG-box)
529172	TCF8	-2.20	Human zinc finger homeodomain protein mRNA, complete cds
339577	TGM2	-2.66	Human transglutaminase mRNA, complete cds
13097680	TGM2	-2.20	Similar to transglutaminase 2 (C polypeptide, protein-glutamine-gamma-glutamyltransferase), clone MGC:1193
11024699	TIMM13B	-2.02	Homo sapiens translocase of inner mitochondrial membrane 13 (yeast) homolog B (TIMM13B)
5802826	TIMM8B	-2.38	Homo sapiens DDP-like protein mRNA, complete cds

9257247	TIMP2	-2.04	Homo sapiens tissue inhibitor of metalloproteinase 2 (TIMP2), mRNA
2460248	TNNC1	-4.61	Homo sapiens cardiac ventricular troponin C mRNA, complete cds
7706580	TOK-1	-2.25	Homo sapiens cdk inhibitor p21 binding protein (TOK-1), mRNA
5032188	TP53BP1	-3.39	Homo sapiens tumor protein p53-binding protein, 1 (TP53BP1), mRNA
14010353	TPM3	-2.15	Homo sapiens tropomyosin 4-anaplastic lymphoma kinase fusion protein minor isoform mRNA
12803958	TPM4	-2.03	Homo sapiens, tropomyosin 4, clone MGC:3641, mRNA, complete cds
7317562	TPP2	-2.84	Tripeptidyl peptidase II
4759277	U5-100K	-2.62	Homo sapiens prp28, U5 snRNP 100 kd protein (U5-100K), mRNA
13376853	UBXD1	-3.48	Homo sapiens UBX domain-containing gene 1 (UBXD1)
13506764	UCK1	-3.84	Homo sapiens uridine-cytidine kinase 1 (UCK1) mRNA, complete cds
4557872	UROS	-2.24	Homo sapiens uroporphyrinogen III synthase (congenital erythropoietic porphyria) (UROS), mRNA
2735306	VDAC3	-2.27	Human voltage dependent anion channel form 3 mRNA, complete cds
2881843	VDUP1	-2.40	Upregulated by 1,25-dihydroxyvitamin D-3
5454161	VDUP1	-2.01	Homo sapiens upregulated by 1,25-dihydroxyvitamin D-3 (VDUP1), mRNA
2631843	VIL2	-3.19	Villin 2 (ezrin)
11141864	VPS11	-3.06	Homo sapiens vacuolar protein sorting 11 (yeast homolog) (VPS11), mRNA
5730119	YKT6	-3.21	Homo sapiens SNARE protein (YKT6), mRNA
4096984	YWHAE	-2.86	Human epsilon isoform 14-3-3 protein mRNA, complete cds
6005977	ZNF258	-2.19	Homo sapiens zinc finger protein 258 (ZNF258), mRNA
23510456	ZNF41	-3.10	Homo sapiens zinc finger protein 41 (ZNF41), transcript variant 1, mRNA
11129064		-2.09	ESTs
405730		-3.23	H.sapiens protein-serinethreonine kinase gene, complete CDS
824338		-2.04	ESTs
13623280		-2.80	Homo sapiens, hypothetical protein FLJ10647, clone MGC:11318, mRNA, complete cds
12385360		-2.24	ESTs

12749776		-2.49	ESTs
405744		-2.55	H.sapiens protein-serinethreonine kinase gene, complete CDS
1265017		-5.13	Homo sapiens cDNA, 3 end
5769385		-2.86	ESTs, Moderately similar to zinc finger protein (H.sapiens)
10736104		-2.10	ESTs
3308527		-2.91	Homo sapiens clone 25129 mRNA sequence
3178040		-2.77	ESTs
11008259		-4.12	Homo sapiens cDNA FLJ11985 fis, clone HEMBB1001356
1437008		-3.17	ESTs
13281338		-4.03	Homo sapiens, clone IMAGE:3908672, mRNA, partial cds
2457916		-4.31	Homo sapiens cDNA FLJ30840 fis, clone FEBRA2002442
4174746		-2.94	ESTs
16553977		-2.14	Homo sapiens cDNA FLJ25255 fis, clone STM03941
6506313		-2.13	ESTs
13591689		-2.30	Homo sapiens PUMAJFY1 protein mRNA, complete cds
10821160		-2.58	Homo sapiens cDNA: FLJ23031 fis, clone LNG01932
27469755		-2.24	Homo sapiens, clone IMAGE:5310953, mRNA
15930214		-3.10	Homo sapiens, clone IMAGE:3884761, mRNA
1849639		-2.24	ESTs
4072178		-2.05	ESTs, Weakly similar to T12540 hypothetical protein DKFZp434J214.1
3430180		-2.18	Homo sapiens cDNA: FLJ21781 fis, clone HEP00223
3451333		-5.58	Homo sapiens chromosome 19, cosmid F22162
1641998		-2.29	ESTs
10836767		-3.44	ESTs
19731133		-2.51	Homo sapiens cDNA FLJ31833 fis, clone NT2RP6000130
18255994		-2.89	Homo sapiens, clone MGC:30053 IMAGE:5139119, mRNA, complete cds
22800482		-3.19	Homo sapiens, clone IMAGE:4552615, mRNA.
3085925		-2.53	ESTs

2984582		-2.13	Homo sapiens chromosome 9, P1 clone 11659
8331754		-2.22	Homo sapiens X28 region near ALD locus containing DUSP9, ribosomal protein L18a
5232294		-2.97	ESTs
20362593		-2.18	Homo sapiens cDNA FLJ38785 fis, clone LIVER2001329
12661587		-2.75	ESTs
4188996		-2.06	ESTs
21734157		-2.01	Homo sapiens mRNA; cDNA DKFZp686F0137
9513134		-2.31	ESTs
22477667		-2.24	Homo sapiens, clone IMAGE:5223521, mRNA
10951966		-2.48	Human clone JkA8 mRNA induced upon T-cell activation, 3 end.
2012170		-2.61	ESTs
4888084		-2.48	ESTs, Weakly similar to WASP-family protein
1278185		-2.02	Homo sapiens cDNA, 5 end
10914577		-2.38	ESTs
1422999		-2.27	Homo sapiens cDNA, 3 end
10434882		-2.15	Homo sapiens cDNA FLJ13049 fis, clone NT2RP30014
13575205		-2.06	Homo sapiens cDNA FLJ11901 fis, clone HEMBA1007347
11683355		-2.15	ESTs, Weakly similar to S69890 mitogen inducible gene mig-2
13045294		-2.60	ESTs
1301533		-3.37	Homo sapiens 14q32 Jagged2 gene, complete cds
4703703		-2.31	ESTs
770394		-2.07	ESTs
11100686		-2.24	ESTs, Weakly similar to KIAA0681 protein
12654762		-3.48	Homo sapiens, clone MGC:982 IMAGE:3354306, mRNA, complete cds
5037961		-2.66	Homo sapiens mRNA; cDNA DKFZp434C1714
11009912		-2.90	Homo sapiens cDNA FLJ12532 fis, clone NT2RM4000200
3808147		-2.25	Homo sapiens ASMTL gene

5924742		-2.27	Homo sapiens, clone IMAGE:4642241, mRNA
405728		-2.38	H.sapiens protein-serinethreonine kinase gene, complete CDS
7921055		-2.65	Homo sapiens chromosome 14 BAC 98L12
5854235		-2.72	ESTs
12917064		-2.14	ESTs
10456093		-3.75	Homo sapiens partial mRNA for FUSCHOP chimaeric fusion protein (type 9 transcript variant)
12669922		-2.38	ESTs
4664062		-2.09	ESTs
4884256		-2.28	Homo sapiens mRNA; cDNA DKFZp564O222
4738836		-2.71	Homo sapiens cDNA, 3 end
1869771		-2.32	Human DNA sequence from PAC 296K21 on chromosome X contains cytokeratin exon, delta-aminolevulinate synthase (erythroid)
13477192		-2.64	Homo sapiens, Similar to CG5078 gene product, clone MGC:12945, mRNA, complete cds
21040444		-2.87	Homo sapiens, Similar to syndecan binding prote
12384240		-2.09	ESTs
2839126		-2.20	Homo sapiens mRNA; cDNA DKFZp434F0217
10348509		-2.13	ESTs, Moderately similar to T43492 hypothetical protein DKFZp434A219.1 (H.sapiens)
9812380		-3.48	ESTs
10151243		-2.06	Homo sapiens cDNA: FLJ22482 fis, clone HRC10859
5657550		-2.08	ESTs, Moderately similar to ADHUA fructose-bisphosphate aldolase (H.sapiens)
6656370		-2.44	ESTs
2094759		-2.38	Human beta-cytoplasmic actin (ACTBP9) pseudogene
4002364		-2.45	Homo sapiens clone 24627 mRNA sequence
12654408		-2.16	Homo sapiens, Similar to phosphatidylinositol glycan, class O, clone

			MGC:3079
6143075		-2.09	Homo sapiens cDNA: FLJ22807 fis, clone KAIA2887
10964796		-2.56	Homo sapiens mRNA; cDNA DKFZp564N1272
13663829		-2.12	Human mRNA for heat shock protein 90kDa, 5UTR
1470308		-2.34	Phosphoglycerate kinase {alternatively spliced}

Note* For up-regulated genes, totally 359 genes were up-regulated and 153 genes were named.
For down-regulated genes, totally 360 genes were down-regulated and 273 genes were named.

CHAPTER 3
NUCLEAR PYRUVATE KINASE M2 IS A PROTEIN KINASE

3.1 Abstract

Pyruvate kinase isoform M2 (PKM2) is a glycolysis enzyme catalyzing conversion of phosphoenolpyruvate (PEP) to pyruvate with transferring a phosphate from PEP to ADP. We report here that PKM2 is also a protein kinase using PEP as phosphate donor. The protein substrate is bound at the ADP binding site. Our experiments suggest that PKM2 dimer is an active protein kinase, while the tetramer is an active pyruvate kinase. Binding of the tyrosyl phosphorylated proteins at the FBP binding site converts the tetrameric PKM2 to a dimer, and reciprocally regulates the pyruvate kinase and protein kinase activities of PKM2. Expression a PKM2 mutant that exists as a dimer promotes cell proliferation. Growth factor stimulations significantly increase the dimer/tretramer PKM2 ratio in cells. Thus, our study reveals that the regulation of pyruvate kinase and protein kinase activities of PKM2 by growth signals plays an important role in promoting cell proliferation.

3.2 Introduction

An important molecular feature of tumor development is the expression of pyruvate kinase isoenzyme M2 (PKM2) (Elbers, van Unnik et al. 1991; Hacker, Steinberg et al. 1998). The glycolysis catalytically active PKM2 exists as a tetramer and associates with a glycolytic enzyme complex in normal cells (Dombrauckas, 2005; Zwerschke, 1999; Altenberg, 2004). In tumor cells, it is believed that PKM2 dominantly forms a dimer, and appears to be catalytically inactive for conversion of PEP to pyruvate (Ashizawa, McPhie et al. 1991; Mazurek, Boschek et al. 2005). It is believed that the

inactive PKM2 actually provides growth advantage for tumor progression as it helps to channel the carbon source from glycolytic intermediates to biosynthesis, especially syntheses of nucleic acids, lipids, and proteins, to meet the demands for tumor cell proliferation. Recent studies have suggested that PKM2 changes its pyruvate kinase activity, consequently facilitating cell proliferation by binding to tyrosine phosphor-peptide (Christofk, Vander Heiden et al. 2008; Christofk, Vander Heiden et al. 2008), indicating that growth signals regulate the activity of PKM2 in glucose metabolism.

3.3 Results

3.3.1 PKM2 is a Protein Kinase

We previously reported that nuclear PKM2 upregulated the MEK5 gene transcription by activating the transcription co-activator stat3. We showed that expression of PKM2 increased stat3 phosphorylation at Y705 (Gao, et.al. Oncogene revision 2009). We questioned whether PKM2 could act as a protein kinase that directly phosphorylated stat3. However, an in vitro phosphorylation using both the E. coli expressed recombinant PKM2 (rPKM2) and the protein purified from nuclear extracts of mammalian cancer cells in the presence of ATP did yield phosphorylation of a commercially available GST-stat3. Since PKM2 use PEP as phosphate donor to phosphorylate ADP in the glycolysis, we reasoned that the protein may use the same phosphate donor to phosphorylate a protein substrate. Thus, we replaced ATP by PEP in our in vitro phosphorylation reaction. Immunoblot using a commercially available antibody against Y705 phosphorylated stat3 demonstrated that the GST-stat3 was phosphorylated by both the rPKM2 and a HA-tagged PKM2 (HA-PKM2) immunopurified from nuclear extracts of

SW620 cells in the presence of PEP. As observed previously, stat3 was not phosphorylated in the presence of ATP (Fig. 3.1 A&B). These experimental results indicated that PKM2 is a protein kinase using PEP as the phosphate donor.

3.3.2 Dimeric PKM2 is the Active Protein Kinase

We and others previously reported that PKM2 localized to the cell nucleus (Hoshino, Hirst et al. 2007), Gao,et.al. Oncogene revision, 2009). In addition, we observed that the kinase activity of the nuclear HA-PKM2 in phosphorylation of stat3 was substantially higher than that of the rPKM2 expressed in E. coli. We therefore sought to compare the protein kinase activity of the nuclear PKM2 and the cytoplasmic PKM2. We immunopurified the HA-PKM2 from nuclear or cytoplasmic extracts prepared from SW620 cells. The same in vitro phosphorylation reactions using the GST-stat3 as substrate were carried out with the immunopurified HA-PKM2 in the presence of PEP or ATP. It was evident that both the HA-PKM2 purified from the nuclear extracts and the cytoplasmic extracts were active in phosphorylating stat3. However, it was also clear that the HA-PKM2 purified from the nuclear extracts had much higher activity in phosphorylating stat3 than that of protein purified from the cytoplasmic extracts (Fig. 3.1 C&D).

It was reported that the catalytically active tetramer and inactive dimer of PKM2 co-exist in cells with high proliferation rate (Mazurek et al., 2005). Fructose-1,6-bisphosphate (FBP) and tyrosine phosphorylation by viral oncogenic products were identified as the regulators for the conversion between these two forms (Ashizawa, McPhie et al. 1991; Mazurek, Boschek et al. 2005). We therefore questioned whether the

differences in the protein kinase activity of nuclear/cytoplasmic PKM2 and the rPKM2 expressed in *E. coli.* were due to dimer or tetramer of the protein. To investigated whether PKM2 is a dimer or a tetramer both in the nucleus and in the cytoplasm, we first fractioned the nuclear extracts and cytoplasmic extracts of SW620 cells by size exclusion chromatography. Non-specific protein-protein interactions were disrupted by treatment of the extracts with 600 mM 6-aminocaproic acid (6-AcA). The levels of PKM2 in each chromatography fraction were examined by immunoblot using the antibody PabPKM2. Nuclear PKM2 was only detected in fractions 14 – 16, while cytoplasmic PKM2 was mainly detected in fractions 10 – 16 with the highest concentrations in fractions 10 – 12. According to the molecular weight calibration standard (Fig. 3.6 A&B), fraction 11 co-elutes with a molecular weight near 240 kDa, while fraction 14 co-elutes with a molecular weight near 120 kDa (Fig. 3.1E). The gel-filtration chromatography experiments suggested that nuclear PKM2 was completely dimer (120 kDa), while the cytoplasmic PKM2 existed in both dimer and tetramer with a higher population of tetramers. The same chromatography procedure was also employed to analyze whether the rPKM2 is a dimer or tetramer. It was evident that the rPKM2 was detected in the fractions 11 – 14, which indicates that the bacterially expressed rPKM2 is mostly tetramer with very small amount of dimer (Fig. 3.2B). To further probe the dimer/tetramer status of nuclear and cytoplasmic PKM2, nuclear extracts and cytoplasmic extracts made from SW620 cells were separated by a non-denaturing PAGE (8% acrylamide:bis-acrylamide = 40:1) and subjected to immunoblot analyses using the antibody PabPKM2. The extracts were also treated with 600 mM 6-AcA prior to electrophoresis. It was clear that the nuclear PKM2 migrated slightly faster than the BSA

dimer (132 kDa). Conversely, the majority of the cytoplasmic PKM2 approximately co-migrated with Urease (272 kDa) (Fig. 3.6C). Thus, both non-denaturing gel electrophoresis and size exclusion chromatography results strongly suggested a division of PKM2 between a dimer form in the nucleus and mainly a tetramer form in the cytoplasm. The bacterially expressed rPKM2 mainly exist as tetramer. Based on the proceeding experimental observations, we speculated that the dimer form of PKM2 is the active protein kinase, while tetramer is an active pyruvate kinase. Closely examination of the crystal structure of the tetramer human PKM2 (Dombrauckas, Santarsiero et al. 2005) reveals that a positive charged residue R399 may plays a critical role in forming the tetramer of PKM2. It is notable that the R399 forms stable charge-charge interactions with residues E418, D357, and E396 of PKM2 located on the other dimer of the tetramer PKM2 (Fig. 3.2A). We therefore created a mutant R399E to disrupt the charge-charge interaction. Size exclusion chromatography analyses of the wt rPKM2 and the R399E mutant demonstrated that the wild-type rPKM2 existed most as a tetramer with residue amounts of dimer, while the R399E mutant was mostly dimer (Fig. 3.2B). We reasoned that the dimeric R399E mutant would be more active in phosphorylating stat3 compared to the wild-type rPKM2. Thus, the in vitro phosphorylation reactions were carried out with the wild-type rPKM2 and the R399E mutant. It was evident that the protein kinase activity of the R399E mutant was substantially higher than that of the wild-type rPKM2 (Fig. 3.2C), while the pyruvate kinase activity of the mutant was dramatically lower than that of the rPKM2 (Fig. 3.2D). The results supported our speculation that dimeric PKM2 is the active protein kinase.

To further verify the phosphorylation of stat3 by PKM2, we prepared [^{32}P]-labeled PEP according to the methods described by Roossien FF. and co-workers (Roossien, Brink et al. 1983). The same in vitro phosphorylation reaction was carried out with the rPKM2, the rPKM1, and the R399E mutant using the [^{32}P]-labeled PEP. The phosphorylation reaction mixture was separated by SDS-PAGE and subjected to autoradiography. It was clear that the GST-stat3 was phosphorylated by the R399E mutant. The phosphorylation of the GST-stat3 by the rPKM2 was very weak (can only be visualized by a substantial overexposure in autoradiograph). The GST-stat3 was not phosphorylated by the recombinant PKM1 in the presence of the [^{32}P]-PEP (Fig. 3.6D). No phosphorylation can be detected even under very high overexposure in the autoradiograph.

3.3.3 Binding Tyrosyl Phosphor-protein at the FBP Site Converts the Tetramer PKM2 to the Dimmer and Reciprocally Regulates the Protein Kinase and Pyruvate Kinase Activities

Christofk and co-workers reported that PKM2 interacts with phosphor-tyrosine peptide and the interaction plays an important role in promoting cell proliferation (Christofk et al., 2008a; Christofk et al., 2008b), suggesting a possible pathway that growth signals promotes proliferation via protein tyrosine phosphorylation and subsequent action on PKM2. Nevertheless, the interaction between PKM2 and a particular cellular tyrosine phosphor-protein is not revealed. We previously demonstrated that P68 RNA helicase is phosphorylated in cancer cells, and tyrosine phosphorylation of p68 correlates with cancer progression (Yang, Lin et al. 2005). Phosphorylation of p68 at Y593 promotes EMT (Yang, Lin et al. 2006), while phosphorylation of p68 at Y593 and

Y595 mediated resistance to apoptotic-induction (Yang, Lin et al. 2007). In an effort to probe interacting protein with the tyrosyl phosphorylated p68, we used a 14 amino acid sequence segment that includes the Y593 or Y593/595 phosphorylation site (aa 587 to 600). The peptides either carried no phosphorylation (Ref to as PepY593), Y593 phosphorylation (Ref to as PhosPepY593), or Y593/595 double phosphorylations (Ref to as D-PhosPepY593). We also used another control peptide that span different region of p68 (aa 561 – 574) with Y567 phosphorylation (Ref to as PhosPepY567). The peptides were conjugated to agarose beads. Precipitation experiments from nuclear extracts made from T98G cells demonstrated that the DPhosPepY593 pulled-down a nuclear protein that migrated at ~60 kDa (Fig. 3.7A). The interacting protein was identified by MALDI (tof/tof) as PKM2 (pyruvate kinase type M2) (Fig. 3.7A right panel). To verify the interaction of p68 with PKM2, the precipitates by the phosphorylated/non-phosphorylated p68 peptides were examined by immunoblot assay using a polyclonal antibody developed against PKM2. It was clear that the ~60 kDa protein precipitated by the tyrosine phosphorylated p68 peptide was recognized by the PKM2 antibody (Fig. 3.7B). The interaction between p68 and PKM2 was also verified by reciprocal pull-down with the nuclear extracts made from T98G cells using recombinant PKM2 as bait (Fig. 3.7C). PKM2 is a glycolysis enzyme that predominantly localizes in the cytoplasm. Thus, we asked whether p68 also interacts with PKM2 in the cytoplasm. To this end, PKM2 was immunoprecipitated from both the cytoplasmic extracts and nuclear extracts made from T98G cells. Co-imunoprecipitation of p68 with PKM2 was examined by immunoblot using the antibody p68-RGG. It was evident that p68 co-immunoprecipitated with PKM2 both in the cytoplasmic extracts and the nuclear extracts (Fig. 3.7D right

panel). Similar co-immunoprecipitation results were also observed with exogenously expressed HA-PKM2 (Fig. 3.7D, left panel). To further verify that PKM2 and p68 interaction is the p68 phosphorylation dependent, we carried out co-immunoprecipitation experiment with the nuclear extracts of T98G cells in which HA-p68, wt or Y593F (a p68 mutant that can not be phosphorylated), was expressed. It was clear that wt HA-p68 co-precipitated with PKM2, while the Y593F mutant did not (Fig. 3.7E), suggesting that p68 tyrosine phosphorylation is required for PKM2 and p68 interaction.

We questioned whether the interaction of PKM2 with the tyrosine phosphor-p68 might promote the conversion of PKM2 from tetramer to the dimer form, To test this conjecture, we employed three phosphorylated/unphosphorylated peptides, the double tyrosine phosphorylated peptide D-PhosPepY593, the peptide that spans different region of p68 PhosPepY567, and the PepY593. We first examined the interaction of the selected phosphor/unphosphor-peptides with the rPKM2 by monitoring the Trp fluorescence changes of the rPKM2 upon interaction with the peptides. It was clear that the D-PhosPepY593 interacted with the rPKM2 with Kd around 30 μM, while the PhosPepY567 and the PepY593 did not (Fig. 3.8 A, B, and C). It was demonstrated that the tyrosine phosphor-peptide interacts with PKM2 at FBP binding site (Christofk, Vander Heiden et al. 2008). To test whether the phosphor-tyrosine peptide interact with the rPKM2 at FBP binding site, we examined the interaction between the peptide D-PhosPepY593 with the rPKM2 in the presence of excessive amounts of FBP. It was clear that FBP competed with the D-PhosPepY593 for binding to the rPKM2 (Fig. 3.8 A, B, and C). The competition of FBP with p68 for binding to PKM2 was also revealed by co-immunoprecipitation experiment. It was clear that coimmunoprecipitation of p68 with

HA-PKM2 in T98G cell extracts decreased by supplementing the extracts with different concentrations of FBP (Fig. 3.8D). The similar coimmunoprecipitation experiment was also carried out with the rPKM2 and the HA-p68 immunopurified from T98G cell extracts in the presence of various concentrations of FBP. High concentration of FBP decreased the HA-p68 and the rPKM2 interaction (Fig. 3.8E). It is reported that W515–G520 located at the activating loop of C-terminal of PKM2 is critical for the FBP binding (Dombrauckas, Santarsiero et al. 2005). Thus, we created a truncation mutant with deletion of W515 – G531. The interaction of the phosphor-p68 with the PKM2 truncation was examined by the co-immunoprecipitation procedure. It was evident that the deletion of the FBP binding activating loop abolished the interaction between p68 and PKM2 (Fig. 3.8F). Meanwhile, a mutation (K270M) that affects the glycolytic substrate binding (Dombrauckas, 2005) did not affect the interaction between p68 and PKM2 (Fig. 3.8F). These results are consistent with the observations by Christofk and co-workers (Christofk, Vander Heiden et al. 2008; Christofk, Vander Heiden et al. 2008), indicating the phosphor-peptides D-PhosPepY593 and phosphor-p68 interact with PKM2 at the FBP binding site.

To examine the effects of binding the phosphor-peptides on the tetramer and dimmer formation, we used the same size exclusion chromatography method to analyze the molecular sizes of the rPKM2 in the presence or absence of the three tyrosine phosphor/unphosphorpeptides and compared to the chromatography profile of molecular size standard. It was evident that there were substantially more dimeric PKM2 in the presence of phosphor-peptides, DPhosPepY593, while the tetramer and dimer ratio of the rPKM2 was not affected in the presence of the phosphor-peptide PhosPepY567 and non-

phosphor-peptide PepY593 (Fig. 3.3A). The experiments apparently suggested that binding the tyrosyl phosphor-protein converts tetramer PKM2 to a dimeric form.

We further questioned whether binding of the tyrosyl phosphor-protein/peptide would activate the protein kinase activity and inactive pyruvate kinase activity of PKM2. To this end, the in vitro phosphorylation reactions were carried out with the rPKM2 in the presence of different tyrosine phosphor/unphosphor-peptide. Examination of phosphorylation of stat3 by the immunoblot using the anti-phospho-stat3 antibody indicated that phosphorylation of stat3 at Y705 by the rPKM2 was dramatically increased in the presence of phosphor-peptide DPhosPepY593 (Fig. 3.3B). The phosphorylations of stat3 by the rPKM2 were not affected in the presence of the peptide PepY593 without tyrosine phosphorylation. The phosphorylation of stat3 was also not affected in the presence of another tyrosine phosphor-peptide PhosPepY567 that did not bind to PKM2 (Fig. 3.3B). We next tested whether indeed presence of phosphor-p68 would activate the protein kinase activity of PKM2. To this end, we immunopurified HA-p68 from nuclear extracts prepared from T98G cells. Phosphorylation of GST-stat3 by the rPKM2 in the presence or absence of the immunopurified HA-p68 was examined. Clearly, stat3 was much strongly phosphorylated by the rPKM2 in the presence of the purified HA-p68 compared to that in the absence of the purified HA-p68 (Fig. 3.3C). The results support the notion that binding of the tyrosyl phosphor-protein activates the protein kinase activity of PKM2.

PKM2 is a glycolysis enzyme. It is believed that the tetramer form of the protein is catalytic active in catalyzing the conversion of PEP to pyruvate in the glycolysis. Since the binding of the tyrosine phosphor-protein promoted the conversion from tetramer to

dimer, we reasoned that binding the tyrosine phosphor-protein/peptide to PKM2 should result in protein that is less active in catalyzing the conversion of PEP to pyruvate. We used the method similar to that is described by Christofk and coworkers (Christofk, Vander Heiden et al. 2008; Christofk, Vander Heiden et al. 2008) to monitor the pyruvate kinase activity of the rPKM2 in the presence of the tyrosine phosphor-peptides. The rPKM2 catalytic activity was dramatically reduced in the presence of D-PhosPepY593, while the activity was not affected in the presence of the peptides PhosPepY567 and PepY593 (Fig. 3.3D), which indicate that binding of PKM2 to the tyrosine phosphor-proteins converted the protein to dimer and consequently reduced the glycolytic enzyme activity. The notion was further supported by the experiments that the enzymatic activity of the R399E in converting PEP to pyruvate was dramatically decreased compared to that of recombinant wild-type (Fig. 3.2D).

3.3.4 PKM2 Kinase Substrates Bind to the ADP Binding Site for Phosphorylation

PKM2 directly phosphorylates stat3. One interesting question is how the protein substrate is bound to PKM2. Our results showed that PEP was used as phosphate donor by PKM2 in phosphorylation of a protein substrate. It is established that in the catalysis of ADP phosphorylation in glycolysis, PKM2 binds phosphate donor PEP at one site and substrate ADP at the other. Thus, a very logic assumption based on this knowledge is that the protein substrate may bind to the ADP site. To test this conjecture, we carried out competition binding analyses. Co-immunoprecipitation was carried out to detect the interaction between PKM2 and Stat3 mutant in the presence of ADP. The results showed that ADP competed the interaction between Stat3 and PKM2. The interaction between

Stat3 and PKM2 mutants were also probed. Co-IP results showed that the mutant at glycolytic substract binding site, K270M, abolished the interaction between Stat3 and PKM2 (Fig. 3.4B). Our experiments thus far demonstrate that tyrosine phosphor-p68 interacts with PKM2 at the FBP site and strengthen the protein kinase activity of the protein. We therefore predict a three ways interaction among the phosphor-p68, PKM2, and GST-stat3. To test this possible protein interaction, we carried out the GST-pull down using the GST-stat3. Immunoblot demonstrated that both recombinant PKM2 and p68 purified from cell extracts of T98G cells were co-precipitated with GST-stat3 (Fig. 3.4C).

3.3.5 PKM2 Protein Kinase Substrates Bind to the ADP Binding Site

PKM2 directly phosphorylates stat3. One interesting question is how the protein substrate is bound to PKM2. Our results showed that PEP was used as phosphate donor by PKM2 in phosphorylation of a protein substrate. It is established that in the catalysis of ADP phosphorylation in the glycolysis, PKM2 binds phosphate donor PEP at one site and substrate ADP at the other. Thus, a very logic assumption based on this knowledge is that the protein substrate may bind to the ADP site. To test this conjecture, we carried out competition binding analyses. The R399E mutant and stat3 interaction was analyzed in the presence and absence of ADP, PEP, and FBP. The GST-stat3 was immobilized on the glutathione-agarose beads. Recombinant R399E in mixing with buffer, ADP, PEP, or FBP were incubated with the beads. Binding of R399E to the immobilized GST-stat3 was then analyzed by SDS-PAGE followed by immunoblot of R399E and stat3. It was very clear that the interaction of R399E with stat3 was not affected in the presence of 5 mM

FBP, while the interaction was almost not detectable in the presence of 5 mM ADP. The R339E and stat3 interaction was also weakened in the presence of 5 mM of PEP. This was most likely due to phosphorylation of stat3, as the reduction in stat3 and R399E interaction was not PEP concentration dependent, while the R399E and GST-stat3 interaction showed a clear ADP concentration dependent reduction (Fig. 3.3E), indicating the competition of ADP with stat3 in binding R399E. Our experiments thus far demonstrate that tyrosine phosphor-p68 interacts with PKM2 at the FBP site and strengthen the protein kinase activity of the protein. We therefore predict a three ways interaction among the phosphor-p68, PKM2, and stat3. To test this possible protein interaction, we carried out the GST-pull down using the GST-stat3. Immunoblot demonstrated that both the HA-PKM2 and p68 purified from cell extracts of T98G cells were co-precipitated with GST-stat3 (Fig. 3.3F). The three ways interaction was also probed by co-immunoprecipitation experiments using anti-HA antibody. The rPKM2 and GST-stat3 were co-precipitated with HA-p68 that was immunopurified from cellular extracts of T98G cells (Fig. 3.9A). These results provided additional support for the notion that PKM2 protein kinase substrate binds to the ADP binding site. The notion that protein kinase substrate is bound at the ADP binding site of PKM2 was also supported by our early observations that addition of ADP decreased the activity of PKM2 in phosphorylation of stat3, while addition of FBP did not (see Fig. 3.1C and 3.2C).

3.3.6 Expression of R399E Increased Stat3 Phosphorylation in Cells and Promoted Cell Proliferation

We employed a PKM2 mutant R399E. Our experiments showed that the recombinant R399E existed mostly as a dimer and the mutant exhibited strong activity in phosphorylation of GST-stat3. We therefore questioned whether the R399E mutant would be active in phosphorylation of stat3 in cells. To this end, the HA-R399E was exogenously expressed in SW480 cells. Immunoblot examination of the phosphor-stat3 in the nuclear extracts indicated a significantly increase in the levels of Y705 phosphorylated stat3. This increase was not due to increase in cellular levels of stat3 as immunoblot of cell lysate indicated very similar stat3 levels in cells with/without expression of the R399E or wt PKM2 (Fig. 3.4A). The exogenously expressed HA-R399E was subsequently immunopurified from cell lysate. Size exclusion chromatography experiments showed that, unlike the exogenously expressed wild-type HAPKM2, the HA-R399E was almost completely dimer in cell lysate (Fig. 3.4B) In vitro phosphorylation assays indicated that the immunopurified HA-R399E phosphorylated GST-stat3 (Fig. 3.4B). We previously observed that expression of PKM2 led to up-regulation of MEK5 and cell proliferation (Gao et.al., Oncogene 2009 revision). Thus, we tested here if exogenous expression of R399E in SW480 cells would lead to MEK5 up-regulation and cell proliferation. RT-PCR analyses clearly demonstrated that the cellular levels of mRNA of MEK5 increased significantly (Fig. 3.4C). Examination of cell proliferation using a commercial kit that monitoring the cooperation of BrdU demonstrated that expression of R399E led to a strong increase in cell proliferation (Fig. 3.4D).

3.3.7 Growth Factor Stimulations Result in Increase in Dimeric PKM2 in Cells

It is well documented that stimulation of cells by growth factors and cytokines results in activation of various protein tyrosine kinases that subsequently phosphorylates many protein substrates at tyrosine residue (Hunter and Cooper 1985). For instance, we previously demonstrated that PDGF or EGF stimulation led to tyrosine phosphorylation of p68 RNA helicase (Yang, Lin et al. 2005; Yang, Lin et al. 2006). Presently our experiments demonstrated that binding to tyrosine phosphor-protein converted PKM2 from tetramer to dimer therefore activated the protein kinase activity of the protein. We reason whether treatment of cells with growth factors would affect PKM2. Thus, SW480 cells were treated with EGF. The same chromatography procedure used for detecting the PKM2 tetramer vs dimer in crude cell extracts was employed here to analyze the tetramer and dimer ratio of PKM2 in cells under the stimulation of EGF. It was clear that the levels of dimer PKM2 in growth factor stimulated cells were significantly higher than that in corresponding unstimulated cells (Fig. 3.5A). Immunoblot analyses of PKM2 in nuclear and cytoplasmic extracts suggested that growth factor stimulation led to increase in nuclear PKM2 levels (Fig. 3.5B). Analyses of protein tyrosine phosphorylation and p68 tyrosine phosphorylation revealed that there was a substantial increase in protein tyrosine phosphorylation and tyrosine phosphorylation of p68 at tyrosine residue (Fig. 3.5C). These experiments suggested that indeed there is a clear correlation between the levels of protein tyrosine phosphorylations and dimeric PKM2 in cells, which is inducible by growth factors and cytokines.

3.4 Discussion

During tumor progression, growth signals stimulate the conversion of glycolytically active PKM2 to an inactive form, consequently regulating the glycolysis pathway to channel the carbon source from glucose for biosynthesis (Deberardinis, 2008; Garber, 2006; Mazurek, 2003; Christofk, 2008). It is conceivable that tumor cells need to coordinate the metabolism alterations with expression of genes that are related to cell proliferation during tumor progression. Thus, at the same token, the growth signals will also activates protein kinase activity of PKM2, which subsequently target transcription factor and activate transcription of genes that closely associated with cell proliferation. PKM2 has long been recognized as a so-called 'moonlight' enzyme that plays a very important role in tumor progression (Sriram, 2005). Clearly, the protein kinase activity of PKM2 and subsequent activity in transcription regulation is an important 'moonlight' activity of the protein. The functions of PKM2 in regulating expression of genes fulfill the role of feedback signaling from metabolic alterations to gene regulation during tumor malignancy transformation (see model in Fig. 3.5D).

It is intriguing that a glycolytic enzyme can function as a protein kinase and translocate to the nucleus acting on gene transcription. Our studies suggested a molecular base for the activity conversion (Fig. 3.5D). Growth signal (growth factors or cytokines) stimulations lead to activation of protein tyrosine kinases, which phosphorylate a number of downstream targets. A number of tyrosine phosphor-proteins subsequently act on PKM2 by interacting with the protein at the FBP binding site. The tyrosine phosphor-protein and PKM2 interaction results in the conversion of PKM2 from tetramer to a dimer, which consequently lead to decrease in pyruvate kinase activity and increase in protein kinase activity. It was revealed from x-ray crystallography structural analyses of

the tetramer PKM2 that the ADP binding site is formed by a large hydrophobic hole, indicating a great flexibility for nucleotide binding (Muirhead, Clayden et al. 1986; Dombrauckas, Santarsiero et al. 2005). The large hydrophobic hole at the nucleotide binding site is almost completely buried in a tetramer structure, while it would be completely accessible with the dimeric form. Thus, it is conceivable that the nucleotide binding site may be able to accommodate a protein substrate when PKM2 is converted to a dimer. Alternatively, binding the tyrosine phosphor-protein to the FBP site would results in a significant conformation change that will allow PKM2 to accommodate a protein substrate binding. Stat3 is a transcription activator that is activated in response to inflammatory cytokines, such as IL-6 (Gao, 2007; Watson, 2008). Strikingly, activation of stat3 represents probably one of the most important molecular signatures involved in promoting cancer progression. It has been observed that activation of stat3 is detected in almost all cancer types (Frank 2007; Huang, Qiu et al. 2007; Kim, Chan et al. 2007; Groner, Lucks et al. 2008). However, it is generally believed that activations of stat3 in response to growth factor and cytokines are usually transient. A long standing question is "How do the malignant cancer cells maintain constitutive activation of stat3?" Currently, mutation(s) that lead to constitutive activation of stat3 have not been identified. Thus, activation of stat3 by PKM2 in malignant cancer cells potentially provides a very attractive explanation for this long-standing question. Whether stat3 is the only PKM2 substrate for its protein kinase activity is an open question. PKM2 interacts with several other proteins (Garcia-Gonzalo, Cruz et al. 2003; Lee, Kim et al. 2008; Spoden, Morandell et al. 2009). It was also reported that PKM2 purified from hepatoma tumour cells can phosphorylate histone H1 in vitro (Ignacak and Stachurska 2003). Thus, it will

be very interested to identify other PKM2 protein kinase substrates and uncover the putative cellular function of the corresponding protein phosphorylations.

3.5 Materials and Methods

3.5.1 Reagents, Cell lines, and Antibodies

The KLH conjugated peptide spans aa 399 – 412 of PKM2 (IYHLQLFEELRRLAPI) was synthesized by Global Peptide Services. PKM2 polycolonal antibody and anti-HA antibody was raised in the animal facility of Georgia State University. The peptides, D-PhoPepY593, PepY593, and PhosPepY567, were synthesized by AnaSpec. Antibodies against stat3, stat3 (pY705), HA-tag, GAPDH, Lamin A/C, and β-actin were purchased from Cell Signaling, Abnova, SantaCruz, Abcam, and AnaSpec respectively. Recombinant GST-stat3 was purchased from Abcam. Cell lines SW480, SW620, T98G were purchased from ATCC and cultured by following the vendor's instructions.

3.5.2 Plasmids Construction

Human full length cDNA of PKM2 and PKM1 were purchased from OriGene Technologies. The cDNA of PKM2 and PKM1 was subcloned into bacteria expression vector pET30a (+) as well as mammalian expression vectors pHM6. The PKM2 or its mutants were fused at the C-terminal of HA protein tag in pHM6 mammalian expression vector. Site directed mutagenesis were performed using QuikChange® Multi Site-Directed Mutagenesis Kit (Stratagene). All the DNA clones and mutations were verified by auto-DNA sequencing at GSU. The HA-tagged full length p68 (wild type, Y593F

mutant) expression plasmids were constructed in pHM6 vectors as indicated in the previous papers from our lab (Yang, Lin et al. 2006).

3.5.3 Expression and Purification of Recombinant PKM2

Recombinant 6×his-PKM2, 6xhis-PKM1, or 6xhisPKM2 mutants was expressed in bacterial BL21-CodonPlus (DE3)-RIPL. The recombinant protein was expressed and accumulated in the bacterial inclusion body. After extensive washes, the bacterial inclusion bodies were dissolved into 8 M Urea pH = 7.5. The protein was then purified over a HiTrap® his-affinity column. The purified recombinant PKM2, PKM1, and PKM2 mutants was then refold by slow dilution into 10 folds refolding buffer (10 mM tris pH=7.5, 20% glycerol, 0.1 M KCl, 0.1 M EDTA, 1 mM DTT) and dialysis against refolding buffer. Purified protein was verified by immunobloting using antibody against PKM2.

3.5.4 Transfection and RNA Interference, Subcellular Extracts Preparation, Immunoprecipitation and Immuno Blots, and PCR and RT-PCR

The experimental procedures for transfection, cellular extracts preparation, immunoprecipitation and immuno blots, and PCR and RT-PCR were similar to our previous reports (Yang, Lin et al. 2006; Yang, Lin et al. 2007). The primer pairs used in present study were, for RT-PCR analyses of MEK5 gene expression, forward 5'-CATGTCCTTGGAAGAATTGC-3', reverse 5'-ATAGAATTCACCAGCTGAGTG-3', targeted exon 12 – exon 14/15 regions of the MEK5 gene.

3.5.5 Size-exclusion Chromatography and Non-denaturing Gel Electrophoresis

Size exclusion chromatograph was performed with a Superdex 200 10/300GL column using Akta purifier 100 FPLC system. The samples of cytoplasmic extracts, nuclear extract, the rPKM2, the recombinant PKM2 mutants, and the immunopurified HA-PKM2/HA-R399E were prepared in tris-HCl buffer (50 mM tris, 0.15 M NaCl pH 7.2). 6-AcA (600 mM) was added to the protein samples to disrupt the non-specific protein-protein interactions. For the crude cellular extracts, the samples were prepared in 5 – 7 mg/ml of total protein. For the recombinant or the immunopurified proteins, the samples were prepared in concentration of 15 μM. 100 μl of prepared sample was loaded into the Superdex 200 10/300GL column and eluted with elution buffer (50 mM phosphate, 0.15M NaCl pH7.2). The fraction of 300 μl was collected, and 50 μl of each fraction was analyzed by 10 % SDS-PAGE and followed by immunoblot using appropriate antibody. A size exclusion chromatograph calibration kits was purchased from GE Healthcare. The protein standard samples (six high MW proteins) were dissolved in the same buffer with 600 mM AcA at concentrations instructed by the manufacture. Proteins were eluted with the same elution buffer. The fractions (300 μl) were collected with the same FPLC system and conditions. The elution profile was recorded based on the absorbance of elution fractions at 280 nm. The elution profile was plotted against LogMW according to vendor's instructions.

The treated cytoplasmic or the nuclear extracts (6 μl) were loaded on an 8% non-denaturing polyacrylamide gel (40:1 – acrylamide:bis-acrylamide). The gel was subject to immunoblot using the antibody PabPKM2. The molecular weight markers, BSA and Urease (Sigma), were loaded on the same gel and were visualized by ponceau S staining.

3.5.6 PKM2 and Peptide Interaction

Interactions between the rPKM2 and its derived mutants were analyzed by monitoring the changes of tryptophan fluorescence of the recombinant protein PKM2 or the mutants (λex =285 nm, λem =310-410 nm). The binding analyses were carried out with protein concentration 4 μM in the reaction buffer (50 mM tris, pH7.5, 100 mM KCl). Different peptides (100 μM) were titrated into the protein solution. All spectra were recorded at ambient temperature using a PTI spectrofluorimeter with a 1 cm path length cuvette. FBP was added in the protein solution with a final concentration of 2 mM.

3.5.7 *In vitro* Protein Kinase and Pyruvate Kinase Assays

The bacterially expressed recombinant rPKM2/R399E or HA-PKM2/HA-R399E immunopurified from cellular extracts (10 μg/ml) were incubated with GST-stat3 (10 μg/ml) under various conditions (indicated in the figure legends) with kinase buffer (50 mM Tris-HCl pH = 7.5, 100 mM KCl, 50 mM $MgCl_2$, 1 mM Na_3VO_4, 1 mM PMSF, and 1 mM DTT) in 100 μl at room temperature for 1 hours. The phosphorylation reactions were carried out in the presence either 5 mM ATP or 5 mM PEP. The phosphorylation reactions were terminated by addition of 20 μl of 4 x SDS-PAGE loading buffer and heated to 100 °C for 8 minutes. The reaction mixtures were then subjected to 10% SDS-PAGE separation and subsequent analyses.

Pyruvate kinase activity was analyzed by following the experimental procedure similar to that was described by Christofk and co-workers (Christofk, Vander Heiden et al. 2008). Briefly, the rPKM2 or the mutant R399E (at 1 μM) was incubated with the

buffer (100 mM Tris-HCl, pH=7.5, 100 mM KCl, 5 mM $MgCl_2$) containing 1 mM ADP and 0.5 mM PEP. The reaction also contained 200 μM NADH and 10 μM FBP. After incubation at room temperature for 30 minutes, 8 units of LDH (Calbiochem) were added to the reaction. The reactions were then subsequently analyzed by measuring the absorbance at 340 nm. The pyruvate kinase activity was presented as relative pyruvate kinase activity by define the activity of the rPKM2 as 100.

3.5.8 Peptide Pull Down and Protein Identification by Mass Spectroscopy

The peptides, PepY593 CGMNQQAYAYPATAA, PhosPepY593 CGMNQQA[pY]AYPATAA, D-PhosPepY593 CGMNQQA[pY]A[pY]PATAA, and PhosPepY567 CGNPTGT[pY]QNGYDST were purchased from Anaspec Inc. The peptides were conjugated to agarose beads using AminoLink Plus Immobilization kit (Pierce). The peptide-conjugated beads were incubated with 3 mg (total protein) fresh nuclear extract in NETs buffer (150 mM NaCl, 50 mM tris, pH 7.5, 5 mM EDTA, 0.1% NP-40) overnight at 4 °C. The next day, the beads were separated and washed with NETs buffer five times. The proteins precipitated with the peptide beads were separated in 10% SDS-PAGE and stained with GelCode blue stain (Pierce) or silver staining. After destaining, the identified protein bands were excised from the gel and digested with trypsin. The digested peptides were extracted from gel with Trypsin Profiel IGD kit (Sigma). The samples were concentrated with vacuum centrifugation and desalted with ZipTip C18 pipette tips (Millipore). After ZipTip purification, the peptides were eluted from the ZipTip with 50% acetonitrile (ACN)/0.1% trifluoroacetic (TFA) and spotted directly onto a wax-coated MALDI target plates. The peptides were analyzed by

TOF/TOF-MS analysis in Applied Biosystems 4700 Proteomics Analyzer. Peptides with "ion scores" above 30 were considered significant. The MS/MS data was searched in the NCBInr database (Mascot; All Taxa, Human).

3.6 References

Ashizawa, K., McPhie, P., Lin, K.H., and Cheng, S.Y. (1991). An in vitro novel mechanism of regulating the activity of pyruvate kinase M2 by thyroid hormone and fructose 1, 6-bisphosphate. Biochemistry *30*, 7105-7111.

Christofk, H.R., Vander Heiden, M.G., Harris, M.H., Ramanathan, A., Gerszten, R.E., Wei, R., Fleming, M.D., Schreiber, S.L., and Cantley, L.C. (2008a). The M2 splice isoform of pyruvate kinase is important for cancer metabolism and tumour growth. Nature *452*, 230-233.

Christofk, H.R., Vander Heiden, M.G., Wu, N., Asara, J.M., and Cantley, L.C. (2008b). Pyruvate kinase M2 is a phosphotyrosine-binding protein. Nature *452*, 181-186.

Cooper, J.A., Bowen-Pope, D.F., Raines, E., Ross, R., and Hunter, T. (1982). Similar effects of platelet-derived growth factor and epidermal growth factor on the phosphorylation of tyrosine in cellular proteins. Cell *31*, 263-273.

Dombrauckas, J.D., Santarsiero, B.D., and Mesecar, A.D. (2005). Structural basis for tumor pyruvate kinase M2 allosteric regulation and catalysis. Biochemistry *44*, 9417-9429.

Ek, B., Westermark, B., Wasteson, A., and Heldin, C.H. (1982). Stimulation of tyrosine-specific phosphorylation by platelet-derived growth factor. Nature *295*, 419-420.

Elbers, J.R., van Unnik, J.A., Rijksen, G., van Oirschot, B.A., Roholl, P.J., Oosting, J., and Staal, G.E. (1991). Pyruvate kinase activity and isozyme composition in normal fibrous tissue and fibroblastic proliferations. Cancer *67*, 2552-2559.

Frank, D.A. (2007). STAT3 as a central mediator of neoplastic cellular transformation. Cancer Lett *251*, 199-210.

Garcia-Gonzalo, F.R., Cruz, C., Munoz, P., Mazurek, S., Eigenbrodt, E., Ventura, F., Bartrons, R., and Rosa, J.L. (2003). Interaction between HERC1 and M2-type pyruvate kinase. FEBS Lett *539*, 78-84.

Groner, B., Lucks, P., and Borghouts, C. (2008). The function of Stat3 in tumor cells and their microenvironment. Semin Cell Dev Biol *19*, 341-350.

Hacker, H.J., Steinberg, P., and Bannasch, P. (1998). Pyruvate kinase isoenzyme shift from L-type to M2-type is a late event in hepatocarcinogenesis induced in rats by a choline-deficient/DL-ethionine-supplemented diet. Carcinogenesis *19*, 99-107.

Hoshino, A., Hirst, J.A., and Fujii, H. (2007). Regulation of cell proliferation by interleukin-3-induced nuclear translocation of pyruvate kinase. J Biol Chem *282*, 17706-17711.

Huang, Y., Qiu, J., Dong, S., Redell, M.S., Poli, V., Mancini, M.A., and Tweardy, D.J. (2007). Stat3 isoforms, alpha and beta, demonstrate distinct intracellular dynamics with

prolonged nuclear retention of Stat3beta mapping to its unique C-terminal end. J Biol Chem *282*, 34958-34967.
Hunter, T., and Cooper, J.A. (1981). Epidermal growth factor induces rapid tyrosine phosphorylation of proteins in A431 human tumor cells. Cell *24*, 741-752.
Ignacak, J., and Stachurska, M.B. (2003). The dual activity of pyruvate kinase type M2 from chromatin extracts of neoplastic cells. Comp Biochem Physiol B Biochem Mol Biol *134*, 425-433.
Kim, D.J., Chan, K.S., Sano, S., and Digiovanni, J. (2007). Signal transducer and activator of transcription 3 (Stat3) in epithelial carcinogenesis. Mol Carcinog *46*, 725-731.
Lee, J., Kim, H.K., Han, Y.M., and Kim, J. (2008). Pyruvate kinase isozyme type M2 (PKM2) interacts and cooperates with Oct-4 in regulating transcription. Int J Biochem Cell Biol *40*, 1043-1054.
Mazurek, S., Boschek, C.B., Hugo, F., and Eigenbrodt, E. (2005). Pyruvate kinase type M2 and its role in tumor growth and spreading. Semin Cancer Biol *15*, 300-308.
Muirhead, H., Clayden, D.A., Barford, D., Lorimer, C.G., Fothergill-Gilmore, L.A., Schiltz, E., and Schmitt, W. (1986). The structure of cat muscle pyruvate kinase. EMBO J *5*, 475-481.
Roossien, F.F., Brink, J., and Robillard, G.T. (1983). A simple procedure for the synthesis of [32P]phosphoenolpyruvate via the pyruvate kinase exchange reaction at equilibrium. Biochim Biophys Acta *760*, 185-187.
Spoden, G.A., Morandell, D., Ehehalt, D., Fiedler, M., Jansen-Durr, P., Hermann, M., and Zwerschke, W. (2009). The SUMO-E3 ligase PIAS3 targets pyruvate kinase M2. J Cell Biochem *107*, 293-302.
Yang, L., Lin, C., and Liu, Z.R. (2005). Phosphorylations of DEAD box p68 RNA helicase are associated with cancer development and cell proliferation. Mol Cancer Res *3*, 355-363.
Yang, L., Lin, C., and Liu, Z.R. (2006). P68 RNA helicase mediates PDGF-induced epithelial mesenchymal transition by displacing Axin from beta-catenin. Cell *127*, 139-155.
Yang, L., Lin, C., Sun, S.Y., Zhao, S., and Liu, Z.R. (2007a). A double tyrosine phosphorylation of P68 RNA helicase confers resistance to TRAIL-induced apoptosis. Oncogene *26*, 6082-6092.
Yang, L., Lin, C., Zhao, S., Wang, H., and Liu, Z.R. (2007b). Phosphorylation of p68 RNA helicase plays a role in platelet-derived growth factor-induced cell proliferation by up-regulating cyclin D1 and c-Myc expression. J Biol Chem *282*, 16811-16819.

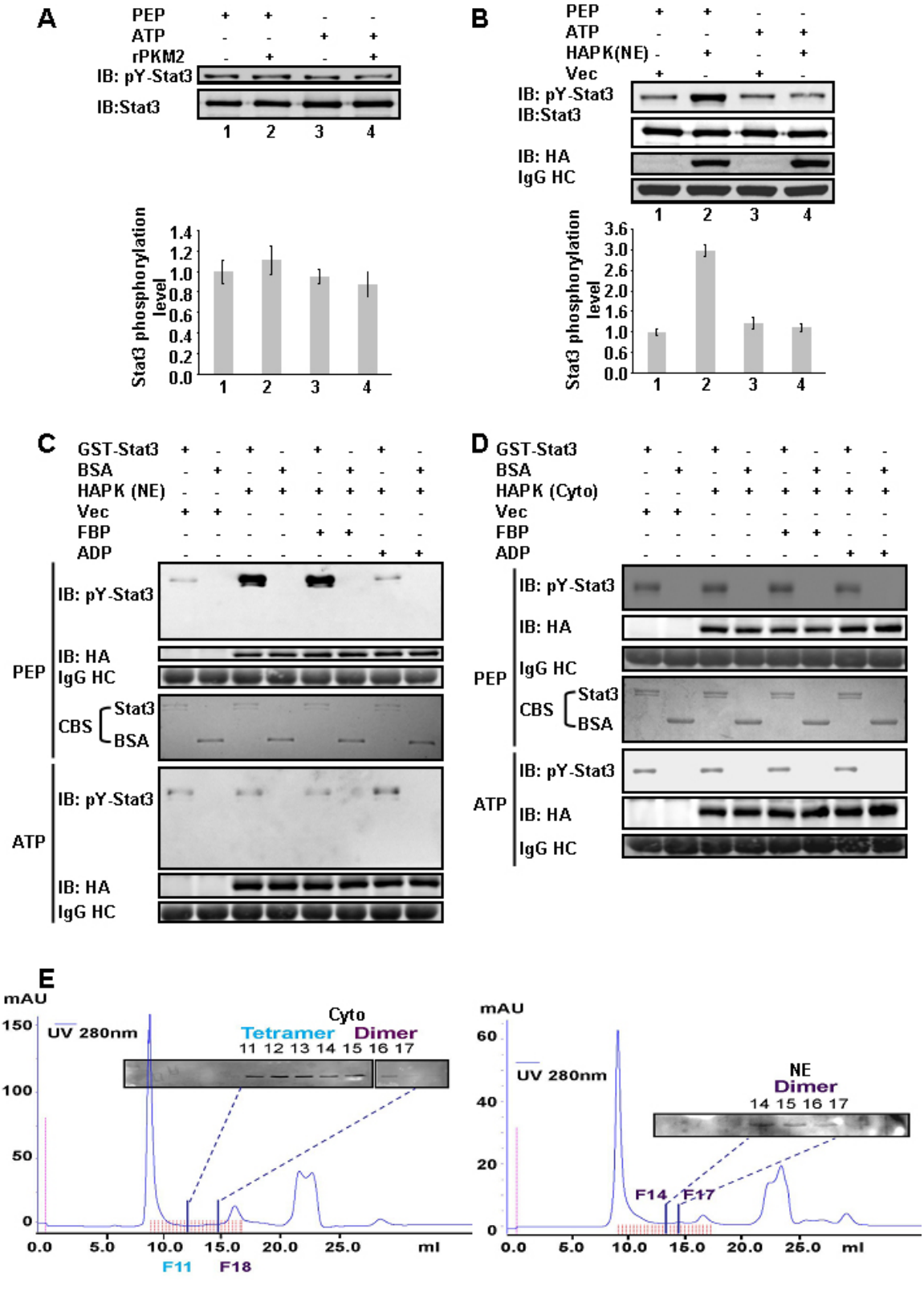
A
PEP
ATP
rPKM2
IB: pY-Stat3
IB:Stat3
1 2 3 4
Stat3 phosphorylation level
B
PEP
ATP
HAPK(NE)
Vec
IB: pY-Stat3
IB:Stat3
IB: HA
IgG HC
C
GST-Stat3
BSA
HAPK (NE)
Vec
FBP
ADP
PEP
ATP
IB: pY-Stat3
IB: HA
IgG HC
CBS
Stat3
BSA
D
GST-Stat3
BSA
HAPK (Cyto)
Vec
FBP
ADP
E
mAU
UV 280nm
Cyto
Tetramer
Dimer
11 12 13 14 15 16 17
F11
F18
ml
NE
14 15 16 17
F14
F17

Fig 3.1 PKM2 Phosphorylates GST-stat3

Phosphorylation of GST-stat3 by the rPKM2 **(A)** and HA-PKM2 immunopurified from nuclear extracts of SW620 cells **(B)** in the presence of 5 mM ATP (ATP) or 5 mM of PEP (PEP) was revealed by immunoblot assays using antibody against Y705 phosphorylated stat3 (IB:pY-stat3). Immunoblot analyses using antibody against stat3 (IB:Stat3) indicates the amounts of GST-stat3 used in each phosphorylation reaction. The bottom panels in (A) & (B) are the quantitative analyses of immunoblot signals. The error bars represent the standard deviations of four measurements. Phosphorylation of GST-stat3 by the HA-PKM2 (HA-PK) immunopurified from the nuclear **(C)** and the cytoplasmic **(D)** extracts of SW620 cells in the presence of 5 mM ATP (ATP) or 5 mM of PEP (PEP) was revealed by immunoblot assays using antibody against Y705 phosphorylated stat3 (IB:pY-stat3). The phosphorylation reactions were also carried out in the presence/absence of 5 mM of FBP (FBP), or 5 mM of ADP (ADP). The immunoblot of HA (IB:HA) indicates the amounts of HA-PKM2 used in each reaction. IgG HC is the ponceau S stain of antibody heavy chain, representing the amounts of antibody used in immunopurification of HA-PKM2 from the extracts. Coomassie blue staining (CBS) indicates the amounts of GSTstat3 and BSA used in each phosphorylation reaction. Vec were the cells infected with virus that carry an empty vector. **(E)** Size exclusion chromatography fractionation of nuclear (NE) and cytoplasmic (Cyto) extracts (100 µl) from SW620 cells. The fractions were collected using a FPLC at 300 µl per fraction. The collected fractions 6 to 17 from cytoplasmic extracts and fraction 9 to 18 from nuclear extracts were immunoblotted using the antibody PabPKM2. Fraction 11 (F11) co-eluted with 240 kDa and fraction 14 (F14) co-eluted with 120 kDa on the same column under identical conditions determined by size exclusion chromatography molecular weight calibration standard (see on-line supplementary Fig. S1 B&C).

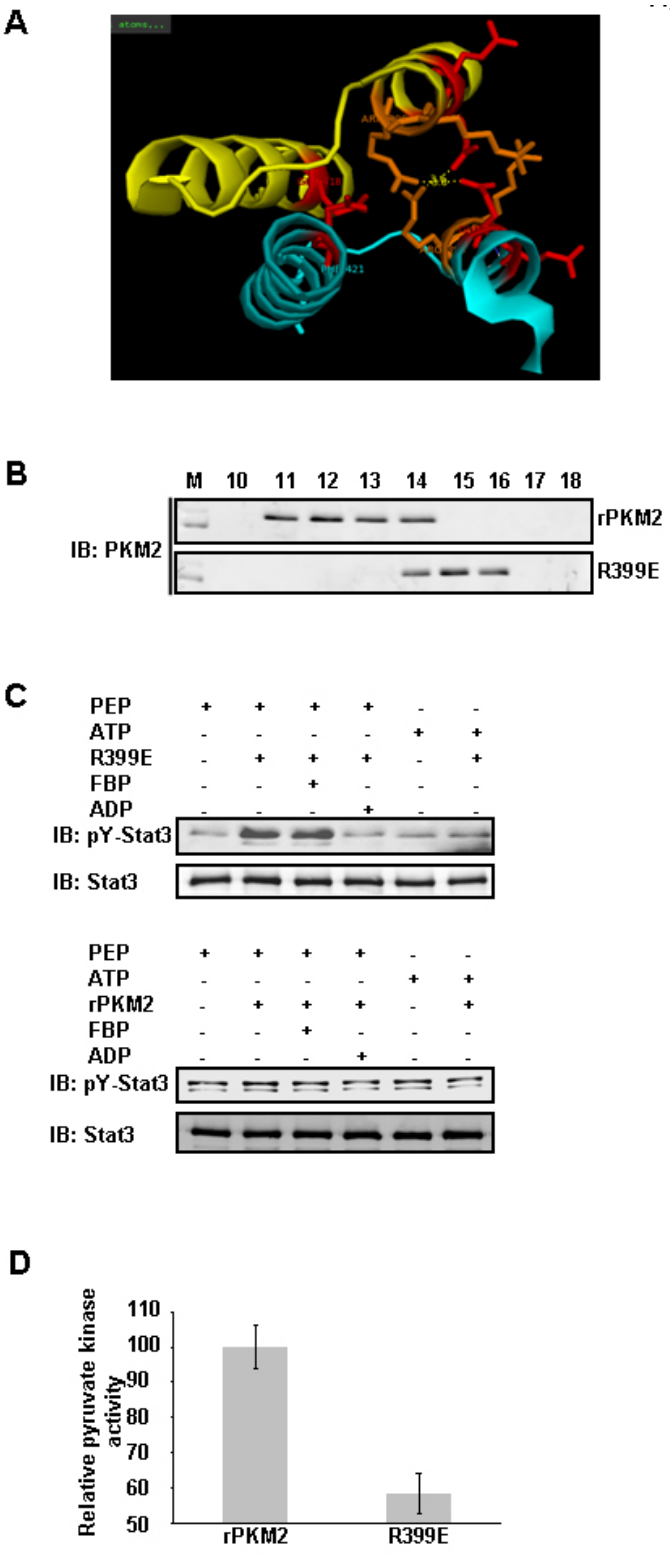
A
B
M 10 11 12 13 14 15 16 17 18
IB: PKM2
rPKM2
R399E
C
PEP
ATP
R399E
FBP
ADP
IB: pY-Stat3
IB: Stat3
PEP
ATP
rPKM2
FBP
ADP
IB: pY-Stat3
IB: Stat3
D
Relative pyruvate kinase activity
110
100
90
80
70
60
50
rPKM2
R399E

Fig 3.2 Dimeric PKM2 is Active Protein Kinase
(A) Part of x-ray crystal structure of human PKM2. The structure was obtained from PDB bank DOI: 10.1021/bi0474923. The residue R399 and its interactive residues E418, D357, and E396 are high lighted in color. **(B)** Size exclusion chromatography fractionation of the wild-type rPKM2 and R399E mutant. The recombinant proteins 100 μl in 1.5 μM were loaded onto column. The chromatography fractions F10 – F18 were collected using a FPLC at 300 μl per fraction. The collected fractions were analyzed by immunoblot using the antibody PabPKM2 (IB:PKM2). **(C)** Phosphorylation of GST-stat3 by the rPKM2 (10 μg/ml) (lower panel) and R399E mutant (10 μg/ml) (upper panel) in the presence of 5 mM ATP (ATP), 5 mM of PEP (PEP), 5 mM of FBP (FBP), and/or 5 mM ADP (ADP) was revealed by immunoblot assays using antibody against Y705 phosphorylated stat3 (IB:pY-stat3). Immunoblot analyses using antibody against stat3 (IB:Stat3) indicates the amounts of GST-stat3 used in each phosphorylation reaction. **(D)** Pyruvate kinase activity of the rPKM2 or R399E mutant (5 μg/ml) was analyzed by the method described by Christofk and co-workers. The pyruvate kinase activity was expressed as relative pyruvate kinase activity by define the activity in the rPKM2 as 100. The error bars represent the standard deviations of four measurements.

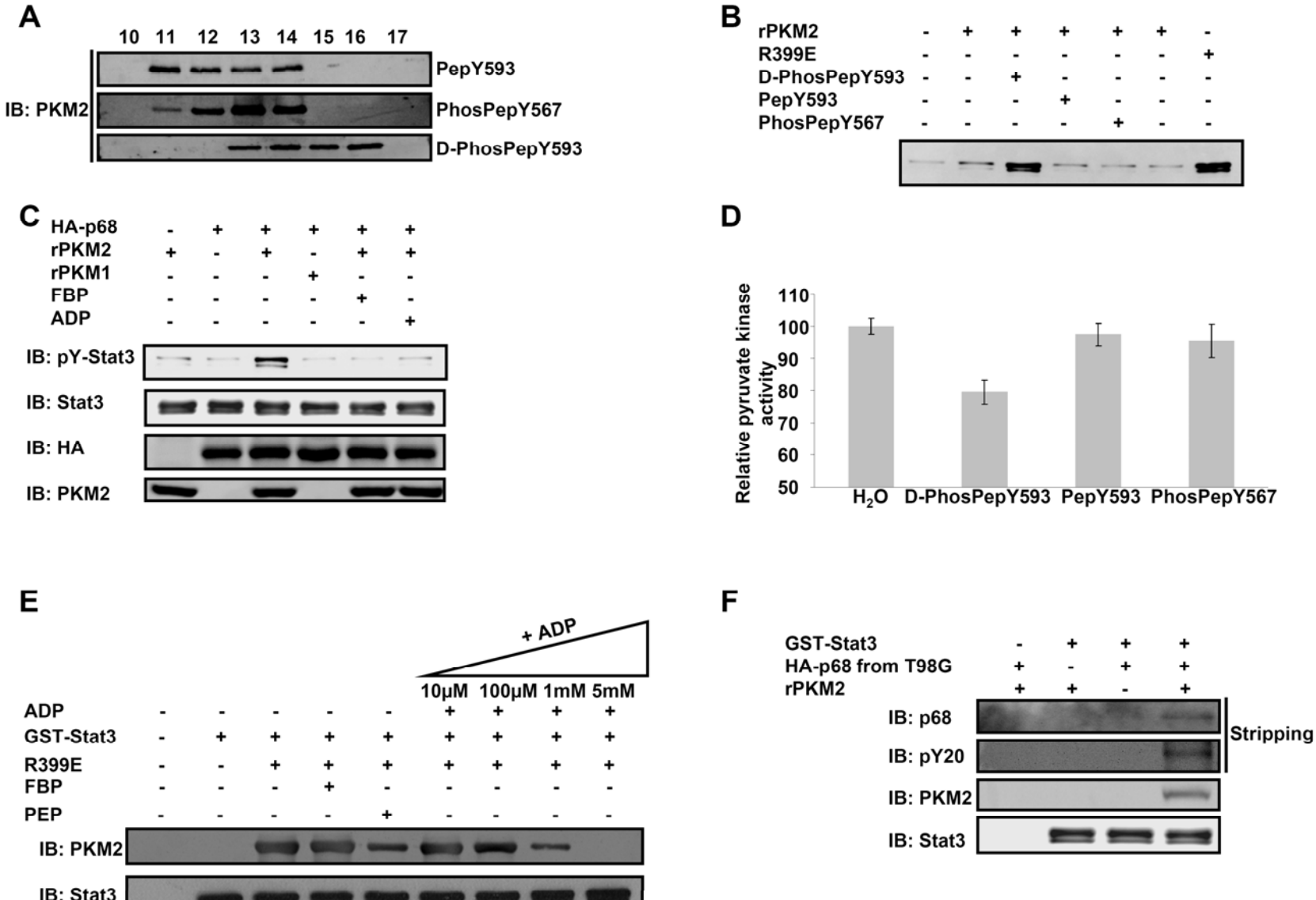
A
10 11 12 13 14 15 16 17
IB: PKM2
PepY593
PhosPepY567
D-PhosPepY593
B
rPKM2
R399E
D-PhosPepY593
PepY593
PhosPepY567
C
HA-p68
rPKM2
rPKM1
FBP
ADP
IB: pY-Stat3
IB: Stat3
IB: HA
IB: PKM2
D
Relative pyruvate kinase activity
110
100
90
80
70
60
50
H2O
D-PhosPepY593
PepY593
PhosPepY567
E
+ ADP
10μM 100μM 1mM 5mM
ADP
GST-Stat3
R399E
FBP
PEP
IB: PKM2
IB: Stat3
F
GST-Stat3
HA-p68 from T98G
rPKM2
IB: p68
IB: pY20
IB: PKM2
IB: Stat3
Stripping

Figure 3.3 Tyrosine Phosphor-peptide Converts Tetramer PKM2 to a Dimer and Activates Protein Kinase Activity

(A) Size exclusion chromatography fractionation of the wild-type rPKM2 in the presence of different peptides (3 μM) D-phosPepY593 (lower panel), PepY593 (upper panel), and phosPepY567 (middle panel). The rPKM2 100 μl in 1.5 μM were loaded onto column. The chromatography fractions F10 – F18 were collected using a FPLC at 300 μl per fraction. The collected fractions were immunoblotted using the antibody PabPKM2 (IB:PKM2). **(B)** Phosphorylation of GST-stat3 by the rPKM2 (10 μg/ml) and the R399E mutant (10 μg/ml) in the presence of different peptides (3 μM) D-PhosPepY593, PepY593, and PhosPepY567 was revealed by immunoblot assays using antibody against Y705 phosphorylated stat3 (IB:pY-stat3). **(C)** Phosphorylation of GST-stat3 by the rPKM2 (10 μg/ml) or the rPKM1 (10 μg/ml) in the presence of HA-p68 that was immunopurified from nuclear extracts of T98G cells and 5 mM of PEP was revealed by immunoblot assays using antibody against Y705 phosphorylated stat3 (IB:pY-stat3). In some phosphorylation reactions, 5 mM of FBP (FBP) or 5 mM ADP (ADP) was added to the reaction. Immunoblots of stat3 (IB:Stat3), HA-p68 (IB:HA), and PKM2 (IB:PKM2) indicate the amounts of GST-stat3, HA-p68, and the rPKM2 used in each phosphorylation reaction. **(D)** Pyruvate kinase activity of the rPKM2 (5 μg/ml) in the presence of different peptides (2 μM) D-PhosPepY593, PepY593, PhosPepY567, or buffer was analyzed by the method described by Christofk and co-workers. The pyruvate kinase activity of the rPKM2 was expressed as relative pyruvate kinase activity by define the activity in the presence of Buffer as 100. The error bars represent the standard deviations of four measurements. **(E)** Interaction of GST-stat3 and R399E mutant in the presence of FBP (5 mM), PEP (5 mM), or various concentrations of ADP (10, 100, 1000 and 5000 μM) was analyzed by GST-pull-down using the glutathione beads. The co-precipitation of R399E with GST-stat3 was detected by immunoblot using the antibody against PKM2 (IB:PKM2). Immunoblots of precipitates using antibody against stat3 (IB:Stat3) indicate the amounts of GST-stat3 that was pulled-down by the glutathione beads. **(F)** Interaction of GST-stat3, the bacterially expressed rPKM2, and the HAp68 immunopurified from T98G cells was analyzed by GST-pull-down using the glutathione beads. The GST-stat3 (2 μg/ml), the rPKM2 (2 μg/ml), and the HA-p68 were incubated in 500 μl at room temperature. The GST-stat3 was precipitated by the GST beads. Co-precipitations of the HA-p68 and the rPKM2 from the mixture were analyzed by immunoblot using antibodies against p68 (IB:p68) and PKM2 (IB:PKM2). The strip blot using anti-phosphor-tyrosine indicates the tyrosine phosphorylation of the precipitated HA-p68. Immunoblot of stat3 (IB:Stat3) indicates the amounts of GST-stat3 that were precipitated by GST beads.

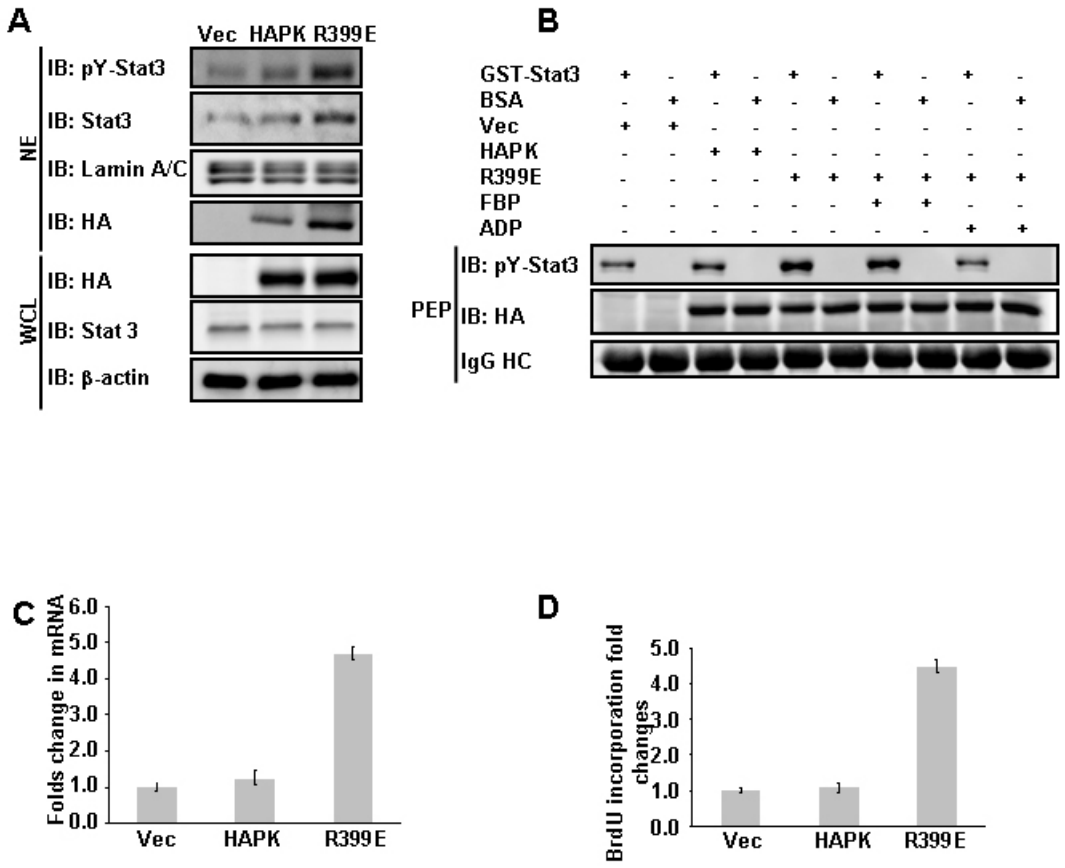
A
Vec HAPK R399E
NE
IB: pY-Stat3
IB: Stat3
IB: Lamin A/C
IB: HA
WCL
IB: HA
IB: Stat 3
IB: β-actin
B
GST-Stat3
BSA
Vec
HAPK
R399E
FBP
ADP
PEP
IB: pY-Stat3
IB: HA
IgG HC
C
Folds change in mRNA
6.0
5.0
4.0
3.0
2.0
1.0
0.0
Vec
HAPK
R399E
D
BrdU incorporation fold changes
5.0
4.0
3.0
2.0
1.0
0.0
Vec
HAPK
R399E

Fig 3.4 The R399E Mutant Phosphorylates Stat3 in Cells and Expression of the Mutant Promotes Cell Proliferation

(A) Phosphorylation of stat3 in SW480 cells was examined by immunoblot analyses of the nuclear extracts (NE) using antibody against the Y705 phosphorylated stat3 (IB:pY-Stat3). PKM2 wild-type (HAPK) or the R399E (R399E) mutant was expressed in the cells by transient transfection. Immunoblots using anti-HA antibody (IB:HA) and anti-stat3 antibody (IB:Stat3) in the nuclear extracts and whole cell lysate (WCL) indicate the levels of stat3 and HA-PKM2/HAR399E in the nuclear extracts and whole cell lysate. **(B)** Phosphorylation of GST-stat3 by the HA-p68 and the HA-R399E mutant that were immunopurified from cell lysate of SW480 cells in the presence of 5 mM of PEP was revealed by immunoblot analyses using antibody against the Y705 phosphorylated stat3 (IB:pY-Stat3). The phosphorylation reactions were also carried out in the presence/absence of 5 mM of FBP (FBP), or 5 mM of ADP (ADP). The immunoblot of HA (IB:HA) indicates the amounts of HA-PKM2 or HA-R399E used in each reaction. IgG HC is the ponceau S stain of antibody heavy chain, representing the amounts of antibody used in immunopurification of the HA-PKM2 or the HA-R399E mutant from the extracts. **(C)** Expression of MEK5 mRNA in SW480 cells was analyzed by RT-PCR HA-PKM2 (HAPK) or HA-R399E (R399E) was exogenously expressed in the cells. The results are presented as fold changes in PCR products before and 48 hours after HA-PKM2 or HA-R399E expression. **(D)** Cell proliferations of SW480 cells were measured using the cell proliferation kit. Cell proliferations were presented as fold changes in BrdU incorporation before and 48 hours after HA-PKM2 (HAPK) or HA-R399E (R399E) expression. The BrdU incorporation of the cells that were transfected with the empty vector (Vec) was defined as 1. Error bars in **(C)** and **(D)** are standard deviations of three independent measurements. Vec in **(A), (B), (C),** and **(D)** are the cells transfected with the empty vector.

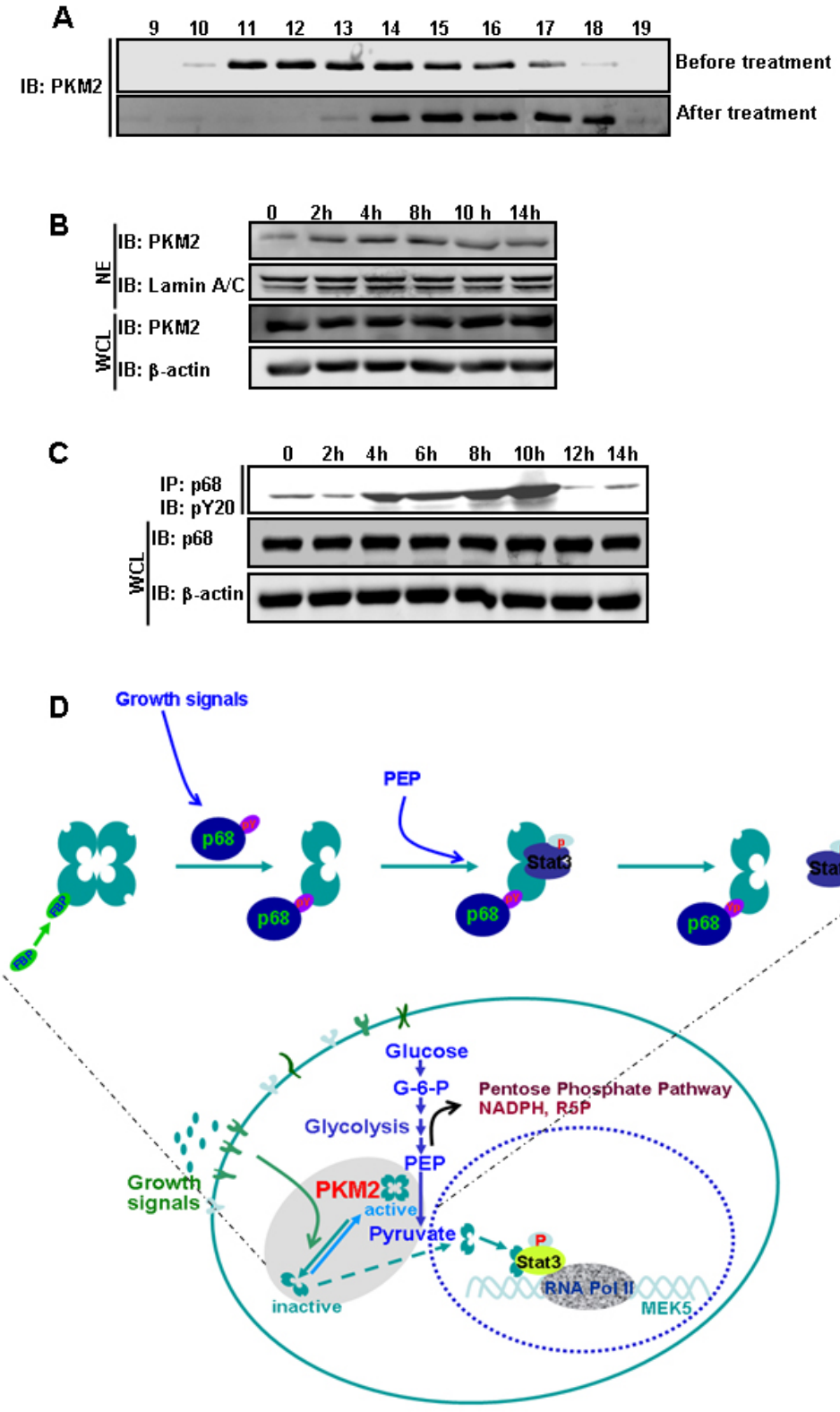
A
9 10 11 12 13 14 15 16 17 18 19
IB: PKM2
Before treatment
After treatment
B
0 2h 4h 8h 10 h 14h
NE
IB: PKM2
IB: Lamin A/C
WCL
IB: PKM2
IB: β-actin
C
0 2h 4h 6h 8h 10h 12h 14h
IP: p68
IB: pY20
WCL
IB: p68
IB: β-actin
D
Growth signals
PEP
p68
Stat3
Glucose
G-6-P
Pentose Phosphate Pathway
NADPH, R5P
Glycolysis
PEP
PKM2
active
inactive
Pyruvate
Growth signals
Stat3
RNA Pol II
MEK5

Fig 3.5 Growth Factor Stimulation Leads to Tetramer to Dimer Conversion of PKM2
(A) Size exclusion chromatography fractionation of cell lysate prepared from SW480 cells that were treated/untreated by 25 ng/ml EGF for 8 hours. The cell lysate (100 μl) were loaded onto the column. The chromatography fractions F9 – F20 were collected using a FPLC at 300 μl per fraction. The collected fractions were immunoblotted using the antibody against PKM2 (IB:PKM2). **(B)** The PKM2 levels in the nuclear extracts (NE) of SW480 cells that were treated with EGF (25 ng/ml) at different time points (indicated) were examined by immunoblot of the nuclear extracts using antibody against PKM2 (IB:PKM2). Immunoblot analyses of PKM2 (IB:PKM2) in the whole cell lysate (WCL) indicate the cellular levels of PKM2. Immunoblot of β-actin (IB:β-actin) and lamin A/C (IB:Lamin A/C) were the loading controls. **(C)** Tyrosine phosphorylation of p68 in the in the nuclear extracts (NE) of SW480 cells that were treated with EGF (25 ng/ml) at different time points (indicated) were examined by immunoblot analyses of p68 that was immunoprecipitated (IP:68) from the extracts using the anti-phosphor-tyrosine antibody (IB:pY20). Immunoblot analyses of p68 (IB:p68) in the whole cell lysate (WCL) indicate the cellular levels of PKM2. Immunoblot of β-actin (IB:β-actin) was the loading control. **(D)** A hypothetic model that illustrates the functions of PKM2 in the glycolysis and gene expression, and the regulation between protein kinase or pyruvate kinase active of the protein.

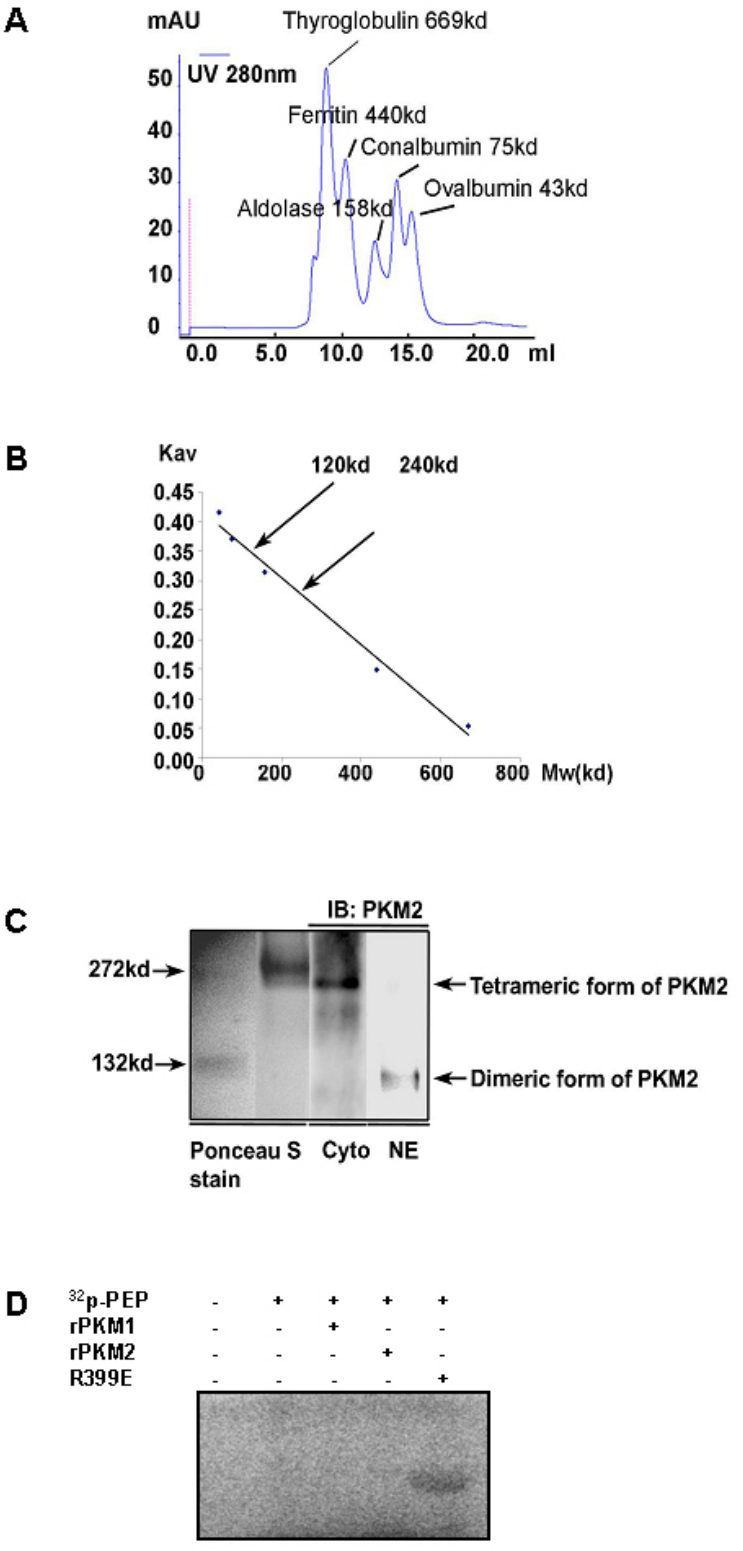
A
mAU
Thyroglobulin 669kd
UV 280nm
Ferritin 440kd
Conalbumin 75kd
Ovalbumin 43kd
Aldolase 158kd
50
40
30
20
10
0
0.0
5.0
10.0
15.0
20.0
ml
B
Kav
120kd
240kd
0.45
0.40
0.35
0.30
0.25
0.20
0.15
0.10
0.05
0.00
0
200
400
600
800
Mw(kd)
C
IB: PKM2
272kd
132kd
Tetrameric form of PKM2
Dimeric form of PKM2
Ponceau S stain
Cyto
NE
D
32p-PEP
rPKM1
rPKM2
R399E

Figure 3.6 Nuclear PKM2 is a Dimeric Form
(A) Chromatographic elution profile of the molecular weight calibration kit proteins (indicated) on the Superdex 200 10/300GL column. The x-axis is the elution volume. The y-axis is the absorbance of the elution at 280 nm. **(B)** The standard curve of elution of the molecular weight calibration kit proteins on the Superdex 200 10/300GL column. The elution volumes were plotted against LogMW. **(C)** Immunoblot analyses of PKM2 in the cytoplasmic (Cyto) and nuclear (NE) extracts of SW620 cells. The extracts (6 μl) were treated (as described in methods) and loaded on an 8% non-denaturing gel electrophoresis. The gel was subjected to immunoblot using the antibody PabPKM2 (IB:PKM2). The molecular weight markers, BSA (dimer) and Urease (trimer), were loaded on the same gel and were visualized by ponceau S staining (ponceau S stain). **(D)** Phosphorylation of GST-stat3 by the rPKM2 (10 μg/ml), the rPKM1 (10 μg/ml), or the R399E mutant (10 μg/ml) in the presence of 32P-PEP (~0.002 μCi) and unlabeled PEP (5 mM). The reaction mixture were separated by 10 SDS-PAGE and subjected to autoradiograph

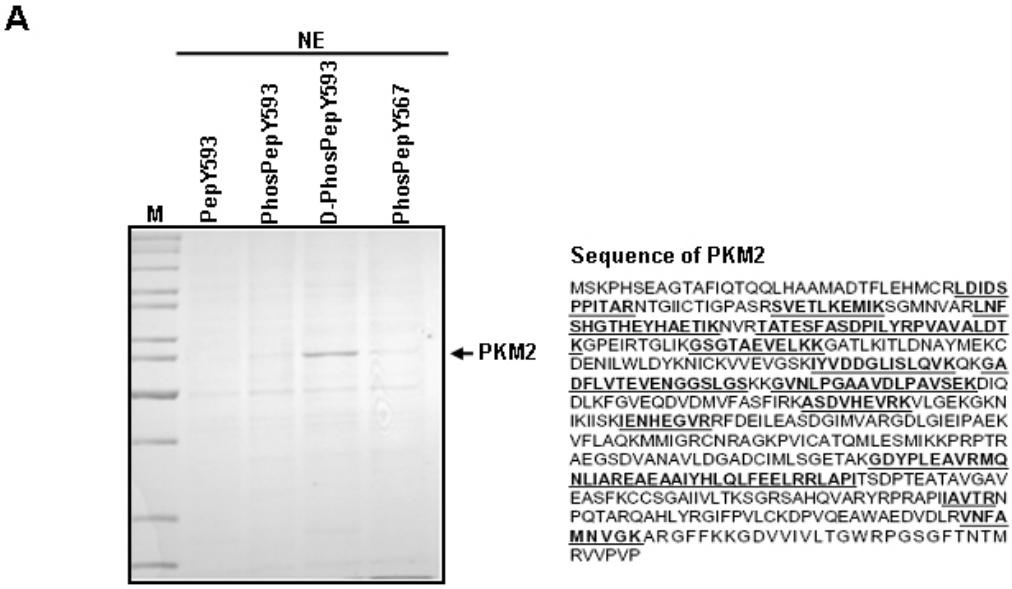
A
NE
M
PepY593
PhosPepY593
D-PhosPepY593
PhosPepY567
PKM2
Sequence of PKM2
MSKPHSEAGTAFIQTQQLHAAMADTFLEHMCRLDIDS
PPITARNTGIICTIGPASRSVETLKEMIKSGMNVARLNF
SHGTHEYHAETIKNVRTATESFASDPILYRPVAVALDT
KGPEIRTGLIKGSGTAEVELKKGATLKITLDNAYMEKC
DENILWLDYKNICKVVEVGSKIYVDDGLISLQVKQKGA
DFLVTEVENGGSLGSKKGVNLPGAAVDLPAVSEKDIQ
DLKFGVEQDVDMVFASFIRKASDVHEVRKVLGEKGKN
IKIISKIENHEGVRRFDEILEASDGIMVARGDLGIEIPAEK
VFLAQKMMIGRCNRAGKPVICATQMLESMIKKPRPTR
AEGSDVANAVLDGADCIMLSGETAKGDYPLEAVRMQ
NLIAREAEAAIYHLQLFEELRRLAPITSDPTEATAVGAV
EASFKCCSGAIIVLTKSGRSAHQVARYRPRAPIIAVTRN
PQTARQAHLYRGIFPVLCKDPVQEAWAEDVDLRVNFA
MNVGKARGFFKKGDVVIVLTGWRPGSGFTNTM
RVVPVP
B
PD: rPKM2
Beads
PepY593
D-PhosPepY593
rPKM2
IB: PKM2
C
NE
PD: rPKM2 Beads
IB: p68
IB: pY20
D
NE
Cyto
Vec HAPK
Vec HAPK
IP: HA
IB: p68
IB: HA
IB: GAPDH
IB: Lamin A/C
IP: PKM2
IB: p68
IB: GAPDH
IB: Lamin A/C
NE
Cyto
E
NE
Vec HA-p68 Y593F
IP: PKM2
IB: HA
IB: HA
IB: H2A

Figure 3.7 Tyrosine-phosphorylated p68 RNA Helicase Interacts with PKM2 both *in vivo* and *in vitro*

(A) (Left panel) GelCode staining SDS-PAGE analyses of proteins pulled down from nuclear extracts of T98G cells by different peptides coupled to agarose beads. The peptides used are: Non-p is the peptide PepY593, Y593-p is the peptide PhosPepY593, Y593/595-p is the peptide D-PhosPepY593, and Y567-p is the peptide PhosPepY567. The arrow indicates the protein band that was cut out and subjected to trypsin digestion followed by MALDI-tof/tof analyses. M is molecular weight markers. (Right panel) The amino acid sequence of PKM2. The bold and underlined sequence indicates the peptide fragments identified by MALDI-tof/tof. **(B)** Interaction of the peptides Non-p and Y593/595-p with recombinant PKM2 (rPKM2). The recombinant PKM2 pull-downs (PD) by the peptides were examined by immunoblot using antibody against PKM2 (IB:PKM2). Beads are the control pull-down using agarose beads alone. **(C)** Pull-down (PD) of p68 from nuclear extracts (NE) of T98G cells by recombinant PKM2 (rPKM2) was examined by immunoblot using antibody p68-RGG (IB:p68-RGG). The tyrosine phosphorylation of p68 was indicated by strip-blot of the pull-down using antibody against phospho-tyrosine (IB:PY20). Beads is the control pull-down using agarose beads alone. **(D)** (Left panel) Co-immunoprecipitations of p68 with exogenously expressed HA-PKM2 from nuclear (NE) and cytoplasmic (Cyto) extracts of T98G cells were examined by immunoblot with antibody p68-RGG (IP:HA, IB:p68-RGG). IBs of HA-PKM2 indicate the immunoprecipitateded HA-PKM2 from the extracts. (Right panel) Co-immunoprecipitations of p68 with endogenous PKM2 from nuclear (NE) and cytoplasmic (Cyto) extracts of T98G cells were examined by immunoblot with antibody p68-RGG (IP:PKM2, IB:p68-RGG). IBs of GAPDH (IB:GAPDH) and lamin A/C (IB:Lamin A/C) are the loading controls. **(E)** Co-immunoprecipitations of exogenously expressed HA-p68s (WT and Y593F, Vec is vector alone) with endogenous PKM2 from nuclear extracts (NE) of T98G cells were examined by immunoblot with anti-HA (IP:PKM2, IB:HA). IBs of the nuclear extracts using anti-HA indicate the expression of HA-p68 (IB:HA). IBs of histone 2A (IB:H2A) are the loading controls.

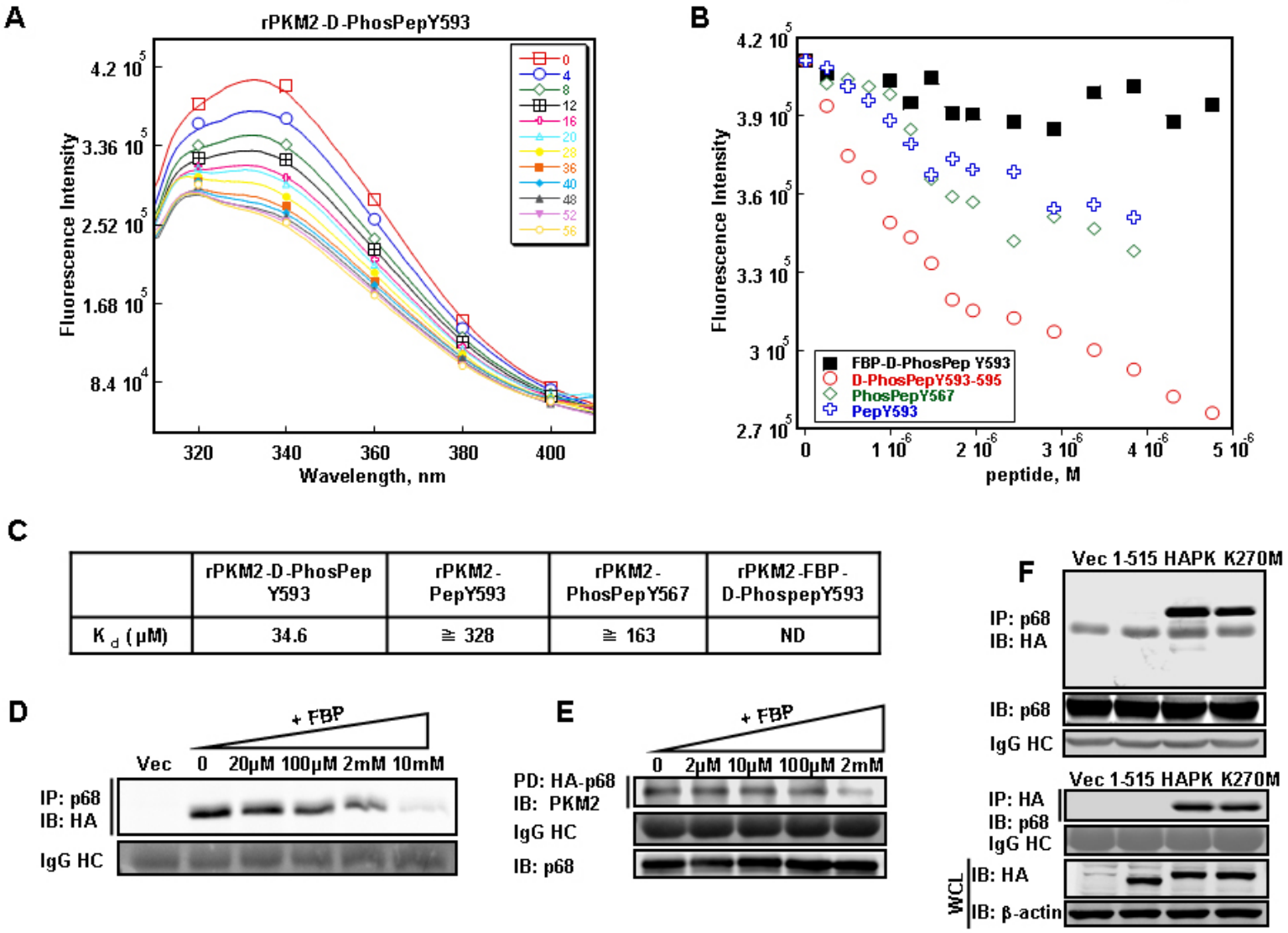
A
rPKM2-D-PhosPepY593
Fluorescence Intensity
Wavelength, nm
0
4
8
12
16
20
28
36
40
48
52
56
B
Fluorescence Intensity
peptide, M
FBP-D-PhosPep Y593
D-PhosPepY593-595
PhosPepY567
PepY593
C
rPKM2-D-PhosPep Y593
rPKM2-PepY593
rPKM2-PhosPepY567
rPKM2-FBP-D-PhospepY593
K d (μM)
34.6
≧ 328
≧ 163
ND
D
+ FBP
Vec
0
20μM
100μM
2mM
10mM
IP: p68
IB: HA
IgG HC
E
+ FBP
0
2μM
10μM
100μM
2mM
PD: HA-p68
IB: PKM2
IgG HC
IB: p68
F
Vec
1-515
HAPK
K270M
IP: p68
IB: HA
IB: p68
IgG HC
IP: HA
IB: p68
IgG HC
WCL
IB: HA
IB: β-actin

Figure 3.8 p68 RNA Helicase Interacts with PKM2 at Its FBP Binding Site
(A) Trp fluorescence emission spectrum of the rPKM2 (4 μM) with the titration of various different concentrations (indicated) of peptide D-PhosPepY593. Binding of the peptide to the rPKM2 was indicated by the decrease in fluorescence intensity at 334 nm. **(B)** Trp fluorescence emission intensity of the rPKM2 at 334 nm in the presence of various peptides (2 μM) D-PhosPepY593 (red circles), PepY593 (blue crosses), PhosPepY567 (green diamonds), and D-PhosPepY593 + 2 mM FBP (black squares). Y-axis is the flurescence intensity at 334 nm. X-axis is peptide concentrations. **(C)** The dissociation constant (Kd) of the rPKM2 with the peptides D-PhosPepY593, PepY593, and PhosPepY567 were determined by the data fitting to langmuir equation (assume 1:1 binding). The Kds were determined based on data fitting on three independent measurements. **(D)** Co-immunoprecipitation of p68 (IP:p68) with exogenously expressed HA-PKM2 in cellular extracts of T98G cells supplementary with various concentrations of FBP was examined by immunoblot using the anti-HA antibody (IB:HA). IgG HC is the ponceau S stain of antibody heavy chain, representing the amounts of antibody used in immunopurification of p68. **(E)** Pull-down of the rPKM2 by the HA-p68 immunopurified from T98G cellular extracts (PD:HA-p68) was analyzed by immunoblot using antibody against PKM2 (IB:PKM2). The Pull-down experiments were performed in the presence of various concentrations of FBP (indicated in figure). IgG HC is the ponceau S stain of antibody heavy chain, representing the amounts of antibody used in immunopurification of HA-p68. IB:p68 indicate amounts of HA-p68 used in the pull-down. **(F)** Co-immunoprecipitation of p68 with the exogenously expressed HA-PKM2 and mutants (indicated) in the cellular extracts prepared from T98G cells. In (upper panel), the antibody p68-RGG was used as immunoprecipitation antibody (IP:p68). Co-immunoprecipitations of HA-PKM2 and mutants with p68 were examined by immunoblot using antibody against PKM2. Immunoblot of p68 (IB:p68) indicated amounts of p68 that was immunoprecipitaed down. In (lower panel), the anti-HA antibody was used as immunoprecipitation antibody (IP:HA). Co-immunoprecipitations of p68 with HA-PKM2 and mutants were examined by immunoblot using antibody against p68 (IB:p68). IgG HC is the ponceau S stain of antibody heavy chain, representing the amounts of antibody used in immunoprecipitations.

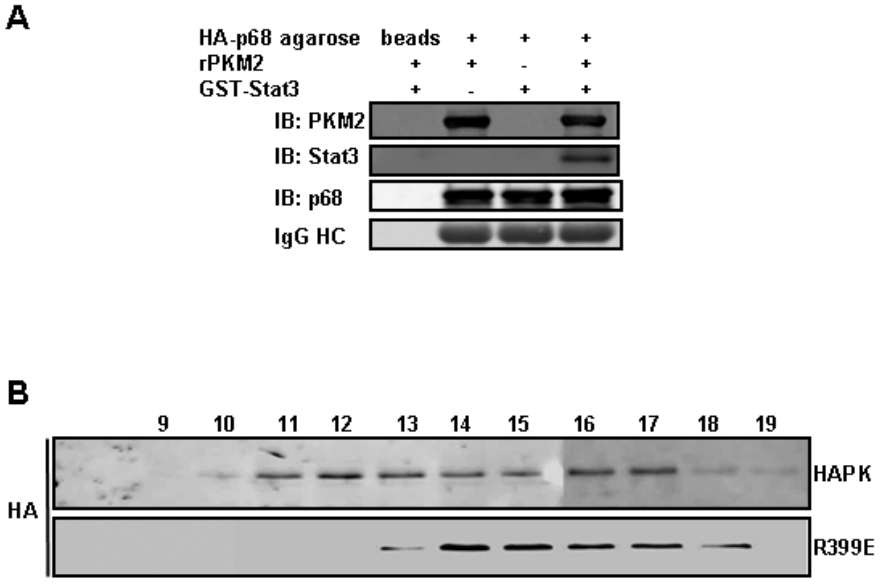
A
HA-p68 agarose beads + + +
rPKM2 + + - +
GST-Stat3 + - + +
IB: PKM2
IB: Stat3
IB: p68
IgG HC
B
9 10 11 12 13 14 15 16 17 18 19
IB: HA
HAPK
R399E

Figure 3.9 PKM2, Stat3 and p68 Forms a Protein Complex
(A) Co-immunoprecipitations of PKM2 and stat3 with HA-p68 in the cellular extracts of T98G cells. The exogenously expressed HA-p68 was immunoprecipitated using anti-HA antibody. The amounts of p68 precipitated from the extracts were examined by immunoblot using antibody against p68. The co-precipitation of PKM2 and stat3 were probed by immunblot using antibodies against PKM2 (IB:PKM2) and against stat3 (IB:Stat3). IgG HC is the ponceau S stain of antibody heavy chain, representing the amounts of antibody used in immunoprecipitation of HA-p68 from the extracts. **(B)** Size exclusion chromatography fractionation of the wild-type HA-PKM2 (wtPKM2) or HA-R399E (R399E) that were immunopurified from SW480 cell lysate. The HA-PKM2 or HA-R399E (100 μl in 0.4 μg/μl) was loaded onto the column. The chromatography fractions F9 – F18 were collected using a FPLC at 300 μl per fraction. The collected fractions were immunoblotted using the anti-HA antibody (IB:HA).

CHAPTER 4: NUCLEAR PKM2 REGULATES CDC14A EXPRESSION TO INDUCE MULTINUCLEUS

4.1 Abstract

The mammalian cell cycle is tightly regulated by multiple protein kinases and their phosphorylation substrates. Exit from anaphase is controlled by anaphase promoting complexes (APC). Cdc14A is a key regulator for cell to exit from anaphase. Overexpression of Cdc14A induces formation of multi-nuclei in cancer cells. The regulatory mechanism governoning the gene Cdc14A transcription is not well defined, yet. We demonstrated here that PKM2 and p68 RNA helicase co-regulated the transcription of Cdc14A gene in less aggressive cancer cells, such as SW480, T98G and LN686. Chromatin immunoprecipitation analysis indicated that the nuclear PKM2 and p68 RNA helicase associated with the Cdc14A promoter. Expression nuclear localization of PKM2 induced formation of multi-nuclei cells. Our experiments suggested that regulation of Cdc14A may mediate the effects of PKM2 expression on the inducation of multi-nuclei cells.

4.2 Introduction

In *Saccharomyces cerevisiae,* exit from mitosis is regulated by a cascade of signals named Cdc Fourteen Early Anaphase Release (FEAR) and Mitosis Exit Network (MEN) (Jensen and Johnston 2002; Bowerman 2004). In anaphase, Cdc14, is induced to export from the nucleolus into the cytoplasm (Bowerman 2004). Cdc14, a serine/tyrosine phosphatase, dephosphorylates and inactivates cyclin B–dependent kinase (Cdk), which

allows the exit from mitosis to continue into a new G1 phase (Bembenek and Yu 2003; de Bettignies and Johnston 2003; Kipreos 2004; Toth, Queralt et al. 2007). In budding yeast, Cdc14 is located in the nucleolus during interphase and is blocked by inhibitors Cfi1/Net1 until metaphase and released into the cytosol in late anaphase (Pereira, Manson et al. 2002; Buonomo, Rabitsch et al. 2003; Bloom and Cross 2007).

In mammalian cells, Cdc14 has two orthologs: Cdc14A and Cdc14B, encodedg by two distinct genes. Cdc14A and Cdc14B have distinct cellular localizations during different stages of the cell cycle. The cellular localization of Cdc14A depends on cell cycle progression. The protein resides in the centrosome during interphase while Cdc14B locates in the nucleolus. During the process of mitosis, Cdc14A is released into the cytoplasm. As an important physiological regulator for cell cycle processes, expression of either Cdc14A or Cdc14B affects genomic stability (Mailand, Lukas et al. 2002). Studies show that Cdc14A overexpression induces the formation of multi-nuclei in mammalian cells by disrupting the process of separation of centrosomes, as well as blocking cytokinesis (Mailand, Lukas et al. 2002). Meanwhile, the depletion of Cdc14B in mammalian cells results in amplification of centrioles (Wu, Cho et al. 2008). Although the biological functions of Cdc14A have been well studied, so far, the molecular mechanism that governs Cdc14A transcription is not well defined.

Pyruvate kinase is an enzyme acting in the glycolysis process. There are four isoforms of pyruvate kinases in mammals: type L, R, M1 and M2. L and R types are generated from one gene with different transcriptional start sites. During tumorigenesis M1 type expression is replaced by M2 type. The replacement of M1 type by M2 type changes the glycolysis rate to produce more phosphoryl intermediates for cell

proliferation. Besides its well-known glycolytic function in the cytosol, little is known for its function in the nucleus. Under the stimulation of interleukin 3 (IL-3), more PKM2 localizes the nucleus to regulate cell proliferation in the IL-3-dependent hematopoietic cell line, Ba/F3 (Hoshino, Hirst et al. 2007). It is reported that PKM2 interacts with Oct-4, an important transcription factor for regulating the pluripotence of embryonic stem cells (Lee, Kim et al. 2008). Interestingly, the N-terminal (a.a.1–348) of PKM2, interacts together with the SUMO-E3 ligase PIAS3 (inhibitor of activated STAT3) in the nucleus of cell of many cell lines, such as NIH3T3 and U-2 OS (Spoden, Morandell et al. 2009). A, Somatosatin, anti-cancer analogue TT-232 interacts with pyruvate kinase in cos-7 cells. The interaction induces nuclear accumulation of PKM2 from the cytosol to trigger caspase-independent apoptosis (Stetak, Veress et al. 2007). PKM2 also plays a role in regulating virus replication. PKM2 interacts with NS5B, the Hepatitis C virus (HCV) RNA-dependent RNA polymerase, in the HCV replicon 9B cells (Wu, Zhou et al. 2008). The downregulation of PKM2 by shRNA in n HCV replicon 9B cells reduces the replication of HCV (Wu, Zhou et al. 2008).

P68 RNA helicase belongs to the DEAD-box family of RNA helicase and has multiple physiological functions in diverse cellular processes, such as cell proliferation, epithelial-mesenchymal transition (EMT) and pre-mRNA splicing. Evidences show that p68 RNA helicase plays an important role in regulating gene transcription by interacting with a number of transcription factors as a co-activator (Warner, Bhattacherjee et al. 2004; Fuller-Pace, Jacobs et al. 2007). P68 interacts with p53 at the C-terminal region of p53 to regulate p53 targeted genes, such as p21, Fas, PIG3 and mdm2 (Bates, Nicol et al. 2005). P68 RNA helicase is reported to be recruited to the pS2 gene promoter, a

downstream target of estrogen receptor alpha (ERα), to regulate pS2 transcription (Watanabe, Yanagisawa et al. 2001). Neither the ATPase activity nor the RNA helicase activity of p68 is required for the function. P68 also interacts with CBP in the C-terminal of CBP to enhance CBP-mediated transcription (Rossow and Janknecht 2003). P68 RNA helicase interacts with Smad3 at the MH2 domains, to form an active transcription regulator complex (Warner, Bhattacherjee et al. 2004). Recently, it was reported that p68 RNA helicase interacts with the androgen receptor (AR) in the nucleus and regulate gene transcription as a co-activator for androgen-dependent and androgen-independent gene expression in malignant prostate cancer cells (Clark, Coulson et al. 2008).

In prsent study, we demonstrated that nuclear PKM2 and p68 RNA helicase induced the formation of multi-nuclei by upregulating Cdc14A expression in cancer cells. Nuclear PKM2 and p68 interacted with the promoter region of Cdc14A to regulate its transcription.

4.3 Results

4.3.1 Exogenous Overexpression of PKM2 and p68 RNA Helicase Induces Multi-nuclei in Cancer Cells

To understand functions of PKM2 in the cell cycle, we analyzed the morphology changes in SW480 cells overexpressing HA-PKM2. Staining nuclear DNA revealed the formation of multinuclei in SW480 cell expressing HA-PKM2 (Fig1A). Statistical analysis indicated that 34% of transfected cells had non-identical double nuclei. 9% of transfected cells had triple nuclei, and 4% of transfected cells showed more than triple nuclei (Fig1B). Very similar phenomenon was also observed with T98G, U87MG and

HEK cells where HA-PKM2 was overexpressed. The results suggested that formation of multi-nucleus by exogenous PKM2 overexpression is a common phenomenon in mammalian cells.

It was reported that Cdc14A overexpression in U-2-OS human osteosarcoma cells induces formation of multi-nucleus due to interfering centrosome separation (Mailand, Lukas et al. 2002). To identify genes that are subject to PKM2 regulation, we carried out expression analyses. PKM2 was expressed in SW480 cells. The RNA profile was examined via Affimetrix human 2.0 microarray. The array analyses revealed that Cdc14A mRNA level was increased to 4 folds in SW480 cell upon expressing PKM2, which indicated a possible transcriptional regulation of Cdc14A by PKM2 in SW480 cells. Thus, we hypothesized that PKM2 regulates Cdc14A expression in SW480 cells and consequently induce the formation of multiple nuclei. To test this hypothesis, the expression level of Cdc14A was examined in SW480 cells with epitoptic PKM2 expression. The Cdc14A expression level was increased more than 4 folds (Fig 2A). Meanwhile, mRNA level of Cdc14A was also examined via RT-PCR. The RT-PCR primers were designed according to Cdc14A pre-mRNA sequence as extended from exon 11 to exons 13-14 interrupted by intron 13-14. It was clear that 3.2 folds increase in Cdc14A mRNA in SW480 cells in which PKM2 was overexpressed (Fig 3B). To verify whether PKM2 overexpression induces multiple nuclei, SW480 cells overexpressing PKM2 were stained with the Lamin B1 antibody. It was clear that PKM2 overexpression induced multiple nuclei in SW480 cells (Fig2 B).

4.3.2 Nuclear PKM2 Regulates the Expression of Cdc14A

PKM2 is an enzyme acting in the glycolysis. The protein is highly expressed and mainly localizes in the cytosol to catalyze ATP production. To investigate whether the regulatory function of PKM2 in controlling Cdc14A expression was by cytoplasmic PKM2 or a nuclear protein, we constructed a mutant PKM2 with addition of nuclear localization signals (NLS) at C- and N- terminal ends. Western blot results showed that over 95% NLS-PKM2 localized in the nucleus. The analyses function of NLS-PKM2 in regulating Cdc14A expression was examined in SW480 cells. Western blot analyses showed that Cdc14A levels were increased when NLS-PKM2 was expressed in SW480 cells (Fig3A). Immunofluorescence stainging results showed that NLS-PKM2 induced formation of mutli-nucleus in SW480 cells

4.3.3 PKM2 and p68 RNA Helicase Co-regulate Cdc14A Protein Expression

Our previous study showed that PKM2 interacts with p68 RNA helicase both in the cytosol and nucleus. p68 RNA helicase is a transcription co-activator (Warner, Bhattacherjee et al. 2004; Bates, Nicol et al. 2005). We questioned whether p68 RNA helicase also plays a role in regulating Cdc14A expression. To this end, p68 RNA helicase was overexpressed in SW480 cells and the Cdc14A expression levels was examined by immnoblot using a commercially avaible Cdc14A antibody. The results showed that Cdc14A expression level was up-regulated upon the overexpression of p68 RNA helicase (Fig2A). RT-PCR analyses showed that Cdc14A mRNA was upregulated 2.3 folds when p68 RNA helicase was expressed in SW480 cells. Meanwhile, the mRNA

level increased 3.8 folds when exogenous NLS-PKM2 was overexpressed in SW480 cells. Cdc14A mRNA level was also upregulated to 2.5 folds when HA-PKM2 was overexpressed (Fig3B).

It is believed that the transcription regulation of p68 RNA heliase does not depend on its ATPase activity (Yang, Lin et al. 2007). To investigate whether the function of p68 RNA helicase in regulating Cdc14A transcription is dependent on its ATPase activity, a p68 mutant (RGLD), which lacks of ATPase activity, was overexpressed in SW480 cells. Western-blot analyses showed that the p68 mutant and wild type have very similar effect in regulating Cdc14A expression (Fig4a). The result indicated that the function of p68 RNA helicase in regulating Cdc14A most likely was ATPase independent.

In our previous study, we showed that PKM2 and p68 RNA helicase interact with each other. However, we speculated that the regulatory function of p68 RNA helicase and PKM2 in Cdc14A are inter-related. To test this conjecture, p68 was knocked down via the RNAi and PKM2 was expressed in p68 knockdown cells. As controls, wild-type p68 and the Y593F mutant were also expressed in the p68 knockdown cells. It was clear that the function of PKM2 in regulating Cdc14A expression was abolished if p68 RNA helicase was knocked down (Fig4b). To further verify that p68 RNA helicase was required for regulating Cdc14A by nuclear PKM2, NLS-PKM2 was introduced in p68 knocked down cells. Consistently, Cdc14A expression level was not affected by the overexpression of cytosolic and nuclear PKM2 (Fig4c). On the other hand, the requiremtn of PKM2 for p68 RNA helicase in regulating Cdc14A expression was tested. PKM2 was knocked down by RNAi in SW480 cells and wild type p68 RNA helicase were introduced into the p68 knocked down cells. The experiments showed that the

function of p68 RNA helicase in regulating Cdc14A transcription was almost abolished (Fig4d). Taken together, our results showed that the p68 and nuclear PKM2 co-regulate Cdc14A transcription.

4.3.4 PKM2 and p68 RNA Helicase Bind to Cdc14A Promoter Region

PKM2 and p68 RNA helicase co-regulated the transcription of Cdc14A gene. It is reported that p68 RNA helicase is a gene transcriptional co-activator (Bates, Nicol et al. 2005). In our previous report, nuclear PKM2 associated with the promoter region of MEK gene to regulate its transcription. To investigate transcriptional role of PKM2 in cancer cells, the ChIP-on-chip experiments were carried out to examine the interaction of PKM2 with promoter. The ChIP-on-chip data showed that PKM2 was associated with the Cdc14A promoter. ChIP-on-chip analyses using antibody against p68 also showed that p68 RNA helicase associated with the same promoter region of Cdc14A promoter. The Chip-on-Chip analyses suggested a possibility that nuclear PKM2 and p68 RNA helicase bind to the same promoter region of Cdc14A gene to regulate its transcription. To confirm the Chip-on-chip analyses, chromatin immunoprecipitation experiment was carried out. Primers were designed according to Chip-on-chip analyses. Chip analyses showed that p68 RNA helicase and nuclear PKM2 indeed interacted with Cdc14A promoter at the same region (Fig5).

4.3.5 Cdc14A Mediates the Effect of PKM2 in Induction of Formation of Multinuclei

To further investigate whether Cdc14A is the target mediating the effects of PKM2 in induction of multinucleus, PKM2 was knocked down in SW480 cells using SMARTpool RNAi and the expression level of Cdc14A was then examined. The expression of Cdc14A in both protein and mRNA levels were decreased around 3 folds when PKM2 was knocked down (Fig 6 c, d). Immunostaining experiments were carried out to examine the multinuclei in PKM2 knocked down cells. The cell numbers with multi-nuclei was decreased 2 folds when PKM2 was knocked down in SW480 cells (Fig 6E).

4.3.6 PKM2 Overexpression Induces formation of Multi-nucleus Only in Less Aggressive Cancer Cells

The effects of PKM2 on induction the formation of multi-nuclei were different from cell line to cell line. We suspected the expression of Cdc14A in different cancer cell line were different. Thus, Cdc14A expression level in 13 cancer cell lines were examined including LN686, M4C1, SW480, SW620, WM115, WM266, H146, H460, T98G, U87MG, HeLa and HEK cells. Expression of Cdc14A in T98G, U87MG, SW480, HEK cells was clearly evident. The expression of Cdc14A in other cell lines, such as SW620, HeLa, WM115 and WM266 could not be detected (Fig 7). To examine whether expression of PKM2 induces formation of multi-nucleus in these cell lines, the cells expression of PKM2 were stained with antibody against γ-tubulin 48 hours after PKM2 overexpression. The formation of multi-nucleus was not observed with WM115, WM266, HeLa and SW620 cells (data not shown). The formation of multi-nuclei clearly correlated with Cdc14A expression in testing cancer cells. Furthermore, expression of

Cdc14A was examined in SW620 cells where the epitogic PKM2 was expressed. Western blot analyses showed that Cdc14A expression level was not increased, even when PKM2 reintroduced in SW620 cells. Consequently, immunofluorescence staining did not show the formation of multi-nucleus in SW620 cells in which epitomic PKM2 or p68 RNA helicase were expressed (Fig7C right panel). All these data indicated that PKM2 regulated Cdc14A expression results in formation of multi-nucleus.

4.4 Discussion

The glycolysis is an important metabolic pathway which provides energy as well as phosphor intermediates for macromolecules synthesis in cancer cells. Many glycolytic enzymes have cellular functions other than glycolysis. Oxidative stress induces cytoplasmic Glyceraldehyde-3-phosphate dehydrogenase (GAPDH) nuclear translocation. Nuclear GAPDH induces ATG12 expression lead to resist to caspase-independent cell death (Colell, Ricci et al. 2007). Studies from ours and other demonstrated that, PKM2, translocate to the nucleus of cancer cells. PKM2 translocate into the nucleus under the stimulation of Interleukin-3 in BB13 cells and nuclear PKM2 promotes Ba/F3 cells proliferation (Hoshino, Hirst et al. 2007) . Contrary, Stetak et al reported that nuclear PKM2 may induce apoptosis in Cos-7 cells by a caspase independent pathway (Stetak, Veress et al. 2007). In our study, nuclear PKM2 regulates Cdc14A expression to induce the formation of multi-nuclei in less proliferation cancer cells. The different functions of nuclear PKM2 may be due to the difference of cell types.

Cdc14A was identified as a downstream target of PKM2 for multi-nuclei cells. The localization of PKM2 in the nucleus may inhibit the action of PKM2 in induction of

centrosome separation. The centrosome is the microtubule organization center, which regulates the formation of bipolar spindle during mitosis (Khmelinskii and Scheibel 2008). Abnormal regulation of the centrosome separation may lead to aneuoploidy. Centrosomes duplicate in S phase and the number is tightly controlled in normal mammalian cells. Recently, studies showed that Cdc14B knockdown induces the amplification of centrosomes (Wu, Cho et al. 2008). Meanwhile, centrosome separation is critical for cells to maintain chromosome numbers. One possibility is the overexpression of Cdc14A may deregulate the dephsophorylation of Cdh1, which cause the malfunction of APC complex resulting in aneuploidy in the tumor cells.

The background level of multi-nucleus cells for SW480 is around 5±2%. As shown in Fig7A, The multi-nucleus caused by Cdc14A overexpression was not completely abolished by Cdc14A knocked down. This is probably due to incomplete knocked down. Alternatively, additional mechanism contributes to the formation of multinucleus cells. In this study, 11 cell lines were screened for the expression of Cdc14A. The expression levels of Cdc14A vary in different cell lines. However, there is a clear correlation between the expression levels of Cdc14A with the formation of multinuclei in less proliferation cancer cell lines. The multinuclei cells may undergo apoptosis. This indicated the distinct functions of nuclear PKM2 in different cancer cells. That is, in more proliferating cancer cells, expression of PKM2 in the nucleus promotes cell proliferation via regulating MEK5 gene transcription (Gao et al, Oncogene, revised, 2009). In less proliferating cancer cells, expression of PKM2 in the nucleus may lead to cell apoptosis by regulating Cdc14A gene transcription to form multinuclei.

4.5 Materials and Methods

4.5.1 Plasmids Construction, Reagents and Antibodies

cDNA of PKM2 and PKM1 were purchased from OriGene Technologies. The cDNA of PKM2 was cloned into bacteria expression vector pET30a and mammalian expression vectors pHM6, PC3.1 et al. The primers and empty pET30a vector were digested with EcoR1 and Not1 two enzymes. The digestion products were purified with mini kit from QIAGENE and ligated with ligase enzyme. The HA-tagged full length of p68 (wild p68, Y593F, Y595F, and LGLD) expression plasmids were constructed in pHM6 vectors as indicated in the previous papers from our laboratory. Mutations in pHM6 vector were obtained via multisites mutation method (QuikChange® Multi Site-Directed Mutagenesis Kit, Stratagene). Cdc14A, γ-tubulin, Lamin A/C, GAPDH and β-actin antibodies were purchased from Abcam and Cellsignal.

4.5.2 Cell culture, Transient Transfection Assays

SW480, SW620, T98G, HeLa, U87MG, H146, H460 Cell lines were purchased from ATCC and cultured by following the vendor's instructions. Cells were transiently transfected using Fugene-HD reagent (Roche) according to the manufacture's instruction. Briefly, 2ug of the plasmid was combined with 5ul of the HD reagent in 100ul of optimum medium, the mixture was added to the wells after 20 minutes incubation. For fluroscent immunostainning experiments, cells were seeded into chambers 24 hours

before transfection. For IP or western-blot experiments, cells were harversted 48 hours after transfection.

4.5.3 Relative Real Time PCR (RT-PCR)

Total RNA was extracted from cells under appropriate treatments using RNeasy kit by following the manufacturer's instruction (Qiagen). Reverse transcription process was performed with ImProm-II reverse transcription system (Promega). RT-PCRs were performed with 1 μg of cDNA and Fast SYBR green master mix (Applied biosystems). RT-PCR process was performed in Applied Biosystems Real-Time PCR 7500. Standard RT-PCR primer set was purchased from RealTimePrimers.com. RT-PCR primers was designed as 5'-CCTAGATGATATGTCTATTGGTGG-3'

5'-TGAACTTAATCTGAAAGGCTGG-3'

4.5.4 Chromatin Immunoprecipitation

Chromatin immunoprecipitation method was performed as we describe before (Yang et al, Cell, 2006). Generally, for one T-150 flask of SW620 cells, cells was fixed with 1% formaldehyde solution by incubating 10min in 37°C and stopped with 125mM glycine. The fixed cells were washed with cold PBS supplemented with protease inhibitors three times and lysated in 1ml SDS lysis buffer (Imgenex) with protease inhibitors. The cell lysate was sonicated on ice 2 min and centrifuged at 15,000 rpm to pellet insoluble material. The shearing performance was examined with 1% TAE agarose gel. The supernatant was aliquot and pre-cleared with 100ul salmon sperm DNA/protein G agarose by incubating for 2 hours. The antibody was added to the clear supernatant and

rotated at 4°C overnight. 100 ul of salmon sperm DNA/protein G agarose was added to each tube and rotated for 2 hours. The immuno-complex was eluted with elution buffer (Imgenex) after extensive washing 8 times. The cross-link was reversed by adding 4ul of 5M NaCl and incubating at 65°C overnight. The released DNA was purified using the phenol chloroform extraction method. Regular PCR was performed in Mastercycle® Gradient PCR machine (Eppendorf) and the result was analyzed with 2% agarose.

4.5.5 RNA Interference

The duplex RNA oligonucleotides of SMARTpool for PKM2 and Cdc14A were purchased from Dharmocon. The RNA interference method was performed as described below. Briefly, cells were grown to 30-50% confluence and transfected with siRNA (150 pmole) using lipo2000 transfection agent. 24 hours later, mutants were transfected using FuGene HD following the manufacturer's instrument. For transient expression of WT p68 or mutants in p68 knockdown cells, the cells were harvested with an additional 48 hours after knockdown.

4.5.6 Subcellular Extracts Preparation, Co-immunoprecipitation and Western blot

Whole cell lysate, nuclear extract, cytoplasm were made fresh. Briefly, for whole cell lysate, cells with appropriate treatments were harvested and lysated in RIPA buffer supplemented with complete proteases inhibitors. Co-IP experiments were performed in RIPA buffer supplemented with complete proteases inhibitors as well as phosphatase inhibitors (1mMSoV, 5mMNaF). Whole cell lysate or subcellular extracts were diluted with RIPA buffer and incubated with appropriate primary antibody overnight at 4□. The

next day, 30ul of protein G agarose bead slurry was added into reaction tube and was rotated for 2h at 4°C. The immuno-complexs were harvested with centrifuging at 800 rpm for 10min. The immuno-complex samples were washed with 600 µl of NETS buffer (150 mM NaCl, 50 mM tris-HCl [pH 7.5], 5 mM EDTA, 0.05% NP-40) five times and were denatured with SDS-PAGE loading buffer by incubating at 95°C for 8 mins. The immuno-complexes were separated in SDS-PAGE and transferred to nitrocellular membranes. Appropriate primary antibodys were incubated with the membranes overnight at 4°C. After washing with TBST buffer three times, secondary antibody was incubated with the membranes for additional 2 hours at room temperature. The blotting signals were detected with SuperSignal West Dura Extended Duration Substrate (Pierce).

4.5.7 Immunostaining and Multinucleated Cells Analysis

SW480, SW620, T98G, HeLa cells were seeded in 6 cell plates to 30% density. 24 hours later cells were fixed with cold methanol for 15 min at -20°C. The cells were washed with PBS 3 times and peameablized with 1%Trixon-X for 20 min. The cells were blocked with 2.5% BSA (in PBS) for 30min at room temperature. The cells were incubated with γ-tubulin or HA-flurescent primary antibody with appropriate dilutions overnight at room tempature. The next day, the cells were washed with PBS three times and secondary Goat anti-Rabbit antibody was incubated with cells for additional two hours. For multinucleated cell analysis, DAPI (1mg/ml) was applied to stain transfected cells and examined with Confocal microscope. 150 cells were counted from each slide to analyze the percentage of multinucleated cells.

4.6 References

Bates, G. J., S. M. Nicol, et al. (2005). "The DEAD box protein p68: a novel transcriptional coactivator of the p53 tumour suppressor." EMBO J 24(3): 543-553.

Bembenek, J. and H. Yu (2003). "Regulation of CDC14: pathways and checkpoints of mitotic exit." Front Biosci 8: d1275-1287.

Bloom, J. and F. R. Cross (2007). "Novel role for Cdc14 sequestration: Cdc14 dephosphorylates factors that promote DNA replication." Mol Cell Biol 27(3): 842-853.

Bowerman, B. (2004). "Cell division: timing the machine." Nature 430(7002): 840-842.

Buonomo, S. B., K. P. Rabitsch, et al. (2003). "Division of the nucleolus and its release of CDC14 during anaphase of meiosis I depends on separase, SPO12, and SLK19." Dev Cell 4(5): 727-739.

Clark, E. L., A. Coulson, et al. (2008). "The RNA helicase p68 is a novel androgen receptor coactivator involved in splicing and is overexpressed in prostate cancer." Cancer Res 68(19): 7938-7946.

Colell, A., J. E. Ricci, et al. (2007). "GAPDH and autophagy preserve survival after apoptotic cytochrome c release in the absence of caspase activation." Cell 129(5): 983-997.

de Bettignies, G. and L. H. Johnston (2003). "The mitotic exit network." Curr Biol 13(8): R301.

Fuller-Pace, F. V., A. M. Jacobs, et al. (2007). "Modulation of transcriptional activity of the DEAD-box family of RNA helicases, p68 (Ddx5) and DP103 (Ddx20), by SUMO modification." Biochem Soc Trans 35(Pt 6): 1427-1429.

Hoshino, A., J. A. Hirst, et al. (2007). "Regulation of cell proliferation by interleukin-3-induced nuclear translocation of pyruvate kinase." J Biol Chem 282(24): 17706-17711.

Jensen, S. and L. H. Johnston (2002). "Complexity of mitotic exit." Cell Cycle 1(5): 300-303.

Khmelinskii, A. and E. Scheibel (2008). "Assembling the spindle midzone in the right place at the right time." Cell Cycle 7(3): 283-286.

Kipreos, E. T. (2004). "Developmental quiescence: Cdc14 moonlighting in G1." Nat Cell Biol 6(8): 693-695.

Lee, J., H. K. Kim, et al. (2008). "Pyruvate kinase isozyme type M2 (PKM2) interacts and cooperates with Oct-4 in regulating transcription." Int J Biochem Cell Biol 40(5): 1043-1054.

Mailand, N., C. Lukas, et al. (2002). "Deregulated human Cdc14A phosphatase disrupts centrosome separation and chromosome segregation." Nat Cell Biol 4(4): 317-322.

Pereira, G., C. Manson, et al. (2002). "Regulation of the Bfa1p-Bub2p complex at spindle pole bodies by the cell cycle phosphatase Cdc14p." J Cell Biol 157(3): 367-379.

Rossow, K. L. and R. Janknecht (2003). "Synergism between p68 RNA helicase and the transcriptional coactivators CBP and p300." Oncogene 22(1): 151-156.

Spoden, G. A., D. Morandell, et al. (2009). "The SUMO-E3 ligase PIAS3 targets pyruvate kinase M2." J Cell Biochem 107(2): 293-302.

Stetak, A., R. Veress, et al. (2007). "Nuclear translocation of the tumor marker pyruvate kinase M2 induces programmed cell death." Cancer Res 67(4): 1602-1608.
Toth, A., E. Queralt, et al. (2007). "Mitotic exit in two dimensions." J Theor Biol 248(3): 560-573.
Warner, D. R., V. Bhattacherjee, et al. (2004). "Functional interaction between Smad, CREB binding protein, and p68 RNA helicase." Biochem Biophys Res Commun 324(1): 70-76.
Watanabe, M., J. Yanagisawa, et al. (2001). "A subfamily of RNA-binding DEAD-box proteins acts as an estrogen receptor alpha coactivator through the N-terminal activation domain (AF-1) with an RNA coactivator, SRA." EMBO J 20(6): 1341-1352.
Wu, J., H. P. Cho, et al. (2008). "Cdc14B depletion leads to centriole amplification, and its overexpression prevents unscheduled centriole duplication." J Cell Biol 181(3): 475-483.
Wu, X., Y. Zhou, et al. (2008). "Isoform-specific interaction of pyruvate kinase with hepatitis C virus NS5B." FEBS Lett 582(15): 2155-2160.
Yang, L., C. Lin, et al. (2006). "P68 RNA helicase mediates PDGF-induced epithelial mesenchymal transition by displacing Axin from beta-catenin." Cell 127(1): 139-155.
Yang, L., C. Lin, et al. (2007). "Phosphorylation of p68 RNA helicase plays a role in platelet-derived growth factor-induced cell proliferation by up-regulating cyclin D1 and c-Myc expression." J Biol Chem 282(23): 16811-16819.

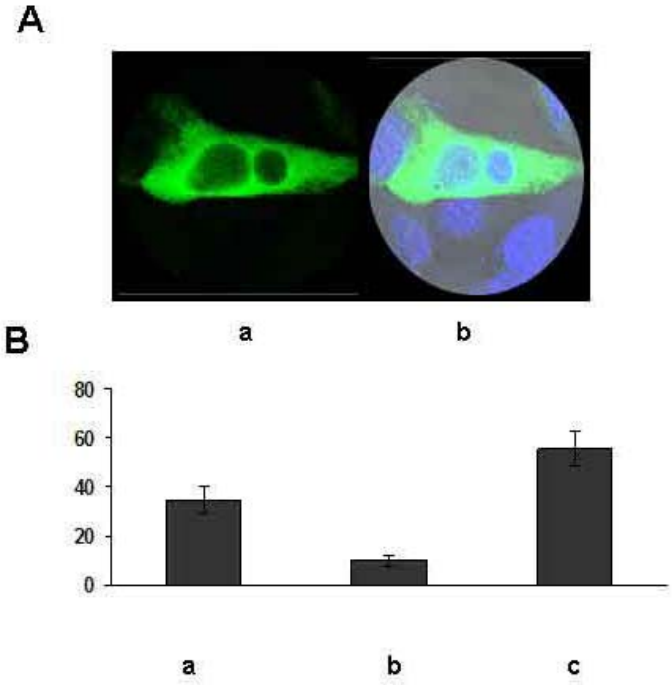
A
a
b
B
80
60
40
20
0
a
b
c

Fig 4.1 HA-PKM2 Expression Induces the Formation of Multinuclei in SW480 Cells
(A) Fluroscent immunostaining of exogenous expressed PKM2 using the antibody PabHA in SW480. The green signal represents staining of exogenous PKM2 in the cells (a). (b) is the overlay of HA antibody staining and DAPI staining. The blue signal represents DAPI staining of DNA. **(B)** shows the percentage of the number of multinuclei cells in the whole populations of expressing HA-PKM2. (a) is the population of two nuclei in the whole populations of expressing HA-PKM2. (b) is the percentage of triple nuclei population in the whole populations expressing HA-PKM2. (c) is the percentage of single nucleus population in the whole population expressing HA-PKM2. Error bars in (B) are standard deviations of three measurements

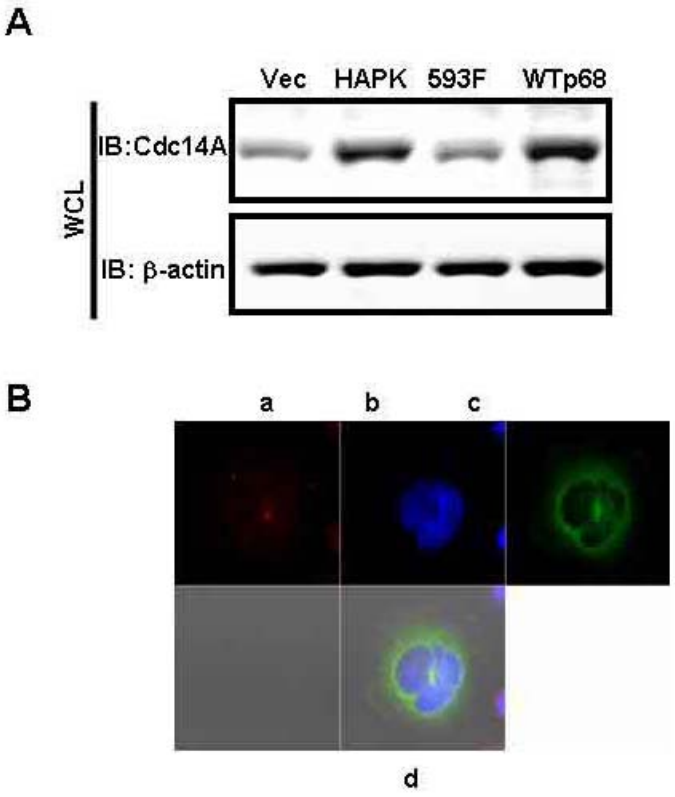
A
Vec
HAPK
593F
WTp68
WCL
IB:Cdc14A
IB: β-actin
B
a
b
c
d

Figure 4.2 Cdc14A Expression is Up-regulated by PKM2 and p68 RNA Helicase
(A) Cellular levels of Cdc14A in SW480 cells 48 hours after transfection of the cells with plasmids vectors that carry PKM2 cDNA expression vector (HAPK), p68 RNA helicase (WTp68), Y593F mutant of p68 RNA helicase (593F) or empty vector (Vec) were analyzed by immunoblot with anti-Cdc14A (IB: Cdc14A). The exogenously expressed HA-PKM2 or p68 was examined by immunoblot using anti-HA antibody. Immunoblot of β -actin (IB: β -actin) were loading control. **(B)** is the centrosome staining in multi nuclei cell induced by PKM2 overexpression. (a) The red signal represents staining of γ-tubulin. (b) The blue signal represents DAPI staining of DNA. (c) The green signal represents staining of exogenous expression of PKM2 in in the cells. (d) is the overlay of HA antibody, γ-tubulin and DAPI staining.

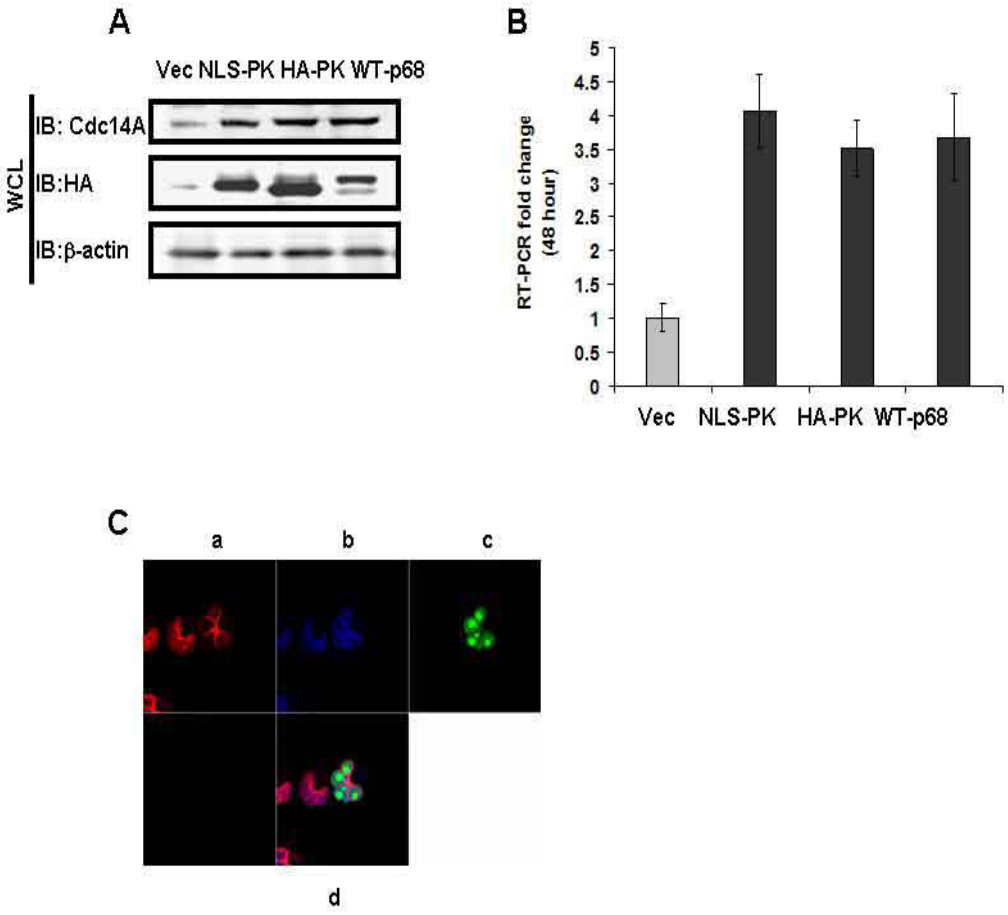
A
Vec NLS-PK HA-PK WT-p68
WCL
IB: Cdc14A
IB:HA
IB:β-actin
B
RT-PCR fold change (48 hour)
5
4.5
4
3.5
3
2.5
2
1.5
1
0.5
0
Vec
NLS-PK
HA-PK
WT-p68
C
a
b
c
d

Figure 4.3 Nuclear PKM2 Regulates Cdc14A Expression
(A) Cellular levels of Cdc14A in SW480 cells 48 hours after transfection of the cells with plasmids vectors that carry PKM2 cDNA expression vector (HAPK), p68 RNA helicase (WTp68), nuclear localization signal mutant of PKM2 (NLS-PK) or empty vector (Vec) were analyzed by immunoblot of anti-Cdc14A (IB:Cdc14A) in whole cell lysate. The exogenously expressed HA-PKM2, p68 was examined by immunoblot using anti-HA. immunoblot of β-actin (IB: β-actin) is loading control. **(B)** RT-PCR experiment was applied to examine Cdc14A mRNA expression level. The RT-PCR primers were designed according to Cdc14A pre-mRNA sequence as extend from exon 11 to exon 13-14 interrupted with intron 13-14. Error bars are standard deviations of three measurements. **(C)** Immunostaining of exogenous nuclear PKM2 induced multinuclei in SW480. The red signal represents staining of Lamin B1 (a). The blue signal represents DAPI staining of DNA (b). The green signal represents staining of HA. (d) is the overlay of HA antibody and DAPI staining.

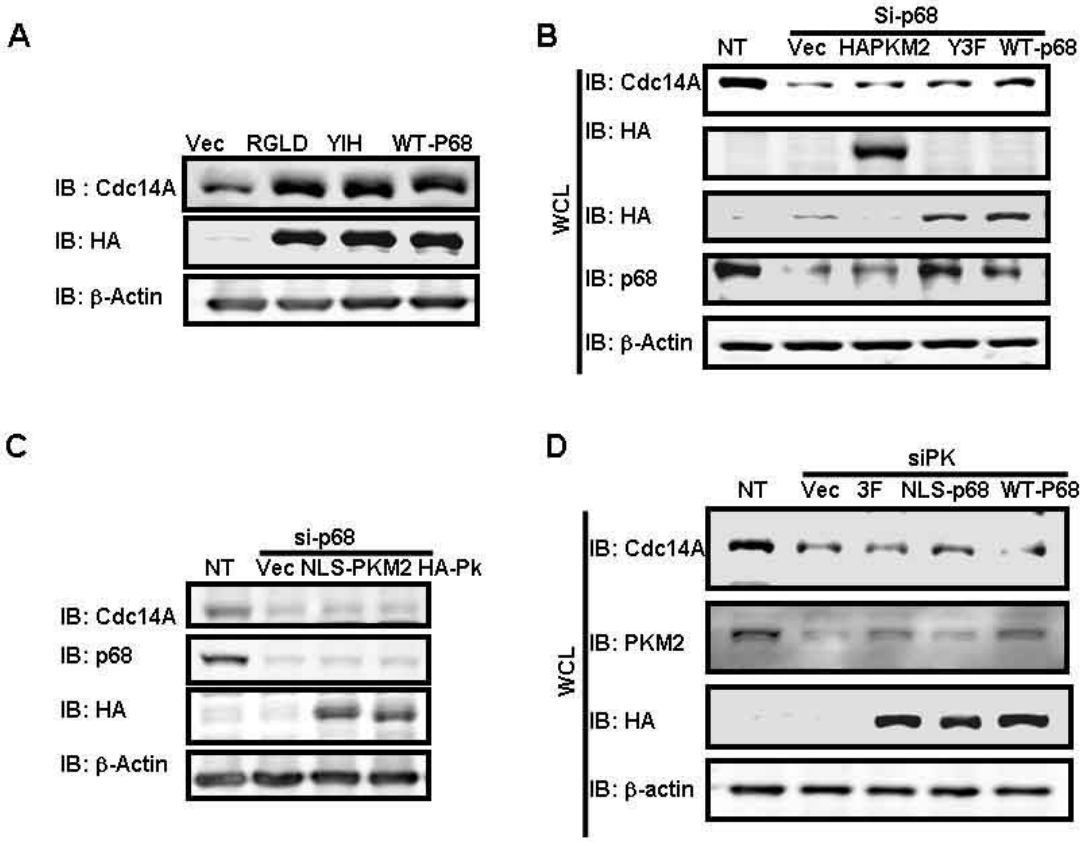
A
Vec
RGLD
YIH
WT-P68
IB : Cdc14A
IB: HA
IB: β-Actin
B
Si-p68
NT
Vec
HAPKM2
Y3F
WT-p68
WCL
IB: Cdc14A
IB: HA
IB: HA
IB: p68
IB: β-Actin
C
si-p68
NT
Vec
NLS-PKM2
HA-Pk
IB: Cdc14A
IB: p68
IB: HA
IB: β-Actin
D
siPK
NT
Vec
3F
NLS-p68
WT-P68
WCL
IB: Cdc14A
IB: PKM2
IB: HA
IB: β-actin

Figure 4.4 Cdc14A Expression is Co-regulated by PKM2 and p68 RNA Helicase.
(A) The regulatory function of p68 for Cdc14A transcription was helicase activity independent. Cellular levels of Cdc14A and exogenously expressed p68 RNA helicase (WTp68), Y593F mutant of p68 RNA helicase (593F) , RNA helicase inactive mutant of p68 RNA helicase (RGLD) or empty vector (Vec) in SW480 were analyzed by immunoblot using antibodies against Cdc14A (IB:Cdc14A) and HA (IB:HA). **(B)** p68 was required for the regulatory function of PKM2 to Cdc14A transcription. Endogenous p68 was knocked down with RNAi (sip68). Exogenous PKM2, wild type or mutant p68 was expressed in p68 knocked down cells. **(C)** p68 was required for the regulatory function of nuclear PKM2. p68 in the cells was knocked down with RNAi (sip68). Wild type or mutant PKM2 was exogenously expressed in p68 knocked down cells. **(D)** PKM2 was required for the regulatory function of p68. PKM2 was knocked down with RNAi (siPK). Wild type or mutant p68 was exogenously expressed in PKM2 knocked down cells. In (A), (B), (C) and (D) Immunoblot of β-actin (IB:β-actin) is a loading control. The exogenously expressed PKM2 or p68 (wild type or mutants) was examined by immunoblot using anti-HA antibody.

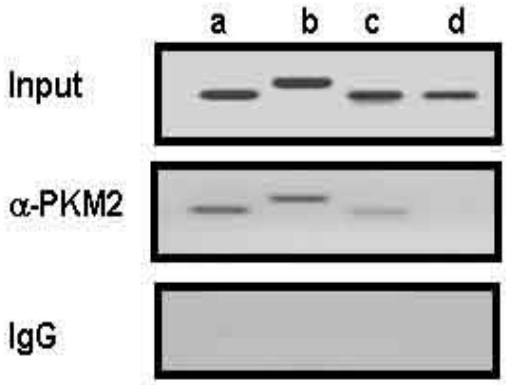
a
b
c
d
Input
α-PKM2
IgG

Fig 4.5 PKM2 Interacts to Cdc14A Gene Promoter
ChIP analyses of Cdc14A promoter using PKM2antibody in SW480 cells (αPKM2). ChIP analyses using rabbit IgG (IgG) was a negative control. Inputs were PCR products from DNA extracts without ChIP. (a) ChIP-using PCR primer pair targeting to promoter reion Cdc14A gene. Chip-1 primers: Forward 5'-GAAGGAGGATCCGGAGCAG-3' Reverse 5'-CCTGGGAAACGCAGACCAG-3' (b) ChIP-using anthour PCR primer targeting to promoter region of Cdc14A gene. Chip-2 primers: Forward 5'-TCGGGTTCCCCTCGGAATG-3' Reverse 5'-AAGCGAGATACGCACGGGG-3' (c) ChIP– using PCR primer pair targeting a down stream region of exon 1 of Cdc14A gene is a negative control. (d) ChIP targeting GAPDH using antibody against PKM2 was another negative control

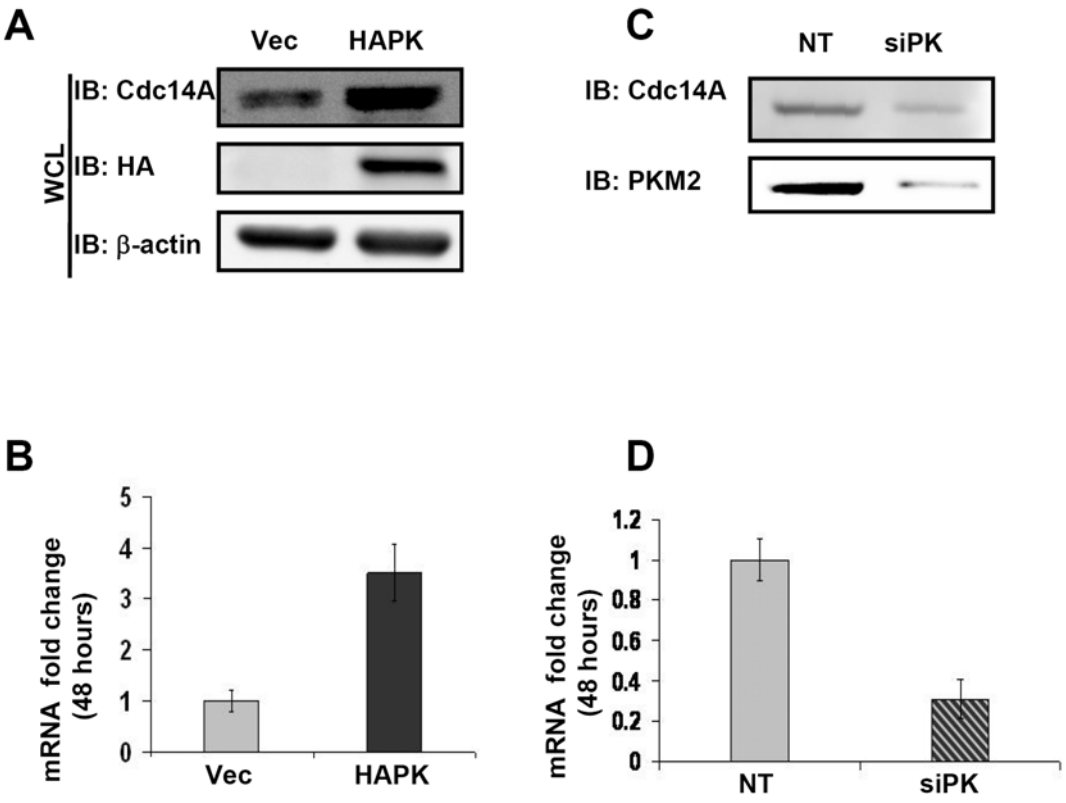
A
Vec
HAPK
IB: Cdc14A
WCL
IB: HA
IB: β-actin
C
NT
siPK
IB: Cdc14A
IB: PKM2
B
mRNA fold change (48 hours)
5
4
3
2
1
0
Vec
HAPK
D
mRNA fold change (48 hours)
1.2
1
0.8
0.6
0.4
0.2
0
NT
siPK
E
120
100
80
60
40
20
0
a
b
c

Fig4.6 Cdc14A Transcription is Regulated by PKM2 Expression
(A) & (C) Expressions of Cdc14A (IB: Cdc14AMEK5) in SW480 were analyzed by immunobloting whole cell lysate (WCL) prepared from the cells in which PKM2 was knocked down by RNAi (PKM2, IB: PKM2). Expression of HA-PKM2 in SW480 was examined by immunobloting whole cell lysate with anti-HA (IB: HA). The blot of β-actin (IB:β-actin) are the loading controls. **(B) & (D)** were RT-PCR results corresponding to (A), (C). **(E)** shows the percentage of the number of multinuclei cells in the whole populations of PKM2 knocked down cells. (a) is the population of two nuclei in the whole populations of PKM2 knocked down cells. (b) is the percentage of triple nuclei population in the whole populations PKM2 knocked down cells. (c) is the percentage of single nucleus population in the whole population PKM2 knocked down cells. Error bars in (E) are standard deviations of three measurements

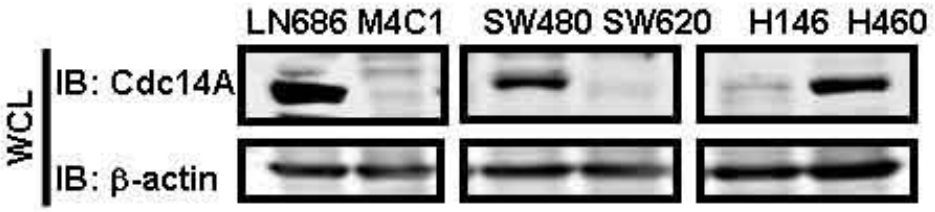
LN686 M4C1
SW480 SW620
H146 H460
WCL
IB: Cdc14A
IB: β-actin

Fig 4.7 Cdc14A Expression in Cancer Cell Lines
Expressions of Cdc14A in SW620/SW480, LN686/M4C1, and H146/H460 were analyzed by immunobloting whole cell lysate (WCL) with anti-Cdc14A. The blot of β-actin (IB: β- actin) are the loading controls.

CHAPTER 5 CONCLUSIONS AND DISCUSSIONS

5.1 Conclusions

The Warburg effect has been known for decades. The detailed mechanism of the Warburg effect is still not known. It has been shown that metabolic adjustment benefits cancer cells in many aspects. For example, the change provides phosphor intermediates for macromolecule synthesis as well as help cancer cells to avoid apoptosis. In this study, we discovered that there were more nuclear PKM2 in metastatic cancer cells than the non-metastatic cancer cells. The nuclear PKM2 levels were correlated with cancer cell proliferation rates. PKM2 regulated MEK5 gene transcription to promote cell proliferation. Nuclear PKM2 phosphorylated Stat3 at Y705 site using PEP as a phosphoryl group donor to regulate MEK5 gene transcription. Our study also showed that double phosphorylated p68 RNA helicase at Y593/595 residues interacted with PKM2 at its FBP binding site. Under the stimulation of growth factors, p68 interacted with PKM2 to promote its protein kinase activity. The transcription regulatory function of nuclear PKM2 was also defined in regulating Cdc14A gene transcription resulting in a multi-nucleus phenomenon in less aggressive cancer cells. These results provided part explanations for Warburg effect.

5.2 Nuclear PKM2 Interacts with Tyrosine-phosphorylated p68 RNA Helicase

p68 RNA helicase is a multifunctional protein dominantly localized in the nucleus, and plays a crucial role in RNA biogenesis as well as tumorigenesis. The phosphorylations of p68 RNA helicase have diverse functions (Huang and Liu 2002; Liu 2002). In 2007, Yang et al reported that p68 RNA helicase is double phosphorylated at

Y593 and Y595 residues in some cancer cells, such T98G and HeLa cells (Yang, Lin et al. 2007). The double phosphorylated p68 RNA helicase facilitates cancer cells in resistance of TRAIL induced-apoptosis. To further examine p68's physiological functions in cancer cells, it was important to uncover proteins that interacted with phosphorylated p68 RNA helicase in the nucleus. PKM2 was found to interact with p-Y593/595 peptides. However, this method did not detect other associated proteins with low enrichment to tyrosine-phosphorylated peptides due to the limitation of its sensitivity, or the weak interactions with phoshprylated p68. Meanwhile, whether nuclear PKM2 has functions in regulating RNA biogenesis with p68 RNA helicase remains elusive.

5.3 Tyrosine-phosphorylated p68 Peptides Change the Quaternary Structure of PKM2

In 2008, Cantley's group reported that PKM2 binds to tyrosine phosphorylated peptides in tumor cells. The binding of phosphorylated peptides to PKM2 releases fructose-1,6-bisphosphate (FBP), the allosteric activator of PKM2. Binding to the phopshorylatd peptides also inhibits its pyruvate kinase activity (Christofk, Vander Heiden et al. 2008; Christofk, Vander Heiden et al. 2008). The inhibitory effect of tyrosine phosphopeptides on PKM2 also exists in living cells. However, the interaction example of a tyrosine phospho protein with PKM2 is not yet revealed. In our study, we found a tyrosine phospho peptides, p-Y593/595, derived from p68 RNA helicase, interacted with PKM2 at FBP binding site. Our experiments further demonstrate the

interaction of the phosphor-p68 with PKM2. The pyruvate kinase activity of PKM2 was decreased when interacting with p68 RNA helicase.

During tumorigenesis, PKM2 is converted to dimeric form in tumor cells. The dimeric form has a low affinity to PEP. The low affinity to PEP slows down the glycolysis so that more phosphorylated intermediates from glycose are used to synthesize nucleic acids and amino acids for cell proliferation. One interesting question is how to convert the tetrameric PKM2 to a dimer in living cells. It is conceivable to think that the binding of tyrosine phosphopeptides to PKM2 changes its quaternary structure from a tetramer to a dimer so that the glycolytic activity of PKM2 is decreased and FBP is released. In our study, the binding of p-Y593/595 to PKM2 changed its quaternary structure from tetrameric to dimeric. The pyruvate kinase activity of PKM2 is decreased to certain level to benefit cancer cells for macromolecule synthesis. On the other hand, the dimeric PKM2 was shuttled into the nucleus by p68 RNA helicase to regulate gene transcription for promoting cell proliferation. Therefore, PKM2 plays a central role to modulate both cancer cell motabism and gene transcription.

In addition, phosphorylation can occur at Serine, Threonine as well as Tyrosine residues. What are the functions of Serine and Theronine phosphorylated proteins binding to PKM2? Do they have the similar functions as Tyrosine phosphorylated proteins binding to PKM2 to affect cell proliferation as well as the glycolysis process? It will be very interesting to find out the physiological roles of these phosphorylated proteins to PKM2.

5.4 Nuclear PKM2 Regulates MEK5 Gene Transcription to Promote Cell Proliferation

To analyze the function of nuclear PKM2, we screened the nuclear PKM2 levels in five pairs of cancer cell lines. The levels of nuclear PKM2 correlated with the proliferation status of cancer cells. According to these studies, we hypothesized that nuclear PKM2 may function in gene transcription in cancer cells to promote cell proliferation. Both expression array and Chip-on-chip suggested that PKM2 plays a role in MEK5 gene transcription. Our results showed that regulation of MEK5 gene transcription mediated the role of PKM2 in promoting cell proliferation. Our results also indicated that MEK5 was highly expressed in more metastatic cancer cells than in less aggressive cancer cells from the same tissues, such as lung, melanoma and colorectal cancer cells. According to our expression array analysis, there were also many other genes related to cell proliferation, such as ribosomes proteins and cyclin D1. Further studies will be carried out with these genes.

Interestingly, PKM2 is not the only metabolism enzyme acting in gene tranascription in the nucleus. It was reported that some other glycolytic proteins played roles in the regulation of gene transcription in the nucleus, such as GAPDH. GAPDH interacts with the Oct-1 transcriptional factor in the nucleus as a co-activator to regulate H2B gene transcription (Zheng 2003). Nuclear GAPDH binds to DNA as well as RNA to play multiple roles in many other cellular processes, such as nuclear tRNA transport, DNA replication and repair (Sirover, 2005). It was also reported that GAPDH induces ATG12 expression to resist the caspase-independent cell death process {Colell, 2007

#6009}. Another example is Lactate dehydrogenase (LDH), which catalyzes the pyruvate to lactate conversion, was also discovered as a DNA-helix-destabilizing protein, which plays roles in gene transcription in the nucleus. LDH-A and LDH-B are transcriptional co-activators with functions in cell-cylce regulation. Hexokinase 2 induces transcriptional repression in the nucleus of yeast {Rodriguez, 2001 #6013}. An isoform of Enolase 1 represses the transcriptional activity of the c-Myc gene in HeLa cells [Ghosh *et al.*, 1999]. In addition, some other glycolytic proteins, such as phosphoglycerate kinase and aldolase, are also detected in the nucleus {Ronai, 1993 #6010}. It is very interesting to investigate whether nuclear PKM2 also regulates other gene transcriptions to perform diverse biological functions, such as nuclear tRNA transport, DNA processing and apoptosis.

5.5 Nuclear PKM2 Phosphorylates Stat3 in the Nucleus to Regulate its Transcriptional Activity

PKM2 does not have a clearly defined DNA binding motif. Thus, an open question is how PKM2 is able to function in gene transcription. We hypothesized that nuclear PKM2 acts as a co-activator to regulate gene transcription and PKM2 may target other transcription factors. It was reported that Stat3 regulateed MEK5 transcription (Song, Jin et al. 2004). It was also shown that Stat3 was a tyrosine phosphopeptides binding proteins. Thus, we questioned whether Stat3 interacted with PKM2 in the nucleus. Our experiments indeed showed the interaction between nuclear PKM2 and Stat3. In this study, the transcription activity of the downstream target of Stat3 is MEK5. MEK5 is the major effector in the control of cell proliferation regulated by nuclear PKM2. The

transcriptional activity of other downstream targets of Stat3, such as Cyclin D1, remains to be elusive. Whether nuclear PKM2 interacts with other transcriptional related-factors to play a role in regulating gene transcription is not yet known. Further study needs to be carried out in this direction.

5.6 Overexpression PKM2 Forms Multinucleus in Less aggressive Cancer Cells

The overexpression of PKM2 in less aggressive cancer cells, such as T98G, SW480 cells, induces formation of multinucleus cells. The molecular mechanism that leads to the formation of multinuclear cells is not clear. Gene array analysis demonstrated that PKM2 control Cdc14A expression. The regulation function of PKM2 in regulating Cdc14A expression depends on the expression of p68 RNA helicase, which provided another example of the function of p68 RNA helicase as a co-activator. In addition, p68 RNA helicase activity was not related to its gene regulation function. One possible mechanism for formation multinucleus phenomenon induced by PKM2 overexpression is the overexpression of Cdc14A dephosphorylated Cdh1, which activated the APC complex to exit mitosis, resulting in aneuploidy, an abnormal number of chromosomes, in tumor cells. The aberrant mitosis may result in apoptosis in these cancer cells after a certain number of generations. Under these circumstances, overexpression of PKM2 may not promote cell proliferation, which explains well why PKM2 does not promote cell proliferation in less aggressive cancer cells. On the other hand, aneuploidization is found in many cancer cells. After more than a hundred years, it is still debatable whether aneuploidy, is a cause of cancer (von Hansemann, D. (1890) Boveri, T. (1914)). It was also reported that Cdc14A upregulation induced aberrant, premature centrosome

splitting. The centrosome is the microtubule organization center, which plays pivotal roles in regulating the formation of bipolar spindles during mitosis. The pre-mature splitting of centrosomes in the S phase may cause formation of multinucleus in these cancer cells.

5.7 Dimeric PKM2 Phosphorylates Stat3 Using PEP as Phosphoryl Group Donor

Both nuclear and cytoplasmic PKM2 exist in different quaternary structures in many cancer cell lines, such as SW480 and SW620 cells. Nuclear PKM2 does not form a tetramic structure like the cytosolic version. Whether nuclear PKM2 forms a dimer or exists as a monomer is not yet determined. We observed that nuclear PKM2 purified from SW620 cells migrated at 120KD position in a native gel. However, it is not known whether nuclear PKM2 has a post-translational modification that lead to the change in mobility in PAGE. Recently, it was reported that PKM2 was sumoylated and the sumoylation promotes nuclear localization (Spoden, Morandell et al. 2009). It will be interesting to test whether the band shift is due to PKM2 sumoylation or possibly other modifications.

Tetrameric forms of PKM2 have a higher affinity to PEP, which is regulated by FBP binding. Our results showed that nuclear PKM2 phosphorylated Stat3 uses PEP as a phosphoryl group donor. The phosphorylation of Stat3 by PKM2 was also observed with PKM2 purified from cytosolic extract. However, the cytosolic PKM2 exhibited much week activity in phosphorylating Stat3 compared to that of nuclear PKM2. This is most likely due to cytosolic PKM2 exists mostly as a tetramer. Another possibility is that the tetrameric PKM2 can not bind to Stat3 because the binding sites for Stat3 are buried

according to structural analysis of PKM2. The binding site for Stat3 on PKM2 is located an ADP binding cleft, which is located between the two dimers. In the glycolysis process, ADP is small enough to access to the site. Stat3 is a large molecule, around 80 KDa. Thus, the access to the binding site is blocked.

5.8 Arginine 399 Changes the Quaternary Structure of PKM2

Arginine 399 is crucial for maintaining the tetrameric structure of PKM2 by forming charge-charge interaction with Glutamic Acid 418, Aspartic Acid 357, Glutamic Acid 396. To test the conjecture, a mutant was made to eliminate the interactions. Studies showed that this mutant interfered with the interaction between the two dimers of PKM2 both *in vivo* and *in vitro*. Interestingly, an NES signal was detected in the PKM2 sequence using the peptide graft technique. The NES signal is also expressed in the interface between the two dimers. The mutant in this region destroyed the formation of tetrameric PKM2. This NES mutant also diminishes the FBP binding site of PKM2. Interestingly, the recombinant R399E mutant protein was shown to phosphorylate Stat3 proteins *in vitro*. This result also confirmed that R399E mutant may share a similar function with nuclear PKM2 to phosphorylate Stat3.

5.9 References

Christofk, H. R., M. G. Vander Heiden, et al. (2008). "The M2 splice isoform of pyruvate kinase is important for cancer metabolism and tumour growth." Nature **452**(7184): 230-233.

Christofk, H. R., M. G. Vander Heiden, et al. (2008). "Pyruvate kinase M2 is a phosphotyrosine-binding protein." Nature **452**(7184): 181-186.

Colell, A., J. E. Ricci, et al. (2007). "GAPDH and autophagy preserve survival after apoptotic cytochrome c release in the absence of caspase activation." Cell **129**(5): 983-997.
Huang, Y. and Z. R. Liu (2002). "The ATPase, RNA unwinding, and RNA binding activities of recombinant p68 RNA helicase." J Biol Chem **277**(15): 12810-12815.
Liu, Z. R. (2002). "p68 RNA helicase is an essential human splicing factor that acts at the U1 snRNA-5' splice site duplex." Mol Cell Biol **22**(15): 5443-5450.
Rodriguez, A., T. De La Cera, et al. (2001). "The hexokinase 2 protein regulates the expression of the GLK1, HXK1 and HXK2 genes of Saccharomyces cerevisiae." Biochem J **355**(Pt 3): 625-631.
Ronai, Z. (1993). "Glycolytic enzymes as DNA binding proteins." Int J Biochem **25**(7): 1073-1076.
Sirover, M. A. (2005). "New nuclear functions of the glycolytic protein, glyceraldehyde-3-phosphate dehydrogenase, in mammalian cells." J Cell Biochem **95**(1): 45-52.
Song, H., X. Jin, et al. (2004). "Stat3 upregulates MEK5 expression in human breast cancer cells." Oncogene **23**(50): 8301-8309.
Spoden, G. A., D. Morandell, et al. (2009). "The SUMO-E3 ligase PIAS3 targets pyruvate kinase M2." J Cell Biochem **107**(2): 293-302.
Yang, L., C. Lin, et al. (2007). "A double tyrosine phosphorylation of P68 RNA helicase confers resistance to TRAIL-induced apoptosis." Oncogene **26**(41): 6082-6092.
Zheng, L., R. G. Roeder, et al. (2003). "S phase activation of the histone H2B promoter by OCA-S, a coactivator complex that contains GAPDH as a key component." Cell **114**(2): 255-266.

CHAPTER 6 MATERIAL AND METHODS

6.1 Nucleic Acids Related Techniques

6.1.1 Mini Preparation for DNA

DNA Spin Mini Kit (Qiagen) was applied to isolate DNA plasmids from bacteria. Single colony was picked using a sterile inoculation loop from agar plates and resuspended in 1 ml LB culture medium containing appropriate antibiotics (50 ng/ml Kanamycin or Ampicillin). The bacteria were incubated at 37°C on a rotary shaker with 220 rpm overnight. The next day, the bacteria medium was transferred into an Eppendoft tube and centrifuged at 13,000 rpm for 2 min. Then, the bacteria pellet was completely resuspended in 250 ul resuspension buffer. 250 ul of lysate buffer, P2, containing RNase was added into the tube. The tube was gently inverted back and forth 5-6 times to completely lysate the bacteria. Then, 350ul of neutralization buffer, N3, was added into the tube and inverted gently 5-6 times to completely neutralize the lysate. The lysate solution was then transferred into a spin column and centrifuged at 13,200 rpm for 1 min to allow DNA to be captured to the membrane. Then, the membrane was washed with 500 ul of buffer PB by centrifuging at 13,000 rpm for 1 min to remove trace nuclease activity. Next, the membrane was washed with 0.75 ml of PE buffer to purify DNA by centrifuging at 13,000 rpm for 1 min. With additional 1 min centrifuging at 13,000 rpm, the membrane was dried. 20~30 ul ddH_2O or TE buffer was loaded to the membrane to elute DNA from the membrane by centrifuging at 13,000 rpm for 1 min. The eluted DNA was confirmed by either gel electrophoresis or DNA sequencing.

6.1.2 Midi Preparation for DNA

Bacteria containing DNA plasmid were cultured in 1 ml LB medium supplemented with appropriate antibiotics (50 ng/ml Kanamycin or Ampicillin). Then, the bacteria culture was transferred into 150 ml warm LB medium and cultured overnight to amplify plasmid DNA. The next day, the culture was centrifuged at 6,000 rpm for 10 min to get cell pellet. The bacteria pellet was resuspended in 3 ml of resuspension buffer and lysated with 3 ml of lysate buffer. The lysate was neutralized with the adding of 3 ml of neutralization buffer. Then, the solution was centrifuged at 15,000 for 20 min and the supernatant was carefully collected into a 50 ml conical tube. 10ml of DNA purification resin provide with the kit was added to the tube and mixed gently with the supernatant containing DNA plasmids. The mixture was loaded to a midi preparation column and applied to vacuum equipment to remove supernatant. The resin beads with DNA plasmids were washed with washing buffer twice (10 ml each time). After the washing buffer completely passed through the column, the vacuum was applied to the column for additional 1 min to dry the resin. The leftover of washing buffer was removed by centrifuging at 10,000 rpm for 1 min. During this time, 2 ml of ddH_2O or TE buffer was heat to 70°C in a heat blocker. 300 ul of warmed ddH_2O was added into the column and incubated for 2 min. Then, DNA plasmid was eluted from the column by centrifuging at 13,200 rpm for 1 min. The DNA plasmid was purified with Phenol/Chloroform/Ethanol method and the concentration was measured with spectrometry at OD260nm.

6.1.3 Agarose Gel Electrophoresis and Gel Extraction of DNA

DNA plasmids or DNA fragments could be visualized by using a double stranded DNA binding dye, Ethidium Bromide, under a UV transilluminator. 1 % agarose gel was prepared by adding 1 g of agarose beads into 100 ml TAE buffer. The solution was heated with microwave to completely liquefy agarose beads. The solution was quickly cooled down to 50-60 °C with a water bath for 1 min. 6 ul of Ethidium Bromide was added into 100 ml warmed agarose solution and the solution was poured into a gel casting apparatus. Well inserts was set up in the gel casting apparatus to make suitable wells. 10 ul of DNA ladder was loaded into one well to refer to molecular weight of DNA fragments. The gel was run at constant voltage of 120 V until the blue dye reached to the middle of agarose gel.

6.1.4 Quantification of DNA and RNA

Nucleic acids concentration was measured using a spectrophotometer (UV-1700 Spectrophotometer, Shimadzu Co.) at OD260 nm. The absorbance obtained at OD260 nm was applied to this formula: DNA concentration (ug/ml) = (OD260nm) X (dilution factor) X (50 ug DNA/ml) / (1 OD260nm unit). The purity of DNA was measured by the ratio of the absorbance of OD260nm /OD280nm. The purify was acceptable when the ratio was between 1.8 and 2.0.

6.1.5 Polymerase Chain Reaction (PCR) Method

PCR method was applied to amplify a target sequence from plasmid DNA or mutate specific nucleic acids of a plasmid vector. Generally, 0.5 ug of template DNA was mixed with 1 mM dNTP, 0.5 ug forward and reverse primers, and 2 unit of pfu polymerase in 1X reaction buffer. The reaction mixture was denatured at 95 °C for 2 min and then was followed by 25-35 cycles: 95 °C denaturation for 30 seconds, 57-62 °C annealing for 45 seconds, 72 °C elongation for 45 seconds. An additional elongation step at 72 °C for 10 min was performed to stabilize the double strands. The PCR product might be visualized by agarose gel electrophoresis.

6.1.6 Restriction Enzyme Digestion and Plasmids Construction.

To exogenous introduce proteins into mammalian cells or express recombinant proteins in bacteria, cDNA of target genes must be constructed into expression vectors. Restriction enzyme digestion was applied to generate the specific restriction enzyme digestion sites. DNA sequence maps of these vectors were available from companies. According to the detailed description of these restriction enzyme sites, two suitable restriction enzymes would be chosen to digest PCR products or targeting cDNA sequences. To apply the restriction enzymes correctly, cDNA or PCR products sequence must be scanned by computer with the sequences of restriction enzymes to avoid mis-targeting. All restriction enzymes have optimum conditions for their activities. To perform two restriction enzymes digestion simultaneously (double digestion), two enzymes must have compatible reaction conditions. Otherwise, the restriction digestions should be carried out one by one. In general, for 1ug DNA or 30ul PCR product, 1ul enzyme (20 unit) was used. ddH_2O was added to the tube to make the final digestive

system to 30 ul or 50 ul. The mixture was incubated at a temperature ranging from 30 °C to 37 °C for 1 to 2 hours. Agaorse gel electrophoresis was performed to separate the digested vectors.

T4 ligase was applied to ligase the digested DNA into the vector. T4 ligase can join the 3'-OH of one nucleic acid and the 5' phosphate of the other nucleic acid. The ratio of insert DNA to vector was critical to make the ligation successful. An optimum ratio of insert DNA to plasmid vector was around 3:1. The ligation process was performed in 1x ligation buffer with 2 ul of T4 ligase. The mixture was incubated at 4 °C overnight. The next day, the ligation product was transformed into competent bacteria.

6.1.7 Site-directed Mutation Method

Site-directed mutation was carried out using QuikChange II XL site-directed mutagenesis kit (Stratagene). The primers were designed using an on-line program--The QuikChange®Primer Design Program. 0.5 ug of primers was applied to PCR system. 2 ul of Dpn1 enzyme (20 unit) was added to the reaction system to digest unmutated plasmid vectors. The reaction was performed at 37°C for 2 hours. After purification, the mutated plasmid vectors were transformed into XL1-Blue competent cells. The transformed XL1-Blue cells were cultured in agar plates containing appropriate antibiotics overnight. The next day, 6-12 colonies were picked to be cultured in 1 ml LB medium overnight. The following day, mini-prep was performed to isolate plasmid DNA from XL-1 Blue cells and the mutated DNA sequences were confirmed with DNA sequencing technique at the core facility of Georgia State University.

6.1.8 DNA Sequencing

DNA sequencing experiment was performed to examine a DNA sequence from a mutation or ligation experiment. The sequencing primer was designed according to plasmid vector maps, which was 50-100 nucleic acids upstream of the target sequence. The sequencing primer was diluted in 20 uM. The plasmid vector was diluted to 0.1-0.2 ug/ul. Some sequencing primers were provided by the core facility of Georgia State University, such as T7, S4 primers.

6.1.9 Ethanol Purification of DNA

Ethanol purification was performed to remove any salt or protein contaminations in DNA samples. Firstly, 1/10 volume of 3 M sodium acetate was added to DNA sample and mixed thoroughly. 2 volumes of 100% ethanol was added into the mixture and placed in -20°C for 30 min. the mixture was centrifuged at full speed for 10 min at room temperature to pellet DNA. The DNA pellet was washed with cold 70% ethanol twice and centrifuged at 4°C. DNA pellet was dried by air at room temperature until the pellet becomes transparent. Then, the pellet was dissolved in ddH_2O and the concentration was measured with a spectrophotometer at OD260nm.

6.1.10 RNA Extraction

Total RNA was isolated from mammalian cells by using RNeasy Plus Kit (Qiagen). Mammalian cells were cultured in a 6-well plate and washed with cold PBS twice. Then, 350 ul of RLT buffer supplemented with 3ul of 2-Mercaptoethanol was added to each well. The attached cells were lifted from the culture plate with a cell lifter

and loaded onto a QiaShredder column (Qiagen) to be homogenized. The loaded column was centrifuged at full speed for 2 min in a microcentrifuge machine. The eluted samples were loaded onto a gDNA eliminator spin column to remove genomic DNA. After centrifuging at 13,200 rpm for 2 min, the eluted solution was mixed thoroughly with one equivalent volume of 70 % ethanol. The mixture was loaded onto an RNeasy spin column and centrifuge at full speed for 1 min. Then, the column was washed with 700 ul of RW1 buffer once and RPE buffer twice. The column was centrifuged for one more minute to dry the membrane. Finally, RNA was eluted with 30 ul of RNase-free H_2O twice. The elution was combined together and RNA concentration was measured with a spectrophotometer at OD260 nm. RNA samples were stored at -80°C for a couple months.

6.1.11 Reverse Transcription PCR

Reverse transcription was performed to generate cDNA from mRNA. 1 ug of total RNA extract was mixed with 1 ul of oligo dt15 to a final volume of 5 ul with adding of RNase-free H_2O. The mixture was incubated at 25 °C for 5 min and followed by incubating at 70 °C for 5 min. Then, the mixture was incubated on ice for 5 min. To each reaction, 1 ul of reverse transcriptase, 1 ul of RNase inhibitor, 4 ul of $MgCl_2$ (25 mM) and 4 ul 5X reaction buffer were mixed thoroughly. The reaction was incubated at 25 °C for 5 min, 45 °C for 1 hour and 70 °C for 15 min. The final products were stored at -80 °C.

6.1.12 Relative Real Time PCR

Total RNA was extracted from cells using a RNeasy kit. Reverse transcription process was performed with ImProm-II reverse transcription system (Promega). RT-PCR process was performed in Applied Biosystems Fast Real-Time PCR 7500. RT-PCRs were performed with 1 μg of cDNA and 25 ul of Fast SYBR green master mix (Applied biosystems). The solutions were mixed in a 0.5 ml PCR tube and loaded to a RT-PCR plate. The plate was tightly sealed with a piece of adhesive film. The plate was centrifuged at 1,000 rpm for 2 min at room temperature and loaded onto real-time PCR machine. The amplification process was carried out by the following the cycles: 95 °C for 15 seconds, 95 °C for 3 seconds and 60 °C for 30 seconds. The amplification was analyzed with the Applied Biosystems SDS v1.4 program. After the cycles, a dissociation curve was generated by increasing the temperature to 95 °C for 30 min. Standard RT-PCR primer set was purchased from RealTimePrimers.com.

6.1.13 Chromatin Immunoprecipitation

Mammalian cells were cultured in normal medium to 70% confluence. Then, cells was fixed with 1% formaldehyde solution by incubating 10 min at 37 °C and the reaction was stopped with the adding of 125 mM glycine. The fixed cells were washed with cold 1X PBS three times supplemented with protease inhibitors and lysated in 1 ml SDS lysis buffer (Imgenex). The cell lysate was sonicated on ice for 2 min and centrifuged at 15,000 rpm to pellet insoluble material. The success of shearing was examined with agarose gel. The supernatant was aliquoted and pre-cleared with 100 ul salmon sperm

DNA/protein G agarose by incubating for 2 hours. The primary antibody (10~20 ul) was added to the supernatant and incubated at 4 °C overnight. The next day, 100 ul of salmon sperm DNA/protein G agarose was added to each tube and incubated for 2 hours. The immuno-complex was eluted with 200 ul elution buffer. The cross-link was reversed with 4 ul of 5 M NaCl incubating at 65° overnight. The released DNA was purified using the phenol chloroform extraction method. Regular PCR was performed in Mastercycle® Gradient PCR machine (Eppendorf) and the result was analyzed on a 2% agarose gel.

6.1.14 ChIP-on-chip

For ChIP-on-chip analysis, GeneChip human promoter 1.0R array was applied in this research. The immuno-complex from Chromatin Immunoprecipitation was cleaned up with phenol chloroform extract method. The immunoprecipitated DNA targets were amplified with PCR method with random primers. The amplified DNA targets were fragmented using cDNA fragmentation buffer (GeneChip WT Double-stranded DNA terminal labeling kit). The fragmented DNA was labeled with DNA labeling reagent (GeneChip WT Double-stranded DNA terminal labeling kit) and examined with gel-shift analysis. The labeled target was hybridized with arrays in hybridization oven (Hybridization Oven 640 Affymetrix) at 60 rpm for 16 hours. The arrays were then scanned with Affymetrix GeneChip 3000 scanner. The ChIP-on-chip data was analyzed with affymetrix Tiling Analysis software 1.1 and Integrated Genome Browser. All parameters were set up as described in the tiling analysis software tutorial from Affymetrix website.

6.1.15 Microarray analysis

GeneChip® Human Genome U133 Plus 2.0 Array was performed in this research. Total RNA from cells expressing HA-tagged PKM2 or control was extracted with RNeasy kit by following the manufacturer's instruction (Qiagen). The total RNA concentration was determined by spectrometer reading at OD 280 nm. 10ug of total RNA of each sample was used for synthesizing the (−) strand cDNA with ImProm-II reverse transcription system (Promega). Synthesized cDNA were purified with the phenol-chloroform extraction method. In vitro transcription reaction was performed by using the GeneChip® IVT Labeling Kit (Affymetrix). The labeled cRNA was fragmented in fragmentation buffer (Affymetrix) and hybridized to GeneChip® Human Genome U133 Plus 2.0 Array. The arrays were scanned with Affymetrix GeneChip 3000 scanner. The data were analyzed by Affymetrix GeneChip Operating Software (GCOS) Version 1.0.

6.1.16 Electrophoretic Mobility Shift Assay.

Stat3 consensus binding probe 5'-GATCCTTCTGGGAATTCCTAGATC-3' was purchased from Santa Cruz. The DNA probes were labeled with γ-^{32}P using T4 polynucleotide kinase. Nuclear protein extracts (10 ug each) were incubated with the ^{32}P labeled Stat3 consensus-binding probe for 20 minutes at room temperature in binding buffer (5 % glycerol, 1 mM MgCl2, 0.5 mM EDTA, 0.5 mM DTT, 50 mM NaCl, 10 mM Tris-HCl, 0.05 mg/ml poly(dI-dC)). For supershift analyses, the nuclear extracts were preincubated with Stat3 monoclonal antibody (invitrogen) for 1hour at room temperate before loading. The protein-DNA complexes were separated in 4 % native

polyacrylamide gel (acrylamide: polyacrylamide 60:1). The 4 % native polyacrylamide gel was pre-run at 200 V for 45 min in 0.5X TBE buffer at 4 °C. Protein-DNA complexes were loading in wells with loading buffer and run at 200 V until the blue dye migrated to ¾ length of the gel. The gel was transferred to Whatman paper. The gel was covered with Saran Wrap and dried at 80 °C in vacuum dryer for 2hours. The gel was placed in phosphoimagine plate in 4 °C overnight. The gel plate was read in Storm 840 phosphoimager, Amersham Biosciences and analyzed with ImageQuant TL.

6.2 Bacterial Techniques

6.2.1 Bacterial Culture and Storage

The *E. coli* strains, such as JM109, XL1-blue, BL-21 were used for plasmid DNA amplification or recombinant protein expression. *E. coli* stains were inoculated in autoclaved Luria Broth (LB) medium prepared in 1 % bacto-tryptone w/v, 0.5 % bacto-yeast-extract w/v and 1 % NaCl w/v. 50μg/ml of Ampicillin or Kanamycin was added into warmed LB medium (50~60 ºC) for antibiotic resistant strains selection. The bacteria were cultured in shakers or incubators in 37 ºC. Agar plates were prepared in LB medium with the addition of 1.5% Agar prior to autoclaving. For long term storage of transformed bacteria, the transformed strains were mixed with sterile 30 % glycerol w/v and preserved at -80 ºC.

6.2.2 Transformation

For large scale plasmid DNA preparation, transformation was carried out in JM109 *E.coli* strain. JM109 competent cells were thawed on ice and 100ul of JM109 was

aliquoted into a test tube. 1~5 μg of plasmid DNA was added into the tube and incubated with JM109 competent cells for 30min on ice. Heat shock was performed to the mixture at 42 ºC for 90 seconds. The mixture was chilled on ice for additional 2 min and 200 ul of warmed LB were added into the tube. Then, the tube was incubated at 37 ºC in a shaker with 220 rmp for 1 hour. The transformed bacteria were spread onto agar plates containing appropriate antibiotics and incubated at 37 ºC overnight. The next day, colonies were picked with sterile plastic sticks from the agar plates and dipped into antibiotics containing LB medium for large scale amplification.

6.3 Protein Techniques

6.3.1 Recombinant PKM2 Protein Expression and Purification

Human PKM2 cDNA was constructed into pET30a bacteria expression vector. BL-21 expression host was transformed with PKM2-pET30a vector and cultured in LB medium containing 50 ng/ml Kanamycin. BL-21 was cultured in 50 ml LB and the next day was transferred into 1L warmed LB medium shaking at 220 rmp at 37 °C until OD600nm reached between 0.4 and 0.6. Isopropyl-β-D-thiogalactoside (IPTG) was added to LB medium to a final concentration at 1mM to induce recombinant protein expression. 4 hours later, bacteria were collected with centrifuging at 6,000 rpm at 4 °C for 10 min. Bacteria pellet was washed with cold PBS twice and lysated in lysis buffer containing 1mg/ml lysozome. The bateria lysate was sonicated for 1 min on ice and centrifuged at 17,000 rpm for 20 min. The expression of recombinant PKM2 was detected with SDS-PAGE gel. Most recombinant PKM2 protein was expressed in inclusion bodies. The pellets were washed with washing buffer (0.5M Urea and 50mM

phoshorylate buffer pH7.4) twice and lysated in a denature buffer (8 M Urea and 50 mM phosphorylate buffer, pH7.4). The inclusion body was lysated at RT for 1 hour and centrifuge at 16,000 rpm for 30 min. The supernatant was collected and diluted dropwise with 50 mM phosphorylated buffer till 0.5 M Urea. Recombinant PKM2 protein was purified with HiTrap column using Akta purifier 100 FPLC system. Recombinant PKM2 protein was gradient eluted with 0.5 M imidazole. The eluted protein was collected and dialysis in buffer (50 mM Tris, pH 7.5, 0.1 M KCl, and 20% glycerol). 25mM DTT was added into the buffer and dialysis into the refolding buffer (50 mM Tris, pH 8.0, 0.1 M KCl, 20% glycerol, 0.1 M EDTA, 1 mM DTT)

6.3.2 Gel Filtration

Size filtration chromatograph was applied to separate tetrameric and dimeric PKM2 from the subcellular extracts. The separation process was performed in Superdex 200 10/300GL column with Akta purifier 100 FPLC system. Superdex 200 10/300GL column can separate proteins molecular weight range from 10KD~600KD. Blue dextran, 2,000 KD, was applied to measure void volume (Vo) of the column. 100 ul of blue dextran was loaded into the column with concentration at 1 mg/ml. The column was calibrated with molecular weight standards, such as Aprotinin 6.5 KD, Ribonuclease A 13.7 KD, Carbonic Anhydrase 29 KD, Ovalbumin 44 KD, Conalbumin 75 KD, Ferritin 440 KD, Thyroglobulin 669 KD. These standards were dissolved in the same buffer as subcellular extracts or recombinant proteins with salt concentration higher than 0.15M. The protein standards concentration was 3 mg/ml or 4 mg/ml. UV280nm protein detector was applied to monitor the chromatography. The flow rate was 0.4 ml/min. The standard curve was

calculated by following the manufacture's instruction. 100 ul cytosolic or nuclear extract (500 ug) was loaded into Superdex 200 10/300GL column and eluted with elution buffer (50 mM sodium phosphate buffer pH7.2, 0.15 M NaCl). The elution fraction was collected in 300 ul aliquots. The molecular weight of each aliquot was calculated based on the calibration curve made from standard proteins. 30 ul of each aliquot was analyzed with 10 % SDS/PAGE gel followed by western blot procedure.

6.3.3 Protein Quantification

Protein concentration was determined with BioRad Protein Assay. The standard curve was generated with a serial of diluted Bovine Serum Albumin (BSA) at the range of 2.0-10.0 ug/ul. The standard curve was generated according to the absorption values of BSA using Microsoft Excel. 1-2 ul of sample solution was diluted in 800 ul ddH_2O mixed with 200 ul BioRad dye solution. The optical density was examined with a spectrophotometer at a wavelength of 595 nm. The protein concentration was calculated according to the absorption values.

6.3.4 Sodium Dodecyl Sulfate Polyacryalmide Gel Electrophoresis (SDS-PAGE)

SDS-PAGE gel was applied to separate protein complexes according to their electrophoretic mobilities. The electrophoresis apparatus was assembled according to the manufacturer's instructions. Separating gel was prepared by following the recipes. The solution was mixed in a 100 ml glass beaker and poured between the glass plates. 500 ul isopropanol was poured on top of separating gel to remove air bubbles. Roughly, it took 45 min for separating gel to be polymerized. After the separating gel was polymerized,

isopropanol was poured off and the top of the separating gel was rinsed with ddH_2O gently. The leftover of ddH_2O was removed by a small piece of filter paper. Then, 4 % stacking gel was prepared and poured on top of the separating gel. A comb was inserted into the stacking gel to generate wells. The prepared SDS-PAGE gels were overlaid with 1X SDS-PAGE running buffer at 4 °C for a couple days. Protein samples were mixed with 5X loading buffer and boiled at 95 °C for 8 min. Protein samples were loaded into the wells with fine tips. The unused adjacent wells were loaded with 1X sample buffer. SDS-PAGE running buffer was added into both the inner chamber and the outer chamber. Run the gel at 60 V until the dye had reached the front of separating gel and then switch to 120 V until the blue dye running out of the gel.

Separating gel buffer

375 mM Tris-HCl; pH 8.8

0.1% SDS

4% Stacking gel buffer

125 mM Tris-HCl; pH 6.8

0.1% SDS

SDS-PAGE running buffer

25 mM Tris; pH 8.3

250 mM Glycine

0.1% SDS

pH = 8.3

5X protein gel sample loading buffer

50 mM Tris-HCl; pH 6.8

2% SDS

10% Glycerol

1% β-Mercaptoethanol

0.02 % Bromophenol Blue

12.5 mM EDTA

6.3.5 Coomassie Blue Staining

Proteins on SDS-PAGE gel can be detected with Coomassie blue stain. The gel was washed with ddH_2O for 2 min. Then, gel was stained with Coomassie blue solution for 30 min. The gel was destained with destaining buffer to remove extra coomssive blue dyes.

Coomssive blue solution

0.1 % Coomassive Brilliant Blue

20% Methanol

10% Acetic Acid

Destain buffer

40%Methanol

10% Acetic Acid

6.3.6 GelCode Staining

Small amount of proteins on SDS-PAGE Gels can be detected with GelCode staining (Pierce). The gel was washed with ddH_2O twice (5 min/each) at room temperature. GelCode staining buffer without dilution was added into the staining tray that would just cover the gel. The gel was stained for 2 hours at room temperature and

destained with ddH_2O for 2 hours. The protein bands were visualized with a UV transilluminator with CCD camera.

6.3.7 Native Gel Preparation

Native gel was prepared and run by following the method of SDS-PAGE in the absence of SDS.

6.3.8 Protein In-gel Digestion

Protein complexes were separated in SDS-PAGE gel or native gel. The presences of interested protein bands were stained with Coomassie blue, SYPRO Rube dye, or GelCode. The protein bands were carefully cut from the gel using a scalpel. The gel piece were placed in a siliconized Eppendorf tube and destained with 200 ul of destaining solution twice. The destaining process might be incubated in 37 ºC. The gel piece was dried using a Speed Vac for 30 min. 20 ul (0.4ug of Trypsin) of Trypsin solution and 50 ul of the Trypsin reaction buffer were added into the tube and incubated with the gel piece at 37 ºC overnight. The next day, the liquid was removed from the tube and transferred into a new tube. 50 ul of peptide extraction solution was added to the gel piece and incubated at 37 ºC for 30 min. The peptide extraction solution was removed from the tube and combined with the liquid recovered from the previous step. Then, the sample was ready for MALDI-MS analysis.

6.3.9 Protein Identification by Peptide Mass Fingerprinting

The proteins complexes were separated in SDS-PAGE and digested with Trypsin. The sample solution was concentrated with a Speed Vac to less than 10 ul. Then, the sample was desalted with ZipTip (uC18) tips. 1.5 ul of neat formic acid was added into the sample and mixed thoroughly. 8.5 ul of 0.1 % TFA was added into the tube and mixed with the sample. The tip was wet with wetting solution (50 % ACN) twice and equilibrated with 0.1 % TFA several times. The sample solution was aspirated and dispensed with the tip 5 times. The bound sample was washed with 0.1 % TFA 10 times. The sample was eluted from the ZipTip with 50 % ACN/0.1 % formic acid and spotted directly onto a wax-coated MALDI-TOF plate. The matching of the experimental peptide mass with database was examined with Peptident proteomic tools in ExPASy Molecular Biology Server (http://www.expasy.ch/). The MALDI-TOF/TOF database was from NCBInr.

6.3.10 Antibody Generation and Purification

Rabbits were immunized with KLH-conjugated peptides or recombinant proteins to generate antibodies. KLH-conjugated peptides were synthesized in Global Peptide Services Com. Recombinant proteins were expressed in BL-21 and purified with HiTrap columns in FPLC systems. For each rabbit, 5 ml pre-immune blood was harvested from the auricular artery for test controls. The blood was allowed to clot at room temperature and the serum was collected by centrifuging at 3,000 rpm for 15 min at

4°C. 0.1 % NaN3 was added to the serum and the serum was stored at -80 °C. Antigens (peptides or recombinant proteins) were emulsified by mixing with an equal volume of complete Freund's adjuvant. The emulsified antigen was injected into three subcutaneous dorsal sites in each rabbit. 0.2 mg of peptides or 0.5 mg of proteins was used per immunization. Two weeks later, 0.2 mg peptides or 0.5 mg of proteins were emulsified with incomplete Freund's adjuvant and injected into three subcutaneous dorsal sites of the same rabbits. Four weeks later, 20 ml of production blood was bled from the rabbits. The serum was collected by centrifuging at 3,000 rpm for 15 min at 4 °C and stored at -80 °C. Seven weeks later, 0.2 mg peptides was mixed with equal volume of incomplete Freund's adjuvant and injected into rabbits. Eight weeks later, the second bleeding was carried out and 20 ml blood was harvested from the auricular artery. Nine weeks later, the rabbits were immunized with 0.2 mg peptides mixed with equal volume of incomplete Freund's adjuvant. Ten weeks later, 50 ml production was bled.

6.3.11 Kinase Assay

SW620 cells were cultured in Leibovitz's L-15 Medium in flasks. SW620 cells were seeded to 70% confluence in T150 flasks and infected with 200 ul adenoviruses lysate ($1X10^{13}$ pfu/ml) packed with PKM2 cDNA per flask. The infected cells were harvested after 3 days and the nuclear extract were prepared. 100 ul of anti-HA antibody was incubated with the nuclear extract from SW620 cells in NETs buffer supplemented with protease inhibitors overnight. The next day 200 ul of agarose G beads were added and incubated for 2 hours. The immunoprecipated complex was harvested with centrifuging 500 rpm at 4 ºC for 5 min. The beads were washed with NETs buffer 4 times and high

salt solution (20mM Tris.HCl, 1M NaCl, pH7.5) for two times. Then the beads were washed with kinase buffer twice. The kinase assay was performed in kinase solution (100mM Tris.HCl, 100mM MgCl2, 2mM DTT, and 50 KCl). The recombinant protein Stat3 was incubated with purified HA-PKM2 in agarose beads at 4 ºC for 1hours. The reaction was stopped by adding 5XSDS-PAGE loading buffer and heating at 95 ºC for 8 min. The phosphorylation level of recombinant Stat3 was analyzed with phosphor-Tyr-705-Stat3 antibody.

6.4 Mammalian Cell Techniques

6.4.1 Mammalian Cell Culture and Storage

LN686, M4C1, SW480, SW620, WM115, WM266, T98G, U87MG, H146 and H460 cell lines were purchased from ATCC and cultured by following the vendor's instructions. To freeze cells, cells were cultured to 60-70 % confluence in a T75 flask and trypsinized. Cell numbers were measured using hemocytometer. Cell pellets were harvested with centrifuging at 1,000 rpm for 10 min. Then, cells were resuspended in freezing medium (10% v/v DMSO, 10% FBS, 80%culture medium) and aliquoted into freezing vials (5 x 10^6 cells/vial). The vials were stored in a freezing container at -80°C overnight. The next day, freezing vials were transferred to a liquid nitrogen reservoir for longer storage.

6.4.2 Transient Transfection Method

Mammalian cells applied in this project were transiently transfected with Fugene-HD reagent (Roche) by following the manufacture's instruction. Mammalian cells were

cultured in normal medium in 6-well plates. The next day, cell density would reach 70-90% confluence depending on cell types. The plasmids DNA-Fugene-HD mixture was prepared in polystyrene transfection tubes. For each well, 2 ug of plasmid DNA was added into 100 ul Opti-MEM medium and mixed thoroughly. Then, 5 ul of Fugen-HD reagent was added into the tube and mixed with plasmid DNA thoroughly. The transfection complex would be formed in 20 min at room temperature. The plates were washed with fresh normal medium twice and fed back with 1ml normal medium. Then, the transfection complex was added to each well dropwise. The transfected cells were cultured in an incubator with/without 5 % CO_2 at 37 °C for 48-72 hours before harvested. For immuno-stain experiments, cells were cultured in chambers 24 hours after transfection. Fluorescent microscope was applied to examine the fluorescent tagged protein 48 hours after transfection.

6.4.3 RNA Interference

RNA interference technique was applied to knock down endogenous protein expressions. Cells were seeded to 30-50 % confluence in 6-well plate in normal medium one day before knockdown experiment performance. The next day, 2 ml Opti-MEM medium was used to wash each well to remove FBS. siRNA duplex for PKM2, p68, MEK5 or Stat3 were purchased from Dharmacon RNA Technologies. RNA duplex was dissolved in DEPC-treated H_2O to 40 pmol/ul. 200 pmol siRNA duplex was diluted in 250 ul Opti-MEM medium. 5 ul of transfection reagent, lipofectamine RNAiMAX (invitrogen), was diluted into 250 ul Opti-MEM medium. The two solutions were combined together and incubated for 30 min at room temperature. 0.75 ml of Opti-MEM

medium was added into each well. Then, the mixture was added into each well dropwise. Fresh medium might be added into each well next day. For re-expression wild type or mutant proteins in knockdown cells, 24 hours later, knockdown cells were transfected using FuGene HD by following the manufacturer's instruction. 48 hours later, cells were lifted by cell lifter and harvested by centrifuging at 1,000 rpm for 10 min at 4 °C.

6.4.4 Growth Factor Treatment of Cells

For growth factors stimulation, mammalian cells were starved for 6-12 hours with Opti-MEM medium prior to treatment. Growth factors dissolved in either DMSO or ddH_2O were diluted in Opti-MEM medium. The starved cells were cultured in Opti-MEM medium containing growth factor for a given amount of time. DMSO or ddH_2O was used as a control. The cells were harvested once the treatment was done and stored at -80 °C immediately.

6.4.5 Whole Cell Lysate Preparation

Mammalian cells were washed with cold 1X PBS twice and collected by centrifuging at 1,000 rpm for 10 min at 4ºC. Whole cell lysate was prepared with cold 1X RIPA buffer (50 mM Tris-HCl, pH7.4, 150 mM NaCl, 0.25 % deoxycholic acid, 1 % NP-40 and 1 mM EDTA) supplemented with Protease Inhibitors Cocktail (PIC) (Sigma) and phosphatase inhibitors cocktail (Pierce). In general, $1X10^6$ cells were resuspended in 1 ml cold RIPA buffer and incubated for 1 hour on a rotary plate at 4 ºC. Then, cells were centrifuged at 13,200 rpm for 10min at 4°C to get cell debris pellet. The supernatant was removed carefully and stored at -80 ºC for later applications.

6.4.6 Nuclear Extract and Cytoplasmic Extract Preparation

Nuclear extract and cytosolic proteins were made with a nuclear extraction kit from Active Motif. Mammalian cells were washed with cold 1X PBS twice supplemented with PIC to completely remove culture medium. The attached cells were harvested gently with a cell lifter. The suspension cells were harvested with centrifuging at 1,500 rpm for 10 min at 4 ºC. In general, $1X10^6$ cells were resuspended in 1 ml of 1X hydrophobic buffer supplemented with PIC and incubated on ice for 15 min. Then, 50ul of detergent was added into tube and the tube was vortexed at maximum speed for 30 seconds. The supernatant was collected and stored at -80 ºC up to 2 months. The pellet, which was the nucleus, was washed with cold 1XPBS twice to avoid cytoplasmic protein contamination. Then, the nuclear pellet was resuspended in AM1 lysis buffer containing PIC and 1 mM DTT and incubated at 4 ºC for 1hour. Next, the tube was centrifuged at 13,200 rpm for 10 min at 4 ºC. The supernatant was collected and stored at -80ºC for further applications.

6.4.7 Suspension Growth of HeLa S3 Cell

HeLa S3 cells were firstly cultured in MEM medium supplemented with 10 % FBS on 2-3 plates. Medium was changed every 2 days until cell density reached 95 % confluent. Then, cells were trypsinized and spinned down in a 15 ml conical tube. Cells were resuspended in fresh medium and cell density was approximately $4X10^5$ /ml. Cells were transferred into a small spinner flask using 10 ml peptides from side arms. The volume was around 100 ml in small spinner flask. The top lid and side arms was sealed with parafilm tightly. The next day, cell density was carefully measured and cells were

spinned down in 50 ml tubes. Then, cells were resuspended in fresh medium in a large spinner flask to reach a density of $4X10^5$ /ml. Cells were fed every day with flash medium and cell density was maintained to $4\sim5x10^5$ /ml. Finally, cells were cultured in a one liter spinner flask and cell density might reach $6\sim7x10^5$ /ml. Cells were collected with centrifuging at 1,500 rpm for 10 min and were ready for later use.

6.4.8 Large Scale Nuclear Extract Preparation

To prepare large scale of nuclear extract for proteomic applications, we applied this method to extract nuclear proteins from mammalian cells. Suspension cells were harvested in 800 ml glass bottles spinning at 1,500 rpm for 10 min at 4°C. Cell pellets were transferred in cold 1xPBS to 50 ml Falcon tubes. The tubes were spinned at 3,000 rpm for 5 min at 4 °C and the packed cell volume was noticed. The cell pellets were resuspended in 5 times the packed cell volume of buffer A and quickly centrifuged at 3,000 rpm for 5 min at 4°C. A small sample was taken for microscope slide. The cell pellets were resuspended in 2 times the packed cell volume of buffer A and allowed to swell in buffer A for 10 min on ice. Then, the cells were homogenized in a large 40 ml glass Dounce homogeniser with a B type pestle for 20 up and down strokes. The cell lysate was examined under microscope. Additional strokes might be taken until cell lysis was greater than 90%. The swollen nuclei were about the same size as unlysed cells. The solution was transferred into a plastic tube and centrifuged at 4,000 rpm for 15 min at 4°C. The supernatant, the cytoplasmic fraction, was removed and the volume was estimated. 0.11 volumes of buffer B was added to the supernatant and transferred to a plastic tube. The mixture was centrifuged at 3,400 rpm for 1 hour at 4°C. The supernatant

was dialyzed with the nuclear fraction later. The pellet volume was carefully estimated and ½ volume of buffer C (low salt) was added to the nuclear fraction. The mixture was then transferred to a small cold baked glass beaker at 4°C. ½ volume of buffer D was added to the beaker dropwise. Stirring was continued for 30 min. The mixture was transferred to plastic tubes and centrifuged at 8,000 rpm for 30 min at 4°C. The supernatant was collected and dialyzed in buffer E. The supernatant was distributed in eppendorf tubes and spinned for 20 min at 4°C. The supernatant was collected and stored at -80°C.

Buffer A (hypotonic)

10mM Tris pH7.9

1.5mM MgCl2

10mM KCl

0.5mM DTT

0.2 mM PMSF

Buffer B

0.3 M Tris pH7.9

1.4M KCl

30mM MgCl2

0.5mM DTT

Buffer C (low salt)

20mM Tris pH7.9

25% Glycerol

1.5mM MgCl2

20mM KCl

0.2mM PMSF

0.5Mm DTT

Buffer D (high salt)

20mM Tris pH7.9

25% Glycerol

1.5mM MgCl2

1.2M KCl

0.2mM PMSF

0.5Mm DTT

Buffer E

20Mm Tris Ph7.9

20% Glycerol

0.1M KCl

0.2mM EDTA

0.5mM DTT

6.4.9 Immunoprecipitation (IP) and Co-immunoprecipitation (Co-IP)

IP and Co-IP experiments were performed in 1X RIPA buffer supplemented with 1X PIC and phosphatase inhibitors (1mM SoV, 5mM NaF). 500ug of whole cell lysate or subcellular extract were incubated with appropriate primary antibody in 1X RIPA buffer overnight at 4°C. The next day, 50ul protein G agarose bead slurry was added into the

reaction tube and incubated on a rotating platform for 2 hours at 4 °C. The beads were washed with 600 µl 1XRIPA or NETS buffer (150 mM NaCl, 50 mM Tris-HCl [pH 7.5], 5 mM EDTA, 0.05 % NP-40) five times. The tubes were centrifuged at 1,000 rpm for 5 min at 4 °C. The immuno-complex samples were denatured with equal volume of 2XSDS-PAGE loading buffer by incubating at 95 °C for 8 min. The immuno-complexes were separated in SDS-polyacrylamide gel electrophoresis (PAGE) and the presence of interested protein bands were detected with western blot technique.

6.4.10 Western Blot

Certain amount of recombinant proteins, whole cell lysate, subcellular lysate or immuno-complex was mixed with 5X SDS-PAGE loading buffer and denatured by incubating at 95 ºC for 8 min. Proteins complex were separated in 8~10% SDS-PAGE and transferred to nitrocellular membranes. Nitrocellular membranes, sponges and filter papers were firstly soaked in transfer buffer (Tris-HCl, pH8.3, Glycine and 40 % methanol) for 10 min. The transfer sandwich was assembled by following the manufacturer's instructions. The transferring was carried out at 100 mA for 1hour. After transferring, the transfer sandwich was disassembled and the nitrocellular membranes was stained with Pancrea S dye for 10 seconds and destained with ddH_2O for 1 min to remove extra dye. The protein bands would be visualized on the membranes. The membranes were washed with TBST for 10 min to remove Panceau S dye completely. The membranes were incubated with primary antibody with suitable dilutions in 2%BSA-TBST buffer at 4 °C for 2 hours to overnight. The next day, the membranes were washed with TBST buffer three times totally for 15~20 min. Then, membranes were incubated

with the secondary antibody (1:2,000 dilutions in TBST buffer) for 2 hours at room temperature. The membranes were incubated with SuperSignal West Dura Extended Duration Substrate (Pierce) for 2 min and the blotting signals were detected with a CCD camera.

6.4.11 Cell Proliferation Assay

Cell proliferation rate was measured with BrdU cell proliferation assay by following the manufacture's instructions (Calbiochem). Briefly, cells were seeded into a 96 well culture plate ($1X10^4$ cells/well). The next day, cells were transfected with adenovirus containing expression plasmid vectors. Two days later, BrdU was diluted in a working solution with fresh culture medium. 20 ul of working solution was added into each well and incubated with cells in a cell culture incubator. 24 hours later, culture medium was removed and cells were fixed with 50ul Fixative/Denaturing solution. Then, 20 ul of anti-BrdU antibody was added into each well and incubated with cells for 1 hour at room temperature. After extensive washing with washing buffer, secondary antibody conjugated with HRP was added into wells and incubated with cells for 30 min at room temperature. The plates were flooded with ddH_2O and incubated with substrate solution for 15 min. 50ul of stop solution was added into each well and absorbance was measured using a spectrophotometric plate reader (Wallac 1420 multilabel counter) at wavelengths of 450-540nm.

6.4.12 Recombinant Adenovirus Generation and Infection in Mammalian Cells

PKM2 cDNA was purchased from OriGene Technologies. Recombinant adenoviruses expressing PKM2 was constructed according to the method reported by Dr. Tong-Chuan He (Luo J et al, Nature protocols, 2007, 2(5), 1236-1247). Briefly, PKM2 cDNA was cloned into a shuttle vector pAdEasy-1 with EcoRI and NotI restriction endonuclease sites. The resultant plasmid was digested with Pme1 and transformed into competent AdEasier cells containing the adenoviral backbone plasmid pAdEasy-1 by electroporation method (BJ5183-AD-1, Stratagene). Recombinants were selected for kanamycin resistance and further confirmed by restriction endonuclease analyses. The confirmed plasmid with PKM2 cDNA was digested with PacI restriction endonuclease and transformed into HEK-293 cells expressing adenovirus E1 (Stratagene). The production of recombinant adenoviruses in HEK-293 cells was examined with GFP expression under fluorescent microscope. The amplified virus was released from HEK-293 cells by four freeze-thaw-vortex cycles. Cell debris was removed by centrifugation at 500 rpm at 4 °C for 15min. The recombinant adenoviruses were amplified three rounds in HEK-293 cells to get higher titers. Titers were measured with GFP expression in HEK-293 cells with a series of 10 folds dilutions of virus lysate. The titer in the initial lysate was around $1.43X10^{9}$ pfu/ml. After three rounds of amplification the titer reached $1.09X10^{13}$ pfu/ml. All viral lysates was stored in -80 °C for further appluications. To infect cells, cells were seeded in 48-well plates to 70~80 % confluence one day before infection. 50ul of viral lysate ($1.09X10^{13}$ pfu/ml) was added to each well of a 48-well plate and incubated with cells for 3-5 hours. For 24-well and 6-well plates, the scales were increased according to the plate sizes. Fresh medium was changed 3~5 hours later. The expression of HA-PKM2 was examined by Western blot 48 hours later.

6.4.13 Metabolism Measurement

Pyruvate, lactate, and glucose assay kits are purchased from BioVision. Mammalian cells overexpressing HA-PKM2 or control vectors were lysated in corresponding assay buffers. The cell lysate were centrifuged at 13,000 rpm to precipitate insoluble material. 10 ul of the clear extracts was applied for assay test. The standard curves were generated using probes supplied with the kits. Pyruvate, lactate, and glucose amounts were measured by following the manufacture's instruction.

6.5 Materials

Table 2 Antibody List

Name	Antigen	Source	Company
8E4	β-catenin	Mouse	Upstate
12CA5	HA	Mouse	Roche
124H6	Stat3	Mouse	Cell sigaling
27E8	His	Mouse	Cell signaling
β-actin	Actin	Rabbit	Cell Signaling
γ-tubulin	γ-tubulin	Rabbit	Abcam
Anti-HA conjugated with fluorescent dye	HA	Mouse	Roche
Anti-HA poly	HA	Rabbit	Georgia State University, Animal center facility
Beta-catenin poly	Beta-catenin	Rabbit	Cell Signaling
Biotin-labeled antibody for IHC		Rabbit	KPL
CRM1	CRM1	Rabbit	Abcam
D2E12	Jak2	Rabbit	Cell signaling
D3A7	p-Tyr-Stat3 (Tyr705)	Rabbit	Cell signaling
DCS-291	Cdc14A	Mouse	Abcam
Eg5	Eg5	Rabbit	Abcam
Fibrillarin	Fibrillarin	Rabbit	Abcam
GAPDH	GAPDH	Mouse	Cell signaling
Histone 2A	Histone	Mouse	Cell Signaling
KPNA2	KPNA2	Rabbit	Abcam
Lamin A/C	Lamin A/C	Rabbbit	Cell Signaling
Lamin B1	Lamin B1	Rabbit	Abcam
MAP2K5 antibody, clone 1B4,	MAP2K5	Mouse	Abnova
MAP2K5(pSer311/Thr315)	MAP2K5	Rabbit	AnaSpec
NTF97/importin β	NTF97	Mouse	Abcam
P68	P68 RNA helicase C-terminal	Rabbit	Georgia State University, Animal center facility
P68-rgg	P68 RNA helicase	Mouse	Auburn University Hybridoma Facility
Phosphor S10	Hstone H3	Mouse	Abcam
PKM2	PKM2 specific sequences	Rabbit	Georgia State University, Animal center

			facility
PY20	Phosphor-Tyrosine	Mouse	Abcam
p-Tyr-100	Phosphor-Tyrosine	Mouse	Cell signaling
RNA polymerase II	RNA polymerase II	Mouse	Abcam
Tyr1007/1008	p-Jak2	Rabbit	Cell signaling

Table 3 Primers List

Construction	Primers	Vector
His-PKM2	5’-GGGGAATTCTCGAAGCCCCATAGTGAAGC-3’ 5’-GGGGCGGCCGCCGGCACAGGAACAACACGC-3’	pET30a
HA-PKM2	5’-GGGGAATTCCTCGAAGCCCCATAGTGAAGC-3’ 5’-GGGGCGGCCGCTTCGGCACAGGAACAACACGC-3’	pHM6
NLS-PKM2	5’-GGGGAATTCCCCTAAGAAGAAGCGCAAGGTGTCGAAGCCCCATAGTGAAGC-3’ 5’-GGGGCGGCCGCTTCACCTTGCGCTTCTTCTTAGGCGGCACAGGAACAACACGC-3’	pHM6
eGFP-PKM2	5’-GGGGATATCAATCGAAGCCCCATAGTGAAGC-3’ 5’-GGGGCGGCCGCTTACGGCACAGGAACAACACGC-3’	pcDNA3.
GST-PKM2	5’-GGGGGATCCTCGAAGCCCCATAGTGAAGC-3’ 5’-GGGGAATTCGCTTACGGCACAGGAACAA-3’	pGEX2T
K433E-PKM2		pHM6
R399E-PKM2	5'-CAATTATTTGAGGAACTCGAGCGCCTGGCGCCCATTACC-3' 5'-GGTAATGGGCGCCAGGCGCTCGAGTTCCTCAAATAATTG-3'	pHM6
NLS-PKM2	5'-CATAATCGTCCTCACCGAGTCTGGCAGGTCTGC-3' 5'-GCAGACCTGCCAGACTCGGTGAGGACGATTATG-3'	pHM6
PKM2- C-terminal deletion mutant	5’-GGGGAATTCCATGTCGAAGCCCCATAGTGA-3’ 5’-GGGGCGGCCGCTTTCAGCTGGTAATGGGCGCCAG-3’	pHM6
L398A of PKM2	5’-GCAGCTGAGGAAGCCCGCCGCCTGGC-3’ 5’-GCCAGGCGGCGGGCTTCCTCAGCTGC-3’	pHM6
L401A of PKM2	5’-GAAGCCCGCCGCGCGGCGCCCATTAC-3’ 5’-GTAATGGGCGCCGCGCGGCGGGCTTC-3’	pHM6
P403A of PKM2	5'-GCCGCGCGGCGGCCATTACCAGCG-3' 5'-CGCTGGTAATGGCCGCCGCGCGGC-3'	pHM6

I404A of PKM2	5'-CGCGCGGCGGCCGCTACCAGCGACCC-3' 5'-GGGTCGCTGGTAGCGGCCGCCGCGCG-3'	pHM6
K270M of PKM2	5'-AAGAACATCAAGATTATCAGCATGATCGAGAATCATGAGGGGGTTC-3' 5'-GAACCCCCTCATGATTCTCGATCATGCTGATAATCTTGATGTTCTT-3'	pHM6 pET30a +
1-432 truncating mutant of PKM2	5'-GGGGAATTCCTCGAAGCCCCATAGTGAAGC-3' 5'-GGGGCGGCCGCTAGGTGAGGACGATTATGGCCC-3'	pHM6
1-515 truncating mutant of PKM2	5'-GGGGAATTCCTCGAAGCCCCATAGTGAAGC-3' 5'-GGGGCGGCCGCTATCCGGTCAGCACAATGACC-3'	pHM6
1-269 truncating mutant of PKM2	5'-GGGGAATTCCTCGAAGCCCCATAGTGAAGC-3' 5'-GGGGCGGCCGCTAGCTGATAATCTTGATGTTCTTTC-3'	pHM6
270-432 truncating mutant of PKM2	5'-GGGGAATTCCAAAATCGAGAATCATGAGGGG-3' 5'-GGGGCGGCCGCTAGGTGAGGACGATTATGGCCC-3'	pHM6

Table 4 Mammalian Cell Lines

Name	Company	Origin	Culture medium
SW480	ATCC	Human colorectal adenocarcinoma cells	Leibovitz L-15 + 10 % FBS
SW620	ATCC	Human colorectal adenocarcinoma cells derived from metastatic site: lymph node	Leibovitz L-15 Medium + 10% FBS
WM115	ATCC	Human skin melanoma cells	MEM + 10 % FBS
WM266	ATCC	Human skin metastatic melanoma cells	MEM + 10 % FBS
H460	ATCC	Human primary lung	DMEM + 10 % FBS
H146	ATCC	Human metastatic lung	DMEM + 10 % FBS
T98G	ATCC	Human brain glioblastoma cells	MEM + 10 % FBS+1mM pyruvate kinase+1mM non-essential amino acid
U-87 MG	ATCC	Human brain astrocytoma cells	MEM +10 % FBS+1mM pyruvate kinase+1mM non-essential amino acid
HeLa S3	ATCC	Human cervix adenocarcinoma cells	F12K/DMEM + 10 % FBS
HEK293	ATCC	Human kidney epithelial cells immortalized by adenovirus 5 DNA	DMEM+ 10 %FBS
HEL 299	ATCC	Human lung normal fibroblast cells	MEM + 10 % FBS
NIH/3T3	ATCC	Mouse embryo fibroblast cells	DMEM + 10 % FBS

Table 5 Chemicals

Name of chemical	Company
α-Cyano-4-hydroxycinnamic acid	Agilent Tech, Santa Clara
[γ-^{32}P] ATP	PerkinElmer, Waltham
2-Mercaptoethanol	Sigma Aldrich, St. Louis
Acetic acid	VWR International, West Chester
Acetone	VWR International, West Chester
Acrylamide/bisacrylamide solutions	Fisher BioReagent, Fairlawn
Agar	Sigma-Aldrich, Saint Louis
Agarose	MP Biomedicals, Aurora
Ammonium persulfate	Sigma-Aldrich, Saint Louis
Anhydrous acetonitrille	Applied Biosystems, Foster City
Bacto Yeast Extract	BD Bioscience, Spark
Bacto Tryptone	BD Bioscience, Spark
Bovine serum albumin	Promega, Madison
Bromophenol Blue	EMD Biosciences, San Diego
Coomassie blue	Sigma-Aldrich, Saint Louis
Deep purple total protein stain	Amersham Biosciences, Piscataway
Dithiothreitol	Shelton Scientific, Shelton
Ethanol	AAPER Alcohol & Chemical, Shelbyville
Ethidium bromide	Sigma-Aldrich, Saint Louis
Ethylenedinitro-tetraacetic acid (EDTA)	Sigma-Aldrich, Saint Louis
Fetal calf serum	HyClone, Logan
Formaldehyde	Calbiochem, San Diego
Formic acid	EMD Biosciences, San Diego
FuGENE 6 Transfection Reagent	Roche Applied Science, Indianapolis
GelCode Blue Stain Reagent	Pierce, Rochford
Glycine	MP Biomedicals, Aurora
HiTrap affinity columns	Amersham Biosciences, Piscataway
Hydrochloric acid	VWR International, West Chester
Imidazole	Sigma-Aldrich, Saint Louis
Isopropyl-ß-D-thiogalactopyranosid	Sigma-Aldrich, Saint Louis
Isopropanol	VWR International, West Chester
Kanamycin solution	Teknova, Hollister
Lipofectamine 2000	Invitrogen, Carlsbad
Lipofectamin RNAiMAX	Invitrogen, Carlsbad
Lysozyme	Sigma-Aldrich, Saint Louis
Magnesium Chloride	Fisher Biotech, Fairlawn
Methanol	VWR International, West Chester
Molecular weight marker (DNA)	MBI Fermentas, Hanover
Molecular weight marker (protein)	MBI Fermentas, Hanover
N- (2-hydroxyethyl) piperazine-N`-(2-	Sigma-Aldrich, Saint Louis

ethanesulfonic acid) (HEPES)	
Nickel-nitrilotriacetic acid (Ni-NTA) agarose	Qiagen, Hilden
Ni-TED™ Silica	Active Motif, Carlsbad
N, N, N', N'-Tetramethylethylenediamine	Promega, Madison
Nonidet P40	Roche Applied Science, Indianapolis
Normal goat serum (10%)	KPL, Gaithersburg
Phenol/Chloroform	Promega, Madison
Phenylmethylsulfonyl fluride	Fluka, Switzerland
Phosphatase inhibitor cocktail	Sigma-Aldrich, Saint Louis
Poly-L-lysine solution	Sigma-Aldrich, Saint Louis
Ponceau S	Sigma-Aldrich, Saint Louis
Protease inhibitor cocktail tablets	Roche, Germany
Protein G agarose	Upstate, Charlottesville
Protein G sepharose 4 fast flow	Amersham Biosciences, Piscataway
Sephadex G-25	Amersham Biosciences, Piscataway
Superdex 200 HR 10/30	Amersham Biosciences, Piscataway
Sodium acetate	Promega, Madison
Sodium azide	Fluka, Switzerland
Sodium bicarbonate	Sigma-Aldrich, Saint Louis
Sodium chloride	Fisher BioReagent, Fairlawn
Sodium dodecyl sulfate	Fisher BioReagent, Fairlawn
Sodium fluoride	Fluka, Switzerland
Sodium hydroxide	Fisher BioReagent, Fairlawn
Sodium orthovanadate	EMD Biosciences, San Diego
Sodium pyruvate	Cellgro, Herndon
Triton X-100	Sigma-Aldrich, Saint Louis
Trypan Blue	Sigma-Aldrich, Saint Louis
Trypsin proteomics grade	Sigma-Aldrich, Saint Louis
Tween-20	Sigma-Aldrich, Saint Louis
Urea	Fisher Biotech, Fairlawn
X-tremeGene siRNA Transfection Reagent	Roche, Germany

Table 6 Experimental Kits

Name	Company
AminoLink Plus Immobilization Kit	Pierce, Rockford
BrdU cell proliferation assay	Calbiochem,
ChIP-IT kit	Active Motif, Carlsbad
DAB reagent set	KPL, Gaithersburg
EZ-link NHS-PEO solid phase biotinylation kit	Pierce, Rochford
Glucose Assay Kit	BioVision, Mountain View
Improm-II Reverse Transcription System	Promega, Madison
Lactate Assary Kit	BioVision, Mountain View
MinElute PCR Purification Kit	Qiagen, Valencia
Nuclear Extract Kit	Active Motif, Carlsbad
ProteoSliver Plu Sliver Stain Kit	Sigma-Aldrich, Saint Louis
Pyruvate Assay Kit	BioVision, Mountain View
RNeasy Plus Kit	Qiagen, Valencia
Qiaprep Spin Mini-Prep	Qiagen, Valencia
Qiaquick Gel Extraction Kit	Qiagen, Valencia
QuickChange II XL site-directed Mutagenesis Kit	Stratagene, La Jolla
Quick-ChIP	Imgenex, San Diego
Trypsin Profile IGD kit for in-gel digests	Sigma-Aldrich, Saint Louis

CHAPTER 7: APPENDIX

7.1 Detection of Associated Nuclear Proteins to Phosphorylated p68 RNA Helicase

7.1.1 Abstract

P68 RNA helicase, a member of DEAD box family, is involved in pre-mRNA splicing progress as well as many other important biogenesis processes. P68 RNA helicase is phosphorylated at its tyrosine residues, which plays crucial roles in cancer developments. Here we applied MALDI-TOF method to detect its phosphorylation sites from HeLa cells. We also performed proteomic methods to examine the associated nuclear proteins to p68 RNA helicase, which may be important for further study about p68 biological functions in the nucleus.

7.1.2 Introduction

P68 is a member of the DEAD (Aspartic acid–Glutamic acid–Alanine–Aspartic acid) box family proteins. DEAD box proteins have been shown to be involved in a wide range of biological processes, such as pre-mRNA splicing, ribosome biogenesis and translation (Liu 2002; Kahlina, Goren et al. 2004) . Protein phosphorylation is one of the major post-translational modifications playing important roles in signal transduction pathways. P68 RNA helicase is phosphorylated at its tyrosine residues in cancer cells (Yang, Lin et al. 2005). Phosphorylation at Y593 tyrosine residue is required for colon cancer cells proliferation and epithelial to mesenchymal transition (EMT) stimulated by PDGF (Yang, Lin et al. 2007). Phosphorylation at Y593 residue of p68 promotes β-catenin translocate into the nucleus in colon cancer cells (Yang, Lin et al. 2006). To

further illustrate the physiological functions of phosphorylated p68 in cancer cells, we examined the nuclear associated proteins to phosphorylated p68 with proteomic methods.

7.1.3 Methods

7.1.3.1 Co-Immunoprecipitation and Peptide Pulldown

IP and Co-IP experiments were performed in NETS buffer (150 mM NaCl, 50 mM tris-HCl[pH 7.5], 5 mM EDTA, 0.05% NP-40). SDS was added to a final concentration of 1%. 30 ul of p68 mono-antibody was incubated with 500 ug of nuclear extract in 1 ml NETS buffer for 3 hr at 4 °C. 100 ul of protein G agarose bead slurry was added into the tube and incubated for 2 h. The beads were recovered by centrifuging at 1000 rpm for 10 min and washed with 600 µl of NETS five times. The proteins complexes were separated in SDS-PAGE gel. For peptide pulldown experiment, 500 ug of nuclear extract was pre-cleared with 50 ul of naked beads by incubating for 30 minutes at 4 °C. After centrifuging, 100 ul of beads conjugated with phosphorylated or non-phosphorylated peptides were incubated with the supernatant at 4 °C overnight. The tube was centrifuged at 1,000 rpm for 10 min at 4 °C. The precipitated mixture was washed with 600 µl of NETS five times and with 1% SDS twice.

7.1.3.2 Two-Dimensional SDS-PAGE Analysis

Protein samples were washed with 1 ml ddH2O twice. The protein samples were then solubilized in re-hydration buffer (7 M Urea, 2 M thiourea, 2% CHAPS, 0.8% ampholyte, 0.02% bromophenol blue, and 65 mM DTT). A dry strip was removed from -

20 °C and was equilibrated in equilibration buffer [0.38 M Tris-base, pH 8.8, 6 M urea, 2% (w/v) SDS and 20% (v/v) glycerol] at room temparature for 15 min. The samples were loaded into the rehydration tray. A paper wick was palaced at both ends of the focusing try channel covered with 30 ul ddH2O. The tray was set into IEF cell and run the following program: 250V for 20 min, 8000 V for 2.5 h and 8000 v for 20,000 Volt-Hours. The next day, IPG strip was taken out from IEF cell and set in a clean tray with gel side up. 3.5 ml Equilibration buffer was added into IEF cell and incubated with the strip for 10 min. The IPG strip was dipped in 1X SDS-PAGE gel running buffer. Then, the strip was laid onto the top of the prepared SDS gel and sealed with 1% agarose in gel box. The gel box was filled with 1X running buffer (25 mM Tris, 190 mM glycine and 0.1% SDS) and run at 60 volt for 20 min, then the volt was changed to 100 volt. After electrophoresis, the gel was wash with ddH2O for 5 min. The gel was stained with Deep Purple fluorescent dye or silver stain (Amersham Biosciences) according to the manufactures instructions.

7.1.3.3 Protein Identification by Peptide Mass Fingerprinting

The proteins complexes were separated in 10% SDS-PAGE or 2-D gel. The targeting proteins spots were picked up with Ettan spot picker. The samples were digested with trypsin. After ZipTip purification, the digested peptide solution was eluted from ZipTip with 50% ACN/0.1% formic acid and spotted directly onto a wax-coated MALDI target plates. Nano LC MALDI TOF/TOF MS analysis was performed in Applied Biosystems 4700 proteomics analyzer. The matching of the experimental

sequences with tryptic peptide masses from database was performed with Peptident proteomic tools in ExPASy Molecular Biology Server (http://www.expasy.ch/). The MALDI-TOF/TOF database was from NCBInr.

7.1.4 Results and Discussions

7.1.4.1 Identification of Phosphorylated Residues of p68 RNA Helicase with MALDI-TOF

Matrix-assisted laser desorption/ionization (MALDI)-time of flight (TOF) MS is a well established tool for peptide or protein identification. The addition of a phosphate monoanion to a hydroxyl group of tyrosine results in mass increases of the proteins or peptides by 79.966 Da in monoisotopic mass. It is possible to estimate the number of phosphates on a protein by comparing the mass shift between the modified and original peptides. The strength of peptide signals in MALDI-TOF is important for detecting the mass shift. In most cases, the protein staining method in SDS-PAGE gel may affect the enrichment of peptide signals. To this purpose, we applied two protein staining methods to detect p68 peptides digested by trypsin. The results showed that GelCode staining was more sensitive for MALDI-TOF signal enrichment of the digested peptides than Coomassive blue staining (Fig 7.1). Therefore, we applied Gelcode staining method in the following experiments to detect the phosphorylated residues of p68. P68 RNA helicase was immunoprecipated from the nuclear extract of HeLa cells. The presence of p68 in the immunoprecipitated complex was confirmed by western-blot. P68 RNA helicase was in-gel digested with trypsin and the presence of peptides was detected with MALDI-TOF. Our results showed that the detected peptide signals were recovered

around 70% by comparing with control (matrix only). The recovered peptides, including 1336.6 D, 1348.6 D, 1389.6 D, 1574.7 D, 2131.9 D, 2361.4 D, matched with theoretical peptide masses (Fig 7.2). All the peptides above 1000 D were detected in MALDI-TOF except one peptide, whose molecular weight was 5967.4D. Our result showed a peak around 5571.8 D in the peptide complex. Whether this peak was due to the hydrolysis effect or some other modifications was not known. The peptide, 2396.4 D, was found 163.4 D shift from 2133.04 D peptides whose compose was FVINYDYPNSSEDYIHR including three tyrosine sites (Fig 7.2). According the prediction from Netphos 2.0, Y418 and Y425 sites had the high potential possibilities of phosphorylation. The shifted peak may be the two phosphorylatd sites from Y418 and Y425. These phosphorylation sites needs to be further confirmed with other biological methods, such as mutagenesis.

7.1.4.2 Detection of p68 Associated Nuclear Proteins Using 2-D Gel

P68 RNA helicase plays crucial roles in many biological process. To elucidate its other functions in the nuclear, it is important to examine the associated proteins. To this end, Co-IP experiment was performed to precipitate these associated proteins with p68 antibody. Three antibodies generated from the C-terminal sequence and one from N-terminal sequence of p68 were applied to immunoprecipitate p68-associated proteins. The precipitated protein complexes were separated in 2-D gel. The results showed that some associated proteins specially precipated by the C-terminal antibody, which indicated these proteins may be only associated with the C-terminal phosphorylated p68 RNA helicase (Fig 7.2). Some spots were picked up and will be identified with MALDI-TOF/TOF peptide fingerprinting method.

7.1.4.3 Analysis of Nuclear Associated Proteins to Phosphorylated p68 using Peptide-protein Interaction Screening Method

To specificly identify phosphorylated p68 RNA helicase associated proteins, we synthesized two peptides according to its C-terminal sequences. One had double phosphorylation sites at tyrosine residues, Y593 and Y595. The other was non-phosphorylated peptide with the same amino acid sequence. The synthesized peptides were coupled to agarose beads. The associated proteins were pull down with agarose beads conjugated with peptides. 2-D gel was performed to separate the protein complexes. The results showed that three proteins spots specificly presented in the complex precipitated with phosphorylated peptides, not with non-phosphorylated peptides. Nine proteins spots specially presented in the protein complex pulled down with non-phosphorylated peptides. These targeting proteins will be identified by MALDI-TOF/TOF (Fig 7.3).

7.1.5 References

Kahlina, K., I. Goren, et al. (2004). "p68 DEAD box RNA helicase expression in keratinocytes. Regulation, nucleolar localization, and functional connection to proliferation and vascular endothelial growth factor gene expression." J Biol Chem **279**(43): 44872-44882.

Liu, Z. R. (2002). "p68 RNA helicase is an essential human splicing factor that acts at the U1 snRNA-5' splice site duplex." Mol Cell Biol **22**(15): 5443-5450.

Yang, L., C. Lin, et al. (2005). "Phosphorylations of DEAD box p68 RNA helicase are associated with cancer development and cell proliferation." Mol Cancer Res **3**(6): 355-363.

Yang, L., C. Lin, et al. (2006). "P68 RNA helicase mediates PDGF-induced epithelial mesenchymal transition by displacing Axin from beta-catenin." Cell **127**(1): 139-155.

Yang, L., C. Lin, et al. (2007). "Phosphorylation of p68 RNA helicase plays a role in platelet-derived growth factor-induced cell proliferation by up-regulating cyclin D1 and c-Myc expression." J Biol Chem **282**(23): 16811-16819.

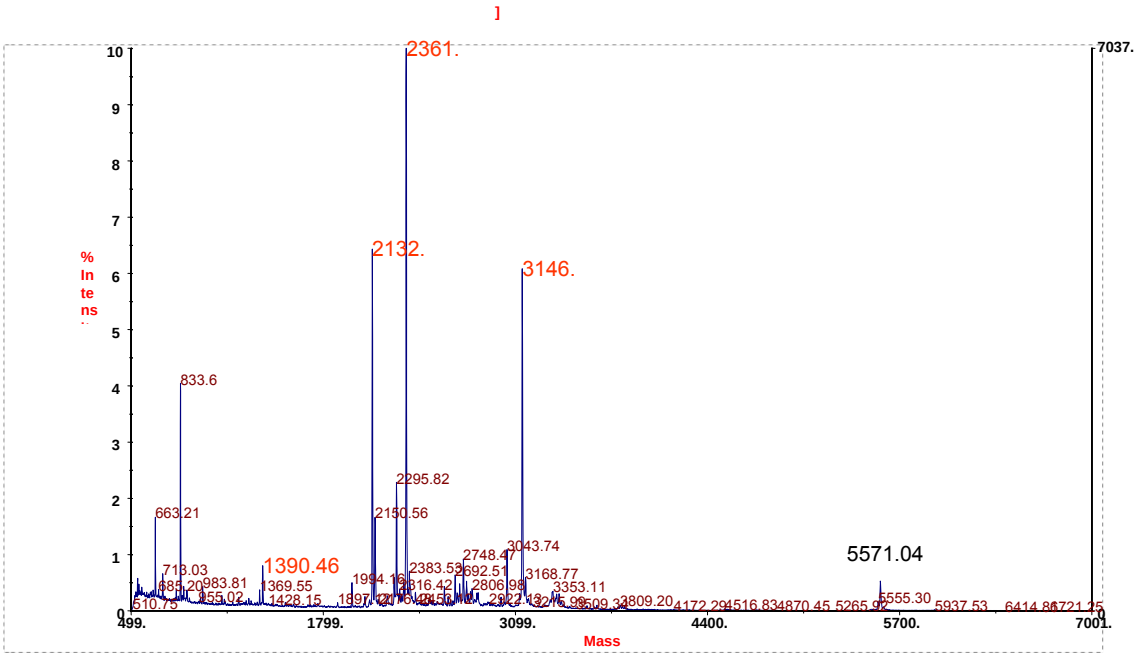

A.

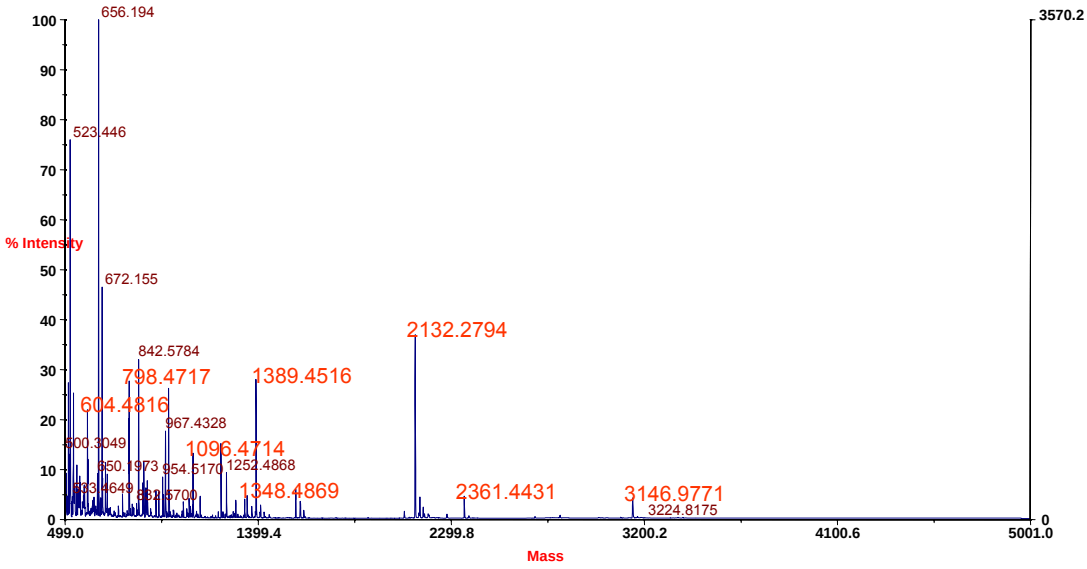
656.194
523.446
672.155
842.5784
798.4717
1389.4516
604.4816
967.4328
1096.4714
1252.4868
1348.4869
2132.2794
2361.4431
3146.9771
3224.8175
% Intensity
Mass
100
90
80
70
60
50
40
30
20
10
0
499.0
1399.4
2299.8
3200.2
4100.6
5001.0
3570.2

B

Fig 7.1.1 P68 Post-translation Modifications Analysis with MALDI-TOF.
(A) shows digested peptides of p68 by trypsin via GelCode staining. **(B)** shows digested peptides from p68 by trypsin via Coomassive blue staining.

A

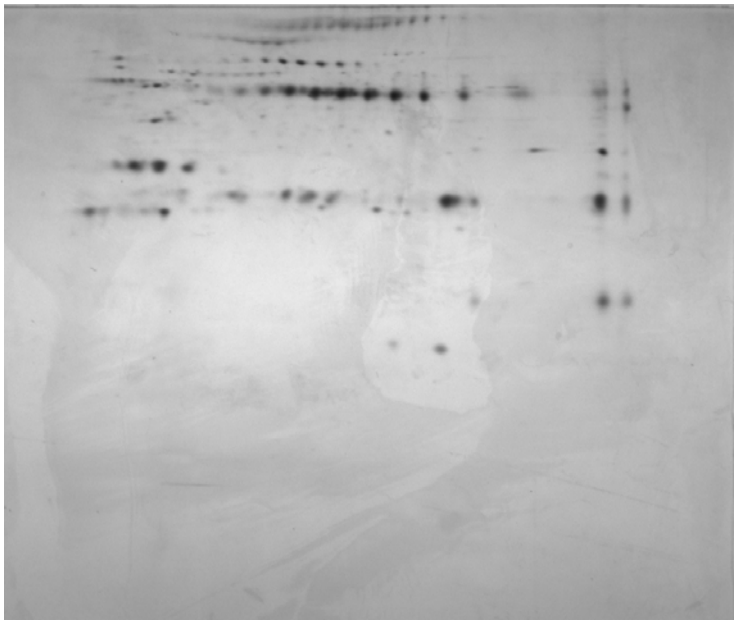

B

Fig 7.1.2 2-D Gel Analyses of p68-associated Nuclear Proteins Immunoprecipitated with p68 Antibodies

(A). 2-D gel analysis of p68 associated nuclear proteins immunoprecipitated by p68 antibody generated from the recombinant protein derived from C-terminal sequence of p68. **(B).** 2-D gel analysis of p68 associated nuclear proteins immunoprecipitated by p68 antibody generated from the recombinant protein derived from N-terminal sequence of p68. In **(A)** and **(B),** both gels were stained with silver staining.

60KD

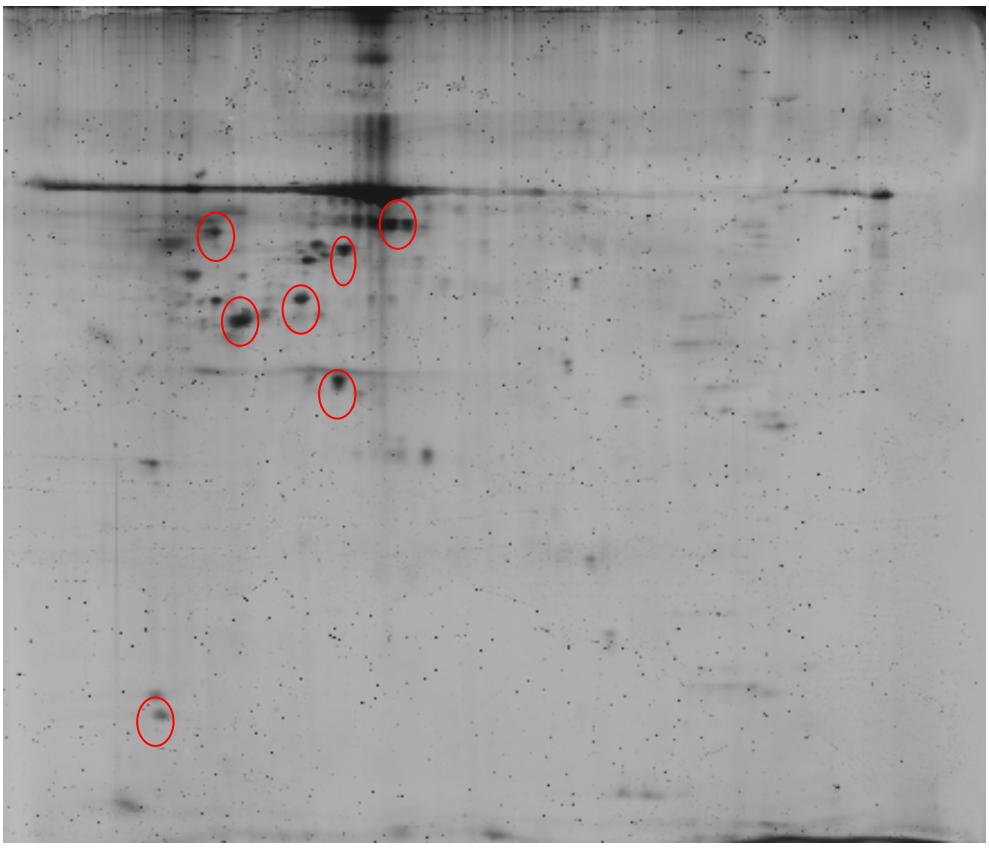

A

60KD

50KD

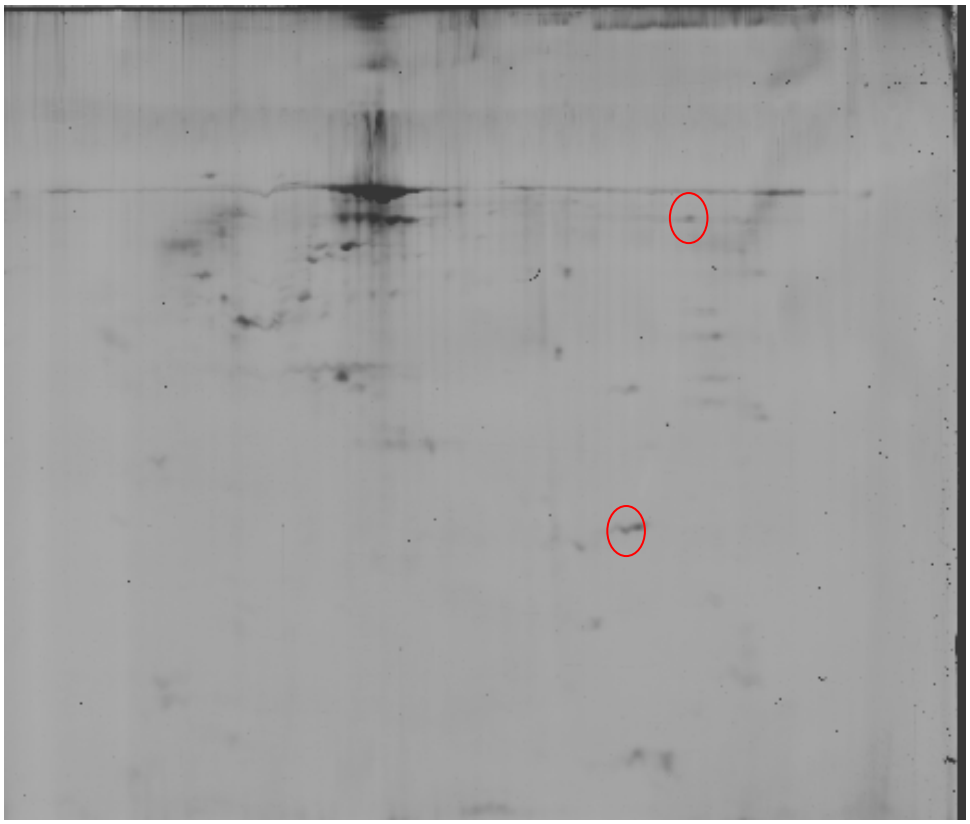

Fig 7.1.3 2-D Gel Analysis of p68-associated Nuclear Proteins Pulled Down with Phophorylated Peptides Derived from p68
(A). 2-D gel analysis of p68 associated nuclear proteins pulled down using non-phosphorylated peptides derived from C-terminal sequence of p68. The cycled spots showed the specific associated protein to non-phosphorylated peptides **(B).** 2-D gel analysis of p68 associated nuclear proteins pulled down by phosphorylated peptide derived from N-terminal sequence of p68. The cycled spots showed the specific associated protein to phosphorylated peptides. In **(A)** and **(B),** both gels were stained with silver staining.